Entwicklung neuer Borhydrid-basierter Materialsysteme für Wasserstoffspeicheranwendungen

Von der

Fakultät für Maschinenbau

der

Helmut-Schmidt-Universität
Universität der Bundeswehr Hamburg

zur Erlangung des akademischen Grades eines

Doktor Ingenieurs (Dr.-Ing.)

genehmigte

Dissertation

vorgelegt von

Nils Bergemann
aus Rostock

Hamburg 2019

Vorsitzender des Prüfungsausschusses:	Univ.-Prof. Dr. rer. nat. habil. Markus Bause
1. Gutachter:	Univ.-Prof. Dr.-Ing. habil. Thomas Klassen
2. Gutachter:	Univ.-Prof. Dr. habil. Chiara Milanese
Tag der mündlichen Prüfung:	25.01.2019

Development of Novel Borohydride-Based Material Systems for Hydrogen Storage Applications

Doctoral Thesis

approved by the

Department of Mechanical Engineering

of the

Helmut-Schmidt-University
University of the German Federal Armed Forces

for obtaining the academic degree of

Doktor Ingenieur (Dr.-Ing.)

presented by

Nils Bergemann
from Rostock

Hamburg 2019

Chairman of the examination committee:	Univ.-Prof. Dr. rer. nat. habil. Markus Bause
1. referee:	Univ.-Prof. Dr.-Ing. habil. Thomas Klassen
2. referee:	Univ.-Prof. Dr. habil. Chiara Milanese
Date of the oral examination:	25.01.2019

Development of Novel Borohydride-Based Material Systems for Hydrogen Storage Applications

Nils Bergemann

Abstract

In this work, a new class of Reactive Hydride Composites $M(BH_4)_n$-Mg_2NiH_4 is studied for potential hydrogen storage applications. After a screening of the composites based on the most interesting alkali and alkaline earth metal borohydrides ($M \in \{Li, Na, K, Mg, Ca\}$) with respect to phase formation and reversibility, the two most promising systems, $LiBH_4$-Mg_2NiH_4 and $Ca(BH_4)_2$-Mg_2NiH_4, are selected for comprehensive in-depth studies. At elevated hydrogen pressures, a mutual destabilisation mechanism between either of the two borohydrides and Mg_2NiH_4 is proven. The enthalpies of these concerted dehydrogenation reactions are extraordinary low, with values below $20\,kJ\,(mol\,H_2)^{-1}$. Upon dehydrogenation, boron is reversibly transferred to $MgNi_{2.5}B_2$ and no significant amounts of $[B_{12}H_{12}]^{2-}$ compounds or elemental boron are present among the desorption products. In fact, $Ca(BH_4)_2$-Mg_2NiH_4 is the first $Ca(BH_4)_2$ based Reactive Hydride Composite that features such a reversible boron exchange with the reaction partner. As the transfer of boron within these systems is a crucial process, the underlying mechanisms are characterised. A yet unknown Mg-Ni-B phase is identified as an intermediate dehydrogenation product at hydrogen pressures low enough to allow for the decomposition of Mg_2NiH_4 and thus the formation of Mg_2Ni. Independent of the boron donor, Mg_2Ni is found to be an essential reactant for the formation of the new phase. The presented results suggest that several phenomena, including the formation of the intermediate Mg-Ni-B phase and the presence of a certain homogeneity range of $MgNi_{2.5}B_2$, are governed by limited solid-state diffusion rates. The insights presented in this work can be used to optimise the investigated systems' hydrogen sorption conditions, control specific reaction steps and design new hydrogen storage solutions.

Entwicklung neuer Borhydrid-basierter Materialsysteme für Wasserstoffspeicheranwendungen

Nils Bergemann

Zusammenfassung

In dieser Arbeit wird eine neue Klasse Reaktiver Hydrid-Komposite $M(BH_4)_n$-Mg_2NiH_4 für potentielle Wasserstoffspeicheranwendungen erforscht. Nach einer Reihe grundlegender Untersuchungen der auf den interessantesten Alkali- sowie Erdalkalimetallborhydriden ($M \in \{Li, Na, K, Mg, Ca\}$) basierenden Komposite hinsichtlich Phasenbildung und Reversibilität werden die beiden vielversprechendsten Systeme, $LiBH_4$-Mg_2NiH_4 und $Ca(BH_4)_2$-Mg_2NiH_4,

für tiefergehende Charakterisierungen ausgewählt. Bei erhöhten Wasserstoffdrücken kann ein wechselseitiger Destabilisierungsmechanismus zwischen diesen beiden Borhydriden und Mg_2NiH_4 aufgezeigt werden. Die Enthalpien dieser abgestimmt ablaufenden Wasserstoffdesorptionsreaktionen sind mit weniger als $20\,kJ\,(mol\,H_2)^{-1}$ außergewöhnlich gering. Im Zuge der Wasserstofffreisetzung wird Bor reversibel zu $MgNi_{2.5}B_2$ übertragen, sodass keine nennenswerten Mengen von $[B_{12}H_{12}]^{2-}$-Verbindungen oder elementarem Bor unter den Desorptionsprodukten nachweisbar sind. Tatsächlich stellt $Ca(BH_4)_2$-Mg_2NiH_4 somit das erste $Ca(BH_4)_2$-basierte Reaktive Hydrid-Komposit dar, das einen derartigen reversiblen Boraustausch mit dem Reaktionspartner ermöglicht. Da der Transport des Bors innerhalb dieser Systeme einen entscheidenden Prozess darstellt, werden die zugrundeliegende Mechanismen untersucht. Eine bisher unbekannte Mg-Ni-B-Verbindung wird als Zwischenprodukt bei der Desorption unter Wasserstoffdrücken identifiziert, die so niedrig sind, dass eine Zersetzung von Mg_2NiH_4 und somit die Bildung von Mg_2Ni ermöglicht werden. Unabhängig von der jeweiligen Verbindung, welche das Bor für die Reaktion zur Verfügung stellt, wird Mg_2Ni als essentieller Reaktionspartner für die Bildung der Übergangsphase ermittelt. Die vorgestellten Ergebnisse legen den Schluss nahe, dass mehrere Phänomene, darunter die Bildung des Mg-Ni-B-Zwischenprodukts sowie das Vorliegen einer gewissen Phasenbreite von $MgNi_{2.5}B_2$, durch begrenzte Diffusionsraten innerhalb der festen Phasen dominiert werden. Die in dieser Arbeit dargestellten Erkenntnisse können dazu genutzt werden, die Wasserstoffsorptionsbedingungen der jeweiligen Systeme zu optimieren, bestimmte Reaktionsschritte zu kontrollieren und neue Wasserstoffspeicherlösungen zu entwickeln.

Contents

1 Introduction and Motivation

Since the Industrial Revolution in the late 18^{th} century, all developed and all developing countries based their economic prosperity and growth on energy obtained from fossil fuels. The amount of their available reserves might be discussed controversially but, without any doubt, our future infrastructure must be based on sustainable ways of energy generation. The first indisputable evidences of climate change made many people realise the importance of new concepts for the generation, distribution and storage of energy. Ideally, these new concepts should be renewable and non-polluting. More and more creative solutions to utilise the planet's renewable sources are currently being developed or have already reached the market. The typically decentralised infrastructure of renewable energy generation sets the demands for modern smart power grids. Due to the non-continuous power generation of most renewables (e. g. wind energy or solar power), efficient ways of storing excess energy become crucial technologies in future power grids. With different local conditions and diverse forms of supplying sustainable power into the grid, not just one energy storage solution but several complementary concepts will be required. Besides solutions for mechanical energy storage (e. g. compressed air, flywheels or pumped hydro), electrical energy storage (e. g. batteries, flow batteries, super capacitors or super conducting magnets) and thermal energy storage (e. g. sensible or latent heat storage), also chemical energy storage technologies are promising concepts [1–4]. In this field, hydrogen technology can play a key role. By dissociating water into hydrogen and oxygen, energy obtained from renewable sources is converted into chemical energy which can be stored, transported and eventually converted into electrical power. A closed hydrogen cycle is accomplished making renewable energies widely available for society. This is schematically visualised in figure 1.1. Herein, storing the hydrogen efficiently is one of the major challenges.

1.1 Storage of Hydrogen as Energy Carrier

Hydrogen can be considered as promising energy carrier for mobile as well as stationary applications. In a fuel cell it reacts with oxygen forming solely pure water. Therefore, the power generation from hydrogen is completely clean and causes none of the problems associated with the combustion of fossil energy carriers, such as the steady rise of the global CO_2 concentration or increased levels of NO_x and fine particles in the inner cities. There are different concepts of storing the hydrogen. Detailed introductions into these approaches and explanations on the physical, chemical and technical backgrounds can be found for instance

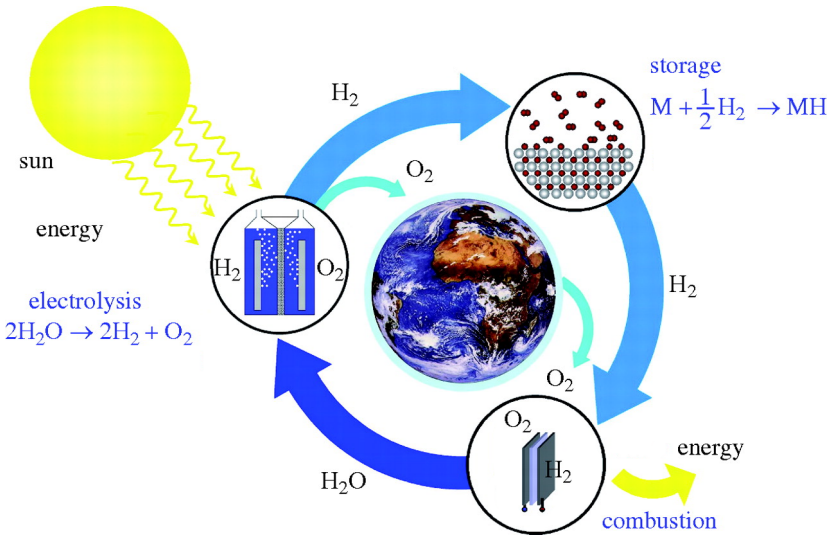

Figure 1.1: A closed hydrogen cycle: renewable energy is used to dissociate water into hydrogen and oxygen. The hydrogen is stored and thus utilised as energy carrier. Its recombination with oxygen produces solely pure water and releases the stored energy (adapted from [5]).

in the books "Hydrogen as a Future Energy Carrier" [6] or "Handbook of Hydrogen Storage: New Materials for Future Energy Storage" [7]. Here just a summarising overview shall be provided. The most acquainted and commercially available way to store hydrogen certainly is the storage in the gaseous state: due to (cryo-)compression large amounts of hydrogen can be filled into especially designed high pressure tanks [8, 9]. For instance, the hydrogen powered cars Toyota Mirai (introduced in 2014) and Hyundai NEXO (introduced in 2018) store the gaseous fuel in 700 bar vessels [10, 11]. If larger amounts of hydrogen are to be stored, also liquifaction represents an option. At atmospheric pressure, the boiling point of liquid hydrogen is at 21.2 K. Typically the Joule-Thompson (or Linde) cycle is employed to liquefy hydrogen. However, almost 40 % of the higher heating value of the hydrogen combustion are consumed in this process. In addition, all liquid hydrogen storage vessels suffer from a continuous hydrogen boil-off, i. e. evaporation losses due to inevitable introduction of external heat into the system. Since these heat fluxes into the vessel are directly controlled by the surface area and the thermal insulation of the tank walls, the relative boil-off rates decrease significantly as the tank volume increases. Therefore, possible applications for liquid hydrogen storage are limited to cases where large amounts of this gas are consumed in a short time. In addition to the compression and the liquefaction, the bonding of hydrogen to solid materials has a great potential [12–15]. In this regard, two concepts must be distinguished: the bonding of molecular and of atomic hydrogen. In the former case, the H_2 molecules are attracted to the surface of the adsorbent by weak van der Waals forces. Typically, this process – which is called physical adsorption or physisorption – is non-activated and thus offers fast kinetics. However, due to the low binding energies of normally 1 kJ $(\mathrm{mol\,H_2})^{-1}$ to 10 kJ $(\mathrm{mol\,H_2})^{-1}$, physisorption usually takes place only at low temperatures. As a consequence, for hydrogen storage applications the respective systems

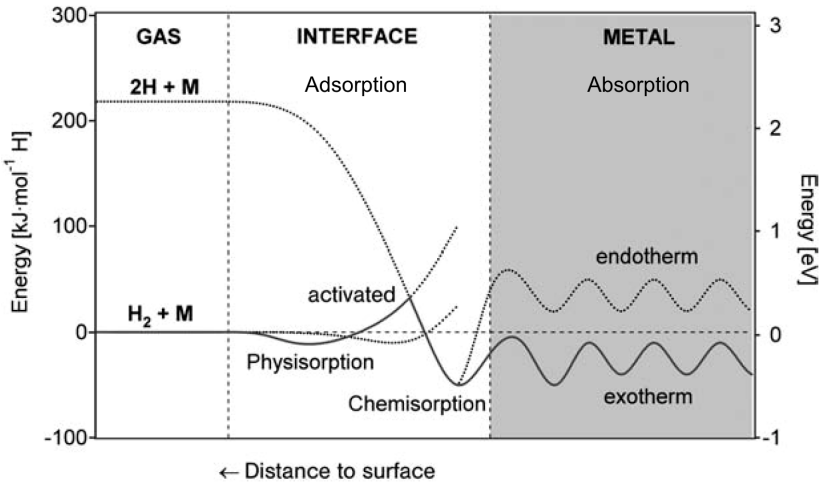

Figure 1.2: A simplified one-dimensional potential energy diagram for the hydrogen adsorption and absorption: as hydrogen comes near the metal surface, the bonding of H_2 molecules in the interface region (physisorption) is the first type of interaction. With further approach the bonding of H atoms to the metal surface atoms (chemisorption), i. e. the dissociation of the hydrogen molecule, is the energetically more favourable state. If the atoms penetrate the surface layer and diffuse into the bulk lattice they are absorbed by the metal (adapted from [6]).

must be cooled down below room temperature, often to liquid nitrogen temperature of 77 K. This constraint drastically reduces the possible fields of application. The second concept is the bonding of atomic hydrogen to the solid compounds. This is possible because certain materials form chemical bonds with hydrogen. In this process, the so-called chemisorption, the molecular H-H bonds are dissociated as energetically more favourable bonds to the surface atoms are established. The dissociation typically involves overcoming of an activation barrier, i. e. a certain temperature is required to enable this reaction step. The higher strength of the chemical bonds with respect to the physisorbed state generally stabilises these systems at room and elevated temperatures allowing for a broader range of technical applications. A simplified one-dimensional potential energy diagram for the two types of hydrogen adsorption is presented in figure 1.2. In a next step, the chemisorbed hydrogen atoms may jump in the subsurface layer and eventually diffuse into the bulk lattice. This is called the absorption of hydrogen by the host material and shown as well in the energy diagram in figure 1.2. For simple hydride-forming intermetallic compounds, such as $LaNi_5$, the further hydrogen enrichment proceeds in three stages involving two hydrogen-metal phases. At low hydrogen concentrations the hydrogen atoms dissolve in the metal, i. e. they form a solid-solution, the so-called α-phase. In this phase the hydrogen atoms are located randomly on the interstitial sites of the host material and cause a lattice expansion that is proportional to the hydrogen concentration by about $2\,\text{Å}^3$ to $3\,\text{Å}^3$ per hydrogen atom. The higher the gas pressure p, the higher the concentration c of dissolved hydrogen (Sieverts' law: $c \propto \sqrt{p}$). Depending on the temperature and the thermodynamic properties of the metal-hydrogen system, upon pressure increase the hydride phase starts to nucleate and grow once a very specific hydrogen concentration is reached. This new phase, the so-called

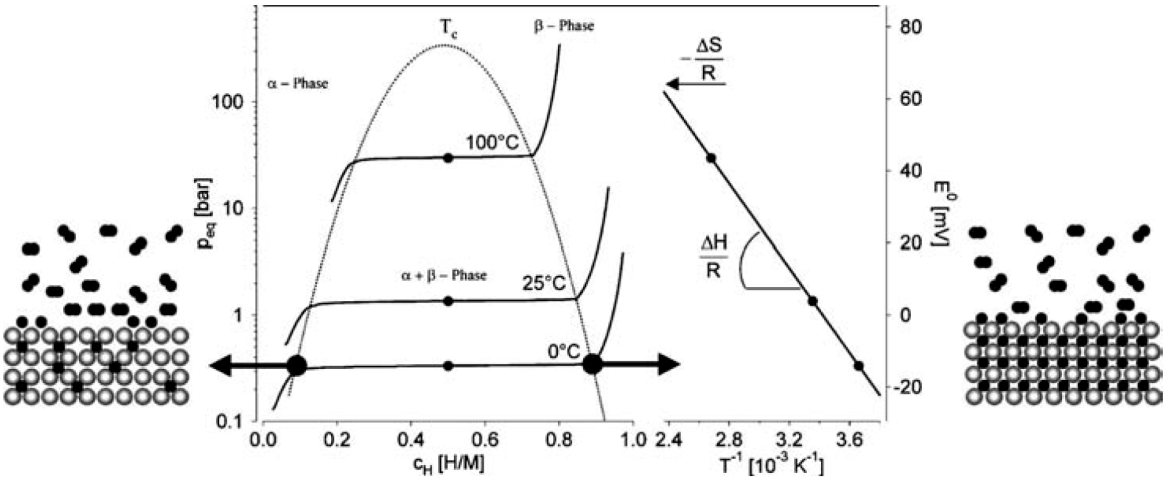

Figure 1.3: The hydrogenation of a typical intermetallic compound: pressure-composition isotherms for three different temperatures (left hand-side) and the corresponding van 't Hoff diagram (right hand-side), from [6].

β-phase, is well-ordered and has a specific hydrogen to metal atomic ratio. Initially the two phases coexist but upon further hydrogen supply the α-phase steadily converts into the β-phase until all material is hydrogenated. This absorption process can be measured and analysed by means of pressure-composition isotherms as depicted in figure 1.3 for a typical intermetallic compound. The coexistence region of the solid-solution and the hydride phase is (ideally) characterised by a flat pressure plateau. If this equilibrium pressure is determined at different temperatures, a van 't Hoff diagram can be constructed. This is shown on the right hand-side in figure 1.3. According to the van 't Hoff equation,

$$\ln\left(\frac{p_{\mathrm{eq}}}{p_{\mathrm{eq},\,0}}\right) = \frac{\Delta H_0}{R}\cdot\frac{1}{T} - \frac{\Delta S_0}{R}, \tag{1.1}$$

the plot's slope and intercept allow to determine the changes of enthalpy ΔH_0 and entropy ΔS_0 for hydrogenation. Since the total entropy change is usually dominated by the entropy of molecular hydrogen gas, for many hydrides it is similar to the standard entropy of hydrogen $S_{300\,\mathrm{K}} = 130.77\,\mathrm{J\,(K\,mol)^{-1}}$ [16]. As a consequence, the reaction enthalpy ΔH_0 can be taken as a measure for the thermal stability of the hydride. For hydrogen storage applications those systems are desired that feature low desorption temperatures which typically correspond to low values of ΔH_0. Thermodynamically rather interesting systems are the so-called room temperature hydrides, such as $LaNi_5$, TiFe or $TiMn_2$. These are interstitial hydrides that allow to store and discharge the hydrogen at temperatures well below 100 °C. This is possible because no structural change of the crystal occurs upon hydrogenation as hydrogen atoms just occupy interstitial sites and cause a lattice expansion. Due to the absence of typical thermally activated processes such as solid-state diffusion of metal atoms or heterogeneous nucleation and growth of phases other than the β-phase, activation energies are low in these systems. Early research activities to utilise interstitial hydrides as hydrogen

stores date back to the 1970s [17, 18]. However, the crucial disadvantage of these systems is the rather low gravimetric hydrogen storage capacity of typically less than 2 mass% due to the comparatively high molar mass of the host crystal (mainly composed of transition metals). In contrast, there are other hydrides based on lighter elements that feature much higher mass-related storage capacities. Since covalent or ionic bonds to the hydrogen atoms are established in these systems, the hydrogenated phase is usually rather stable and has a different crystal structure than the dehydrogenated phase. Although thermodynamic equilibrium temperatures of these metal-hydrogen systems are already comparatively high, experimentally determined sorption temperatures are often even considerably higher. This can be attributed to the high kinetic barriers associated with the restructuring of the crystal during hydrogen uptake and release that demand for a certain thermal activation. For instance, the ionic hydride MgH_2 stores up to 7.6 mass% H_2. MgH_2 is typically considered as a high-temperature hydride since it dehydrogenates only above approximately 300 °C (at $p_{H_2} \gtrsim 1$ bar). This high operation temperature is a direct consequence of the high reaction enthalpy of $-74.4\,\mathrm{kJ\,(mol\,H_2)^{-1}}$ [19]. However, for coarse MgH_2, i. e. mechanically unprocessed material (e. g. ball milling), without addition of any additives, also desorption temperatures above 350 °C are not unusual and can be attributed to kinetic constraints. This example clearly illustrates that higher gravimetric hydrogen capacities very often come at the cost of unfavourable thermodynamic and/or kinetic properties and thus significantly increased operation temperatures. Approaches to develop hydrogen storage solutions with good gravimetric capacities that operate at relatively low temperatures include the improvement of reaction kinetics and thermodynamic destabilisation. Kinetic improvements can be realised e. g. by optimising the materials' preparation conditions. This includes nano-structuring by mechanical agitation and the use of suitable additives that may have catalytic activity. In this regard some milestone discoveries should be mentioned. In 1999, Zaluska *et al.* [20] and Huot *et al.* [21] described the superior reaction kinetics of MgH_2 with nano-scaled crystallite size distributions and highly enlarged specific surface areas as a result of high energy ball milling. Oelerich *et al.* [22] reported on the accelerated hydrogen sorption kinetics of MgH_2 due to the catalytic effects of different oxide based additives in 2001. The discovery of reversibility in Ti-doped $NaAlH_4$ by Bogdanović *et al.* [23] in 1997 was certainly one of the most crucial achievements in the field of solid-state hydrogen storage. The catalyst enables the rehydrogenation of desorbed $NaAlH_4$ which is otherwise kinetically hindered. This finding motivated and initiated a series of important research activities as it demonstrated that complex hydrides, i. e. compounds with complex anions such as $[AlH_4]^-$, $[BH_4]^-$ or $[NH_2]^-$, have the potential to release their hydrogen reversibly and can thus be utilised for technical applications. Due to their rather high gravimetric hydrogen capacity, light metal borohydrides, e. g. $LiBH_4$, $NaBH_4$, $Mg(BH_4)_2$ or $Ca(BH_4)_2$, have been regarded as potential candidates for hydrogen storages applications and hence been thoroughly investigated [24–28]. At this point it is worth mentioning that these compounds are also of great interest in other areas of sustainable energy research. For instance, the discovery of the excellent ion conductivity

of many borohydrides or closo-boranes led to increased research efforts for employing such hydrides in battery applications. The usage of these materials as electrolytes for lithium, sodium and magnesium batteries is investigated intensively [29, 30]. In addition, also the potential to use complex metal borohydrides as active layers of solar cells was emphasised [31]. Regarding the utilisation of borohydrides as reversible hydrogen storage materials, a significant breakthrough was achieved by Barkhordarian *et al.* [32, 33] and Vajo *et al.* [34] in 2004. The two groups discovered independently that the combination of $LiBH_4$ with MgH_2 not only reduces the dehydrogenation temperatures of $LiBH_4$ but also, more significantly, enables the full recovery of the borohydride upon rehydrogenation under relatively mild temperature and hydrogen pressure conditions. The $LiBH_4$-MgH_2 system is a so-called Reactive Hydride Composite, i. e. the reactions between the two components improve the hydrogen sorption properties of the mixture. As the concept of Reactive Hydride Composites is one the most promising approaches to create hydrogen storage solutions with favourable thermodynamic properties, many similar systems based on different borohydride-hydride combinations were introduced since then.

1.2 The Concept of Reactive Hydride Composites

The high gravimetric hydrogen capacities of many borohydrides – for instance 18.5 mass% in $LiBH_4$ and 14.8 mass% in $Mg(BH_4)_2$ – make these compounds interesting for hydrogen storage applications. However, the reaction enthalpies of many borohydrides are fairly high and thus rather unsuitable for most applications. There are ways to address this issue, i. e. to tailor reaction enthalpies. For example the partial cation substitution by elements with higher Pauling electronegativity was shown to reduce the enthalpy change upon dehydrogenation and therefore the desorption temperature [25, 35, 36]. Another effective approach was demonstrated by Reilly and Wiswall already in 1967 [37]. They could show how a hydride MH_x can be destabilised by combination with a suitable reactant A:

$$MH_x + y\,A \longrightarrow MA_y + \tfrac{x}{2}\,H_2. \tag{1.2}$$

The authors investigated the system MgH_2-$MgCu_2$ that forms Mg_2Cu upon hydrogen release. Later, this approach to tailor reaction enthalpies was also applied to borohydrides as, for instance, mixtures of $LiBH_4$ with metals such as aluminium, magnesium or titanium were characterised [38–40]. A major disadvantage of these systems is the considerable reduction of gravimetric hydrogen capacity due to the additional weight of the metal. The use of an appropriate hydride instead of the pure metal reduces this effect because of the additional hydrogen stored in this compound which also contributes to the system's total storage capacity. Such systems are called Reactive Hydride Composites (RHCs). The basic concept of a general RHC is schematically illustrated in figure 1.4. Upon dehydrogenation the two hydrides form – similar to Reilly and Wiswall's approach – one or more common reaction

products, i. e.

$$AH_m + BH_n \longrightarrow AB + \tfrac{m+n}{2} H_2. \tag{1.3}$$

The total hydrogen capacity in such RHCs is the weighted average of the capacities of the individual hydrides. The thermodynamic destabilisation in these systems is based on the exothermic heat of formation of the new compound(s). This reaction might occur either directly between the two initial hydrides – such reactions are called mutual or concerted – or involve their respective desorption products. As exemplified in figure 1.5, this exothermic process partially compensates for the independent, endothermic dehydrogenation enthalpies of the individual hydrides. To be more precise, the overall reaction enthalpy $\Delta H_{r,total}$ is reduced by the standard enthalpy of formation $\Delta H_f^0(AB)$ of the new compound(s):

$$\Delta H_{r,total} = \Delta H_f^0(AB) - \left(\Delta H_f^0(AH_m) + \Delta H_f^0(BH_n)\right). \tag{1.4}$$

As a consequence, such thermodynamically destabilised systems offer significantly reduced dehydrogenation temperatures. Up to now, a variety of different RHCs was investigated. These systems are not necessarily based on borohydrides. In fact, one of the first reported composites that can be regarded as RHC was the $LiNH_2$-LiH system described by Chen *et al.* in 2002 [42]. Nevertheless, especially for borohydrides the RHC approach attracted a lot of attention, in particular after the encouraging experimental results about the system $LiBH_4$-MgH_2 published by Barkhordarian *et al.* [32] and Vajo *et al.* [34]. Upon

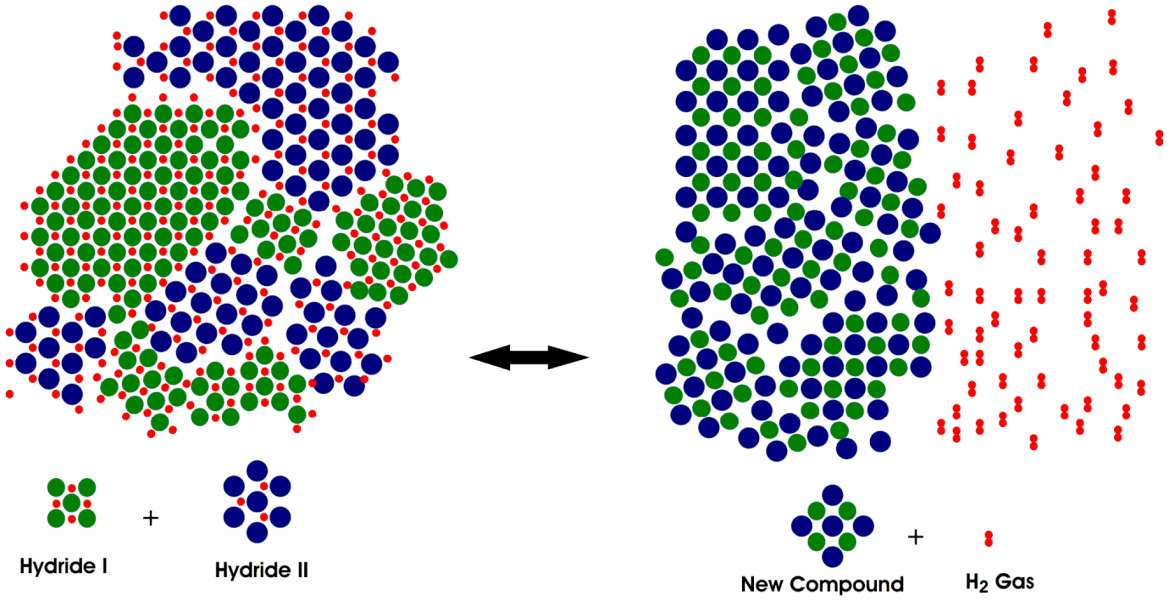

Figure 1.4: Schematic illustration of the reaction processes in a Reactive Hydride Composite (from [41]).

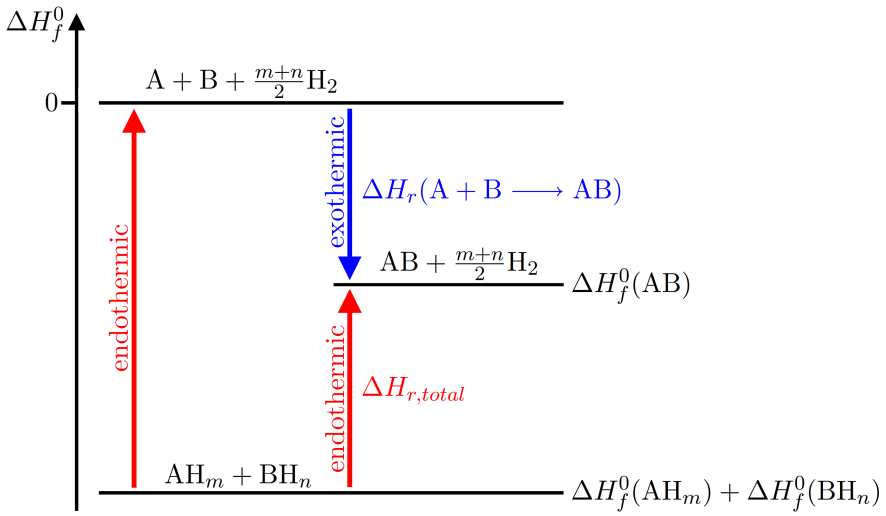

Figure 1.5: Schematic enthalpy diagram demonstrating the thermodynamic tailoring of the reaction enthalpy in a Reactive Hydride Composite. The dehydrogenated state is stabilised by the exothermic formation of at least one new compound.

dehydrogenation of $LiBH_4$-MgH_2, boron is transferred to magnesium and MgB_2 is formed:

$$2\,LiBH_4 + MgH_2 \longrightarrow 2\,LiH + MgB_2 + \underbrace{4\,H_2}_{11.4\,\text{mass\%}}. \tag{1.5}$$

This boron transfer proved to be crucial to allow for relatively mild rehydrogenation conditions and simultaneously preserve the system's storage capacity upon hydrogen cycling. After decomposition of pure $LiBH_4$ the solid residues contain LiH, elemental boron and/or $Li_2B_{12}H_{12}$. The presence of elemental boron and $M_n[B_{12}H_{12}]$ phases among the decomposition products of borohydrides is rather common. However, these compounds are typically considered as boron sinks as the recovery of the original borohydride demands extreme temperature and pressure conditions. For instance, in the case of pure $LiBH_4$ rehydrogenation was achieved at 350 bar H_2 and 600 °C [43]. As opposed to this, MgB_2 turned out to be a highly potent boron donor for the formation of borohydrides [33]. In the dehydrogenated $LiBH_4$-MgH_2 system the hydrogen uptake starts already at around 250 °C and 50 bar H_2 [34, 44]. Good reaction kinetics for isothermal hydrogenation are obtained at the same pressure and temperatures around 350 °C [45–47]. Barkhordarian *et al.* explained the superior kinetic properties of borohydride formation in systems based on MgB_2 by the particular crystal structure of this compound which is composed of alternating magnesium and boron layers [48]. Within each boron layer all atoms are bonded covalently to three other boron atoms. In contrast, in elemental boron as well as in $[B_{12}H_{12}]^{2-}$ anions each atom establishes five boron-boron bonds, though. Consequently the authors attributed the low reactivity of these compounds to high activation barriers associated with breaking the larger number of bonds per atom (i. e. higher binding energy per boron atom). This example shows that in an efficient

and reversible RHC not only the dehydrogenation temperatures are effectively lowered but at the same time the common reaction product(s) must allow for the reverse reaction and possibly even promote the recovery of the initial hydrides upon hydrogen absorption in order to facilitate high degrees of reversibility even after many sorption cycles.

1.3 Challenges for new Borohydride-based Reactive Hydride Composites

As promising as the concept of Reactive Hydride Composites for the utilisation of high-capacity borohydrides may appear, there are reoccurring problems and limitations that could not completely be addressed yet. For instance, although the titanium doped $LiBH_4$-MgH_2 system experimentally stores an amount of hydrogen equivalent to more than 9 mass% over more than twenty full sorption cycles providing a high degree of reversibility at a capacity loss of only roughly 0.04 mass% per cycle [46, 47] and therefore surely belongs to the best storage solutions introduced thus far, the dehydrogenation temperatures of this system are fairly high and could not be lowered significantly and permanently yet. In fact, the calculated equilibrium temperature at 1 bar H_2 is approximately 225 °C [34] but the experimentally determined desorption temperatures are typically well above 300 °C. In order to release hydrogen at reasonable rates, temperatures around 400 °C must often be applied. These high temperatures can be attributed to kinetic barriers related to processes such as the diffusion of boron or metallic species or the nucleation and growth of the newly formed phases. Moreover, it could be demonstrated that the dehydrogenation does not occur in a concerted reaction between $LiBH_4$ and MgH_2 [44, 49]. Instead, the first reaction step always appears to be the independent decomposition of MgH_2. Hence, the dehydrogenation proceeds *via* an – in terms of the Gibbs free energy G – activated state, i. e. $LiBH_4$-Mg. In addition, also the formation of stable side products must be considered: if the dehydrogenation pressure is lower than approximately 3 bar H_2, the partial decomposition of $LiBH_4$ into $Li_2B_{12}H_{12}$, LiH and hydrogen is observed.

Another noteworthy example for a very promising high-capacity borohydride with crucial limitations still preventing its use as reversible hydrogen store is $Ca(BH_4)_2$. At a hydrogen capacity of 11.5 mass% and a relatively low thermal stability [50–53] compared to other light metal borohydrides like e. g. $LiBH_4$ or $NaBH_4$, also $Ca(BH_4)_2$ seems to be an attractive candidate for many hydrogen storage applications. However, upon closer examination several problems become evident. As reported in the literature, pure $Ca(BH_4)_2$ dehydrogenates along

different reaction paths:

$$Ca(BH_4)_2 \longrightarrow CaH_2 + 2B + 3H_2 \quad [51, 54, 55] \quad (1.6)$$

$$Ca(BH_4)_2 \longrightarrow \tfrac{2}{3}CaH_2 + \tfrac{1}{3}CaB_6 + \tfrac{10}{3}H_2 \quad [51, 54, 56–58] \quad (1.7)$$

$$Ca(BH_4)_2 \longrightarrow \tfrac{1}{6}CaB_{12}H_{12} + \tfrac{5}{6}CaH_2 + \tfrac{13}{6}H_2 \quad [57–59] \quad (1.8)$$

$$Ca(BH_4)_2 \xrightarrow[\text{reaction}]{\text{intermediate}} CaB_2H_6 + H_2 \quad [54, 58, 59]. \quad (1.9)$$

These reaction paths depend on the dehydrogenation conditions, i. e. on external parameters such as temperature, hydrogen pressure or heating rate [54, 59, 60]. The formation of amorphous boron and $CaB_{12}H_{12}$ was identified to restrict reversibility as these compounds are rather stable [55, 59, 60]. Although the evolution of these phases can be largely suppressed by limiting the temperature from 320 °C to 350 °C (in vacuum), this approach comes at the expense of highly reduced rates of hydrogen evolution [54, 61, 62]. Also with the RHC approach the obstacles to utilise $Ca(BH_4)_2$ for hydrogen storage purposes have not been overcome successfully yet. In all characterised composites boron was either not transferred to the reaction partner (e. g. [63–66]) or the reaction proved to be irreversible (e. g. [67, 68]). For example, the well-investigated $Ca(BH_4)_2$-MgH_2 system [56, 63, 64, 69, 70] dehydrogenates very differently to the $LiBH_4$-MgH_2 Reactive Hydride Composite (chemical equation 1.5). The final reaction products do not contain MgB_2 and therefore reaction path 1.10,

$$Ca(BH_4)_2 + MgH_2 \longrightarrow CaH_2 + MgB_2 + 4H_2, \quad (1.10)$$

was experimentally disproved. Instead, despite the addition of MgH_2 boron remains exclusively with calcium based compounds as CaB_6 and $CaB_{12}H_{12}$ are formed upon dehydrogenation or it is released into the elemental state:

$$Ca(BH_4)_2 + MgH_2 \longrightarrow \tfrac{2}{3}CaH_2 + \tfrac{1}{3}CaB_6 + Mg + \tfrac{13}{3}H_2 \quad [56, 63] \quad (1.11)$$

$$Ca(BH_4)_2 + MgH_2 \longrightarrow \tfrac{5}{6}CaH_2 + \tfrac{1}{6}CaB_{12}H_{12} + Mg + \tfrac{19}{6}H_2 \quad [63] \quad (1.12)$$

$$Ca(BH_4)_2 + MgH_2 \longrightarrow CaH_2 + 2B + Mg + 4H_2 \quad [56]. \quad (1.13)$$

The formation of CaB_6 was confirmed to be the reason for the partial reversibility of approximately 55 % between subsequent sorption cycles [56, 64, 69]. The drop in reversible hydrogen capacity is caused by the formation of $CaB_{12}H_{12}$ and amorphous boron which have too high kinetic barriers to allow for the recovery of $Ca(BH_4)_2$ under moderate temperature and hydrogen pressure conditions [63]. Therefore, these two kinetically stable phases act as boron sinks upon cycling. Compared to pure $Ca(BH_4)_2$ the improved reversibility of the $Ca(BH_4)_2$-MgH_2 composite was attributed to an effect occurring during dehydrogenation: magnesium, which is formed at higher temperatures, was suggested to promote the formation

of CaB_6 by acting as an agent for the heterogeneous nucleation of this compound due to the low d-value mismatch $\{111\}_{CaB_6}/\{1011\}_{Mg}$ of only 0.6 % [64]. Consequently, $Ca(BH_4)_2$-MgH_2 cannot be considered as a true RHC because the enthalpy of the desorbed state is not lowered by the formation of mutual reaction products between the initial hydrides.

These obstacles define the demands on new borohydride-based Reactive Hydride Composites. An ideal system should address the drawbacks outlined above and simultaneously meet the high expectations of solid-state hydrogen storage materials. The challenges are summarised in the following points:

- High hydrogen capacity: In order to preserve the high storage capacities of light metal borohydrides, the destabilising hydride should have a rather high gravimetric hydrogen density, too. Therefore, the metallic host material should be light-weight and/or bind a comparatively large number of hydrogen atoms per metal atom.
- Low dehydrogenation temperature: For many purposes high dehydrogenation temperatures are a serious impediment. Especially for mobile applications a thermal coupling of the storage tank and a fuel cell is an energetically favourable approach. For that purpose the dehydrogenation temperature of the RHC must match the operation temperature of the fuel cell. This can be realised by an effective thermodynamic destabilisation of the borohydride.
- High reversibility: The sorption process must be highly reversible in order to allow for many hydrogen charge-discharge cycles without significant capacity loss. This also implies that the boron exchange must be reversible and complete, i. e. no side reactions should occur that produce stable boron sinks.
- Fast sorption kinetics: For technical applications the kinetics of hydrogen sorption must be reasonably fast within the desired temperature range. For instance, the dehydrogenation rates of the storage tank must be high enough to ensure a sufficient and stable hydrogen supply for the fuel cell.

1.4 Scope of Work

The objective of this work is the development of novel borohydride-based RHCs capable to address the challenges listed in the previous section providing at the same time key insights into the mechanism of boron transfer between the reaction partners. The focus is set on systems based on alkali and alkaline earth metal borohydrides. As outlined in the previous section, the selection of the reaction partner is the crucial step. Among the variety of potentially suitable hydrides Mg_2NiH_4 [71–77] emerged as the most promising candidate. This ternary hydride stores an amount of hydrogen equal to 3.6 mass% and is less stable than MgH_2, i. e. it decomposes at lower temperatures.

As the first reaction step in Reactive Hydride Composites is typically the desorption of the less stable hydride, the comparatively low decomposition temperature of Mg_2NiH_4 was expected to facilitate similarly low operation temperatures for borohydride-Mg_2NiH_4 mixtures. Of course, this assumption presupposed that Mg_2NiH_4 – or its dehydrogenated phase Mg_2Ni – could indeed destabilise the borohydride effectively, i. e. the composite must be reactive below the decomposition temperature of the borohydride. Ideally, in this reaction all boron should be taken up and bonded in the mutual product(s) which, at the same time, should allow for the recovery of the borohydride upon rehydrogenation. As a matter of fact, first preliminary experiments with the $LiBH_4$-Mg_2NiH_4 system showed that the ternary boride $MgNi_{2.5}B_2$ is formed upon dehydrogenation. In addition, the reaction appeared to be at least partially reversible. A literature review revealed that some research activities on the combination of light-metal borohydrides with Mg_2NiH_4 had been done before. Vajo *et al.* obtained similar results with a mixture of $LiBH_4$ and Mg_2NiH_4: the authors reported the formation of $MgNi_{2.5}B_2$ upon desorption and the partial recovery of $LiBH_4$ during rehydrogenation [78, 79]. Furthermore, Afonso *et al.* could confirm a similar reaction pathway for the composite $NaBH_4$-Mg_2NiH_4 [80].

Therefore, the first major task of this thesis is devoted to studying composites of the most interesting alkali and alkaline earth metal borohydrides $M(BH_4)_n$ ($M \in \{Li, Na, K, Mg, Ca\}$ and $n \in \{1, 2\}$) and Mg_2NiH_4. The experiments are chosen to provide first fundamental insights into these systems' individual potentials for hydrogen storage applications. In particular, the dehydrogenation reactions should be described and possible similarities as well as differences between the five hydride composite systems revealed. Also the reversibility of the sorption process is of considerable interest. In this context, the results of Vajo *et al.* and Afonso *et al.* should be revised and complemented. Afterwards, based on the initial set of results, the further experiments are planned. Given the extent of experimental work necessary to characterise each system in detail, the scope of work has to be limited to the two system with the most appealing features.

These systems are then investigated comprehensively applying several complementary methods. All research efforts aim at the clear determination of the different reaction steps and their dependency on experimental parameters. In particular the impact of the hydrogen pressure and the temperature chosen for dehydrogenation should be evaluated since variations of these parameters are known to affect the reaction path, the dehydrogenated state and thus also the reversibility of the system in general. As most borohydrides tend to form rather stable $[B_xH_y]^{n-}$ phases at elevated temperatures or even decompose into elemental boron, an important aspect of this study is to find out whether such side products are also formed in the hydride composites investigated here. In addition, the stabilities of the systems' storage capacities upon hydrogen cycling, i.e. the reversibilities of the sorption reactions, are of specific interest. Furthermore, the transfer of boron between the different compounds and the transport within these phases should be investigated. For that purpose both crystalline and non-crystalline compounds are considered. Intermediate phases are taken into account

as well in order to develop a comprehensive understanding of the transport of boron atoms during the sorption processes. For this thorough approach the structural diversity of the different boron containing compounds should be analysed and considered also. Eventually, the processes and discovered effects should be correlated to the experimental conditions to deduct general mechanisms and strategies for systematic further improvements of promising new RHC materials.

2 Experimental Part

This chapter describes the fundamental experimental details for the results presented in chapter 3. In the first section specific material properties as well as synthesis and preparation methods are depicted. The second section deals with the employed sample characterisation techniques and the experimental conditions for the different analyses. It should be noted that all described experiments and presented measurements were carried out by myself unless another collaborating researcher is explicitly mentioned in section 2.2. This includes the preparation of all samples and the described syntheses of new compounds. Also, I personally processed the raw data, evaluated the results and interpreted my findings (see chapter 3).

2.1 Materials, Sample Preparation and Synthesis Methods

Most chemical compounds used in this work are commercially available and were purchased from different suppliers. In order to reduce the impact of impurities on the prepared samples, i. e. on their hydrogen storage properties, only highly pure materials were used. A categorised list of the different compounds stating the respective purity and the supplier is provided in table 2.1. Mg_2NiH_4, $MgNi_{2.5}B_2$ and $Ca_4Mg_3H_{14}$ are not commercially available and were synthesised in-house following the procedures described separately at the end of this section.

As many materials utilised in the experiments described below are sensitive to oxygen and/or humidity, they had to be handled carefully to prevent contaminations. Therefore, all investigated samples were prepared in argon-filled gloveboxes with oxygen and water levels lower than 1 ppm. In addition, the materials were stored in gas-tight sample vials that were also used to safely carry the samples outside the gloveboxes.

In order to ensure homogeneity of the multi-component materials and improve the reactivity of these mixtures, all powders underwent a mechanical treatment by means of high energy ball milling. Also the pure compounds were processed in a similar way as the mixed materials prior to all experiments to enable the development of comparable microstructural and thus kinetic properties for all samples. Two different types of milling devices were employed. In particular, a SPEX SamplePrep 8000 Mill with hardened steel milling vials was used for the preparation of all standard samples. For that purpose the powders were milled for 300 min using hardened steel balls with a diameter of 1 cm and employing a ball-to-powder ratio of 10 : 1. An overview of all multi-component materials used for the experiments described hereafter is given in table 2.2. For each composite the molar ratio of the individual compounds are listed as well as the section in which the corresponding

Table 2.1: Categorised overview of all commercially available materials used in the present work indicating the respective purities and the suppliers.

category	material	purity [%]	supplier
borohydrides	$LiBH_4$	95	Alfa Aesar
	$NaBH_4$	98	abcr GmbH
	KBH_4	98	Alfa Aesar
	$Mg(BH_4)_2$	95	Sigma-Aldrich
	$Ca(BH_4)_2$	95	KatChem
binary hydrides	LiH	97	Alfa Aesar
	KH	98	Sigma-Aldrich
	MgH_2	95	
	CaH_2	95	
closo-dodecaborates	$Li_2B_{12}H_{12}$	95	KatChem
	$CaB_{12}H_{12}$	95	
borides	MgB_2	95	Alfa Aesar
	CaB_6	99.5	
others	$TiCl_3$	99.9	Sigma-Aldrich
	B	99	
	Ni	99.8	Alfa Aesar

experiments are described. The second milling device, a Fritsch Planetary P6, was used to prepare larger amounts of material for the syntheses of Mg_2NiH_4 and $MgNi_{2.5}B_2$. Here, the mechanochemical processing was performed either in Al_2O_3 or WC milling vials with appropriate 1 cm balls.

A particular specimen of CaH_2-$MgNi_{2.5}B_2$-MgH_2 was prepared in a different manner. The aim was to improve the reactivity of this material by a sequence of intense ball milling cycles. The reduction of diffusion path lengths due to the decrease of the material's mean particle size, the enlargement of interface areas between the different phases as well as the increased number of crystallographic defects induced by the strong mechanical stress were supposed to enhance reaction kinetics [81, 82]. For that purpose, the three components CaH_2, $MgNi_{2.5}B_2$ and MgH_2 were pre-milled individually for 48 h in the planetary mill at a rotation speed of 350 rpm. These initial milling treatments were conducted with WC vials and balls. A ball-to-powder ratio of 40 : 1 was applied. Afterwards a stoichiometric mixture of the pre-milled compounds was filled into a stainless steel high pressure vial. Heptane (99 % from Sigma-Aldrich) was added in a fluid-to-powder mass ratio of 4 : 1 to avoid particle agglomeration upon milling [83, 84]. The obtained suspension was milled for 72 h at 400 rpm with a ball-to-powder ratio of 20 : 1. Subsequently the powder was separated from the liquid

Table 2.2: Overview of all composite materials investigated in the experiments described in this thesis. The molar ratios of the different samples are listed as well as the sections in which the corresponding experiments are presented.

composite material	molar ratio	section
$LiBH_4$-Mg_2NiH_4	2 : 2.5	3.1.1, 3.2.1
$4LiBH_4$-Mg_2NiH_4	4 : 1	3.2.2
$4LiBH_4$-Mg_2NiH_4-$TiCl_3$	4 : 1 : 0.05	3.2.2
$LiBH_4$-MgH_2-$TiCl_3$	2 : 1 : 0.025	3.2.2
$NaBH_4$-Mg_2NiH_4	2 : 2.5	3.1.2
KBH_4-Mg_2NiH_4	2 : 2.5	3.1.3
$Mg(BH_4)_2$-Mg_2NiH_4	1 : 2.5	3.1.4
$Ca(BH_4)_2$-Mg_2NiH_4	1 : 2.5	3.1.5, 3.3
KH-$MgNi_{2.5}B_2$-MgH_2	2 : 1 : 4	3.1.3
CaH_2-$MgNi_{2.5}B_2$-MgH_2	1 : 1 : 4	3.3
CaH_2-$MgNi_{2.5}B_2$	2 : 1	3.3
$Ca_4Mg_3H_{14}$-$MgNi_{2.5}B_2$-MgH_2	1 : 4 : 13	3.3
$Ca_4Mg_3H_{14}$-$MgNi_{2.5}B_2$	1 : 1	3.3
$MgNi_{2.5}B_2$-MgH_2	1 : 5	3.1.4, 3.3
Mg_2NiH_4-$Li_2B_{12}H_{12}$-LiH	15 : 1 : 10	3.2.1
Mg_2NiH_4-$CaB_{12}H_{12}$	15 : 1	3.3
Mg_2NiH_4-CaB_6	7.5 : 1	3.3
Mg_2NiH_4-B	1.25 : 1	3.3

in a Büchner funnel with applied vacuum. Afterwards, in order to remove all residues of the solvent, the material was dried under continuous vacuum at 70 °C for 18 h.

Autoclaves from Parr Instrument with an inner volume of 25 ml were employed for all high-pressure hydrogenation procedures. They allow the application of a maximum pressure of 450 bar at 400 °C. A manometer makes it possible to monitor the internal pressure. For heat treatment, the autoclaves were placed into an external furnace from Nabertherm. Due to the rather high equilibrium pressures of many material systems investigated in this work, most hydrogen absorption attempts could not be done in the instruments typically employed for this purpose, e. g. the volumetric apparatuses, because of these devices' limited operation pressures. Instead, the hydrogenations had to be carried out in the high-pressure autoclaves. In addition, these reactors were also used for the syntheses of Mg_2NiH_4 and $Ca_4Mg_3H_{14}$ as the materials were eventually heated under high hydrogen pressures. The experimental approach consisted of three steps: first the material was filled into the autoclave, then the vessel was charged with hydrogen at room temperature and subsequently heated to

the desired temperature setpoint. In order to perform hydrogen absorption experiments with several samples under the same conditions, steel inserts were used to fill the reactor simultaneously with different specimens without the risk of cross contamination. Typically rather high pressures were applied for hydrogenations with the intention of exceeding the sorption equilibrium pressures of the respective material system, increasing the absorption kinetics and maximising the conversion yield.

Hydrogen cycling experiments were conducted in another device. A 250 ml autoclave manufactured by Estanit was employed. This vessel allows the application of a maximum pressure of 385 bar at temperatures up to 500 °C. It is possible to charge and discharge hydrogen during a running synthesis. Moreover, since the temperature is accurately regulated by a PID controller and both the temperature as well as the pressure are recorded, this device is predestined for high-pressure cycling experiments.

2.1.1 Synthesis of Mg_2NiH_4

Since Mg_2NiH_4 could not be obtained commercially it had to be synthesised in-house. The material was prepared from the starting reactants MgH_2 and nickel according to chemical equation 2.1:

$$2\,MgH_2 + Ni \longrightarrow Mg_2NiH_4. \tag{2.1}$$

The two compounds were mixed in a molar ratio of 2 : 1 and milled for 4 h in the planetary mill using Al_2O_3 vials and balls. A ball-to-powder ratio of 5 : 1 was applied and the rotation speed was set to 300 rpm. Subsequently, the mixture was annealed at 400 °C under a hydrogen pressure of 225 bar. As the powdery material already contained all hydrogen required for the formation of Mg_2NiH_4, the rather high pressure value was chosen solely to prevent any dehydrogenation reactions upon heat treatment. The diffraction patterns of the as-milled and the annealed material are presented in figure 2.1. Mg_2NiH_4 exists in two polymorphic structures. At temperatures below approximately 250 °C the monoclinic modification (space group $C12/c1$, No. 15) [75] is the thermodynamically stable form. Above that temperature only the cubic polymorph (space group $Fm\bar{3}m$, No. 225) [73] can be found. As can be seen in figure 2.1, Mg_2NiH_4, i. e. a mixture of both polymorphs, was partially formed already upon ball milling. After the heat treatment only minor amounts of the initial reactants are recognised indicating a purity of approximately 90 %. The final material is a composition of the low- and high-temperature polymorph of Mg_2NiH_4.

2.1.2 Synthesis of $MgNi_{2.5}B_2$

Similar to Mg_2NiH_4 also $MgNi_{2.5}B_2$ [85–87] could not be purchased and thus had to be prepared in-house. This compound was synthesised from a mixture of MgB_2 and nickel,

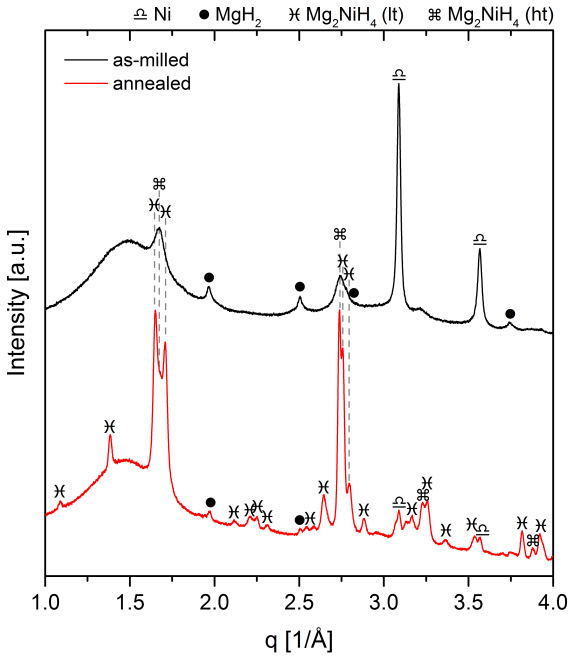

Figure 2.1: X-ray diffractograms of as-milled and annealed "$2\,MgH_2 + Ni$".

i. e. in a process according to reaction 2.2,

$$MgB_2 + 2.5\,Ni \longrightarrow MgNi_{2.5}B_2. \tag{2.2}$$

The two reactants were combined in a molar ratio of 1 : 2.5 and subsequently milled for 4 h in the planetary mill employing Al_2O_3 vials and balls. For this purpose a ball-to-powder ratio of 5 : 1 and a rotation speed of 300 rpm were applied. Afterwards, the powder was annealed in argon atmosphere at 930 °C for 24 h. Diffractograms of as-milled and annealed material are shown in figure 2.2a. The as-milled powder only features the reflections of Ni and MgB_2, however, after the heat treatment no signals of these two compounds are discernible anymore. Instead, only intense reflections of $MgNi_{2.5}B_2$ are identified. The ^{11}B MAS NMR spectra of pure[1] MgB_2 and annealed "MgB_2 + 2.5 Ni" are presented in figure 2.2b. It can be seen clearly that the resonance of MgB_2 vanished completely in the latter sample. Only minor quantities of boron containing impurities with resonances between 10 ppm and 20 ppm can be distinguished. Overall, the purity of as-synthesised $MgNi_{2.5}B_2$ is higher than 95 %.

2.1.3 Synthesis of $Ca_4Mg_3H_{14}$

$Ca_4Mg_3H_{14}$ [88–90] is the third chemical compound that had to be synthesised in-house. This was achieved by mixing CaH_2 and MgH_2 in a molar ratio of 4 : 3. The intended chemical

[1] The as-milled mixture of "MgB_2 + 2.5 Ni" could not be investigated by means of MAS NMR technique due to the ferromagnetic nature of nickel.

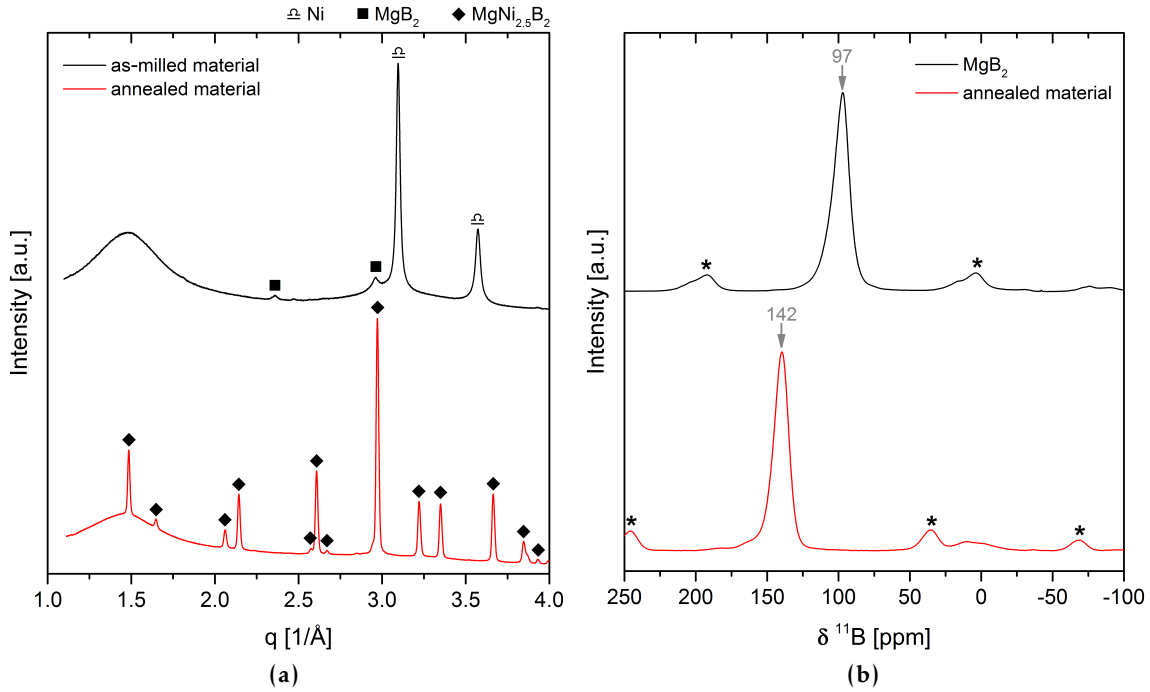

Figure 2.2: The chemical composition of "MgB_2 + 2.5 Ni" before and after heat treatment: (a) PXD analyses of as-milled and annealed material and (b) ^{11}B MAS NMR spectra of pure MgB_2 and the annealed mixture (spinning sidebands are marked with asterisks ⋆).

reaction 2.3 is:

$$4\,CaH_2 + 3\,MgH_2 \longrightarrow Ca_4Mg_3H_{14}. \tag{2.3}$$

The mixture was milled in the SPEX mill for 100 min with a ball-to-powder ratio of 10 : 1. Subsequently, the material was filled into an autoclave and heated to 400 °C under a hydrogen atmosphere with a final pressure of 200 bar. As no additional hydrogen is necessary to form $Ca_4Mg_3H_{14}$ from the 4 : 3 mixture of CaH_2 and MgH_2, the rather high but arbitrary hydrogen pressure was applied exclusively to prevent potential dehydrogenation reactions. The X-ray diffraction patterns of as-milled and annealed material are shown in figure 2.3. It can be seen that minor amounts of $Ca_4Mg_3H_{14}$ were already formed upon ball milling. After annealing only weak reflections of CaH_2 remained visible besides the intense diffraction pattern of $Ca_4Mg_3H_{14}$. A purity of more than 90 % was reached.

2.2 Characterisation Techniques

2.2.1 Volumetric Analyses

The temperature dependent release of hydrogen from the investigated materials was evaluated by non-isothermal volumetric measurements performed using a Sievert's type apparatus designed by Hydro-Québec/HERA Hydrogen Storage Systems Inc. or a similar in-house

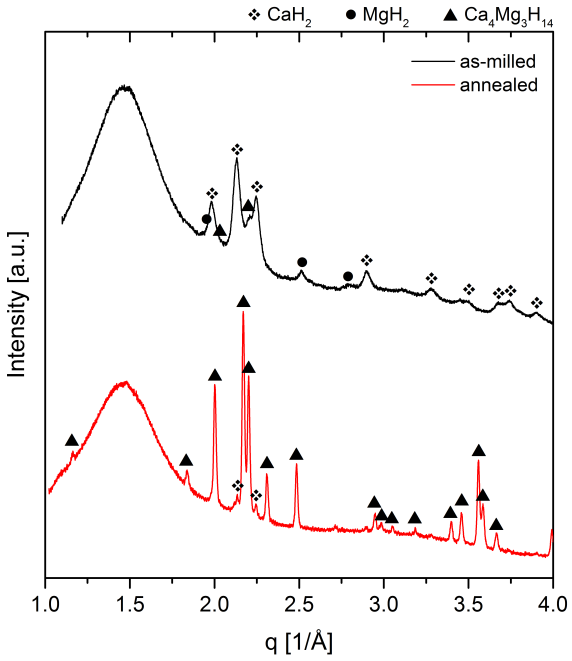

Figure 2.3: X-ray diffractograms of as-milled and annealed "$4\,CaH_2 + 3\,MgH_2$".

custom build device. Both machines operate in the differential principal, i. e. the sample volume and an equal but separate reference volume are connected by a differential pressure gauge. Therefore, all temperature induced pressure changes are compensated and only differences due to sorption processes are recorded. By considering the exact sample mass – typically around 180 mg – the pressure changes are converted into changes of the gravimetric hydrogen content of the investigated samples, i. e. the results are given in the unit "mass% H_2". All measurements were conducted in hydrogen atmosphere with pressures of at least 1 bar. The applied pressure value depends on the respective experiment. The samples were heated from room temperature with rates of $3\,K\,min^{-1}$ or $5\,K\,min^{-1}$.

The combined calorimetric and volumetric measurements presented in section 3.3.1 were conducted by Prof. Chiara Milanese at the Pavia Hydrogen Lab of the University of Pavia (Pavia, Italy). For the volumetric analyses a PCTPro-2000 from Setaram & Hy-Energy was employed. Roughly 50 mg of material were used per measurement. The samples were heated at a rate of $5\,K\,min^{-1}$ from room to the maximum temperature in the particular experiment. All measurements were carried out in hydrogen atmosphere with pressures of 1 bar, 7.5 bar, 20 bar and 50 bar, respectively.

2.2.2 X-ray Diffraction Analyses

X-ray diffraction belongs to the most powerful techniques to obtain fundamental insights into crystalline materials. The experiments are used for many purposes, e. g. to determine the chemical composition of multi-component samples, characterise the crystal structures or microstructural properties of the investigated phases or identify impurities. Instead

of the Bragg angle 2θ the scattering vector $q = (4\pi/\lambda)\sin(2\theta/2)$ is given in all the results to promote easy comparability of the different data collected with the lab diffractometer or at the synchrotron facilities.

2.2.2.1 *Ex Situ* Powder X-ray Diffraction (PXD) Measurements

Ex situ PXD measurements were used to determine the chemical compositions of the crystalline phases in various samples. The data was collected with a Bruker D8 Discover diffractometer operating in Bragg-Brentano geometry. The instrument is equipped with a copper K_α source ($\lambda = 1.541\,84\,\text{Å}$) and a VÅNTEC-500 area detector from Bruker. The diffractograms were acquired in seven steps in the 2θ range from 10° to 90° (detector centre position) with an acquisition time of 450 s per step. In order to prevent samples from oxidation or hydrolysis, a sample holder featuring an argon-filled PMMA dome was employed during the measurements. X-rays scattered by this dome are the cause of the broad background distributed around $q \approx 1.5\,\text{Å}^{-1}$ that is present in each diffractogram.

2.2.2.2 *In Situ* Synchrotron Radiation Powder X-ray Diffraction (SR-PXD) Experiments

In situ SR-PXD experiments are a powerful technique to determine the temperature and time dependent evolution of crystalline phases and the sequences of chemical reactions. The measurements were conducted at the synchrotron facilities PETRA III (beamline P02.1) at DESY (Hamburg, Germany) and MAX II (beamline I711) at MAX-lab (Lund, Sweden). The X-ray wavelengths at PETRA III and MAX II were $\lambda \approx 0.21\,\text{Å}$ and $\lambda \approx 0.99\,\text{Å}$, respectively. At PETRA III the diffraction patterns were collected using a Perkin Elmer XRD 1621 detector with a 2048 x 2048 pixel array and a pixel size of $(200 \times 200)\,\mu\text{m}^2$. An Agilent Titan CCD detector featuring a 2048 x 2048 pixel array with a pixel size of $(60 \times 60)\,\mu\text{m}^2$ was employed at MAX II. For the acquisition of each two-dimensional diffraction pattern exposure times of 15 s and 20 s were used at PETRA III and MAX II, respectively, for all experiments.

The experiments were performed in Debye-Scherrer geometry with a special *in situ* diffraction setup that allows for sample temperature and gas pressure recording [91, 92]. A schematic drawing of this setup is shown in figure 2.4. The specimens were filled into a sapphire capillary (outer diameter 1 mm, inner diameter 0.6 mm) which was positioned directly in the X-ray beam. This capillary was mounted into the sample holder body with gas tight connections. A thermocouple was inserted into the capillary with its tip almost in contact with the sample allowing for accurate temperature measurements. A pressure transducer connected to the sample holder was employed to ensure proper evacuation prior to as well as steady pressure in the course of each *in situ* experiment. All measurements were conducted in hydrogen atmosphere with a pressure of at least 1 bar. An electrical heating block positioned below the sapphire capillary and operated by a PID controller increased the sample temperature with the desired heating rate to the respective maximum. In order to determine the X-ray wavelength and the instrumental broadening precisely, LaB_6 powder

was used. The obtained two-dimensional images were carefully masked to exclude single crystal diffraction spots, e. g. from the sapphire capillary, and then radially integrated to one-dimensional diffractograms by means of the program FIT2D [94, 95]. Subsequently, all diffractograms collected in the experiment were combined to a two-dimensional (temperature *vs.* q-vector) colour-coded intensity map using the software Origin [96].

2.2.2.3 Rietveld Refinements

A Rietveld refinement is a computational approach to analyse a measured diffraction pattern quantitatively. For that purpose, a mathematical model is used to describe the diffractogram as a function of the scattering angle. The theoretical line profile is based on many parameters that are directly related to the sample's chemical composition, microstructure and crystallographic properties. The Rietveld method uses a least squares approach to refine the profile function and minimise the difference to the experimental data [97–99].

The program MAUD [100, 101] was used to perform Rietveld refinements of *ex situ* and selected *in situ* diffractograms. Structural data of the different chemical compounds were included either with Crystallographic Information Files (CIF) taken from the ICSD catalogue [102] or by transferring the crystallographic properties directly from the original publications.

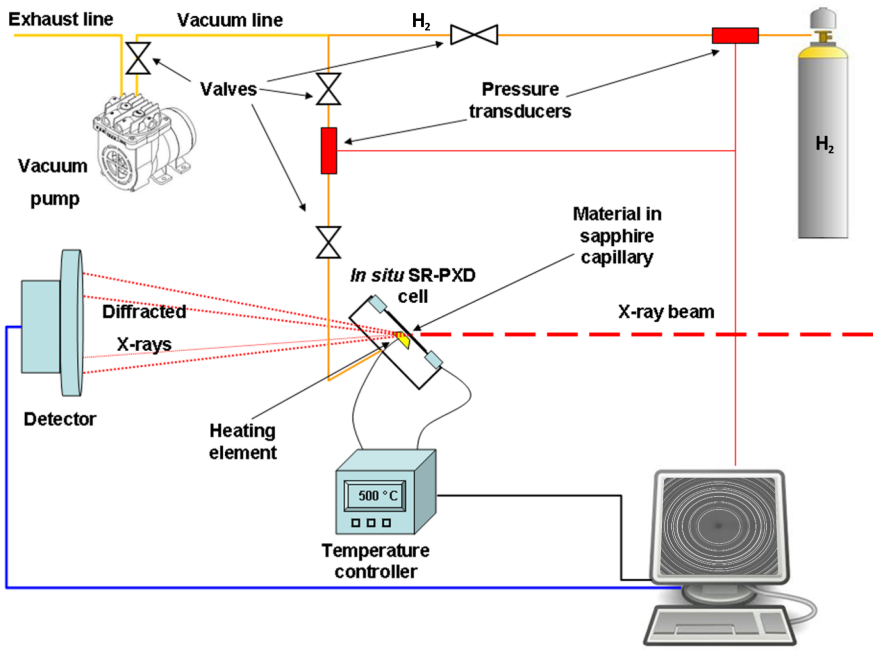

Figure 2.4: Schematic drawing of the experimental setup for the *in situ* SR-PXD measurements (adapted from [93]).

2.2.3 Differential Scanning Calorimetry (DSC) Analyses

DSC analyses were used to determine the sequence of thermal events upon dehydrogenation and precise onset temperatures for each transition. The calorimetric measurements were carried out in a Netzsch DSC 204 HP heating the samples (about 10 mg each) from room to the respective maximum temperature of the experiment at a rate of 5 K min^{-1}. All measurements were conducted in hydrogen atmosphere with constant pressures of 1 bar, 20 bar or 50 bar.

The DSC analyses shown in section 3.2.2 were carried out by Prof. Chiara Milanese from the Pavia Hydrogen Lab of the University of Pavia (Pavia, Italy). In addition, she performed combined calorimetric and volumetric measurements which are presented in section 3.3.1. Her calorimetric analyses were carried out in a Sensys DSC from Setaram. Roughly 50 mg of material were used per measurement. The samples were heated at a rate of 5 K min^{-1} from room to the maximum temperature in the particular experiment. All measurements were carried out in hydrogen atmosphere with pressures of 1 bar, 7.5 bar, 20 bar and 50 bar, respectively.

2.2.4 Solid-State Magic Angle Spinning (MAS) Nuclear Magnetic Resonance (NMR) Spectroscopy

The chemical compositions of samples containing nano-crystalline or amorphous phases were determined by solid-state MAS NMR measurements. Spectra of the ^{11}B nucleus were recorded to characterise the distribution of boron within these samples. The measurements were carried out at the NMR Laboratory of the Autonomous University of Barcelona (Bellaterra, Spain) employing a Bruker Avance 400 MHz (128.33 MHz for the ^{11}B nucleus) spectrometer equipped with a wide-bore 9.4 T magnet and a boron-free Bruker CP-MAS probe. The one-dimensional ^{11}B{^{1}H} MAS NMR spectra were acquired after a 2.7 µs single $\pi/2$ pulse (corresponding to a radio field strength of 92.6 kHz) and with application of a strong ^{1}H signal decoupling by using the two-pulse phase modulation (TPPM) scheme. In order to assess quantitatively molar ratios of samples comprising more than one boron containing compound, the areas of resonances and their corresponding spinning sidebands in the range from 1500 ppm to −1500 ppm were considered.

The NMR analyses shown in sections 3.1 and 3.2 were performed by Dr. Thomas Emmler at Helmholtz-Zentrum Geesthacht (Geesthacht, Germany). He employed a Bruker Avance III HD 500 MHz spectrometer with a Bruker 4 mm standard bore H/X CP-MAS probe. The spectra were collected at 160.42 MHz for the ^{11}B nucleus. Excitation was realised by the ZGBS pulse sequence and signals were recorded after a recovery delay (D1) of 10 s.

The spectra presented in figure 3.40 were measured by Prof. Michele R. Chierotti at the University of Torino (Torino, Italy) with a Bruker Avance II plus 400 MHz instrument using single-pulse excitation (SPE) or DEPTH (for suppressing the probe background signal) sequences ($\pi/2$ pulse = 3.75 µs, recycle delays = 0.2 s, 128 transients).

For all ^{11}B NMR analyses presented in this work the chemical shifts were externally

referenced to $BF_3 \cdot Et_2O$ and reported in parts per million (ppm). For all measurements the samples were filled into 4 mm ZrO_2 rotors that were closed with Kel-F caps. The packing was done inside argon-filled gloveboxes. The rotors were spun at 9 kHz to 14 kHz by applying dry nitrogen gas. For all analyses of samples belonging to the same experiment the same MAS frequency was employed. During the measurements the sample temperature was kept at 20 °C by Bruker BCU units. For the sake of comparability all spectra presented in this work were normalised over their respective spectral intensities.

3 Results and Discussion

In this chapter – which is divided into three main sections – the most important experimental results are presented and subsequently discussed. In the first section, sets of basic experiments are introduced for the five $M(BH_4)_n$-Mg_2NiH_4 hydride composites investigated in this work. These results provide fundamental insights into the systems' general characteristics and individual potentials as hydrogen storage media. At the end of this section, the five hydride composites are compared and assessed. Based on their promising results with respect to hydrogen storage applications and particular, scientifically interesting features, two systems – $LiBH_4$-Mg_2NiH_4 and $Ca(BH_4)_2$-Mg_2NiH_4 – are chosen for more detailed investigations. In the second section, the $LiBH_4$-Mg_2NiH_4 system is characterised thoroughly. More specifically, this section deals with the detailed study of the dehydrogenation reactions and the reversibility of the sorption processes for two different stoichiometric compositions of $LiBH_4$ and Mg_2NiH_4. These two composites, the 2 : 2.5 and the 4 : 1 system, are described in separate subsections. In the last section, comprehensive experiments on the $Ca(BH_4)_2$-Mg_2NiH_4 system are given which complement the results shown in the first section. In particular, the complex processes upon hydrogen release are elucidated as the influences of external experimental parameters and the role of different side reaction products are investigated. In addition, the rehydrogenation reactions are analysed fundamentally.

3.1 Screening of $M(BH_4)_n$-Mg_2NiH_4 Hydride Composites: Phase Formation and Reversibility

In this section five hydride composites are investigated in terms of their potentials for hydrogen storage applications. Each of these composites is composed of one light metal borohydride $M(BH_4)_n$ ($M \in \{Li, Na, K, Mg, Ca\}$ and $n \in \{1, 2\}$) and Mg_2NiH_4. The two hydrides are mixed in molar ratios that allow for the bonding of all boron in the ternary boride $MgNi_{2.5}B_2$ upon dehydrogenation, i. e. it is aimed for a reaction according to the general scheme:

$$2/n\,M(BH_4)_n + 2.5\,Mg_2NiH_4 \longrightarrow 2/n\,MH_n + MgNi_{2.5}B_2 + 4\,Mg + 8\,H_2. \tag{3.1}$$

The different systems are presented in individual subsections. In a last subsection the crucial results of these different composites are summarised and compared and, based on this assessment, the two most interesting composites selected.

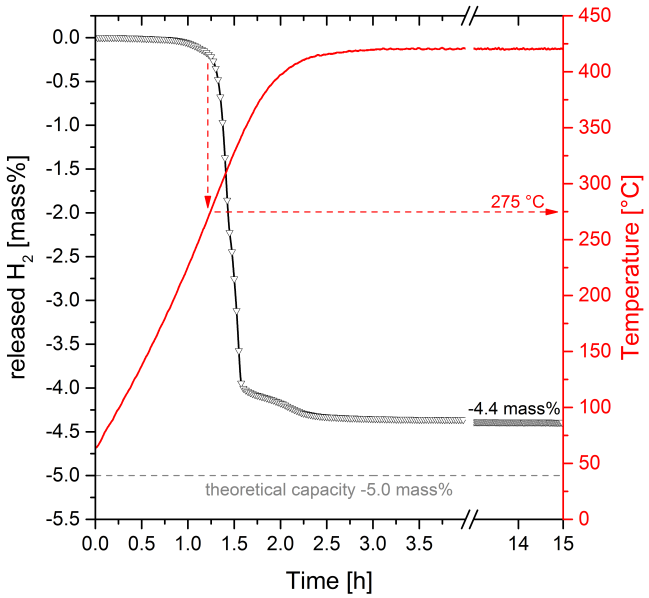

Figure 3.1: Volumetric analysis of the $LiBH_4$-Mg_2NiH_4 composite: at a pressure of 1 bar H_2 the powder was heated from room temperature to 420 °C at 3 K min^{-1}.

3.1.1 $LiBH_4$-Mg_2NiH_4

3.1.1.1 Experimental Results

The temperature dependent evolution of hydrogen from the composite $LiBH_4$-Mg_2NiH_4 (molar ratio 2 : 2.5) was monitored by means of a volumetric technique (figure 3.1). The material was heated from room temperature to 420 °C at a rate of 3 K min^{-1} in a hydrogen atmosphere of 1 bar. The onset temperature for dehydrogenation is approximately 275 °C. The hydrogen is mainly released in one step, although a minor second step can be observed. Altogether, an amount of hydrogen equal to 4.4 mass% is desorbed. The fully dehydrogenated material was rehydrogenated in an autoclave at 360 °C and at a pressure of 200 bar for 20 h. X-ray diffractograms of the as-milled, dehydrogenated and rehydrogenated material are presented in figure 3.2. After milling the powder features reflections of the low-temperature (lt) polymorph of $LiBH_4$ (space group *Pnma*, No. 62) [103] besides those of the two Mg_2NiH_4 modifications, i. e. the low-temperature monoclinic and the high-temperature (ht) cubic. The diffraction pattern of the fully dehydrogenated sample contains reflections of $MgNi_{2.5}B_2$, MgH_2 and Mg. In the rehydrogenated material, reflections of recovered $LiBH_4$ (lt) and Mg_2NiH_4 (both lt and ht) are discernible. However, the strong diffraction intensity of residual $MgNi_{2.5}B_2$ points towards a rather high concentration of unreacted desorbed-state material. In order to assess the sequence of dehydrogenation events in detail, this process was monitored in an *in situ* SR-PXD experiment. For that purpose, as-milled $LiBH_4$-Mg_2NiH_4 was heated from room temperature to 440 °C at a rate of 10 K min^{-1} in 1 bar of hydrogen. As can be seen in figure 3.3, the very first modification of the diffraction patterns occurs at about 111 °C and is associated to the polymorphic transition from lt to ht $LiBH_4$ (space group

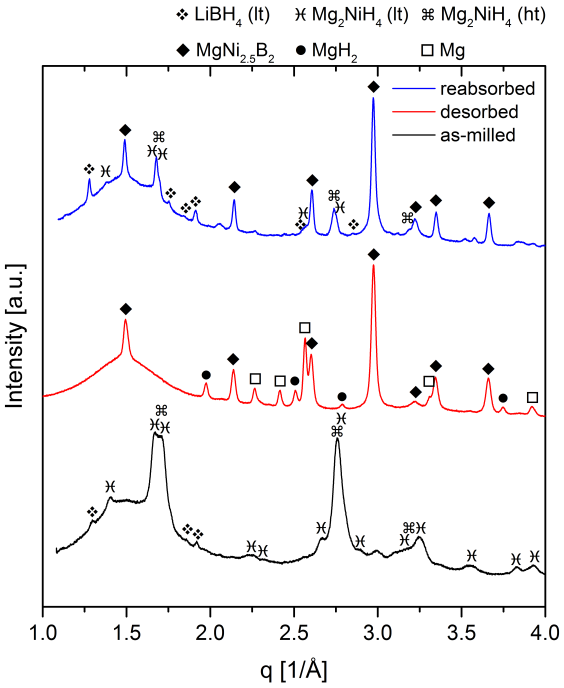

Figure 3.2: X-ray diffractograms of as-milled (black), desorbed (red) and reabsorbed (blue) $LiBH_4$-Mg_2NiH_4 composite.

$P6_3mc$, No. 186) [104]. At roughly 240 °C the transition from Mg_2NiH_4 (lt) to the high-temperature polymorph can be observed. The first chemical reaction occurs at approximately 284 °C as the formation of Mg_2Ni is detected. Shortly after, the reflections of $MgNi_{2.5}B_2$ and MgH_2 can be detected as well. The latter are only present for a very short time and disappear at a temperature of approximately 310 °C. Simultaneously, the diffraction pattern of Mg becomes visible. At about 337 °C the reflections of a yet unknown phase arise and intensify. Hereafter, this unknown phase is uniformly denoted as UP. At nearly the same temperature the diffraction intensity of Mg_2Ni starts to decrease. At slightly higher temperatures also the reflections of UP weaken and above approximately 400 °C these two compounds cannot be identified any more. At termination of the experiment, i. e. after a short dwell time of 5 min at 440 °C, only reflections of $MgNi_{2.5}B_2$ and Mg remain visible.

3.1.1.2 Discussion

The dehydrogenation of the composite $LiBH_4$-Mg_2NiH_4 proceeds according to the overall reaction scheme 3.1, i. e.

$$2\,LiBH_4 + 2.5\,Mg_2NiH_4 \longrightarrow 2\,LiH + MgNi_{2.5}B_2 + 4\,Mg + \underbrace{8\,H_2}_{5.0\,\text{mass\%}}. \tag{3.2}$$

However, the *in situ* diffraction experiment revealed that under the applied conditions the dehydrogenation involves a sequence of intermediate reaction steps. At 1 bar H_2 no direct

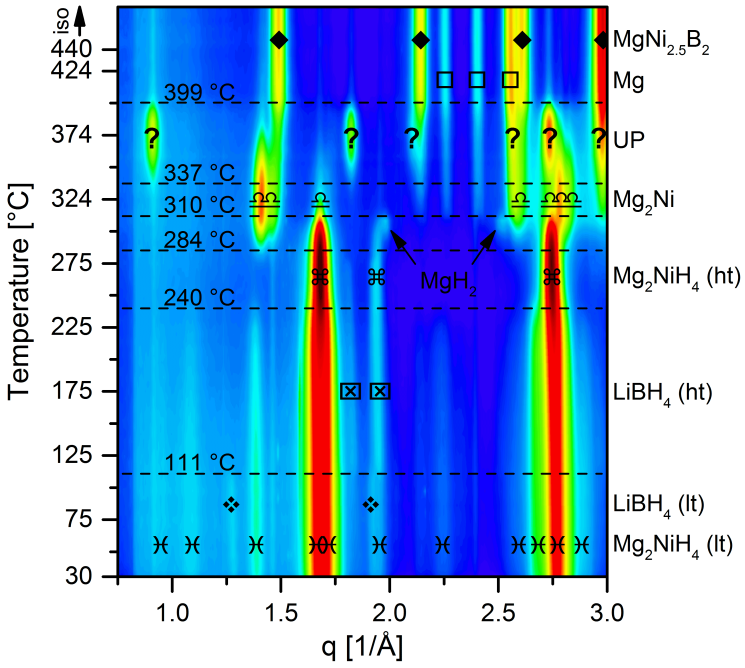

Figure 3.3: *In situ* SR-PXD analysis of the $LiBH_4$-Mg_2NiH_4 composite: the sample was heated from room temperature to 440 °C at 10 K min^{-1} in 1 bar of hydrogen.

formation of the end products is observed. Instead, the first reaction step is the independent desorption of Mg_2NiH_4. In this process only Mg_2Ni and hydrogen are formed but no reaction products with $LiBH_4$. The onset of this dehydrogenation coincides conspicuously with the melting of $LiBH_4$, though. In addition – considering the applied hydrogen pressure – the experimentally determined desorption temperature of Mg_2NiH_4 is comparatively low in this composite. Therefore, it appears possible that liquid $LiBH_4$ might have a destabilising effect on Mg_2NiH_4 or reduce kinetic barriers for dehydrogenation. This influence was also described by Vajo *et al.* who investigated the $LiBH_4$-Mg_2NiH_4 composite and reported that the measured hydrogen release temperature of the system was even lower than those of the individual compounds [78]. The authors proposed a concerted reaction between $LiBH_4$ and Mg_2NiH_4, i. e. the direct formation of $MgNi_{2.5}B_2$, MgH_2 and LiH from the two constituting hydrides. However, this mechanism of mutual destabilisation could not be confirmed under the given experimental conditions as the presence of Mg_2Ni reflections prior to those of any other reaction product rather suggests that all other compounds are formed in two subsequent reactions between Mg_2Ni and $LiBH_4$. The first is leading to $MgNi_{2.5}B_2$, MgH_2/Mg (depending on the temperature and hydrogen pressure) and LiH, the second is producing UP and its associated reaction products. Since the exact composition of this new compound is still unknown, it is currently not possible to depict the respective reaction path. In this system UP must be considered as an intermediate phase because it reacts completely upon dehydrogenation. The sequence of the reflection intensities for the different phases suggests that UP is a yet unreported Mg-Ni-B phase which is depleted in a consecutive

reaction producing $MgNi_{2.5}B_2$. It is noteworthy that the formation of UP was not mentioned by Vajo *et al.* Since the authors did not conduct *in situ* diffraction experiments, they were not able to identify this intermediate compound. The reflections of LiH could be observed neither in the *ex situ* diffractogram of fully dehydrogenated material nor in any of the diffraction patterns collected in the *in situ* experiment. Since the composition of the detected diffractive compounds supports a dehydrogenation according to reaction path 3.2, the absence of LiH reflections must be explained by the low scattering intensity of this material. Indeed, for both LiH and $MgNi_{2.5}B_2$ the (200) reflections are the most intense. However, the structure factor $|F_{200}(MgNi_{2.5}B_2)|$ is approximately 13.4 times larger than $|F_{200}(LiH)|$ leading to an about 180 times higher diffraction intensity. In addition, at scattering vectors of $q_{200}(MgNi_{2.5}B_2) = 2.98\,Å^{-1}$ and $q_{200}(LiH) = 3.08\,Å^{-1}$ these two reflections are partially overlapping and thus making it even more difficult to distinguish the contributions of LiH. Therefore, the absence of distinct LiH reflections does not contradict the proposed dehydrogenation path. According to reaction 3.2 a capacity of 5.0 mass% is expected. At a mass loss of 4.4 % the released amount of hydrogen matches roughly 88 % of this value which is consistent with the purity of the initial reactants (see section 2.1). Although the hydrogenation of desorbed material was incomplete, the presence of recovered $LiBH_4$ and Mg_2NiH_4 in the rehydrogenated sample proves the reversible character of the sorption process. Since no side products are observed, the reduced hydrogen uptake could be attributed to kinetic limitations such as low solid-state diffusion rates or phase segregation due to the presence of a liquid compound. Therefore, it appears rather likely that improved reversibility can be achieved if the experimental conditions are optimised, more suitable material preparations are performed or an adequate additive is found.

3.1.2 $NaBH_4$-Mg_2NiH_4

3.1.2.1 Experimental Results

In order to study the release of hydrogen as a function of temperature for the system $NaBH_4$-Mg_2NiH_4 (molar ratio 2 : 2.5) a non-isothermal volumetric analysis was performed. The sample was heated in a hydrogen atmosphere of 1 bar from room temperature to 420 °C at a rate of $3\,K\,min^{-1}$. As can be seen in figure 3.4, the dehydrogenation proceeds in two distinct steps. The onset temperature of the first desorption step is approximately 295 °C, the second step starts at around 400 °C. During the first event 2.4 mass% of hydrogen are released and another 1.6 mass% in the second event achieving an overall hydrogen loss of 4.0 mass%. The fully dehydrogenated material was reabsorbed in 100 bar H_2 at a temperature of 360 °C for 20 h. The chemical composition of the sample before and after rehydrogenation was determined by means of X-ray diffraction. These two PXD patterns are presented in figure 3.5 along with the one of the as-milled material. The diffractogram of the as-milled sample features only the reflections of $NaBH_4$ (space group $Fm\bar{3}m$, No. 225) [105] and Mg_2NiH_4 (lt and ht). After dehydrogenation the diffraction peaks of the initial reactants

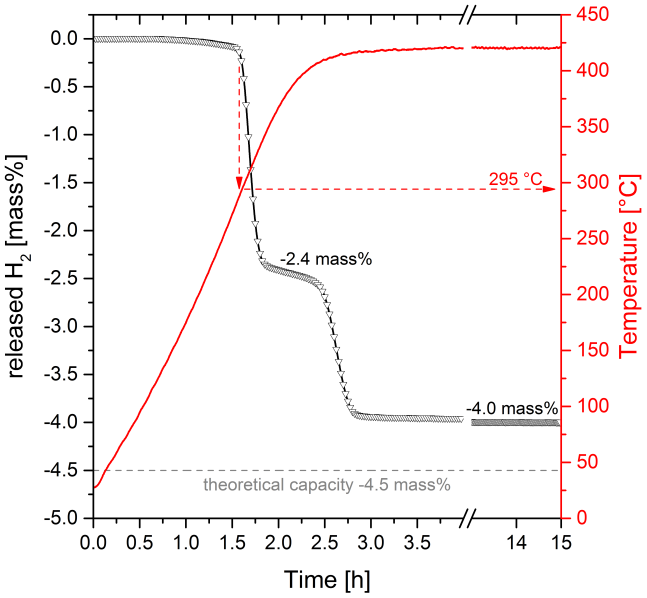

Figure 3.4: Volumetric analysis of the $NaBH_4$-Mg_2NiH_4 composite: the sample was heated from room temperature to 420 °C at 3 K min^{-1} in a hydrogen atmosphere of 1 bar.

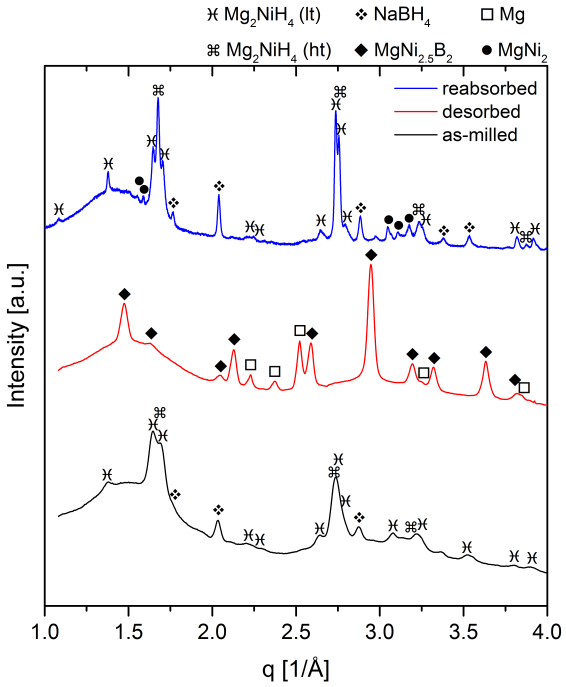

Figure 3.5: X-ray diffractograms of as-milled (black), dehydrogenated (red) and rehydrogenated (blue) $NaBH_4$-Mg_2NiH_4 composite.

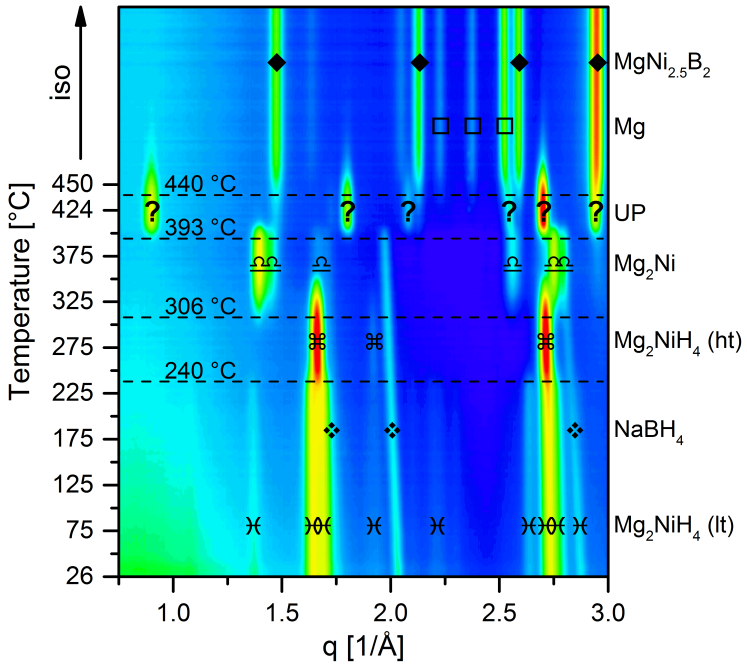

Figure 3.6: *In situ* SR-PXD analysis of the $NaBH_4$-Mg_2NiH_4 composite: the powder was heated from room temperature to 450 °C at 10 K min^{-1} and a hydrogen pressure of 1 bar.

disappeared completely and those of $MgNi_{2.5}B_2$ and Mg are discernible. No other diffractive compounds can be identified among the reaction products. The rehydrogenated sample has a chemical composition similar to the as-milled material as can be seen from the intense reflections of $NaBH_4$ and Mg_2NiH_4 (lt and ht). No residues of $MgNi_{2.5}B_2$ or Mg are detected. However, additionally the reflections of $MgNi_2$ can be distinguished. Detailed insights into the course of dehydrogenation events were obtained by means of an *in situ* SR-PXD study of the composite (figure 3.6). In this experiment the material was heated in a hydrogen atmosphere of 1 bar from room temperature to 450 °C at a rate of 10 K min^{-1}. No changes of the diffraction patterns are observed up to approximately 240 °C. At this temperature the low-temperature modification of Mg_2NiH_4 transforms into the high-temperature polymorph. At about 306 °C Mg_2NiH_4 (ht) starts to decompose and the diffraction pattern of Mg_2Ni emerges. The reflections of UP arise at roughly 393 °C. Simultaneously those of $NaBH_4$ and Mg_2Ni vanish. Approximately at 440 °C the reflections of $MgNi_{2.5}B_2$ and Mg become visible as those of UP fade slowly. At the end of the isothermal period at 450 °C no reflections except for those of $MgNi_{2.5}B_2$ and Mg are discernible.

3.1.2.2 Discussion

The overall dehydrogenation path of the hydride composite $NaBH_4$-Mg_2NiH_4 is in agreement with reaction scheme 3.1, i. e.

$$2\,NaBH_4 + 2.5\,Mg_2NiH_4 \longrightarrow 2\,NaH + MgNi_{2.5}B_2 + 4\,Mg + \underbrace{8\,H_2}_{4.5\,\text{mass\%}}. \tag{3.3}$$

The amount of hydrogen released in this reaction is equal to 4.5 mass%. A capacity of 4.0 mass% H_2 was determined experimentally. This value corresponds to 88 % of the theoretical capacity and is, therefore, in good agreement with the purity of the starting materials (see section 2.1). As confirmed by the *in situ* diffraction experiment, the first reaction step is the independent dehydrogenation of Mg_2NiH_4. The amount of hydrogen expected to evolve in this first step is equivalent to 2.8 mass%. At 2.4 mass% about 86 % of this theoretical value is reached consistently with the purity of Mg_2NiH_4. In the second dehydrogenation step the intermediate compound UP is formed first. As it reacts further, $MgNi_{2.5}B_2$ and Mg are produced. It is important to notice that, as for the system $LiBH_4$-Mg_2NiH_4, also for $NaBH_4$-Mg_2NiH_4 the formation of UP upon dehydrogenation was not reported before. Afonso *et al.* investigated this system but employed only a limited spectrum of experimental techniques [80]. Especially the absence of any *in situ* characterisation methods must be emphasised which, in conjunction with the transient nature of UP in the reaction process, prevented the detection of this compound. However, the authors analysed the thermodynamic properties of the system by measuring pressure-composition isotherms. They identified three distinct plateaus upon dehydrogenation. In compliance with the experimental results presented here, the first plateau is attributed to the independent desorption of Mg_2NiH_4. The second plateau is associated to the formation of $MgNi_{2.5}B_2$, Mg and NaH and the last to the decomposition of the latter compound. By means of a van 't Hoff analysis the corresponding reaction enthalpies were determined to be 67 kJ $(mol\,H_2)^{-1}$, 76 kJ $(mol\,H_2)^{-1}$ and 95 kJ $(mol\,H_2)^{-1}$. Based on these values the enthalpy of the overall reaction 3.3 can be calculated to approximately 70 kJ $(mol\,H_2)^{-1}$. It is noteworthy that this reaction enthalpy is higher than the one of the desorption of Mg_2NiH_4, thus suggesting that the overall reaction cannot occur directly i. e. without the described intermediate events. *A priori*, also another dehydrogenation path appears possible, that is

$$2\,NaBH_4 + 2.5\,Mg_2NiH_4 \longrightarrow 2\,NaH + MgNi_{2.5}B_2 + 4\,MgH_2 + \underbrace{4\,H_2}_{2.25\,\text{mass\%}}. \tag{3.4}$$

The formation of MgH_2 instead of Mg would lower the total reaction enthalpy but concurrently also reduce the overall entropy gain. Assuming an enthalpy of desorption for MgH_2 of 74.4 kJ $(mol\,H_2)^{-1}$ [19], the enthalpy change of reaction path 3.4 is calculated to roughly 67 kJ $(mol\,H_2)^{-1}$ and, therefore, practically matching the value of the independent desorption

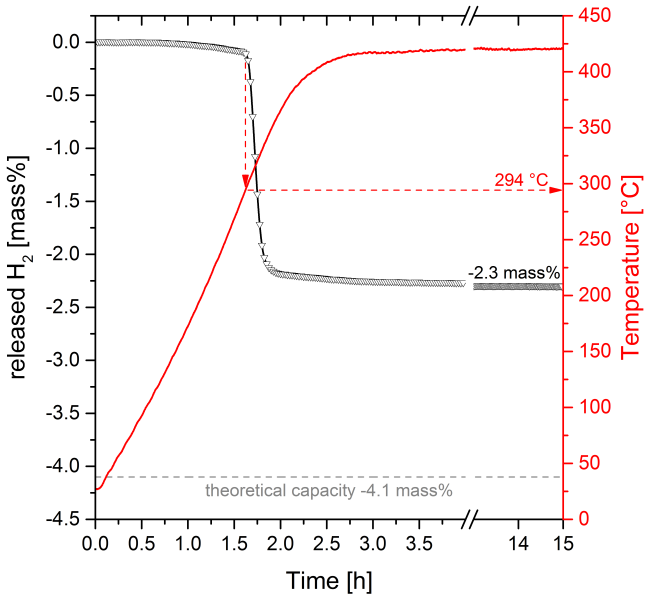

Figure 3.7: Volumetric analysis of the KBH_4-Mg_2NiH_4 composite: at a pressure of 1 bar H_2 the sample was heated from room temperature to 420 °C at 3 K min^{-1}.

of Mg_2NiH_4. Activation energies for the latter process are presumably lower than those of reaction 3.4 because of the lower extent of solid-state diffusion involved and the smaller number of new phases that have to nucleate and grow (one *vs.* three). Thus, it appears plausible to assume that dehydrogenation of the hydride composite $NaBH_4$-Mg_2NiH_4 always starts with the decomposition of Mg_2NiH_4. Consequently, concerted reactions between the two initial hydrides are not expected to take place in this system. At first glance, the rehydrogenation of the desorbed material appears quite promising due to the intense reflections of Mg_2NiH_4 and $NaBH_4$ that are present in the respective diffraction pattern. No residues of $MgNi_{2.5}B_2$ and Mg/MgH_2 can be identified. However, unlike the system $LiBH_4$-Mg_2NiH_4 some $MgNi_2$ is formed upon hydrogen absorption. As this intermetallic is not absorbing (relevant amounts of) hydrogen [106], its presence reduces the possible hydrogen uptake and thus the overall system hydrogen capacity. The formation of this compound was confirmed by Afonso *et al.*, too [80]. The authors reported that the molar fraction of $MgNi_2$ increases upon hydrogen cycling gradually decreasing the reversible hydrogen storage capacity of the $NaBH_4$-Mg_2NiH_4 system.

3.1.3 KBH_4-Mg_2NiH_4

3.1.3.1 Experimental Results

The composite KBH_4-Mg_2NiH_4 (molar ratio 2 : 2.5) was heated in a hydrogen atmosphere of 1 bar from room temperature to 420 °C at a rate of 3 K min^{-1}. The temperature dependent evolution of hydrogen form the materials was monitored by means of a volumetric technique (figure 3.7). As can be seen, the desorption process starts at about 294 °C. All hydrogen

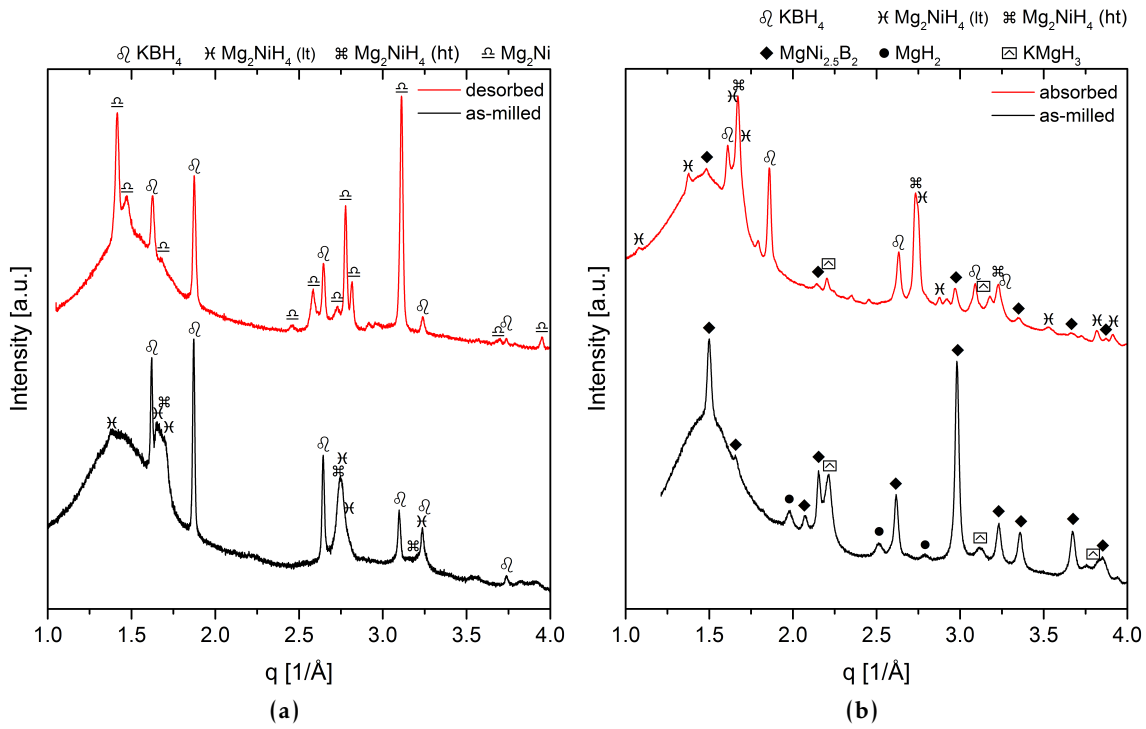

Figure 3.8: PXD analyses of samples in different sorption states: (a) as-milled and dehydrogenated KBH_4-Mg_2NiH_4 and (b) as-milled and hydrogenated KH-$MgNi_{2.5}B_2$-MgH_2.

is released in a single step reaching an overall loss of 2.3 mass%. In figure 3.8a the PXD analyses of the as-milled and the dehydrogenated material are presented. All reflections in the diffractogram of the as-milled sample can be assigned to KBH_4 (space group $Fm\bar{3}m$, No. 225) [107] and Mg_2NiH_4 (lt and ht). The diffraction pattern of the desorbed material features intense reflections of Mg_2Ni but also of KBH_4. No other boron containing phases can be identified. Since the hydrogen stored in this composite was only partially released and the transfer of boron to Mg_2NiH_4/Mg_2Ni, i. e. the formation of $MgNi_{2.5}B_2$ as proposed by reaction scheme 3.1, did not happen, a mixture according to the dehydrogenated state of this reaction scheme was prepared. The as-prepared KH-$MgNi_{2.5}B_2$-MgH_2 (molar ratio 2 : 1 : 4) was investigated in terms of hydrogen absorption capabilities of this desorbed state material. In order to prepare this material avoiding cold welding phenomena during ball milling, MgH_2 was used instead of Mg. A sample of this material was hydrogenated at 360 °C and at a pressure of 100 bar for 20 h. The PXD analyses of the as-milled and the hydrogenated sample are shown in figure 3.8b. The diffractogram of the as-milled material features reflections of $MgNi_{2.5}B_2$, MgH_2 and $KMgH_3$. No contributions of KH to the diffraction pattern are discernible. After hydrogenation the reflections of KBH_4 and Mg_2NiH_4 (lt and ht) are clearly visible besides very weak diffraction peaks of residual $MgNi_{2.5}B_2$ and $KMgH_3$. Since no reaction between KBH_4 and Mg_2NiH_4 could be observed upon dehydrogenation of the composite but only the decomposition of Mg_2NiH_4, this process was not monitored

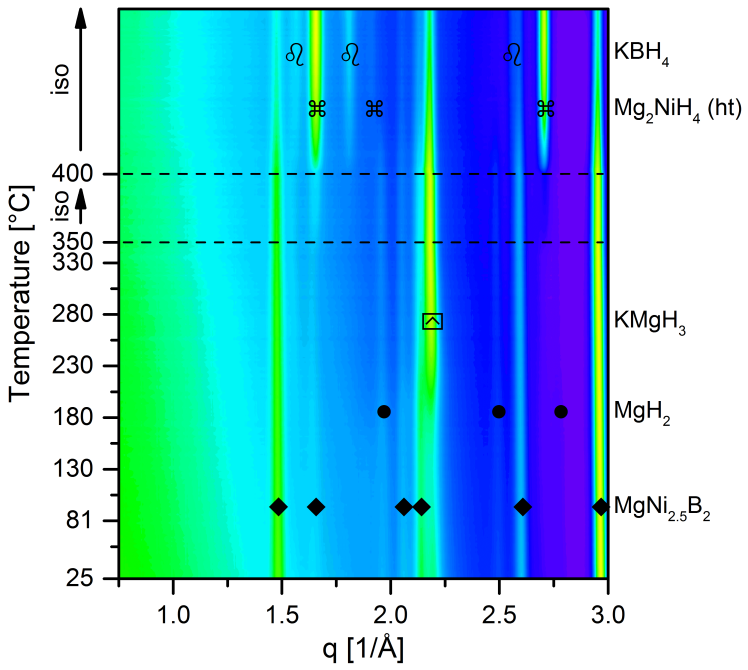

Figure 3.9: *In situ* SR-PXD experiment showing the hydrogenation reactions of as-milled KH-$MgNi_{2.5}B_2$-MgH_2: the sample was heated from RT to 350 °C at 5 K min^{-1} in 170 bar of hydrogen.

by *in situ* SR-PXD technique. Instead, the hydrogenation of as-milled KH-$MgNi_{2.5}B_2$-MgH_2 was analysed by means of this experimental method. The specimen was heated under a hydrogen atmosphere of 170 bar from room temperature up to 350 °C at a rate of 5 K min^{-1} and afterwards kept isothermally for 10 min. Subsequently the temperature was abruptly increased to 400 °C in order to promote reaction kinetics. As shown in figure 3.9, below 350 °C only an intensification of $KMgH_3$ reflections can be observed. At this temperature the diffraction pattern of Mg_2NiH_4 (ht) arises. Within the isothermal region at 350 °C the diffraction intensity of this compound slowly increases. The temperature increment to 400 °C improves the kinetics of Mg_2NiH_4 formation. Simultaneously the reflections of KBH_4 appear. Until termination of the experiment the reflections of both newly formed phases intensify whereas those of the initial compounds weaken.

3.1.3.2 Discussion

Upon dehydrogenation of the hydride composite KBH_4-Mg_2NiH_4 no reactions between the two constituting hydrides are observed for the applied experimental conditions. As a consequence, no common reaction products – in particular no $MgNi_{2.5}B_2$ – are formed that could stabilise the dehydrogenated state and therefore lower the overall reaction enthalpy. Hence, this composite system cannot be considered as Reactive Hydride Composite. Accordingly, the determined dehydrogenation path does not correspond to reaction scheme 3.1 and can

be summarised as

$$2\,KBH_4 + 2.5\,Mg_2NiH_4 \longrightarrow 2\,KBH_4 + 2.5\,Mg_2Ni + \underbrace{5\,H_2}_{2.6\,\text{mass\%}}. \tag{3.5}$$

Mg_2NiH_4 decomposes if its equilibrium temperature is exceeded. In contrast, KBH_4 is stable within the investigated temperature range. As reported in previous publications [108, 109], at more than 550 °C the decomposition temperature of this borohydride is relatively high. The thermal stability of this compound – and perhaps also kinetic constraints – prohibits the formation of $MgNi_{2.5}B_2$ in this system. The low amount of released hydrogen is in agreement with this finding. At 2.3 mass% the experimentally determined amount of evolved gas matches approximately 89 % of the theoretical hydrogen capacity of Mg_2NiH_4 within this system. The value is in good agreement with the purity of this compound (see section 2.1). The high stability of KBH_4 hinders full dehydrogenation according to reaction scheme 3.1. On the contrary, this high stability leads to an easy hydrogenation of KH-$MgNi_{2.5}B_2$-MgH_2, i. e.

$$2\,KH + MgNi_{2.5}B_2 + 4\,MgH_2 + 4\,H_2 \longrightarrow 2\,KBH_4 + 2.5\,Mg_2NiH_4. \tag{3.6}$$

Almost full conversion was achieved after hydrogenation of this mixture. Even in the *in situ* diffraction experiment a rather high degree of absorption was reached within just 40 min of isothermal heating at 400 °C. The ternary hydride $KMgH_3$ was formed already during ball milling. This compound does not hinder hydrogenation towards KBH_4 and Mg_2NiH_4. Instead, it could be possible that this hydride improves reaction kinetics because diffusion lengths are potentially reduced: in the initial mixture KH-$MgNi_{2.5}B_2$-MgH_2 the absorption reaction 3.6 can only occur at the common interfaces of all three compounds. Thus, relatively long diffusion lengths arise from this condition. In contrast, after formation of $KMgH_3$ the two starting reactants KH and MgH_2 are virtually mixed on the atomic level. This could allow for the absorption process to take place at the common interfaces of solely $KMgH_3$ and $MgNi_{2.5}B_2$ resulting in effectively shortened diffusion path lengths. As proven by the *in situ* hydrogenation experiment, the formation of Mg_2NiH_4 and KBH_4 occurs directly i. e. without development of boron containing intermediate phases such as UP. This observation is noteworthy because the latter compound was identified as an intermediate in the dehydrogenation of all other $M(BH_4)_n$-Mg_2NiH_4 composites ($M \in \{Li, Na, Mg, Ca\}$). Therefore, these results could indicate that the reaction paths and mechanisms for absorption and desorption are different in these composite systems.

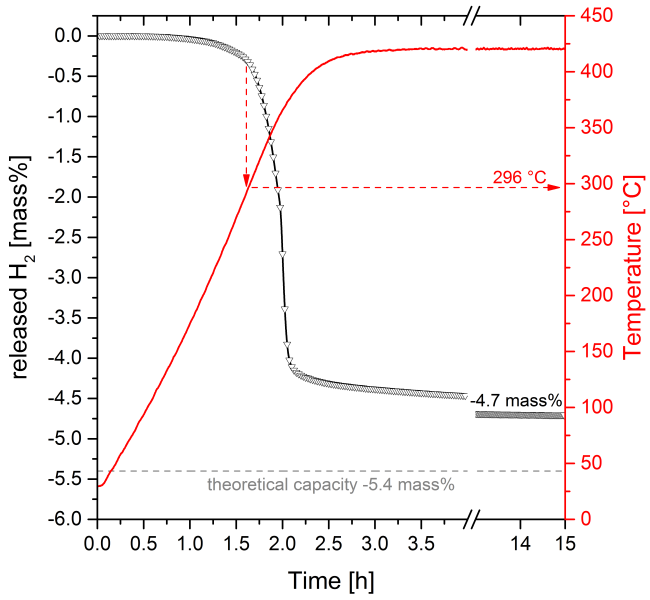

Figure 3.10: Volumetric analysis of the $Mg(BH_4)_2$-Mg_2NiH_4 composite: the sample was heated from room temperature to 420 °C at 3 K min^{-1} in hydrogen with a pressure of 1 bar.

3.1.4 $Mg(BH_4)_2$-Mg_2NiH_4

3.1.4.1 Experimental Results

The temperature dependent evolution of hydrogen from the composite $Mg(BH_4)_2$-Mg_2NiH_4 (molar ratio 1 : 2.5) was measured *via* volumetric technique (figure 3.10). For this purpose the material was heated from room temperature to 420 °C at a rate of 3 K min^{-1} in a hydrogen atmosphere of 1 bar. The onset temperature of dehydrogenation can be estimated at roughly 296 °C. The gas is released continuously in a single step. However, the last 0.3 mass% emerge rather slowly from the solid materials. Altogether, an amount of hydrogen equal to 4.7 mass% is desorbed. The fully dehydrogenated material was rehydrogenated at 400 °C and 450 bar for 24 h. *Ex situ* X-ray diffraction analyses were performed on the as-milled, the dehydrogenated and the rehydrogenated material. These three diffractograms are presented in figure 3.11a. The as-milled material features broad reflections of Mg_2NiH_4 (lt and ht) – the diffraction pattern of $Mg(BH_4)_2$ cannot be recognised, though. After full dehydrogenation the diffractogram comprises the reflections of $MgNi_{2.5}B_2$ and Mg. These are the only compounds that can be observed, hence no indications of residual Mg_2Ni or additional boron containing phases such as MgB_2 are discernible. The diffraction pattern of the rehydrogenated material is composed of the reflections of $MgNi_{2.5}B_2$ and MgH_2. Neither contributions of Mg_2NiH_4 nor $Mg(BH_4)_2$ can be detected. Since $Mg(BH_4)_2$ might be present in nano-crystalline or even (partially) amorphous state (see absence of reflections in diffractogram of as-milled material in figure 3.11a), ^{11}B MAS NMR spectra were collected to gain more insights into the phase composition of the absorbed material. In order to ensure that possible signals of $Mg(BH_4)_2$ can be doubtlessly related to the hydrogenation process

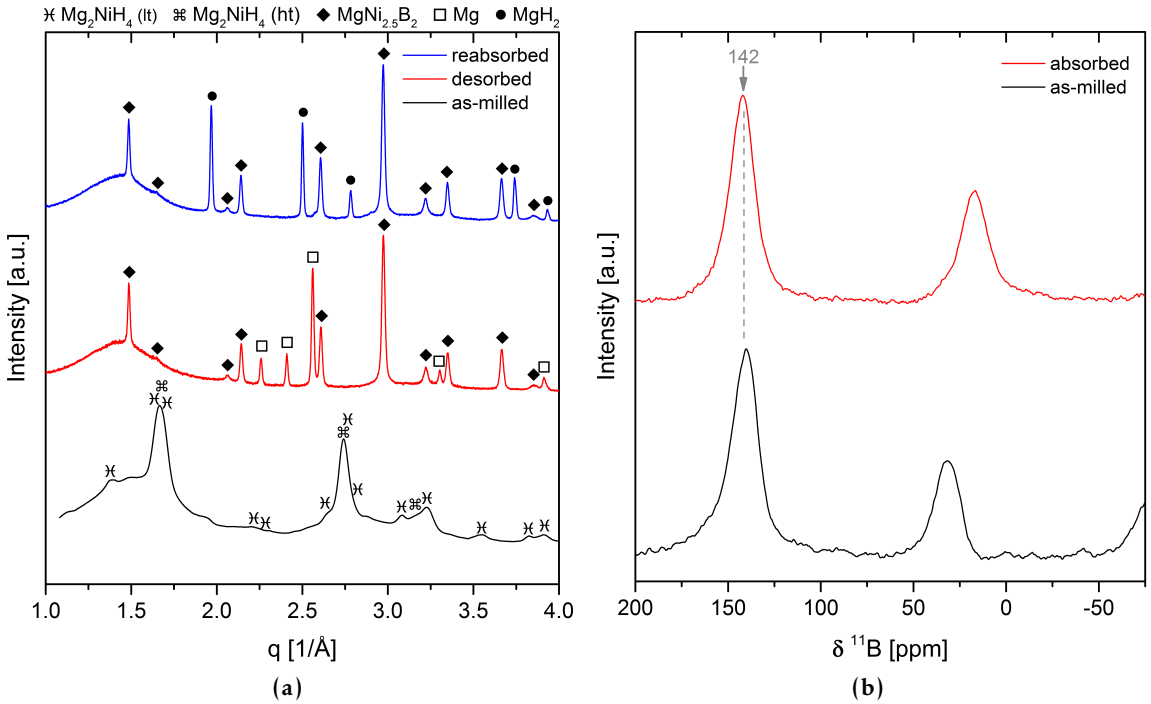

Figure 3.11: Determination of the chemical composition of five samples in different sorption states: (a) PXD analyses of as-milled, dehydrogenated and rehydrogenated $Mg(BH_4)_2$-Mg_2NiH_4 and (b) ^{11}B MAS NMR spectra of as-milled and hydrogenated $MgNi_{2.5}B_2$-MgH_2.

and are not just caused by unreacted residues of the as-prepared compounds, desorbed state material was prepared directly according to reaction scheme 3.1 – as suggested by the PXD analysis of desorbed $Mg(BH_4)_2$-Mg_2NiH_4 shown in figure 3.11a. Thus, $MgNi_{2.5}B_2$ and MgH_2 were mixed in a molar ratio of 1 : 5. Also in this case MgH_2 was used instead of magnesium to prevent cold welding during ball milling. This material was hydrogenated at 450 bar and 400 °C. The NMR spectra of the as-prepared and the hydrogenated sample are presented in figure 3.11b. The two spectra look almost identical. Both feature a single resonance with the centerband at 142 ppm which is attributed to $MgNi_{2.5}B_2$ (see reference material in figure 2.2b). All other peaks are spinning sidebands of this compound. As a consequence of different spinning frequencies, the two analyses differ from each other with respect to the sideband positions. No resonance signal of $Mg(BH_4)_2$ can be detected in the spectrum of the hydrogenated material. The sequence of events upon dehydrogenation of the $Mg(BH_4)_2$-Mg_2NiH_4 composite was investigated by means of *in situ* SR-PXD technique. For this analysis as-milled $Mg(BH_4)_2$-Mg_2NiH_4 was heated from room temperature to 450 °C at a rate of 10 K min^{-1}) in 1 bar of hydrogen. As can be seen in figure 3.12), the first change of the diffraction patterns takes place at approximately 161 °C. At this temperature $Mg(BH_4)_2$ undergoes a polymorphic transition from space group $Ia\bar{3}d$ (No. 230) [110] to space group $P6_122$ (No. 178) [111]. Also the two subsequent modifications of the diffraction patterns are related to polymorphic transitions: at about 200 °C the transition from $Mg(BH_4)_2$ space group $P6_122$ to space group *Fddd* (No. 70) [112] can be observed and at roughly 240 °C Mg_2NiH_4 changes

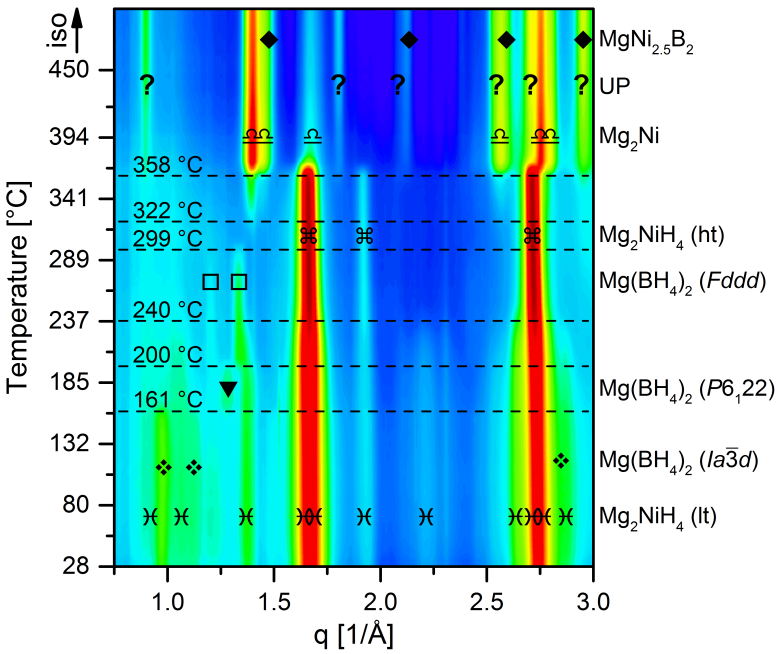

Figure 3.12: *In situ* SR-PXD analysis of the $Mg(BH_4)_2$-Mg_2NiH_4 composite: the specimen was heated from room temperature to 450 °C at 10 K min^{-1} and a pressure of 1 bar H_2.

from its low- to its high-temperature structure. The reflections of $Mg(BH_4)_2$ disappear at about 299 °C and at 322 °C those of Mg_2Ni arise whilst the intensity of Mg_2NiH_4 reflections starts to decrease slowly. Eventually, at approximately 358 °C, the remaining Mg_2NiH_4 vanishes as the reflections of Mg_2Ni intensify quickly and, in addition, the diffraction patterns of UP and $MgNi_{2.5}B_2$ become visible. Due to the very gradual growth of these two phases, the temperatures at which they emerge cannot be determined precisely. Nevertheless, UP not only appears to grow faster than $MgNi_{2.5}B_2$ but also to crystallise first. Until termination of the experiment, the diffraction intensities of UP as well as $MgNi_{2.5}B_2$ increase whereas Mg_2Ni reflections fade out.

3.1.4.2 Discussion

Similar to the other borohydride-Mg_2NiH_4 composites introduced before, the dehydrogenation of $Mg(BH_4)_2$-Mg_2NiH_4 proceeds along several intermediate reaction steps. As revealed by the *in situ* diffraction experiment, the process starts with the disappearance of $Mg(BH_4)_2$ reflections. This could be the consequence of either the melting of $Mg(BH_4)_2$ or its decomposition into non-diffractive compounds. Both scenarios are likely due to the proximity of the melting point to the decomposition temperature [108]. In contrast to $LiBH_4$-Mg_2NiH_4 this event does not seem to affect the dehydrogenation of Mg_2NiH_4 directly because Mg_2Ni reflections do not emerge until 322 °C which is about 23 K above the vanishing temperature of $Mg(BH_4)_2$ reflections. Moreover, the dehydrogenation onset temperature determined in the volumetric analysis (about 296 °C) is consistent with the onset temperature of pure

Mg_2NiH_4 recorded in the same instrument under equal conditions. This result also rather suggests the melting of $Mg(BH_4)_2$ because no significant amounts of gas – that could be related to decomposition reactions – are released prior to the dehydrogenation of Mg_2NiH_4. Also in this system, UP takes part in the desorption process as an intermediate compound. Thus, hinting to the fact that UP is a transitional phase in the formation of $MgNi_{2.5}B_2$ from Mg_2Ni. The presence of considerable quantities of non-diffractive B-H phases or amorphous boron – both typical decomposition products of $Mg(BH_4)_2$ – can also be excluded by X-ray diffraction: the initial ratio between $Mg(BH_4)_2$ and Mg_2NiH_4 was chosen to allow for the bonding of all nickel and all boron in $MgNi_{2.5}B_2$ and, indeed, this compound is the only nickel containing phase observed after full dehydrogenation. Considering that the amplitude of X-ray radiation scattered at a specific atom is proportional to the square of that atom's atomic scattering factor and nickel has the largest scattering factor among all elements within the analysed samples (at $q = 2\,\text{Å}^{-1}$: $f_{Ni} \approx 23.6$, $f_{Mg} \approx 9.3$, $f_B \approx 3.2$ and $f_H \approx 0.6$) [113], relevant amounts of other nickel containing phases would be discernible in the diffractogram of fully desorbed material due to their rather high scattering intensities. This absence of residual Mg_2Ni and other nickel containing compounds strongly suggests that by far the greatest fraction of boron must be bonded in $MgNi_{2.5}B_2$. This finding is in accordance with reaction scheme 3.1. As a consequence, the overall dehydrogenation path can be written as

$$Mg(BH_4)_2 + 2.5\,Mg_2NiH_4 \longrightarrow MgNi_{2.5}B_2 + 5\,Mg + \underbrace{9\,H_2}_{5.4\,\text{mass\%}}. \tag{3.7}$$

Non-diffractive B-H phases or amorphous boron might be present in the desorbed sample, e. g. due to stoichiometric deviations, but only in fairly low concentrations. At 4.7 mass% the measured amount of hydrogen stored in the system matches approximately 87 % of the theoretical capacity of 5.4 mass%. Under the applied experimental conditions, reaction 3.7 proved to be irreversible as no traces of $Mg(BH_4)_2$ could be detected in the ^{11}B MAS NMR spectrum of $MgNi_{2.5}B_2$-MgH_2 after attempted hydrogenation. The rather low thermal stability of $Mg(BH_4)_2$ in combination with the estimated highly negative standard enthalpy of formation[1] of $MgNi_{2.5}B_2$ most likely results in a very low reaction enthalpy that demands for extreme reabsorption conditions, i. e. very high pressures of hydrogen. Furthermore, poor kinetic properties might even raise the requirements for successful (re)absorption: another specimen of $MgNi_{2.5}B_2$-MgH_2 was hydrogenated for 24 h at 1000 bar. However, during that experiment the temperature was limited to a maximum of 300 °C. Also this sample did not show traces of $Mg(BH_4)_2$. Since the applied hydrogen pressure was exceptionally high, the limited temperature could have been the restricting factor for the unsuccessful $Mg(BH_4)_2$ formation.

[1] Vajo *et al.* were able to estimate the standard enthalpy of formation of $MgNi_{2.5}B_2$ by means of their thermodynamic assessment of the $LiBH_4$-Mg_2NiH_4 system and literature values for the formation enthalpies of the other compounds. They calculated a value of $-323\,\text{kJ mol}^{-1}$. On a per atom basis, $MgNi_{2.5}B_2$ (−59 kJ/atom) is almost twice as stable as MgB_2 (−31 kJ/atom) [114].

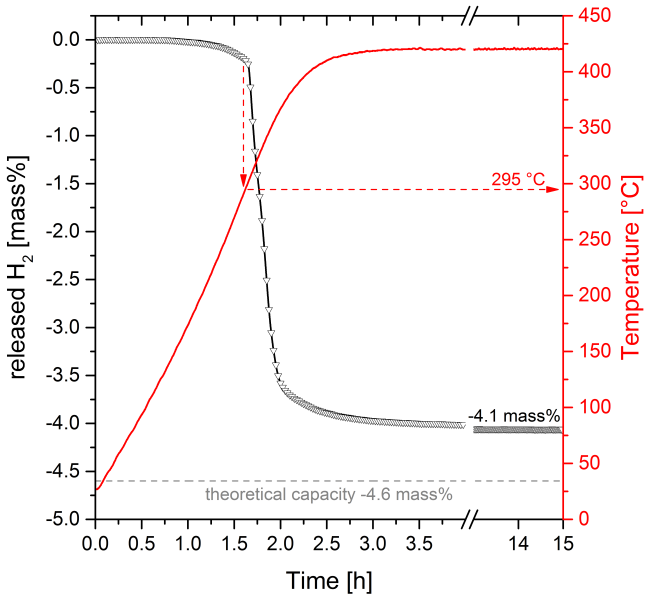

Figure 3.13: Volumetric analysis of the $Ca(BH_4)_2$-Mg_2NiH_4 composite: at a pressure of 1 bar H_2 the sample was heated from room temperature to 420 °C at a rate of 3 K min^{-1}.

3.1.5 $Ca(BH_4)_2$-Mg_2NiH_4

3.1.5.1 Experimental Results

In order to determine the temperature dependent release of hydrogen from the composite $Ca(BH_4)_2$-Mg_2NiH_4 a non-isothermal volumetric analysis was conducted (figure 3.13). The experiment was performed at 1 bar of hydrogen pressure. The specimen was heated from room temperature to 420 °C at a rate of 3 K min^{-1}. As can be seen, the dehydrogenation reaction starts at approximately 295 °C. Afterwards the hydrogen is released from the material in a continuous process yielding a total capacity of about 4.1 mass%. The desorbed sample was rehydrogenated at 375 °C and a pressure of 330 bar for 20 h. The chemical compositions of the specimens in different sorption states were characterised by *ex situ* PXD and ^{11}B MAS NMR analyses (figure 3.14). The three diffractograms of as-milled, dehydrogenated and rehydrogenated material are presented in figure 3.14a. In the diffraction pattern of the as-milled material only the broad reflections of Mg_2NiH_4 (lt and ht) can be distinguished. No reflections of $Ca(BH_4)_2$ are discernible, though. The diffractogram of the dehydrogenated sample features distinct peaks of $MgNi_{2.5}B_2$, CaH_2 and Mg. After rehydrogenating this material, its diffraction pattern is composed of reflections which can be attributed to $MgNi_{2.5}B_2$, $Ca_4Mg_3H_{14}$ and MgH_2. However, no indications of recovered $Ca(BH_4)_2$ are observed. Since pure $Ca(BH_4)_2$ typically decomposes into CaH_2 and compounds that are weakly or even non-diffractive because of their nano-crystalline or amorphous nature (CaB_6, $CaB_{12}H_{12}$, CaB_2H_6 and elemental boron), the chemical state of boron after full dehydrogenation was investigated by means of ^{11}B MAS NMR technique. Due to the absence of $Ca(BH_4)_2$ reflections in the PXD analyses of both the as-milled and the rehydrogenated specimen,

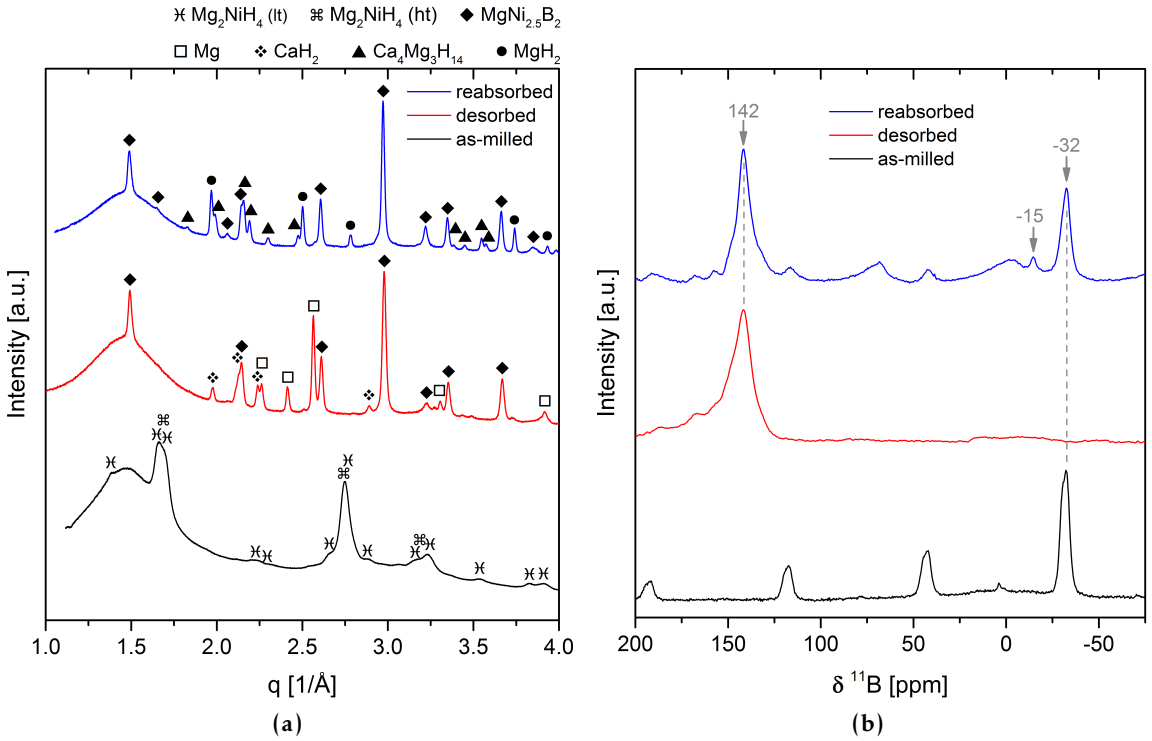

Figure 3.14: Determination of the chemical composition of as-milled, desorbed and reabsorbed $Ca(BH_4)_2$-Mg_2NiH_4 specimens:(a) PXD analyses and (b) ^{11}B MAS NMR spectra.

^{11}B MAS NMR spectra of these materials were recorded, too. The spectra of as-milled, desorbed and reabsorbed material are presented together in figure 3.14b. These results show that the as-milled material comprises only one boron containing phase, that is $Ca(BH_4)_2$ [115]. More precisely, the signal at approximately −32 ppm is a superposition of the two polymorphs α- and γ-$Ca(BH_4)_2$. In contrast, the desorbed sample contains no residues of $Ca(BH_4)_2$ anymore. Instead, just one rather broad resonance at about 142 ppm is visible which is assigned to $MgNi_{2.5}B_2$. No signals of any other boron containing compound can be perceived. The rehydrogenated material features two major resonances: the first at 142 ppm can be assigned to unreacted $MgNi_{2.5}B_2$, the second at −32 ppm clearly belongs to $Ca(BH_4)_2$. In addition, a weak signal at roughly −15 ppm is recorded which cannot be assigned clearly. In order to shed more light on the sequence of dehydrogenation events, an *in situ* SR-PXD experiment was performed applying a temperature ramp of $10\,K\,min^{-1}$ heating from room temperature to 450 °C in 1 bar of hydrogen (figure 3.15). The room temperature diffraction pattern exhibits the reflections of both the low- and the high-temperature form of Mg_2NiH_4. Diffraction peaks of $Ca(BH_4)_2$ can be attributed to the α- (space group $F2dd$, No. 43) [116] and γ-phase (space group $Pbca$, No. 61) [117]. The first event with rising temperature is the polymorphic transition from α-/γ-$Ca(BH_4)_2$ to β-$Ca(BH_4)_2$ (space group $P\bar{4}$, No. 81) [116] which starts at about 174 °C. The second modification in the diffraction patterns is related to another polymorphic transition: monoclinic Mg_2NiH_4 (lt) converts to the cubic phase

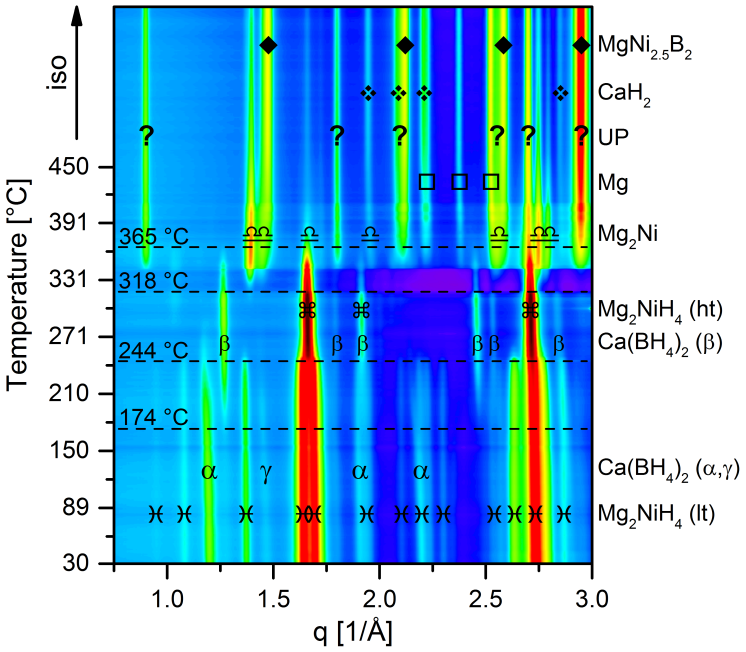

Figure 3.15: *In situ* SR-PXD analysis of the $Ca(BH_4)_2$-Mg_2NiH_4 composite: the powder was heated from room temperature to 450 °C at 10 K min^{-1} and a hydrogen pressure of 1 bar.

(ht) at approximately 244 °C. At about 318 °C, Mg_2NiH_4 starts to decompose to Mg_2Ni and hydrogen. At slightly higher temperatures, the intensities of $Ca(BH_4)_2$ reflections start to decrease while the diffraction patterns of four other phases occur and intensify: $MgNi_{2.5}B_2$, Mg, CaH_2 and UP. Increasing the temperature further, the peaks of Mg_2Ni first grow until the maximum intensities are reached at roughly 365 °C, followed by a quick decline of peak intensities. The reflections of $MgNi_{2.5}B_2$, Mg and CaH_2 grow during the remaining heating period and the following isothermal region at 450 °C. In contrast, those belonging to UP only grow until the highest intensities are attained at about 410 °C, then the reflection intensities reduce much slower than those of Mg_2Ni. Moreover, it must be emphasised that the diffraction peaks of $Ca(BH_4)_2$ vanish already at about 365 °C, that is when $MgNi_{2.5}B_2$ and UP are still growing.

3.1.5.2 Discussion

Evaluating the PXD and NMR analyses, the overall dehydrogenation path of the composite $Ca(BH_4)_2$-Mg_2NiH_4 can be expressed as

$$Ca(BH_4)_2 + 2.5\,Mg_2NiH_4 \longrightarrow CaH_2 + MgNi_{2.5}B_2 + 4\,Mg + \underbrace{8\,H_2}_{4.6\,\text{mass\%}}. \tag{3.8}$$

This dehydrogenation reaction is consistent with the general reaction scheme 3.1. The quantity of hydrogen theoretically released from the materials amounts to 4.6 mass%. Considering the purity of the initial reactants, the measured capacity of 4.1 mass% – that is 89 % of the

ideal value – is in good agreement with reaction 3.8. As shown by the NMR analysis of the desorbed sample, all boron seems to be bonded in $MgNi_{2.5}B_2$. If there were minor amounts of other boron containing phases their quantities would have to be below the sensitivity threshold of the spectrometer. Therefore these amounts would have to be less than roughly 1 to 2 mol%. This result is very important because it shows that none of the typical decomposition products of $Ca(BH_4)_2$, i. e. CaB_6, $CaB_{12}H_{12}$, CaB_2H_6 or amorphous boron, could be detected in the dehydrogenated state of $Ca(BH_4)_2$-Mg_2NiH_4. The formation of the stable phases $CaB_{12}H_{12}$ and amorphous boron is considered as the main reason for the degradation of $Ca(BH_4)_2$ based hydrogen storage systems as these compounds act as boron sinks upon hydrogen cycling. Hence, the absence of these phases may allow for an improved reversibility of the $Ca(BH_4)_2$-Mg_2NiH_4 Reactive Hydride Composite. For that purpose it is crucial that $MgNi_{2.5}B_2$ is not just another boron sink but can serve as boron donor for the formation of $Ca(BH_4)_2$. Considering that $MgNi_{2.5}B_2$ is the only boron containing compound detected in the fully dehydrogenated material, all boron bonded in the recovered $Ca(BH_4)_2$ must have been transferred from $MgNi_{2.5}B_2$ upon reabsorption. In the NMR spectrum of the rehydrogenated material the centerband area of $Ca(BH_4)_2$ conforms roughly 50 % of the $MgNi_{2.5}B_2$ centerband area. Therefore, a significant fraction of all boron in the sample (about 33 %) changed the chemical state upon hydrogen uptake. Consequently, these findings prove that boron can be exchanged reversibly between $Ca(BH_4)_2$ and $MgNi_{2.5}B_2$ in the sorption processes. However, as can be seen from the high fraction of residual $MgNi_{2.5}B_2$ present in the absorbed sample, the rehydrogenation did not complete under the applied experimental conditions. Based on the results presented in this section, no definitive explanation for this limitation can be provided yet. Since no $Ca(BH_4)_2$ reflections are discernible in the X-ray diffractogram of the reabsorbed sample, the crystallites of this compound seem to be rather small. As the nucleation of $Ca(BH_4)_2$ is expected to occur at common interfaces of the three reactants of the desorbed state, i. e. $MgNi_{2.5}B_2$, Mg and CaH_2, the newly formed borohydride may act as a diffusion barrier leading to reduced kinetic rates. This might (partly) explain the incomplete rehydrogenation. The NMR spectrum of the reabsorbed material also shows a minor resonance at −15 ppm. Although this signal cannot be assigned clearly, it is noticed that the chemical shift is similar to $CaB_{12}H_{12}$ and CaB_2H_6 [62, 115]. Thus, this signal is most likely caused by a $(B_xH_y)^{n-}$ compound which could be an intermediate product for $Ca(BH_4)_2$ formation. The *in situ* monitoring of the dehydrogenation reactions of $Ca(BH_4)_2$-Mg_2NiH_4 revealed that the reflections of both $MgNi_{2.5}B_2$ and UP were still intensifying after $Ca(BH_4)_2$ reflections already disappeared. This finding strongly suggests the possibility of Mg_2Ni reacting with decomposition products of $Ca(BH_4)_2$. If that was the case it would also explain the absence of boron containing compounds other than $MgNi_{2.5}B_2$ among the desorption products. It should be noted that the rapid disappearance of $Ca(BH_4)_2$ reflections at about 365 °C clearly suggests an independent decomposition of this borohydride. Furthermore, the sequence of reflection intensity changes for the different phases suggests once more that UP is a yet unreported Mg-Ni-B compound. It is noteworthy as well that – among

all $Ca(BH_4)_2$ based hydrogen storage systems described thus far – the Reactive Hydride Composite $Ca(BH_4)_2$-Mg_2NiH_4 features a unique reaction mechanism. In all other systems boron is either not transferred from the calcium based compound(s) to the reaction partner (formation of CaB_6, $CaB_{12}H_{12}$, CaB_2H_6 and/or amorphous boron) or the boron containing reaction products proved to be irreversible, e. g. [67, 68]. In this respect, the presence of $MgNi_{2.5}B_2$ among the dehydrogenation products of $Ca(BH_4)_2$-Mg_2NiH_4 is quite remarkable because all boron in the system is bonded in this compound and, moreover, it allows for the reversible formation of $Ca(BH_4)_2$.

3.1.6 Conclusion and Assessment

Among the five hydride composites $M(BH_4)_n$-Mg_2NiH_4 ($M \in \{Li, Na, K, Mg, Ca\}$ and $n \in \{1, 2\}$) introduced in this section only four can be regarded as Reactive Hydride Composites. In the case of KBH_4-Mg_2NiH_4 no reactivity between the two components could be observed within the analysed temperature range up to 450 °C. Although the allegedly reverse reaction starting from KH-$MgNi_{2.5}B_2$-MgH_2 is yielding a high conversion to KBH_4 and Mg_2NiH_4, the irreversibility of this process makes the system unattractive from an applicational point of view. Therefore, it was discarded from further investigations. On the contrary, the system $NaBH_4$-Mg_2NiH_4 meets the criteria of a Reactive Hydride Composite. A high degree of recovery of the initial composition was achieved after one full hydrogen cycle. However, the formation of $MgNi_2$ upon rehydrogenation must be considered as major disadvantage, especially since this compound is agglomerating after several cycles [80]. Moreover, the thermodynamic properties of this composite are not favourable: the estimated reaction enthalpy of the whole system is higher than the one of pure Mg_2NiH_4. Consequently, the high working temperatures are not a result of poor kinetics but directly related to the thermodynamics of the system. For these reasons also $NaBH_4$-Mg_2NiH_4 was not considered for additional investigations. The Reactive Hydride Composite $Mg(BH_4)_2$-Mg_2NiH_4 features the highest hydrogen storage capacity among the five systems presented here making it an appealing candidate for hydrogen storage applications. Additionally, the complex chemistry of pure $Mg(BH_4)_2$ is also turning the mixture with Mg_2NiH_4 into a rather interesting object of study. However, the release of hydrogen proved to be irreversible as no traces of $Mg(BH_4)_2$ could be found after the hydrogenation attempt. Therefore, also this composite was discarded from the further studies.

The system $LiBH_4$-Mg_2NiH_4 might be the most promising candidate for technical applications. As a matter of fact, at 5.0 mass% this Reactive Hydride Composite features the second highest hydrogen capacity among the five systems and shows partial reversibility in the first full hydrogen cycle. No side products could be detected after the first rehydrogenation. It is, therefore, very likely that the incomplete hydrogen uptake may be ascribed to kinetic limitations. In that case, this drawback could be addressed by modifying the sorption conditions, i. e. the experimental parameters, optimizing the material preparation

or using an adequate additive. Furthermore, the experimental results indicate that the two hydrides could actually destabilise each other mutually. This becomes even more evident by comparing the dehydrogenation temperatures of all five composites: in contrast to the other four systems, $LiBH_4$-Mg_2NiH_4 evolves hydrogen already above approximately 275 °C. That is roughly 20 K lower than each of the onset temperatures of the other composites. Therefore, $LiBH_4$-Mg_2NiH_4 is a very interesting hydrogen storage solution that was investigated more thoroughly. These results are presented in section 3.2.

The Reactive Hydride Composite $Ca(BH_4)_2$-Mg_2NiH_4 is obviously a very interesting system due to its – for $Ca(BH_4)_2$ based hydrogen storage solutions – exceptional reaction mechanism. In particular the complete boron transfer from $Ca(BH_4)_2$ to $MgNi_{2.5}B_2$, i. e. the absence of stable boron sinks, after full dehydrogenation is remarkable and unique among all reversible $Ca(BH_4)_2$ based Reactive Hydride Composite. Also the clear indications of a reactivity between Mg_2Ni and decomposition products of $Ca(BH_4)_2$ are worth to be addressed with suitable experiments. Moreover, partial reversibility could already be achieved without any optimisations of the sorption conditions, the material preparations or the application of additives. In order to obtain more insights into this system and develop approaches to improve the degree of reversibility, $Ca(BH_4)_2$-Mg_2NiH_4 was the subject of further investigations. The results are described and discussed in section 3.3.

3.2 Reactive Hydride Composites based on $LiBH_4$ and Mg_2NiH_4

Motivated by the promising results introduced in section 3.1.1, more detailed experiments on the Reactive Hydride Composite $LiBH_4$-Mg_2NiH_4 are presented in this section. The first subsection is dedicated to the system $LiBH_4$-Mg_2NiH_4 with the molar ratio 2 : 2.5. Here a set of experiments that complement those shown in section 3.1.1 is reported. In the second subsection the sorption behaviour of the $4LiBH_4$-Mg_2NiH_4 system with the molar ratio 4 : 1 is investigated and described.

3.2.1 $LiBH_4$-Mg_2NiH_4: The RHC with the Molar Ratio 2 : 2.5

The system described in this section is "$2\,LiBH_4 + 2.5\,Mg_2NiH_4$". A set of experiments was conducted to shed light on the influence of the hydrogen pressure on the dehydrogenation reactions. Furthermore, the role of $Li_2B_{12}H_{12}$ or rather the consequence of its formation as a side product is investigated. Eventually, the reversibility of the sorption process is evaluated upon several hydrogen cycles to determine the cycling stability of this system's storage capacity.

3.2.1.1 Experimental Results

The influence of the hydrogen pressure on the dehydrogenation reactions The influence of the hydrogen back pressure on the dehydrogenation reactions of the $LiBH_4$-Mg_2NiH_4 system was determined by a set of complementary experiments. First, the dependency of the hydrogen evolution from the as-prepared material was monitored as a function of temperature at 1 bar, 5 bar and 50 bar H_2. The specimens were heated from room temperature to 400 °C at a rate of $5\,K\,min^{-1}$. The three volumetric analyses are presented in figure 3.16a. By increasing the hydrogen pressure, the dehydrogenation onset temperature shifts from 297 °C to 335 °C and eventually to 385 °C. Unlike the desorption measured at 1 bar that mainly proceeds in one step, the dehydrogenation process at 5 bar features an additional step: an alteration of the gas evolution rate can be perceived at a hydrogen loss of approximately 2 mass%. The determined total hydrogen capacities are similar for the two experiments conducted at 1 bar and 5 bar and amount to roughly 4.8 mass%. It should be noted that at both these pressures the last 0.4 mass% evolve at a slower rate. At a back pressure of 5 bar the desorption process requires several hours to reach a stable plateau. On the contrary, at 50 bar the dehydrogenation stops after the first step and no further release of gas is recorded up to 400 °C. Hence, at this pressure only 2 mass% of hydrogen evolve altogether.

The sequence of thermal transitions was determined by the set of DSC analyses shown in figure 3.16b. To ensure a reliable comparison between these results and the observed evolution of hydrogen (figure 3.16a), the same experimental conditions were applied as for the volumetric analyses. In the temperature range between 50 °C and 400 °C four endothermic thermal events are visible at all applied hydrogen pressures. The respective peaks are

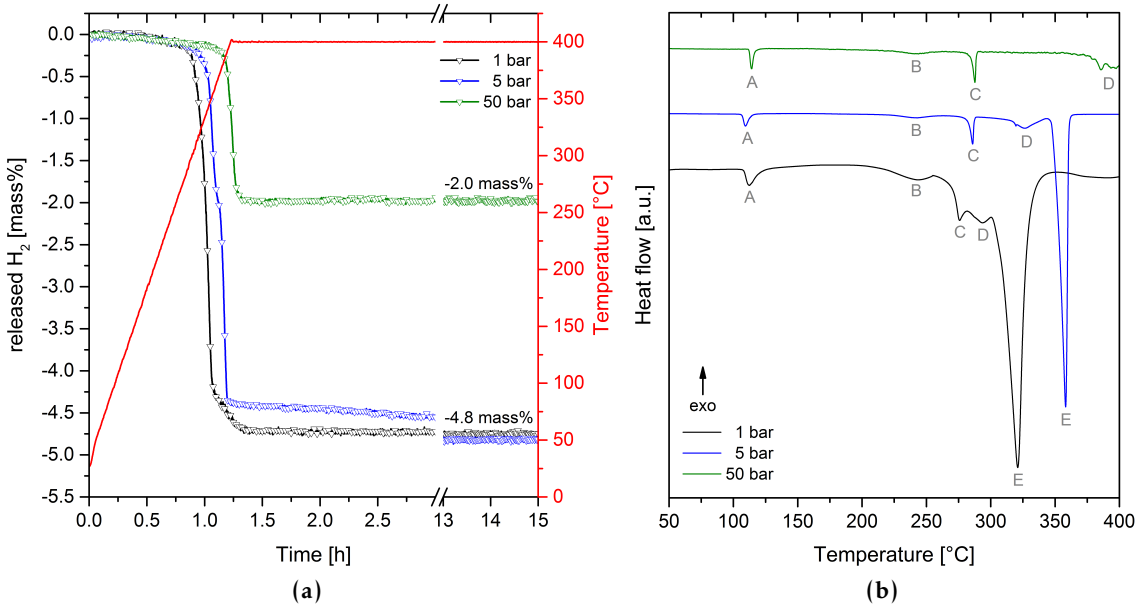

Figure 3.16: Dehydrogenation experiments of the $LiBH_4$-Mg_2NiH_4 system conducted at hydrogen pressures of 1 bar, 5 bar and 50 bar in the temperature range from RT to 400 °C: (a) volumetric analyses and (b) DSC analyses.

denoted by the letters A to D. In case of the two experiments conducted at 1 bar and 5 bar, a fifth endothermic event is discernible which is marked with the letter E. The first two transitions are not affected by the applied back pressure. Their onset temperatures are at roughly 110 °C (peak A) and 230 °C (peak B). At 5 bar and 50 bar H_2 also event C occurs at similar temperatures of about 280 °C. At 1 bar, however, it appears that the onset of this event is slightly shifted to a lower temperature value. Due to the partial overlap of the peaks C and D it is difficult to determine reliable, independent temperatures of these transitions, though. The onset of the superposition of the two peaks can be estimated at approximately 270 °C. In contrast to the other thermal events the transitions D and E feature an apparent pressure dependence. As just pointed out, at 1 bar H_2 the onset temperature of peak D cannot be determined clearly but should be lower than 280 °C. This temperature rises to 315 °C and eventually to about 375 °C if a back pressure of 5 bar and 50 bar is applied, respectively. Also the onset temperature of thermal event E cannot be determined clearly at 1 bar because the respective peak is partially overlapping with peak D. Nevertheless, this temperature is apparently lower than 300 °C and it increases to roughly 345 °C if the pressure is raised to 5 bar.

The chemical composition of the three samples after dehydrogenation was investigated by *ex situ* PXD and ^{11}B MAS NMR analyses (figure 3.17). As can be seen in figure 3.17a, for all hydrogen pressures the most intense X-ray reflections are those of $MgNi_{2.5}B_2$. In addition, all diffractograms contain the pattern of MgH_2. Magnesium can be identified only in the two samples dehydrogenated at 1 bar and 5 bar, though. No reflections of LiH are

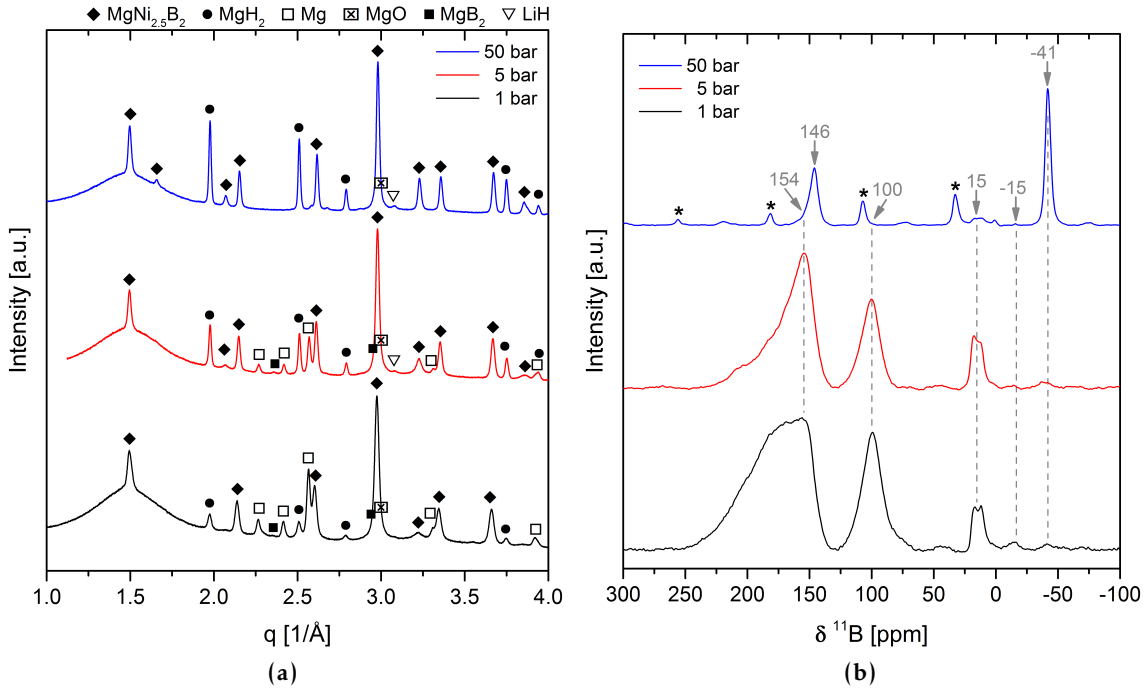

Figure 3.17: Determination of the chemical composition of the three $LiBH_4$-Mg_2NiH_4 samples desorbed at hydrogen pressures of 1 bar, 5 bar and 50 bar (figure 3.16a): (a) PXD analyses and (b) ^{11}B MAS NMR spectra (spinning sidebands are marked with asterisks ⋆).

visible in the diffractogram of the sample desorbed at 1 bar. However, after desorption at the higher pressures the weak (200) reflection can be distinguished. Although the contributions of MgO to the diffraction patterns are not that obvious, Rietveld refinements confirm the presence of small amounts (< 5 mass%) among the dehydrogenation products in all three samples. The chemical state of boron is assessed by means of the ^{11}B MAS NMR analyses. The respective three spectra are presented in figure 3.17b. The distribution of boron atoms in the samples dehydrogenated at 1 bar and 5 bar is similar: most of the boron atoms are bonded in $MgNi_{2.5}B_2$ (resonance at 154 ppm). Surprisingly, also a significant amount of MgB_2 (chemical shift 100 ppm) was formed: the molar ratio of boron atoms bonded in $MgNi_{2.5}B_2$ and MgB_2 is roughly 3 : 1 for both samples. Additionally, a signal at approximately 15 ppm is recorded in case of both these materials. This resonance can be attributed to B-O structures such as $Li_2B_4O_7$ [118, 119]. About 5 % of the boron atoms are bonded in these impurities. Furthermore, weak signals of residual $LiBH_4$ (chemical shift -41 ppm) are detected. The very low intensity of the $Li_2B_{12}H_{12}$ resonance at -15 ppm indicates a low concentration of this compound after dehydrogenation at 1 bar. At 5 bar this resonance barely stands out against the background. Qualitatively and quantitatively the ^{11}B MAS NMR spectrum of the material desorbed at 50 bar differs significantly from the other two. About 66 % of the boron atoms are still bonded in $LiBH_4$ and only 30 % were transferred to $MgNi_{2.5}B_2$. Moreover, no traces of MgB_2 and $Li_2B_{12}H_{12}$ are visible. Some impurities of lithium-boron oxides are

also detected among the dehydrogenation products in a similar concentration[2] as for the other two samples. It is noteworthy that the chemical shift, the width and the shape of the $MgNi_{2.5}B_2$ resonance change remarkably for the different back pressures. At 1 bar and 5 bar the centerband maxima are at roughly 154 ppm. However, the width of the $MgNi_{2.5}B_2$ resonance after dehydrogenation at 1 bar (FWHM ≈ 59 ppm) is substantially larger than the one after dehydrogenation at 5 bar (FWHM ≈ 27 ppm). In addition, the shapes of these peaks are highly asymmetrical, especially at 1 bar the intensity at frequencies higher than the peak maximum declines slowly. In contrast, the spectrum of the material dehydrogenated at 50 bar features a rather narrow (FWHM ≈ 8 ppm) and almost symmetrical $MgNi_{2.5}B_2$ resonance that can be approximated by a Gaussian-Lorentzian profile. At 146 ppm, its chemical shift also differs significantly from the frequencies measured for the other two samples. Compared to the as-synthesised $MgNi_{2.5}B_2$ that has a symmetrical resonance with a chemical shift of approximately 142 ppm (see figure 2.2b), the NMR spectrum of the material formed upon dehydrogenation at 50 bar shows by far the closest resemblance.

The considerable differences in the ^{11}B resonance signal of $MgNi_{2.5}B_2$ are caused by structural variations of this compound that should – to a certain extend – also affect its diffraction pattern. Indeed, upon close examination of the three diffractograms in figure 3.17a it is possible to notice alterations in the diffraction pattern of $MgNi_{2.5}B_2$. Besides different peak widths (decreasing with increasing back pressure) also variations in the relative reflection intensities are discernible. In order to quantify these variations and correlate them to changes of the atomic structure of the $MgNi_{2.5}B_2$ crystal, thorough Rietveld refinements of all three diffractograms in figure 3.17a were performed and compared to the respective analysis of as-synthesised $MgNi_{2.5}B_2$ (see figure 2.2a). The broad background elevation at about 1.5 $Å^{-1}$ caused by the PMMA dome of the sample holder impeded the preparation of good quality refinements. Therefore, the computation was restricted to the q-range from 1.6 $Å^{-1}$ to 5.5 $Å^{-1}$. For illustrative purpose, the final refinement of the diffractogram of the sample dehydrogenated at 5 bar is shown in figure 3.18a: besides the experimental data, the full refinement and the contributions of the individual compounds are presented as well as the residual plot. The two regions from 2.03 $Å^{-1}$ to 2.2 $Å^{-1}$ and from 3.15 $Å^{-1}$ to 3.4 $Å^{-1}$ are highlighted because they contain each one pair of $MgNi_{2.5}B_2$ reflections ((102)/(003) and (104)/(113)) that visualise well the variations in the relative peak intensities for the different dehydrogenation pressures. Both regions are shown enlarged in figure 3.18b. With respect to their neighbouring reflections, the intensities of the (102) and (104) peaks decrease when decreasing the hydrogen pressure. Furthermore, among the three diffractograms a systematic shift of the $MgNi_{2.5}B_2$ reflections (the lower the pressure, the lower the Bragg angles) becomes evident in the expanded view. If the as-synthesised $MgNi_{2.5}B_2$ is regarded as a reference, the corresponding diffraction pattern of this compound obtained upon de-

[2] Due to the high intensity and narrow peak width of the $LiBH_4$ resonance the relative peak intensities of the other phases appear rather low. The integration of center- and sideband areas confirms a fraction of impurities of approximately 5 %.

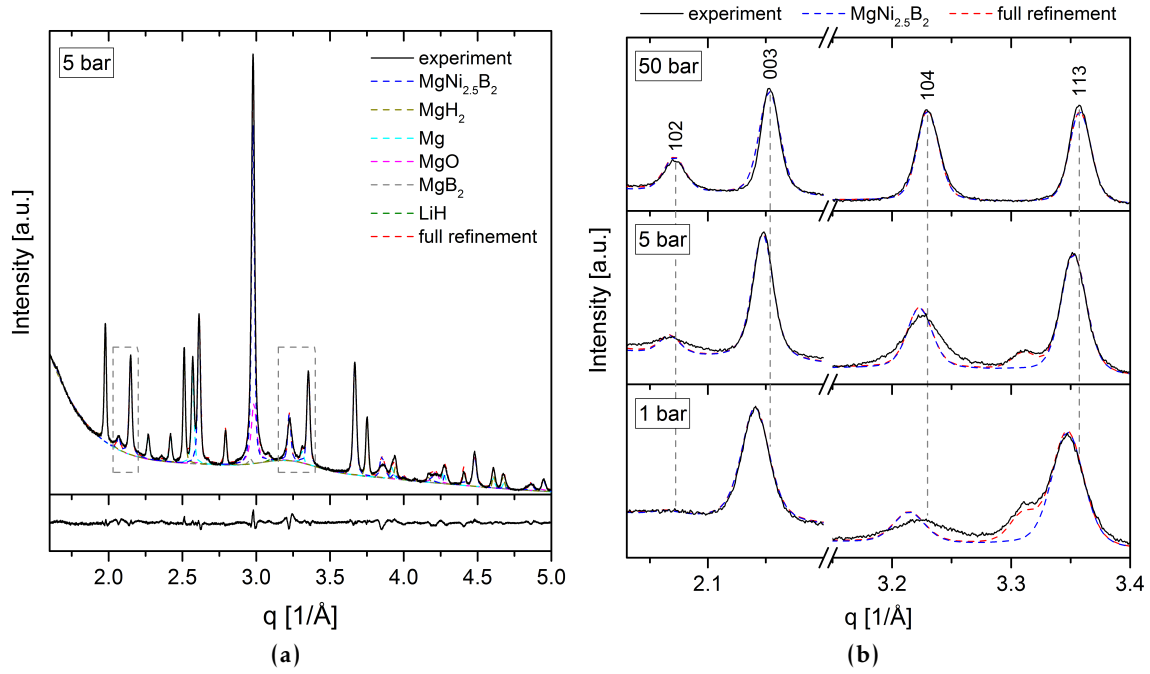

Figure 3.18: Rietveld refinements of the PXD analyses of the three dehydrogenated $LiBH_4$-Mg_2NiH_4 samples presented in figure 3.17a: (a) full refinement of the sample desorbed at 5 bar for the q-range from 1.6 $Å^{-1}$ to 5.5 $Å^{-1}$ and (b) detailed view on the two regions from 2.03 $Å^{-1}$ to 2.2 $Å^{-1}$ and from 3.15 $Å^{-1}$ to 3.4 $Å^{-1}$ to illustrate the modifications of the relative reflection intensities of $MgNi_{2.5}B_2$ for the different dehydrogenation pressures.

sorption of $LiBH_4$-Mg_2NiH_4 at 50 bar clearly shows the closest resemblance. This qualitative observation is supported by the quantitative Rietveld analyses. For the refinements of the diffratograms of the three desorbed samples, the phases $MgNi_{2.5}B_2$, MgH_2, LiH and MgO were considered. For 1 bar and 5 bar Mg and – as suggested by the NMR analyses – MgB_2 were additionally taken into account. The inclusion of the latter compound certainly improves the refinements. For instance, without the contribution of the MgB_2 (101) reflection the calculated intensity of the $MgNi_{2.5}B_2$ (200) reflection (at approximately 3 $Å^{-1}$) is too low to perfectly match the experimental diffraction intensity. In case of the diffraction pattern of the reference material (as-synthesised $MgNi_{2.5}B_2$), only the crystal structures of $MgNi_{2.5}B_2$ and MgO were considered in the refinement process. In order to reach suitable starting parameters for the refinements of the $MgNi_{2.5}B_2$ crystal structure, initially only the crucial parameters were optimised, i. e. the background, the sample displacement, the phase fractions, the cell parameters, the microstructures and the thermal factors. Once the fit could not be improved any further with the given set of free parameters, also the atomic parameters of $MgNi_{2.5}B_2$ (atom positions and site occupancies) were refined. For that purpose the initial atomic configuration was specified according to the ideal values of this crystal structure: all occupancies were set to 1 and all atoms were restricted to their specific sites, i. e. Ni atoms on sites 6*f* and 3*d*, Mg atoms on site 3*a* and boron atoms on site 6*i*. Since the possible substitution of Ni by Mg atoms – as described by Jung [85] – was not taken into account in the refinement process, the scattering capabilities of the atomic sites were solely adjusted by their total occupancies and thermal factors.[3] Initial values for the general atomic coordinates, i. e. those coordinates that do not coincide with symmetry elements of the space group, were taken from the structure reported by Jung [85]. In fact, most atomic coordinates in the $MgNi_{2.5}B_2$ crystal are special positions, i. e. they correspond to the space group's symmetry elements. Only the *z*-coordinate of site 6*f* (Ni) and the *x*- and *y*-coordinates of

[3] The total occupancy O_j of a Wyckoff site as well as the composition of atoms in this site (partial occupancy $\alpha_{n,j}$, $\sum_n \alpha_{n,j} = 1$) but also the thermal factor (mean squared displacement, $U_j = \langle {u_j}^2 \rangle$) influence the site's scattering capability and thus the relative reflection intensities. The intensity I_{hkl} of the reflection with the scattering vector $\vec{q} = \vec{G}_{hkl}$ depends on the structure factor F_{hkl}: $I_{hkl} \propto |F_{hkl}|^2$. This structure factor can be expressed as $F_{hkl} = \sum_j O_j \cdot \langle f_j \rangle \left(\vec{G}_{hkl}\right) \cdot \exp\left[-1/6 \left|\vec{G}_{hkl}\right|^2 \cdot U_j\right] \cdot \exp\left[i\, \vec{G}_{hkl} \cdot \vec{r}_j\right]$, where the sum is over all atoms (positions $\vec{r}_j$) in the basis. Here, $\langle f_j \rangle \left(\vec{G}_{hkl}\right) = \sum_n \alpha_{n,j} \cdot f_{n,j}\left(\vec{G}_{hkl}\right)$ denotes the mean atomic scattering factor which is determined by the ratio of the different types of atoms occupying the same site and their respective atomic scattering factors $f_{n,j}\left(\vec{G}_{hkl}\right)$. As can be seen, the total occupancy O_j solely scales the intensity of a wave scattered at a particular site with a factor between 0 and 1. Modifications of O_j do not affect the q-dependency of that site's scattering capability, though. Since the atomic scattering factors $f_{n,j}(q)$ of different elements are different functions of q, changes of the atomic composition in a site directly influence the course of the mean function $\langle f_j \rangle (q)$. Also the thermal factors U_j affect the intensity of a scattered wave as a function of the scattering vector q: the larger U_j (i. e. the larger the average displacement of the atoms from their equilibrium position), the larger the damping of the scattered wave. This damping increases with increasing q and is often described in the form of a Debye-Waller factor. In order to determine all three contributions to the scattering capability of a Wyckoff site with a reasonable degree of reliability and precision, the quality of the experimental data must be good. Unfortunately, the presented experimental results (uneven background, several phases overlapping, limited resolution of detector) do not allow a trustworthy separation of the described contributions. Therefore, in order to simplify the computation and obtain consistent results for all measurements, only total occupancies and thermal factors were refined.

Table 3.1: Refined parameters of the $MgNi_{2.5}B_2$ crystal for the three $LiBH_4$-Mg_2NiH_4 samples desorbed at different hydrogen pressures (figure 3.17a) and for the reference material (figure 2.2a): cell and atomic parameters were determined directly in the refinement. Atomic ratios are based on calculated occupancies. Discrepancy indices are given in form of weighted profile *R*-factors (R_{wp}) and background subtracted *R*-factors ($R_{wp,bs}$). The calculated occupancy of site 3*a* is 1 for all materials. Values related to boron atoms are depicted in grey due to the relatively high uncertainty.

			atomic parameters					
	cell parameters		site 6*f*		site 3*d*	site 6*i*	atomic ratio	
p_{des} [bar]	*a* [Å]	*c* [Å]	*z*	occ.	occ.	occ.	Mg : Ni : B	R_{wp} / $R_{wp,bs}$ [%]
1	4.892	8.847	0.187	0.87	0.81	0.88	1 : 2.55 : 1.76	2.5 / 10.3
5	4.889	8.816	0.197	0.92	0.91	0.63	1 : 2.75 : 1.26	2.3 / 9.8
50	4.886	8.798	0.206	0.99	1.00	0.53	1 : 2.98 : 1.06	1.7 / 6.4
ref.	4.883	8.793	0.207	1.00	1.00	1.00	1 : 3 : 2	2.8 / 9.8

site 6*i* (boron) are general positions. Due to the low sensitivity of the Rietveld refinement to parameters related to the boron atoms (weak atomic scattering factor) and the limitations of the experimental data, the parameters of site 6*i* could not be refined rigorously. Instead, the atomic coordinates were fixed to the literature values and solely the total occupancy as well as the thermal factor of this site were refined. The crucial parameters of these Rietveld analyses are summarised in table 3.1. The reference material has the smallest cell parameters and consequently the lowest cell volume of 181.57 $Å^3$. In addition, all site occupancies were calculated to be 1 yielding an atomic ratio of Mg : Ni : B = 1 : 3 : 2. With respect to this reference material the cell parameters of the $MgNi_{2.5}B_2$ crystals formed upon desorption of $LiBH_4$-Mg_2NiH_4 are enlarged. At cell volumes of 183.36 $Å^3$ at 1 bar, 182.49 $Å^3$ at 5 bar and 181.90 $Å^3$ at 50 bar, the unit cell expanded approximately 0.99 %, 0.51 % and 0.18 %, respectively, as compared to the as-synthesised $MgNi_{2.5}B_2$. This volume expansion, however, is mainly caused by a growth of the cell in *z*-direction: although cell parameter *c* increases by up to 0.61 %, cell parameter *a* only expands by maximum 0.18 %. Also the atomic parameters of the Ni atoms (sites 6*f* and 3*d*) show a similar behaviour: the lower the dehydrogenation pressure, the larger the discrepancy from the reference values. The calculated occupancies of site 3*a* (Mg) are 1 for all materials. Only the parameters of the boron atoms (site 6*i*) follow a different pattern. Here the highest occupancy was calculated for the structure formed at 1 bar. Instead, at 50 bar a site occupancy of only 0.53 was determined. Due to the low influence of boron on the diffraction pattern of $MgNi_{2.5}B_2$ and the fixation of the atomic coordinates of site 6*i*, the given occupancies of this site should be treated with care, though. Altogether, the resemblance to the as-synthesised material increases with increasing dehydrogenation pressure.

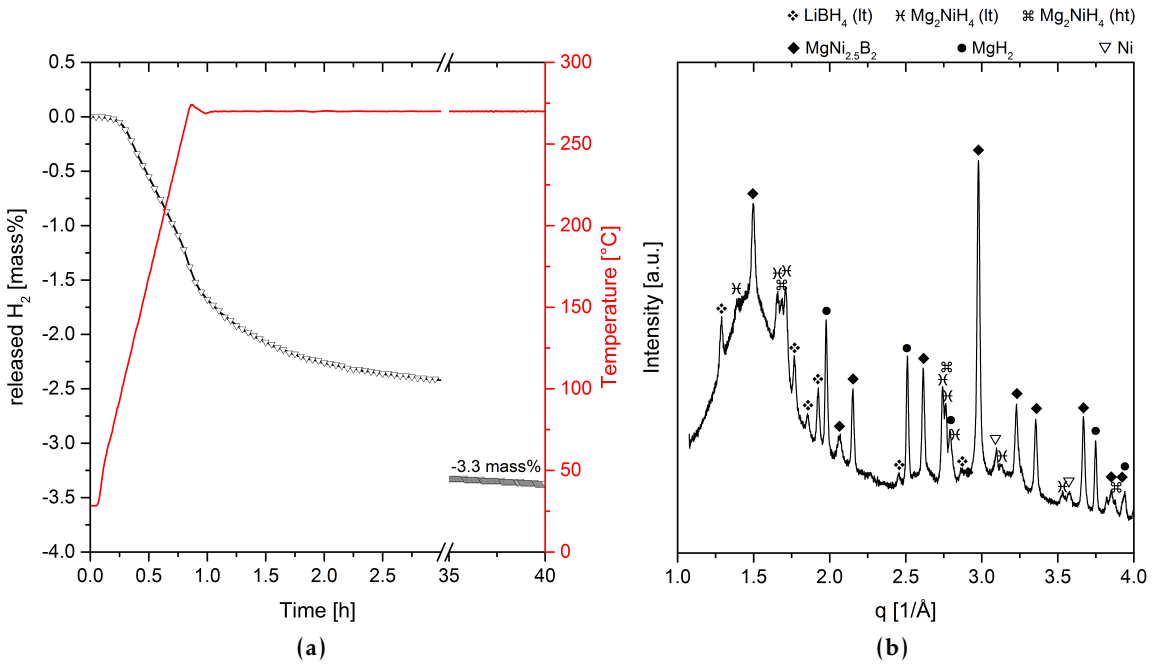

Figure 3.19: Dehydrogenation of the $LiBH_4$-Mg_2NiH_4 system at temperatures below the melting point of $LiBH_4$: (a) volumetric analysis conducted at a hydrogen pressure of 4 bar and a maximum temperature of 270 °C and (b) PXD analysis of the desorbed sample.

Reactivity at temperatures below the melting point of $LiBH_4$ The onset temperature of the reaction associated with the exothermic event D in the DSC analysis conducted at 1 bar (figure 3.16b) is lower than 280 °C and thus lower than the melting temperature of pure $LiBH_4$ [108, 120]. This observation hints at the possibility that Mg_2NiH_4/Mg_2Ni also interacts with solid $LiBH_4$ in a reaction that leads to releasing hydrogen. To verify this assumption, a specimen of $LiBH_4$-Mg_2NiH_4 was heated to 270 °C, i. e. the temperature was kept below the melting point of $LiBH_4$. In addition, a hydrogen pressure of 4 bar was applied to prevent the decomposition of Mg_2NiH_4. The volumetric analysis of this experiment is shown in figure 3.19a. A release of gas could be observed already below 200 °C. Although about 2 mass% of hydrogen were released within the first 90 min of the experiment, the reaction kinetics slowed down significantly afterwards. At termination of the experiment, i. e. after a dwell time of 40 h at 270 °C, only approximately 3.3 mass% H_2 were released. After cooling the specimen down to room temperature the consistency and structure of the material was analysed. It can be described as homogeneous, fluffy powder with very low mean particle size. No hints of a possible melting of $LiBH_4$ were found. The chemical composition of the sample was determined by means of a PXD analysis (figure 3.19b). Besides the reflections of unreacted Mg_2NiH_4 and $LiBH_4$ also those of $MgNi_{2.5}B_2$ and MgH_2 were identified.

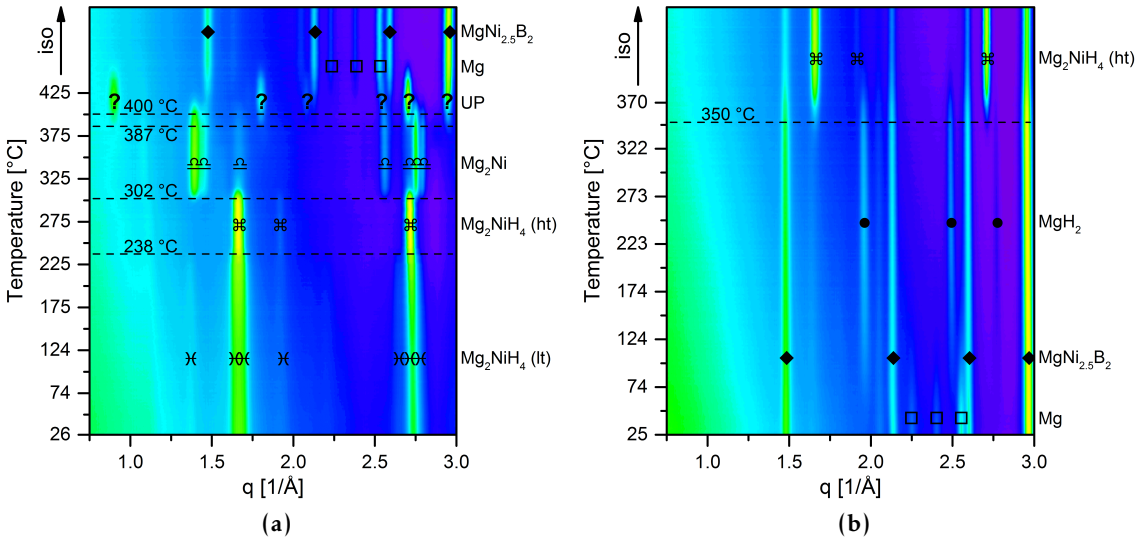

Figure 3.20: SR-PXD experiments demonstrating the reactions between Mg_2NiH_4 and $Li_2B_{12}H_{12}$: (a) dehydrogenation at 1 bar and a maximum temperature of 425 °C and (b) subsequent rehydrogenation at 160 bar and a maximum temperature of 370 °C.

The interaction between Mg_2NiH_4 and $Li_2B_{12}H_{12}$ The ^{11}B NMR spectrum of the composite $LiBH_4$-Mg_2NiH_4 dehydrogenated at 1 bar H_2 (figure 3.17b) only contains a very weak signal that can be attributed to $Li_2B_{12}H_{12}$. However, if pure $LiBH_4$ or composites containing this borohydride are heated above 350 °C without sufficient hydrogen back pressure $Li_2B_{12}H_{12}$ is usually formed in much higher quantities [121–123]. In addition, the volumetric analyses conducted at 1 bar and 5 bar (figure 3.16a) reveal that the last approximately 0.4 mass% of hydrogen are released at noticeably reduced rates. This observation could be related to reactions involving $Li_2B_{12}H_{12}$. Altogether, it appears reasonable to assume that Mg_2NiH_4/Mg_2Ni could react with $Li_2B_{12}H_{12}$ if this compound occurs during dehydrogenation. Since the processes considered here are intermediate reactions, their study is not possible by means of the *ex situ* analyses performed after full dehydrogenation of $LiBH_4$-Mg_2NiH_4. Hence, in order to verify the assumption, Mg_2NiH_4, $Li_2B_{12}H_{12}$ and LiH were mixed in a molar ratio of 15 : 1 : 10. This compositions theoretically allows for the bonding of all boron in $MgNi_{2.5}B_2$ and $LiBH_4$, respectively. A sample of this material was investigated in an *in situ* SR-PXD experiment (figure 3.20). First, this sample was dehydrogenated at a pressure of 1 bar H_2 by heating it from room temperature to 425 °C at a rate of 5 K min^{-1}. After a dwell time of 40 min the sample was cooled down to room temperature. For the subsequent rehydrogenation the hydrogen pressure was raised to 160 bar and the sample temperature was increased to 370 °C at 5 K min^{-1}. After an isothermal heating period of 20 min the experiment was eventually terminated. As can be seen in figure 3.20a, the diffractogram of as-milled material that was collected at room temperature only exhibits intense reflections of Mg_2NiH_4 (lt and ht). At about 238 °C the polymorphic conversion of this hydride is observed i. e. afterwards solely the reflections of the high-temperature form

remain present up to approximately 302 °C. At this temperature Mg_2NiH_4 decomposes and the diffraction pattern of Mg_2Ni arises. At 387 °C the reflections of UP become discernible. Shortly after, at roughly 400 °C, also those of $MgNi_{2.5}B_2$ and Mg emerge. In contrast to the reflections of UP which fade completely in the isothermal period, the diffraction intensities of $MgNi_{2.5}B_2$ and Mg maximise and stabilise in conjunction with the disappearance of UP. Also after cooling down to room temperature $MgNi_{2.5}B_2$ and Mg remain the only diffractive compounds that are discernible with the given experimental resolution (figure 3.20b). The consecutive hydrogenation at 160 bar begins with the conversion of Mg into MgH_2 (figure 3.20b). This process starts already at temperatures lower than 75 °C. However, the second hydrogen absorption step only occurs above 350 °C, i. e. above the melting temperature of $LiBH_4$. The reflections of cubic Mg_2NiH_4 emerge whilst those of $MgNi_{2.5}B_2$ and MgH_2 weaken. The diffraction peaks of the two latter compounds diminish continuously during the isothermal dwell time – MgH_2 almost vanishes. As opposed to this, the diffraction pattern of Mg_2NiH_4 intensifies until the termination of the experiment.

Reversibility upon hydrogen cycling With regard to the utilisation of hydrogen storage systems for technical applications the reversibility of the sorption processes is essential. The agglomeration of inert side products, phase segregation or the development of large, reaction-inhibiting microstructures are phenomena that diminish the system's hydrogen capacity and/or its sorption rates steadily. Thus, it is crucial to investigate such issues in order to adopt appropriate measures to avoid or minimise them. Typically, a first step to carefully characterise the reversibility of a hydrogen storage system is the monitoring of hydrogen release and uptake over several full sorption cycles. Unfortunately, the high absorption pressures of $LiBH_4$-Mg_2NiH_4 prohibit the use of the volumetric apparatuses for these kind of cycling experiments. Therefore, the cycling of the material had to be performed in a temperature controlled autoclave. As a consequence, the storage capacity could not be recorded for the individual cycles. Instead, nine full sorption cycles were performed consecutively. For the dehydrogenation periods a temperature of 420 °C and a hydrogen pressure of 5 bar were applied. The nine rehydrogenations were conducted at 360 °C and pressures between 200 bar and 250 bar. Each of these sorption steps was carried out for at least 15 h. Eventually, the material was removed from the autoclave in the hydrogenated state allowing to monitor the tenth desorption iteration with the volumetric apparatus. In figure 3.21a the temperature dependent release of hydrogen is shown for the first and the tenth dehydrogenation. Although the onset of the desorption reactions appears to be shifted to slightly higher temperatures after cycling, the overall kinetics remain almost unchanged. In total, the cycled material evolved about 4.3 mass% H_2. In comparison to the as-milled sample (4.8 mass%), this corresponds to a reduction of the hydrogen content of approximately 10 %. The chemical composition of the sample after the ninth reabsorption and after the tenth desorption was determined by PXD analyses (figure 3.21b). As can be seen, intense reflections of Mg_2NiH_4 (lt and ht) and $LiBH_4$ dominate the diffraction pattern

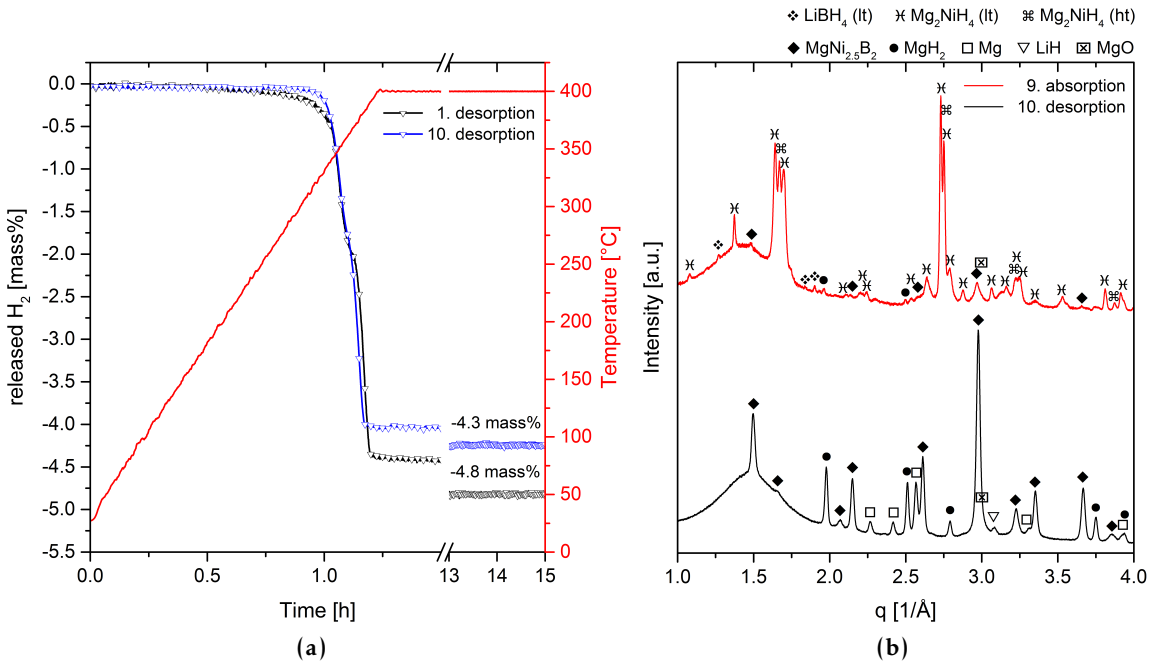

Figure 3.21: Reversibility of the $LiBH_4$-Mg_2NiH_4 system upon hydrogen cycling: (a) comparison of the volumetric analyses of the first and tenth dehydrogenation and (b) PXD analyses of cycled material after the ninth rehydrogenation and the tenth dehydrogenation.

of the hydrogenated material. However, also weak reflections of $MgNi_{2.5}B_2$ and MgO are visible. The diffractogram of the desorbed sample is composed of the reflections of $MgNi_{2.5}B_2$ and Mg but also a small fraction of MgO can be distinguished. However, no other nickel containing phases are detected, especially no Mg_2Ni.

3.2.1.2 Discussion

The dehydrogenation path of $LiBH_4$-Mg_2NiH_4 strongly depends on the applied experimental conditions i. e. the hydrogen back pressure and the temperature. The variation of the hydrogen pressure in the non-isothermal experiments revealed some exceptional properties of this hydride composite. In case of the experiments conducted at 1 bar, the reactions mainly proceed as described in section 3.1.1. A pattern similar to most other hydride composites was discovered: dehydrogenation starts with the decomposition of the least stable hydride, i. e. Mg_2NiH_4. In contrast, if the hydrogen pressure is high enough to prevent the independent desorption of Mg_2NiH_4 another reaction path can be observed. The very first dehydrogenation step is identified as a concerted reaction between $LiBH_4$ and Mg_2NiH_4. The evidence for this behaviour is provided by the DSC analyses presented in figure 3.16b. The peaks in these analyses were denoted with the letters A to E. The first three of them can be clearly attributed to thermal transitions of the individual hydrides: peak A and B are related to the polymorphic changes of $LiBH_4$ (low-temperature orthorhombic to high-temperature hexagonal) [103, 124] and Mg_2NiH_4 (low-temperature monoclinic to high-temperature cubic)

[72, 73], respectively, and peak C to the melting of $LiBH_4$ [108, 120]. Also peak E can be identified unambiguously as decomposition of MgH_2[4] [19, 125]. Since the equilibrium temperature of this hydride exceeds 400 °C at a pressure of 50 bar, its decomposition is not observed in the respective DSC analysis. The peaks denoted with the letter D are related to the reactions between $LiBH_4$ and Mg_2NiH_4 or Mg_2Ni. The comparison of the *in situ* SR-PXD experiment conducted at a pressure of 1 bar (figure 3.3) with the respective DSC analysis shows that at this pressure the dehydrogenation starts with the decomposition of Mg_2NiH_4. Shortly after the appearance of the Mg_2Ni reflections also those of $MgNi_{2.5}B_2$ and MgH_2 arise. The formation of the latter two compounds also explains the low intensity of peak D in the DSC analysis: the exothermic reactions creating $MgNi_{2.5}B_2$ and MgH_2 partially compensate for the enthalpy that is required for the endothermic desorption of Mg_2NiH_4. However, already at a pressure of 5 bar a significant difference in the dehydrogenation process can be identified. At 315 °C the onset of peak D is lower than the equilibrium temperature of Mg_2NiH_4 ($T_{eq}(5\,bar) > 320\,°C$). Consequently, the first dehydrogenation step of the composite $LiBH_4$-Mg_2NiH_4 is a direct reaction between the two hydrides. This becomes even more obvious when evaluating the DSC analysis conducted at 50 bar. At this pressure the decomposition temperature of Mg_2NiH_4 is higher than 440 °C but the onset of peak D is at only 375 °C. Supported by the PXD analyses (figure 3.17a) the chemical equation of this concerted reaction can be depicted as

$$2\,LiBH_4 + 2.5\,Mg_2NiH_4 \xrightarrow{\text{concerted}} 2\,LiH + MgNi_{2.5}B_2 + 4\,MgH_2 + \underbrace{4\,H_2}_{2.5\,\text{mass\%}}. \tag{3.9}$$

It is noteworthy that the enthalpy of this reaction is remarkably low. This can be easily seen by the comparison of the areas of the two DSC peaks D and E at a hydrogen pressure of 5 bar. The area of peak D (chemical equation 3.9) is significantly smaller than the area of peak E (decomposition of MgH_2). To be exact, area D covers only about 18 % of area E. However, in both reactions the same amount of hydrogen is released, namely 4 moles per formula unit. Consequently, the enthalpy of reaction 3.9 can be directly estimated from the ratio of the peak areas and the known enthalpy of MgH_2 ($74.4\,kJ\,(mol\,H_2)^{-1}$, [19]). At roughly $13\,kJ\,(mol\,H_2)^{-1}$ the experimentally determined enthalpy is significantly lower than those of common, reversible hydrides and hydride composites. Considering this low reaction enthalpy, a rehydrogenation of the desorption products would be impossible at the temperature and pressure conditions employed in the absorption experiments if the entropy change associated with the hydrogenation reaction was similar to those of typical hydrides such as MgH_2 or Mg_2NiH_4 (i. e. ΔS well above $100\,J\,(K\,mol\,H_2)^{-1}$) because the equilibrium pressure would be extremely high. Since rehydrogenation was successful at moderate gas pressures, also the entropy change of reaction 3.9 must be exceptionally low. In fact, Vajo *et al.*

[4] The presence of MgH_2 reflections in the diffraction patterns of the two $LiBH_4$-Mg_2NiH_4 samples desorbed at 1 bar and 5 bar (figure 3.17a), respectively, must be attributed to the rehydrogenation of Mg upon cooling down.

were able to estimate thermodynamic data for the composite $LiBH_4$-Mg_2NiH_4 by means of a sequence of non-equilibrium measurements [78]. They performed absorption and desorption experiments with varying hydrogen pressures at several constant temperatures and evaluated the sorption rate. With the assumption that this rate becomes zero if the pressure converges to the equilibrium pressure, the authors could estimate a set of $p_{eq}(T)$-values and construct a van 't Hoff diagram. At 15.4 kJ $(\mathrm{mol\,H_2})^{-1}$ the extracted reaction enthalpy is fairly low but in good agreement with the value determined in this work. The entropy change was specified with 62.2 J $(\mathrm{K\,mol\,H_2})^{-1}$. This value is – as expected – rather low, too. Vajo *et al.* attributed the low entropy change to the properties of the hydrogenated state. They assumed a comparatively high entropy associated with having the two complex hydride anions $[BH_4]^-$ and $[NiH_4]^{4-}$. However, this explanation is not satisfactory because the entropy change for the decomposition of pure Mg_2NiH_4 is reported to be 122.2 J $(\mathrm{K\,mol\,H_2})^{-1}$ [71]. That is almost the entropy value generated with the release of gaseous hydrogen ($S_{300\,K}(H_2) = 130.77\,\mathrm{J\,(K\,mol)^{-1}}$, [16]) suggesting that the moderate entropy excess of Mg_2NiH_4 with respect to Mg_2Ni cannot explain the low entropy change of reaction 3.9. In order to survey the plausibility of the given values, thermodynamic data of several chemical reactions was taken from the literature. Subsequently these reactions were deconstructed and recombined to find estimates for the enthalpy and entropy changes in question. Thermodynamic properties associated with the formation of $MgNi_{2.5}B_2$ are not easy to assess because no independent data is reported in the literature. Therefore, the formation of this compound is evaluated with the help of two additional reactions. The first is the one between $NaBH_4$ and Mg_2Ni as reported by Afonso *et al.*:

$$2\,NaBH_4 + 2.5\,Mg_2Ni \longrightarrow 2\,NaH + MgNi_{2.5}B_2 + 4\,Mg + 3\,H_2. \tag{3.10}$$

For this reaction an enthalpy change of 76 kJ $(\mathrm{mol\,H_2})^{-1}$ was measured. The stated value for the entropy change is 113 J $(\mathrm{K\,mol\,H_2})^{-1}$. The second reaction considered in this context is the decomposition of $NaBH_4$ occurring *via*

$$NaBH_4 \longrightarrow NaH + B + 3/2\,H_2. \tag{3.11}$$

It should be pointed out that this reaction path is purely hypothetical. In reality NaH is not stable at the dehydrogenation conditions of $NaBH_4$ which is why the latter compound actually decomposes into liquid Na, boron and hydrogen [126]. Nevertheless, the standard enthalpies of formation ΔH_f^0 and the standard molar entropies S^0 of $NaBH_4$, NaH, boron and hydrogen are listed in the NIST Chemistry WebBook [127] and summarised in table 3.2. By means of these values the reaction enthalpy and entropy of chemical equation 3.11 can be calculated to 90.3 kJ $(\mathrm{mol\,H_2})^{-1}$ and 93.8 J $(\mathrm{K\,mol\,H_2})^{-1}$, respectively. The combination of

Table 3.2: Standard enthalpies of formation ΔH_f^0 and standard molar entropies S^0 of $NaBH_4$, NaH, boron and hydrogen according to the NIST Chemistry WebBook [127].

compound	ΔH_f^0 $\left[\mathrm{kJ\,mol^{-1}}\right]$	S^0 $\left[\mathrm{J\,(K\,mol)^{-1}}\right]$
$NaBH_4$	-191.8	101.5
NaH	-56.4	40.0
B	0	5.9
H_2	0	130.7

reactions 3.10 and 3.11 allows to determine the enthalpy and entropy change of the reaction

$$2.5\,Mg_2Ni + 2\,B \longrightarrow MgNi_{2.5}B_2 + 4\,Mg \tag{3.12}$$

to −42.8 kJ and 57.8 $\mathrm{J\,K^{-1}}$ per formula unit. Furthermore, in order to estimate the thermodynamics of the concerted reaction 3.9 the decomposition of liquid $LiBH_4$ occurring *via* the reaction path

$$LiBH_4(\mathrm{liquid}) \longrightarrow LiH + B + 3/2\,H_2 \tag{3.13}$$

is considered. According to Price *et al.* the changes of enthalpy and entropy for this reaction are 58.6 $\mathrm{kJ\,(mol\,H_2)^{-1}}$ and 80.1 $\mathrm{J\,(K\,mol\,H_2)^{-1}}$, respectively [128]. Whilst taking into account the dehydrogenation paths and the associated enthalpy and entropy changes of pure Mg_2NiH_4 (64.4 $\mathrm{kJ\,(mol\,H_2)^{-1}}$ and 122.2 $\mathrm{J\,(K\,mol\,H_2)^{-1}}$, [71]) as well as pure MgH_2 (74.4 $\mathrm{kJ\,(mol\,H_2)^{-1}}$ and 135.1 $\mathrm{J\,(K\,mol\,H_2)^{-1}}$, [19]), the combination of reactions 3.12 and 3.13 makes it possible to estimate the enthalpy and entropy changes for the dehydrogenation of $LiBH_4$-Mg_2NiH_4. For that purpose a hypothetical reaction scheme with three individual steps is constructed:

$$\begin{aligned} &2\,LiBH_4 + 2.5\,Mg_2NiH_4 \\ &\longrightarrow 2\,LiH + 2\,B + 2.5\,Mg_2Ni + 8\,H_2 && (3.14)\\ &\longrightarrow 2\,LiH + MgNi_{2.5}B_2 + 4\,Mg + 8\,H_2 && (3.15)\\ &\longrightarrow 2\,LiH + MgNi_{2.5}B_2 + 4\,MgH_2 + 4\,H_2. && (3.16) \end{aligned}$$

The reaction enthalpies and entropies for the steps 3.14, 3.15 and 3.16 are 62.2 $\mathrm{kJ\,(mol\,H_2)^{-1}}$ and 106.4 $\mathrm{J\,(K\,mol\,H_2)^{-1}}$, −42.8 kJ and 57.8 $\mathrm{J\,K^{-1}}$ per formula unit and −74.4 $\mathrm{kJ\,(mol\,H_2)^{-1}}$ and −135.1 $\mathrm{J\,(K\,mol\,H_2)^{-1}}$, respectively. Consequently, according to the given literature data the overall reaction – i. e. the concerted reaction 3.9 – features an enthalpy change of 39.4 $\mathrm{kJ\,(mol\,H_2)^{-1}}$ and an entropy change of 92.2 $\mathrm{J\,(K\,mol\,H_2)^{-1}}$. These values do not support the exceptionally low reaction enthalpies determined in this work and by Vajo *et al.* Also the extraordinarily low entropy change reported by Vajo *et al.* is not confirmed. However,

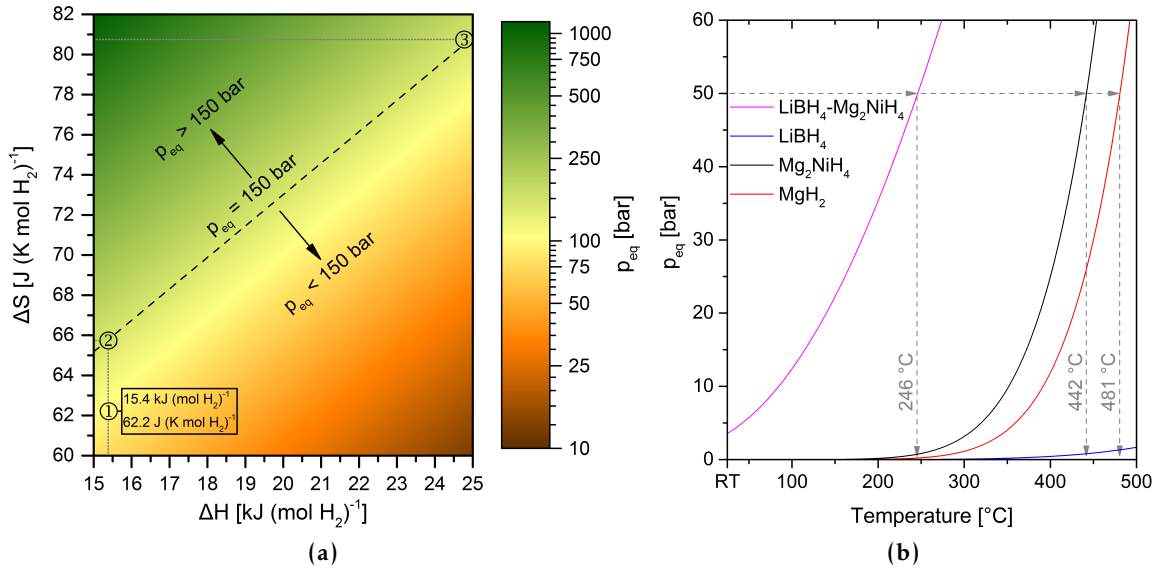

Figure 3.22: Assessment of the thermodynamic properties of the $LiBH_4$-Mg_2NiH_4 system: (a) equilibrium pressure of a general sorption process at 365 °C as a function of the reaction enthalpy ΔH and the entropy change ΔS, the plateau pressure of the concerted reaction 3.9 is located in the lower left part of the diagram ($p_{eq}(365\,°C) < 150\,bar$), (b) equilibrium pressures as a function of the temperature for reaction 3.9 and for the pure compounds $LiBH_4$, Mg_2NiH_4 and MgH_2.

the calculated enthalpy and entropy changes associated with the formation of $MgNi_{2.5}B_2$ are dubious. These calculations rely partially on the data provided by Afonso *et al.* [80]. On closer examination of their raw data it is clear that their results are subject to considerable uncertainty, though. Unfortunately, no other publications on this topic are available that could contribute more trustworthy results. Nevertheless, the close resemblance between the enthalpy values determined for the concerted reaction 3.9 in this work (about 13 kJ $(mol\,H_2)^{-1}$) and by Vajo *et al.* (15.4 kJ $(mol\,H_2)^{-1}$) lets the magnitude appear reasonable. In figure 3.22a the equilibrium pressure of a general sorption process is drawn as a function of the reaction enthalpy and entropy at a temperature of 365 °C. Since rehydrogenation of desorbed $LiBH_4$-Mg_2NiH_4 was successfully performed at 365 °C and a hydrogen pressure of 150 bar, this pressure represents an upper limit for the equilibrium pressure of reaction 3.9. As can be seen, the reaction enthalpy reported by Vajo *et al.* demands an entropy change of less than 66 J $(K\,mol\,H_2)^{-1}$ (point 2). Even if the true reaction enthalpy exceeded the reported value of 15.4 kJ $(mol\,H_2)^{-1}$ by roughly two thirds, the entropy change still would be restricted to values of less than 81 J $(K\,mol\,H_2)^{-1}$ (point 3). Consequently, assuming the enthalpy values determined in this work and by Vajo *et al.* are in the right magnitude, entropy changes of less than 70 J $(K\,mol\,H_2)^{-1}$ are plausible. Unlike the explanation attempt given by Vajo *et al.* not high entropy of the absorbed state is responsible for the low entropy change but rather the reduced entropy of the desorbed state: in reaction 3.9 liquid $LiBH_4$, a high-entropy hydride, and Mg_2NiH_4 decompose but only 50 % of the hydrogen is released into the gas phase. The other half is stored in the low-entropy hydride MgH_2 effectively reducing the entropy change

upon desorption.

Substantiated by these inferences, the equilibrium pressure of $LiBH_4$-Mg_2NiH_4 was calculated based on the thermodynamic data reported by Vajo *et al.* (point 1 in figure 3.22a) and compared to the respective pressures of Mg_2NiH_4, MgH_2 and $LiBH_4$. This is shown in figure 3.22b. At 50 bar H_2 only the composite material features an equilibrium temperature of less than 400 °C confirming once again that the dehydrogenation process observed in the volumetric and DSC analyses is indeed a concerted reaction. However, it can be seen that the measured dehydrogenation onset of this reaction (about 375 °C) is much higher than the calculated equilibrium temperature of 246 °C. Most likely this discrepancy must be attributed to poor kinetic properties. This assumption is supported by the non-isothermal experiments conducted at 1 bar (*in situ* SR-PXD and DSC analyses in figures 3.3 and 3.16b). Although the calculated equilibrium temperature of the concerted reaction is approximately −25 °C at this pressure, the dehydrogenation process starts with the decomposition of Mg_2NiH_4 only at temperatures above 270 °C. It seems that in these experiments with quickly rising temperature the high activation energy of the mutual reaction between $LiBH_4$ and Mg_2NiH_4 does not allow a discernible reaction rate before the decomposition temperature of Mg_2NiH_4 is reached. Nevertheless, also at comparatively low temperatures the concerted reaction can be observed, provided the independent decomposition of Mg_2NiH_4 is inhibited and sufficient time is granted. Even at temperatures below the melting point of $LiBH_4$ the two hydrides effectively destabilise each other. This process is rather unusual because the high kinetic barriers of $LiBH_4$ typically prevent its dehydrogenation in the solid-state. Thus, the discovered behaviour points towards a large driving force (highly negative change of the free energy ΔG) for the mutual reaction which is in agreement with the large deviation between the calculated sorption equilibrium and the measured onset temperature.

After dehydrogenation of $LiBH_4$-Mg_2NiH_4 at 1 bar and 5 bar MgB_2 is identified among the desorption products. This compound is formed in the side reaction between Mg and yet unreacted $LiBH_4$. Upon desorption at 50 bar MgH_2 is stable and, therefore, no MgB_2 is formed. The presence of this compound demands a modification of reaction scheme 3.2 introduced in section 3.1.1. If $LiBH_4$ is partially consumed in the side reaction forming MgB_2 one would expect to find residual Mg_2Ni among the desorption products, i. e. an overall reaction according to

$$\begin{aligned} 2\,LiBH_4 + 2.5\,Mg_2NiH_4 \longrightarrow\ & 2\,LiH + x\,MgNi_{2.5}B_2 + (5x-1)\,Mg + \\ & + 2.5\,(1-x)\,Mg_2Ni + (1-x)\,MgB_2 + \underbrace{8\,H_2}_{5.0\,\text{mass\%}}. \end{aligned} \tag{3.17}$$

Here $x \in [0.2, 1]$ would be understood as a kinetic parameter describing the amount of produced MgB_2. However, no traces of Mg_2Ni could be detected in the powder diffractograms. In fact, except for $MgNi_{2.5}B_2$ no other Ni-containing compounds are discernible in the PXD analyses (figure 3.17a). In addition, no signals of non-diffractive Ni-B based phases are

identified in the NMR spectra (figure 3.17b). Thus, all Ni atoms in these samples must be bonded in $MgNi_{2.5}B_2$. Since boron is partially bonded in MgB_2, the atomic composition of the Mg-Ni-B compound formed upon dehydrogenation at 1 bar and 5 bar must differ from the expected ratio of 1 : 2.5 : 2. This finding could be explained by a certain homogeneity range of $MgNi_{2.5}B_2$, i. e. by a range of atomic compositions with (almost) the same crystal structure (e. g. partial occupancy or atomic substitution). This assumption can also be motivated by the results of the Rietveld analyses (table 3.1). Accordingly, the following modified reaction scheme for $LiBH_4$-Mg_2NiH_4 at 1 bar and 5 bar can be depicted:

$$\begin{aligned} 2\,LiBH_4 + 2.5\,Mg_2NiH_4 \longrightarrow\ & 2\,LiH + Mg_{y(4+x)}Ni_{2.5}B_{2x} + \\ & + (1-y)(4+x)\,Mg + (1-x)\,MgB_2 + \underbrace{8\,H_2}_{5.0\,\text{mass\%}}. \end{aligned} \tag{3.18}$$

The parameter $x \in [0,1]$ specifies the amount of produced MgB_2 but simultaneously determines the ratio of nickel and boron in $MgNi_{2.5}B_2$. Also in this reaction scheme x can be considered as a kinetic parameter that depends on the experimental conditions such as the hydrogen pressure, the heating rate and the maximum temperature but also on certain properties related to the sample itself like the particle size or the presence of impurities. Hence, it can be assumed that different experimental conditions and sample preparations result in different values for x. The parameter $y \in [0,1]$ is linked to structural properties of $MgNi_{2.5}B_2$. Besides the amount of free magnesium it describes the ratio of magnesium and nickel within $MgNi_{2.5}B_2$ and is, therefore, related to their respective site occupancies and substitutional effects. Based on the chemical compositions of the desorbed samples as determined by the PXD and NMR analyses and supported by the Rietveld refinements of the atomic parameters of $MgNi_{2.5}B_2$ (table 3.1), the existence of the aforementioned homogeneity range of this compound must be considered the most plausible explanation for the experimental results. Consequently, "*$MgNi_{2.5}B_2$*" should rather be considered a name than an accurate expression of the actual chemical composition of this Mg-Ni-B phase. For convenience this name is used throughout the whole thesis in order to refer to this compound, though.

The temperature and pressure dependent reaction paths and steps can be summarised and visualised in a simplified schematic reaction diagram (disregarding UP and $Li_2B_{12}H_{12}$) as shown in figure 3.23. The formation enthalpies of the different states are calculated with respect to the fully absorbed state (state 1) that was defined as ground level (0 kJ). The calculations are based on the dehydrogenation enthalpies of Mg_2NiH_4 and MgH_2 reported by Reilly *et al.* [71] and Stampfer *et al.* [19], respectively. In addition, the enthalpy change determined by Vajo *et al.* [78] – which is similar to the value measured in this work – was assumed for the concerted reaction 3.9 i. e. the transition from state 1 to state 2. The formation enthalpy of state 5 depends on the parameters x and y and, therefore, is not a fixed value. Since $MgNi_{2.5}B_2$ can be synthesised from MgB_2 and Ni (see section 2.1.2), this compound must have a more negative standard formation enthalpy (on a per atom basis)

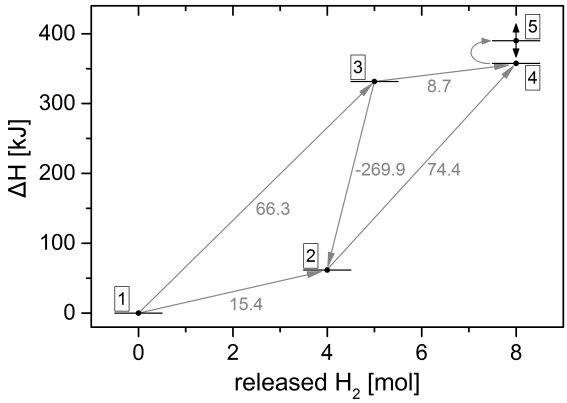

state	composition
1	$2\,LiBH_4 + 2.5\,Mg_2NiH_4$
2	$2\,LiH + MgNi_{2.5}B_2 + 4\,MgH_2 + 4\,H_2$
3	$2\,LiBH_4 + 2.5\,Mg_2Ni + 5\,H_2$
4	$2\,LiH + MgNi_{2.5}B_2 + 4\,Mg + 8\,H_2$
5	$2\,LiH + Mg_{y(4+x)}Ni_{2.5}B_{2x} + + (1-y)(4+x)\,Mg + (1-x)\,MgB_2 + 8\,H_2$

Figure 3.23: Simplified schematic reaction diagram for the $LiBH_4$-Mg_2NiH_4 Reactive Hydride Composite: five thermodynamic states are identified (disregarding UP and $Li_2B_{12}H_{12}$). The grey values at the arrows indicate the reaction enthalpies in kJ $(mol\,H_2)^{-1}$ for the different transitions.

as compared to MgB_2. Consequently, state 5 has the highest formation enthalpy among the five states considered in diagram 3.23. If $LiBH_4$-Mg_2NiH_4 is heated up steadily, the reaction path from state 1 to state 2 is thermodynamically the most favourable and should be enabled first. However, high kinetic barriers suppress this path at low temperatures. Hence, at low hydrogen pressures the transition from state 1 to state 3 (decomposition of Mg_2NiH_4) is observed first. The application of higher hydrogen pressures effectively shifts the sorption equilibrium of Mg_2NiH_4 to higher temperatures and thus allows for the concerted reaction to take place. State 3 is a non-equilibrium state i. e. the system reacts further immediately. If the temperature is lower than the equilibrium temperature of MgH_2 the gradual transition from state 3 to state 2 is observed. As soon as this temperature is exceeded, the fraction of the system in state 2 quickly passes into state 4. The residual fraction of the system in state 3 reacts gradually to state 4, too. Simultaneously, the newly formed magnesium from state 4 reacts with unreacted $LiBH_4$ from state 3 and forms MgB_2. The formation of this compound introduces state 5. This fifth state is thermodynamically less favourable than state 4. However, the presence of MgB_2 after full dehydrogenation, i. e. after a dwelling time of several hours at 400 °C, shows that the transition from state 5 to state 4 is kinetically hindered at this temperature.

If $LiBH_4$ or composites containing this borohydride are heated above 350 °C without the application of sufficient hydrogen pressure, the formation of $Li_2B_{12}H_{12}$ is typically observed. The ^{11}B NMR analyses of dehydrogenated $LiBH_4$-Mg_2NiH_4 only show very weak signals that can be attributed to this compound (figure 3.17b), though. However, it is unlikely that the decomposition of $LiBH_4$ into $Li_2B_{12}H_{12}$, LiH and hydrogen is somehow suppressed in this composite. Instead, it must be assumed that $Li_2B_{12}H_{12}$ is partially formed but then acts as a boron donor for Mg_2Ni in the formation of $MgNi_{2.5}B_2$. The possibility that this reaction occurs under experimental conditions similar to those chosen for the dehydrogenation of $LiBH_4$-Mg_2NiH_4 was demonstrated in the *in situ* SR-PXD experiment shown in figure 3.20a. The composition of the Mg_2NiH_4-$Li_2B_{12}H_{12}$-LiH samples was chosen to allow

for the bonding of all boron and all nickel in $MgNi_{2.5}B_2$. At the end of the dehydrogenation period only $MgNi_{2.5}B_2$ but no residual Mg_2Ni were detected. Considering the described stoichiometry of the as-prepared material, (almost) full consumption of $Li_2B_{12}H_{12}$ must be inferred. This experiment also demonstrates the good kinetics for the boron transfer from $Li_2B_{12}H_{12}$ to $MgNi_{2.5}B_2$. Moreover, also in this experiment UP was found to be an intermediate phase. The presence of UP in this sample simultaneously confirms that its formation is not directly associated to $LiBH_4$ but rather to Mg_2Ni reacting with any boron donor. Upon rehydrogenation of the desorbed sample Mg_2NiH_4 was recovered. Its reflections arose at temperatures above the melting point of $LiBH_4$. Therefore, this borohydride was formed in the liquid state making it non-detectable with diffraction methods. Altogether, $Li_2B_{12}H_{12}$ – if produced in a side reaction – must be regarded as an intermediate compound in the $LiBH_4$-Mg_2NiH_4 system. After complete dehydrogenation all boron is bonded in $MgNi_{2.5}B_2$ and thus a full recovery of $LiBH_4$ is possible. This finding is a crucial advantage for the preservation of this system's hydrogen storage capacity and distinguishes it from the Reactive Hydride Composite $LiBH_4$-MgH_2. As magnesium does not react with $Li_2B_{12}H_{12}$ under moderate conditions (no formation of MgB_2), the latter compound must be regarded as a boron sink in the $LiBH_4$-MgH_2 system. The formation of $Li_2B_{12}H_{12}$ in this RHC causes a gradual degradation of the hydrogen storage capacity as more and more boron is removed from the reversible cycle between $LiBH_4$ and MgB_2. In contrast to this, $Li_2B_{12}H_{12}$ does not constitute a boron sink in the $LiBH_4$-Mg_2NiH_4 system allowing reversible hydrogen cycling without particular pressure or temperature restrictions.

Due to experimental limitations – the plateau pressure at the hydrogenation temperature exceeds the maximum operation pressure of the volumetric apparatuses – the reversibility of the $LiBH_4$-Mg_2NiH_4 system could not be recorded continuously over several hydrogen cycles. Instead, the cycling stability had to be evaluated based on *ex situ* measurements (figure 3.21). The comparison of volumetric analyses of the first and the tenth dehydrogenation revealed that the reaction kinetics remained almost unchanged. To some extend this observation allows to draw conclusions about the stability of the composite's microstructure. Typically, the development of a refined particle size distribution promotes reaction kinetics. In contrast, a noticeably particle growth causes the opposite i. e. it impedes fast sorption rates. Therefore, no significant microstructural changes are expected as a result of cycling procedure. However, a drop of the hydrogen capacity of about 10 % could be observed. Although this reduction can be partially explained by the presence of MgO – which points towards an exposure to oxygen or humidity during the handling of the material – the low concentration of this impurity suggests that the partial oxidation cannot be held liable for the entire capacity drop. The presence of residual $MgNi_{2.5}B_2$ in the hydrogenated state (9. absorption) shows that $LiBH_4$ was not recovered completely during hydrogenation. This finding could be ascribed to several phenomena. For instance, absorption kinetics could reduce sensibly towards the end of the hydrogenation reactions. Such a process could be induced by e. g. the development of new structures and interfaces that impede solid-state diffusion. Another explanation attempt

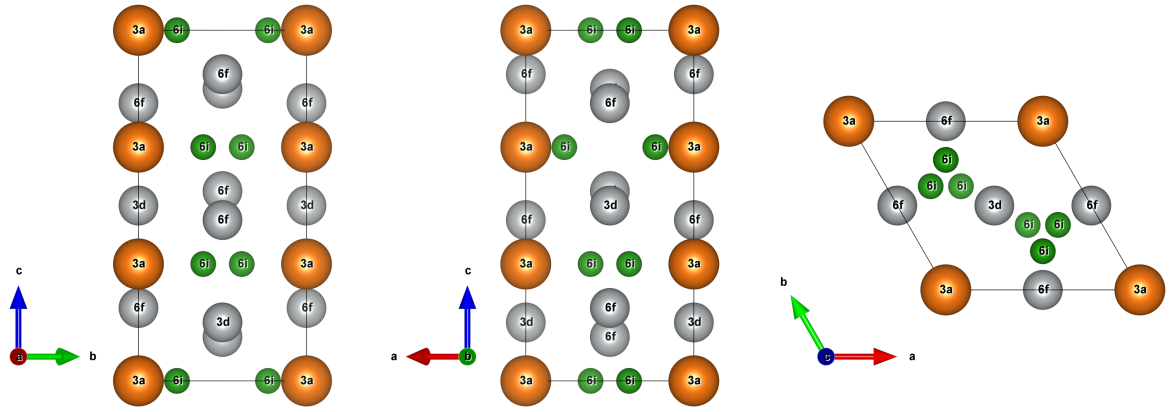

Figure 3.24: The crystal structure of $MgNi_{2.5}B_2$ viewed along the three crystallographic axes. Nickel, magnesium and boron atoms are portrayed as orange, grey and green spheres, respectively.

for the incomplete recovery of the absorbed state could be related to phase segregation which can be motivated by the presence of a liquid phase ($LiBH_4$) in both the absorption and desorption periods. Under the influence of gravity, local deviations from the stoichiometric composition of the $LiBH_4$-Mg_2NiH_4 composite could develop. Nevertheless, without further detailed characterisations by means of more dedicated techniques the observed capacity drop cannot be explained unambiguously.

Interestingly, the achieved degree of reversibility after ten cycles (about 90 %) is much higher than the one obtained by Li and Vajo *et al.* [79]. In their publication, the authors report a boron transfer to $LiBH_4$ that is equivalent to an absorption yield of only approximately 65 %. This rather low value was obtained already for the first three hydrogenations. In contrast to the absorption conditions chosen in this work (360 °C, 200 bar to 250 bar), their hydrogenations experiments were conducted at less absorption-promoting conditions of 160 bar and 350 °C. Considering that the sorption conditions (temperature, pressure and time) and the material properties (no additives, no compaction) were not optimised for the experiments presented in this work, a reversible capacity of 90 % of the starting value after ten full hydrogen cycles must be regarded as good result.

The presented results also provide some insights into the nature of $MgNi_{2.5}B_2$. The crystal structure of this compound was characterised for the first time by Jung in 1977 [85]. He described this ternary boride as hexagonal crystal with the space group $P6_222$ (No. 180). An illustration of the $MgNi_{2.5}B_2$ crystal is presented in figure 3.24. Ni atoms are located at the Wyckoff sites 6*f* and 3*d*, most of the Mg atoms at 3*a* and the B atoms at site 6*i*. However, about one quarter of the Mg atoms occupies as well 6*f* and 3*d* sites. Therefore, these sites are partially occupied by both Ni and Mg. The total occupancies are yet only 89 % (3*d*) and 93 % (6*f*). These crystal structure parameters are summarised in table 3.3. In addition, Jung pointed out that single phase diffractograms can also be obtained for slightly different atomic compositions indicating that $MgNi_{2.5}B_2$ features a certain homogeneity range as expressed above. Since the measured cell parameters are practically independent from these changes of

Table 3.3: Crystallographic parameters, i. e. cell lengths a and c, atomic positions x, y and z and site occupancies n, of $MgNi_{2.5}B_2$ as reported by Jung and of $MgNi_3B_2$ as reported by Gross *et al.*

	$MgNi_{2.5}B_2$, Jung [85] ($a = 4.887$ Å, $c = 8.789$ Å)						$MgNi_3B_2$, Gross *et al.* [86] ($a = 4.880$ Å, $c = 8.786$ Å)					
				n						n		
site	x	y	z	Ni	Mg	B	x	y	z	Ni	Mg	B
6*f*	1/2	0	0.208	4.98	0.59	0	1/2	0	0.208	6	0	0
3*d*	1/2	0	1/2	2.54	0.13	0	1/2	0	1/2	3	0	0
3*a*	0	0	0	0	2.27	0	0	0	0	0	3.01	0
6*i*	0.393	0.786	0	0	0	6	0.385	0.771	0	0	0	6

the atomic composition, Jung explained his results by modifications of the total and partial occupancies of the Wyckoff sites. This assumption is supported by a publication of Gross *et al.* from 1998 [86]. The authors reported the crystal structure of $MgNi_3B_2$ (table 3.3). This compound has similar cell parameters and the same space group as Jung's structure. In contrast to the latter, $MgNi_3B_2$ exhibits no substitution of Ni by Mg on the 6*f* and 3*d* sites. Moreover, all sites are fully occupied. The authors used a different synthesis method as compared to Jung. Hence, it seems that the structure and atomic composition of $MgNi_{2.5}B_2$ (i. e. the site occupancies and the distribution of atoms) are not fixed but depend on the way this compound is formed. With respect to the structural variations of this compound that develop upon dehydrogenation of $LiBH_4$-Mg_2NiH_4 at different hydrogen pressures, the Rietveld analyses (table 3.1) provide a couple of interesting findings. Due to the presence of several diffractive phases, the uneven background functions (scattering at PMMA dome) and the limited resolution of the laboratory diffractometer, some constraints for the interpretation of these results must be considered, though. First, the refinement of the general coordinates of site 6*i* (boron) had to be omitted because the attempted simultaneous optimisation of all atomic parameters of this site led to dubious results. As a consequence, a particular degree of uncertainty for the calculated properties of the boron atoms must be taken into account. Furthermore, the possible substitution of nickel and magnesium on the sites 6*f* and 3*d* was not considered in the refinements. Instead, the scattering capabilities of these Wyckoff sites were solely adjusted by their total occupancies and their thermal factors. Consequently, the calculated occupancy values should rather be regarded as measures for the scattering capabilities of these two atomic sites. For instance, a partial replacement of nickel by magnesium atoms on site 3*d* would lower this site's mean atomic scattering factor $\langle f_{3d} \rangle$ and thus demand a larger total occupancy to produce a similar scattering capability. However, since all Rietveld refinements were conducted in a uniform manner, the presented results are consistent and – within the mentioned limitations – trends between the different

samples can be directly concluded. The high quality of the fits, i. e. the low reliability indices[5] in conjunction with the qualitative (visual) assessment of the calculated fit curves, provides a high degree of credibility for the refined cell lengths and atomic parameters of the nickel and magnesium atoms. The following obvious trends for the development of the $MgNi_{2.5}B_2$ crystal structure upon dehydrogenation of $LiBH_4$-Mg_2NiH_4 can be summarised. The lower the applied hydrogen pressure:

1. the larger the unit cell (expansion mainly in *c*-direction),
2. the smaller the *z*-coordinate of site 6*f* (up to −2 % of cell length *c*),
3. the lower the scattering capabilities of sites 6*f* and 3*d*.

It appears plausible to relate these three trends to a more and more disordered crystalline structure. This assumption is also supported by the increased broadening of the $MgNi_{2.5}B_2$ reflections perceived after desorption of $LiBH_4$-Mg_2NiH_4 at lower hydrogen pressures. This broadening is directly related to a reduced mean crystallite size and increased microstrain. The dimensions of the unit cell and the atomic positions are determined by the overall potential created by all atoms in the crystal. Modifications of the atomic site properties (occupancies, substitutional effects) directly affect this potential and thus the energetically best configuration of the crystal. Therefore, it is reasonable to ascribe not only the reduced scattering capabilities of sites 6*f* and 3*d* to lowered site occupancies and possible substitutions of nickel and magnesium atoms but also the systematic expansion of the unit cell as well as the shift of the *z*-coordinate of site 6*f*. Initially, these occupancy variations and substitutional effects were motivated by the evaluation of the composition of the dehydrogenated $LiBH_4$-Mg_2NiH_4 samples (reaction schemes 3.17 and 3.18) but also the Rietveld analyses support this conclusion. In addition, Jung referred to these effects to best describe the $MgNi_{2.5}B_2$ diffraction patterns he collected [85]. This line of argument is further substantiated by considering the similar effective ionic radii of Ni^{2+} and Mg^{2+} of 69 pm and 72 pm [129], respectively, which make the possible substitution of these two atoms appear quite plausible. However, for a more detailed evaluation of the $MgNi_{2.5}B_2$ crystal structure that develops upon dehydrogenation $LiBH_4$-Mg_2NiH_4 more and better resolved experimental data is required. Especially a combination of synchrotron and neutron diffraction analyses could be highly beneficial for this purpose.

The portrayed variations in the $MgNi_{2.5}B_2$ crystal structure can be correlated directly to the dehydrogenation pressure and thus to the reaction path of $LiBH_4$-Mg_2NiH_4. At 1 bar H_2 the dehydrogenation starts with the decomposition of Mg_2NiH_4. Consequently, $MgNi_{2.5}B_2$ is formed in the reaction between $LiBH_4$ and Mg_2Ni. In addition, the unknown phase UP is produced as an intermediate compound that, upon further reaction, also contributes to

[5] The weighted profile *R*-factors (R_{wp}) are extraordinary low for all refinements. These values are greatly affected by the high experimental background intensity caused by radiation scattered at the PMMA dome. Nevertheless, also the background subtracted *R*-factors ($R_{wp,bs}$) are at maximum 10 % and thus fairly decent.

the $MgNi_{2.5}B_2$ formation. In contrast, at a hydrogen pressure of 50 bar $MgNi_{2.5}B_2$ is formed exclusively in the concerted reaction between $LiBH_4$ and Mg_2NiH_4. Obviously this particular reaction path leads to the more ordered structure of the $MgNi_{2.5}B_2$ crystal which bears a much closer resemblance to the structure of the as-synthesised material (section 2.1.2, figure 2.2) and the ideal configuration of this crystal ($MgNi_3B_2$ structure described by Gross *et al.* [86]). At 5 bar H_2 the dehydrogenation begins with the concerted reaction between $LiBH_4$ and Mg_2NiH_4. However, at this pressure the equilibrium temperature of Mg_2NiH_4 is lower than 400 °C and thus exceeded upon further heating. Afterwards, the formation of $MgNi_{2.5}B_2$ continues with the consumption of Mg_2Ni and, moreover, involves UP. Consequently, the appearance of $MgNi_{2.5}B_2$ after desorption of $LiBH_4$-Mg_2NiH_4 at 5 bar is a mixture of the ordered structure obtained at higher hydrogen pressures and the disordered one formed at lower pressures. The differences between the reactions of $LiBH_4$ with Mg_2NiH_4 and Mg_2Ni, respectively, might be related to different atomic mobilities at the interfaces of these compounds. The crystal structure of the as-synthesised $MgNi_{2.5}B_2$ also appears well ordered. In this case, the high annealing temperature of 930 °C certainly promotes diffusion rates and facilitates the development of an almost ideal structure.

3.2.2 $4LiBH_4$-Mg_2NiH_4: The RHC with the Molar Ratio 4 : 1

The system described in this section is "$4\,LiBH_4 + Mg_2NiH_4$". The motivation to change the molar ratio of the two hydrides is based on the presence of MgH_2/Mg among the desorption products of "$2\,LiBH_4 + 2.5\,Mg_2NiH_4$". First of all, from a thermodynamic point of view it appears rather unfavourable to find elemental magnesium after full dehydrogenation. The formation enthalpy of the desorbed state should be minimised in order to reduce the reaction enthalpy and thus potentially the dehydrogenation temperatures. This thermodynamic stabilisation of the desorbed state can be achieved by finding a suitable reaction partner for magnesium that must be added to the original system. This compound should be light weight and ideally store hydrogen itself. As a matter of fact, $LiBH_4$ appears to be an obvious choice as it reacts with magnesium upon dehydrogenation to form MgB_2, LiH and hydrogen. In order to allow for the conversion of all magnesium formed along with $MgNi_{2.5}B_2$, each mole of Mg_2NiH_4 must be mixed with four moles of $LiBH_4$, i. e. the expected overall reaction proceeds according to the following chemical equation:

$$4\,LiBH_4 + Mg_2NiH_4 \longrightarrow 4\,LiH + 0.4\,MgNi_{2.5}B_2 + 1.6\,MgB_2 + \underbrace{8\,H_2}_{8.1\ \text{mass\%}}. \tag{3.19}$$

Consequently, two different borides should be produced upon full dehydrogenation. The first, i. e. $MgNi_{2.5}B_2$, is expected to be formed in a process similar to the direct reaction between $LiBH_4$ and Mg_2NiH_4 described in the sections 3.1.1 and 3.2.1. The second boride, i. e. MgB_2, would be formed as a result of the reaction between $LiBH_4$ and MgH_2/Mg. This anticipated additional reaction step is well known from the Reactive Hydride Composite $LiBH_4$-MgH_2 (molar ratio 2 : 1) that was introduced independently by Barkhordarian *et al.* [32, 33] and Vajo *et al.* [34] in 2004 and investigated comprehensively ever since [39, 44–47, 49, 130, 131]. This system is considered as a reference material for $4LiBH_4$-Mg_2NiH_4 and was thus included in all experiments presented in this section in order to identify potential improvements but also drawbacks of the new system.

As discussed in section 3.2.1, MgH_2 is among the products of the concerted reaction between $LiBH_4$ and Mg_2NiH_4. From a practical point of view, this is not ideal because this hydride binds half the hydrogen initially stored in the $LiBH_4$-Mg_2NiH_4 system. In order to release all hydrogen, the solid compounds must be heated above the decomposition temperature of MgH_2. On the contrary, in the $4LiBH_4$-Mg_2NiH_4 system additional $LiBH_4$ acts as reaction partner for MgH_2. However, from the $LiBH_4$-MgH_2 system it is well known that these two hydrides do not react mutually, i. e. the dehydrogenation process always starts with the independent desorption of MgH_2. Nevertheless, in $4LiBH_4$-Mg_2NiH_4 magnesium is formed as a side product of the formation of $MgNi_{2.5}B_2$ and thus released continuously on an atomic scale at the reactive interfaces. This could promote reaction kinetics with $LiBH_4$ and hence enable the formation of MgB_2 already below the decomposition temperature of MgH_2.

In case of the $LiBH_4$-MgH_2 system, the positive influence of titanium based additives on

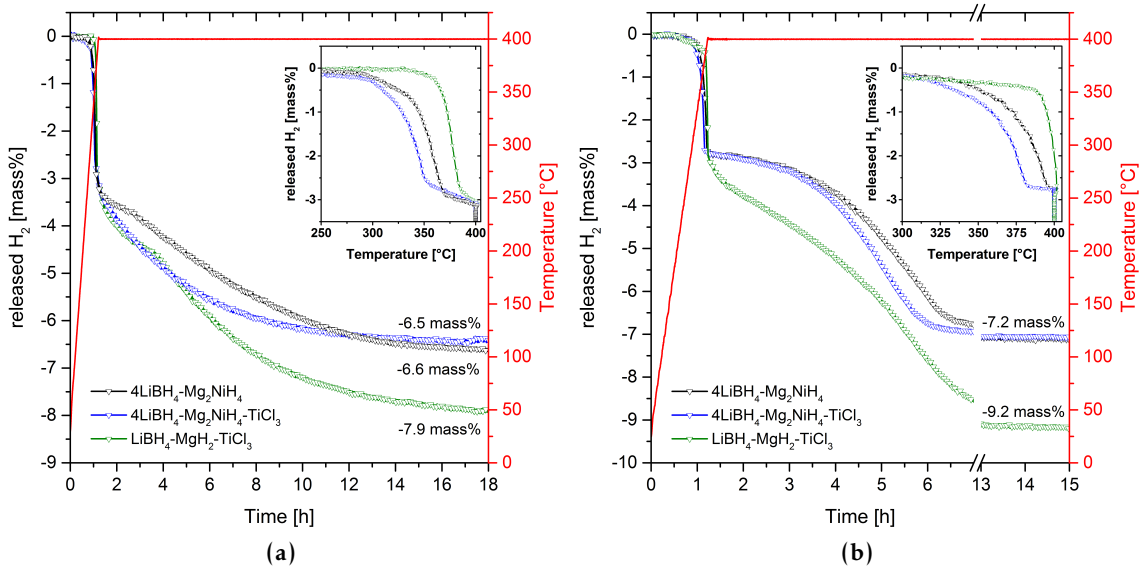

Figure 3.25: Volumetric analyses of the dehydrogenation reactions of $4LiBH_4$-Mg_2NiH_4, $4LiBH_4$-Mg_2NiH_4-$TiCl_3$ and $LiBH_4$-MgH_2-$TiCl_3$ conducted at pressures of (a) 1 bar H_2 and (b) 5 bar H_2. The samples were heated from room temperature to 400 °C at 5 K min^{-1}.

the reaction kinetics is well known [45, 47, 130]. These compounds effectively shorten the incubation period of MgB_2 nucleation and generally enhance the material dehydrogenation and hydrogenation rates. Therefore, 2.5 mol% of $TiCl_3$ was added to the $LiBH_4$-MgH_2 composite. In order to characterise the influence of this additive on the $4LiBH_4$-Mg_2NiH_4 system, besides the pure material also samples doped with 5 mol% of $TiCl_3$ were investigated in the experiments presented hereafter. The addition of $TiCl_3$ decreases the theoretical hydrogen capacity from 8.1 mass% to 7.8 mass%.

3.2.2.1 Experimental Results

The dehydrogenation path and reaction mechanism The dehydrogenation reactions of the $4LiBH_4$-Mg_2NiH_4 system were characterised by means of a set of complementary experiments. In particular the differences between the reaction mechanisms obtained under hydrogen atmospheres of 1 bar and 5 bar were studied. The temperature dependent hydrogen release was determined by means of volumetric analyses for the systems $4LiBH_4$-Mg_2NiH_4 (with and without $TiCl_3$ addition) and $LiBH_4$-MgH_2-$TiCl_3$ (figure 3.25). The samples were heated from room temperature to 400 °C at a rate of 5 K min^{-1} and kept isothermally for several hours. At 1 bar H_2 (figure 3.25a) all materials release hydrogen in multiple steps: a fast first step evolving gas equivalent to roughly 2.8 mass% is identified for all samples. Afterwards the hydrogen evolution proceeds at much lower rates for all materials and probably – as suggested by the shapes of the sorption curves – due to combinations of several overlapping processes. $TiCl_3$ doped $4LiBH_4$-Mg_2NiH_4 has the lowest dehydrogenation onset temperature (about 285 °C) and the fastest sorption rates for the first step. In comparison, the desorption

of pure $4LiBH_4$-Mg_2NiH_4 starts at slightly higher temperatures (approx. 290 °C). The rate of the first reaction step is discernibly lower, though. The $LiBH_4$-MgH_2-$TiCl_3$ system begins to release hydrogen at about 340 °C. After 18 h the latter system released approximately 7.9 mass% H_2. The two $4LiBH_4$-Mg_2NiH_4 samples released almost similar quantities of hydrogen: 6.5 mass% with $TiCl_3$ addition and 6.6 mass% in case of the pure composite. At 5 bar H_2 (figure 3.25b) all three investigated materials release hydrogen in two steps. In case of the two $4LiBH_4$-Mg_2NiH_4 samples again about 2.8 mass% H_2 are evolved in the first step. At roughly 3 mass% $LiBH_4$-MgH_2-$TiCl_3$ appears to set free slightly more gas in the first step. Compared to the experiments conducted at 1 bar all onset temperatures are shifted to higher values: again the $TiCl_3$ doped $4LiBH_4$-Mg_2NiH_4 system starts to desorb hydrogen at the lowest temperature (approx. 300 °C). The desorption onset of pure $4LiBH_4$-Mg_2NiH_4 is only negligibly higher but the kinetics of the first dehydrogenation step are certainly not as fast as for the doped system. At roughly 385 °C $LiBH_4$-MgH_2-$TiCl_3$ begins to release hydrogen at a significantly higher temperature. Both $4LiBH_4$-Mg_2NiH_4 samples appear to feature a short (and slopy) incubation period of approximately 120 min before the second dehydrogenation step starts. Also this second step proceeds faster in case of the material prepared with $TiCl_3$. The $LiBH_4$-MgH_2-$TiCl_3$ sample does not clearly display an incubation period as such. Instead, the second step – although initially rather slowly – seems to start shortly after the first ended. Both $4LiBH_4$-Mg_2NiH_4 samples release 7.2 mass% of hydrogen in total and 9.2 mass% evolve from the $LiBH_4$-MgH_2-$TiCl_3$ specimen.

The addition of $TiCl_3$ appears to promote reaction kinetics of the $4LiBH_4$-Mg_2NiH_4 system to some extent. Simultaneously, the measured hydrogen capacity is reduced just slightly. For this reason the focus for the experiments presented hereafter was set solely on the two $TiCl_3$ containing Reactive Hydride Composites. The sequences of thermal transitions were determined by a set of DSC analyses performed at hydrogen pressures of 1 bar and 5 bar (figure 3.26). The specimens were heated from room temperature to 500 °C at 5 K min^{-1}. At temperatures below 250 °C only polymorphic changes of the individual hydrides are observed. Therefore, to ensure a better overview the temperature axis was restricted to the range from 250 °C to 500 °C. $4LiBH_4$-Mg_2NiH_4-$TiCl_3$ features four thermal events denoted by the black labels A to D. At 1 bar the onset temperature of event A is approximately 284 °C. The events B and C are superimposed. In addition, the onset of these merged DSC peaks overlaps with event A. For this reason only rough estimates of the onset temperatures can be provided. These are 290 °C and 310 °C for the events B and C, respectively. The onset temperature of event D is about 430 °C. At a hydrogen pressure of 5 bar these four transitions can be distinguished more clearly. Their onset temperatures are 284 °C, 295 °C, 350 °C and 430 °C. The Reactive Hydride Composite $LiBH_4$-MgH_2-$TiCl_3$ exhibits three thermal events in the displayed temperature range. These are denoted by the red labels A to C. At 1 bar H_2 the respective onset temperatures are approximately 284 °C, 342 °C and 425 °C. If the pressure is increased to 5 bar, these values change to approximately 285 °C, 375 °C and 427 °C.

The chemical compositions of the two systems $4LiBH_4$-Mg_2NiH_4 and $LiBH_4$-MgH_2 (both

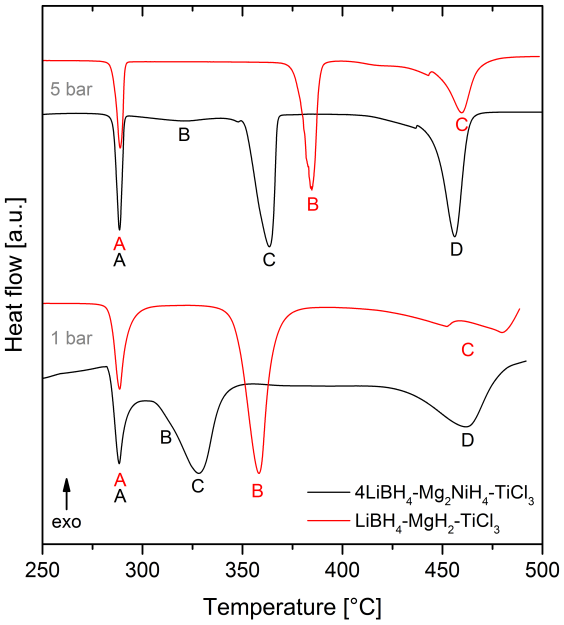

Figure 3.26: DSC analyses showing the thermal events occurring upon dehydrogenation of $4LiBH_4$-Mg_2NiH_4-$TiCl_3$ and $LiBH_4$-MgH_2-$TiCl_3$ at hydrogen pressures of 1 bar and 5 bar. The materials were heated from room temperature to 500 °C at 5 K min^{-1}.

with $TiCl_3$ addition) after full dehydrogenation at 1 bar and 5 bar, respectively, and a temperature of 400 °C were determined by PXD and ^{11}B MAS NMR analyses (figure 3.27). If $4LiBH_4$-Mg_2NiH_4-$TiCl_3$ is desorbed at 1 bar H_2 five crystalline compounds are identified among the decomposition products (figure 3.27a). These are $MgNi_{2.5}B_2$, MgB_2, Mg, MgH_2 and LiH. In contrast, after desorption at 5 bar $MgNi_{2.5}B_2$, MgB_2, LiH and LiCl are discernible but no traces of Mg/MgH_2 were detected. The distributions of boron within these samples are revealed by the respective NMR analyses. Four distinct chemical shifts attributable to $LiBH_4$ (−41 ppm), $Li_2B_{12}H_{12}$ (−15 ppm), MgB_2 (100 ppm) and $MgNi_{2.5}B_2$ (approx. 154 ppm) are emphasised. In addition, elemental boron should be considered which typically causes a rather broad resonance signal at around −1 ppm. The spectrum of $4LiBH_4$-Mg_2NiH_4-$TiCl_3$ desorbed at 1 bar comprises the resonances of five boron containing compounds (figure 3.27b). Besides $MgNi_{2.5}B_2$ and MgB_2 – that were identified already in the X-ray diffractogram – also residual $LiBH_4$ and significant amounts of $Li_2B_{12}H_{12}$ and boron are detected. The formation of the latter two compounds upon dehydrogenation is avoided if a pressure of 5 bar is applied: as can be seen, the NMR spectrum of this material only exhibits the resonances of $MgNi_{2.5}B_2$, MgB_2 and $LiBH_4$. The diffraction pattern of $LiBH_4$-MgH_2-$TiCl_3$ desorbed at 1 bar (figure 3.27a) shows the reflections of Mg, MgH_2, MgB_2, LiH and MgO. The intensities of the MgB_2 peaks are fairly low, though. The application of a hydrogen pressure of 5 bar for the dehydrogenation of this composite changes the chemical composition significantly. The most intense reflections are those of MgB_2. Furthermore, LiH and LiCl is discernible. Also very weak reflections of MgH_2 are identified but none attributed to Mg. The NMR analyses (figure 3.27b) show that both these samples contain weakly or non-diffractive phases. The

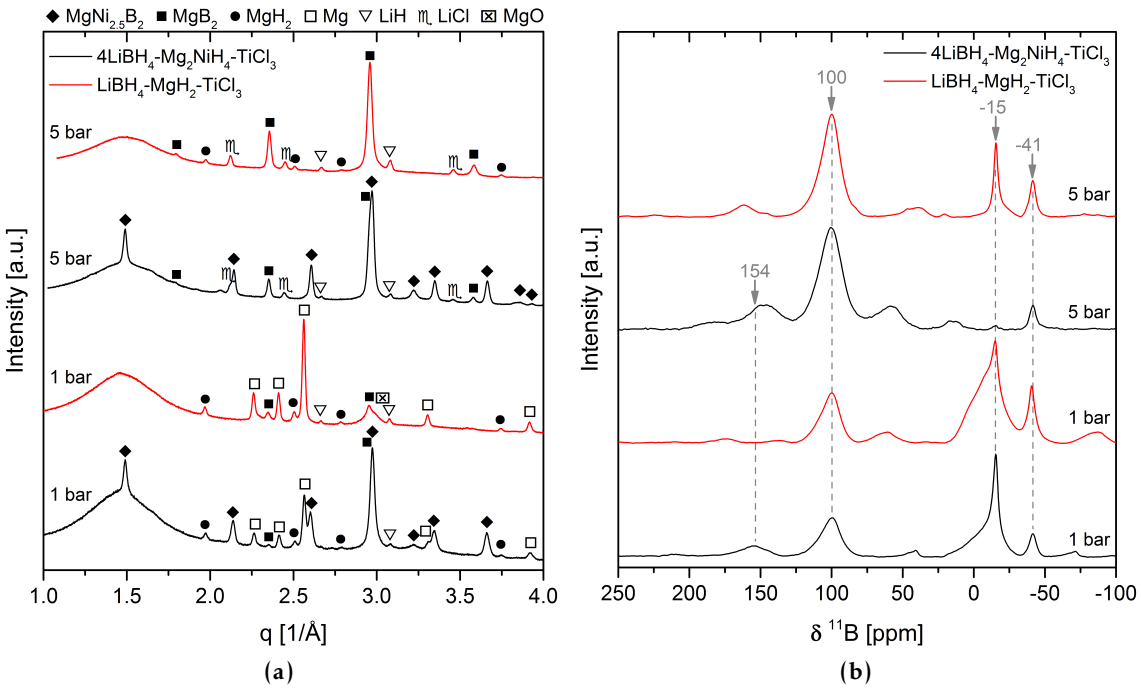

Figure 3.27: Characterisation of the chemical composition of $4LiBH_4$-Mg_2NiH_4-$TiCl_3$ and $LiBH_4$-MgH_2-$TiCl_3$ after dehydrogenation at 400 °C and pressures of 1 bar and 5 bar H_2, respectively: (a) PXD analyses and (b) ^{11}B MAS NMR spectra.

material desorbed at 1 bar features the resonances of unreacted $LiBH_4$, $Li_2B_{12}H_{12}$ and boron besides MgB_2. However, most of the boron atoms are bonded in $Li_2B_{12}H_{12}$ and in amorphous boron itself. As opposed to this, the MgB_2 signal in the spectrum of $LiBH_4$-MgH_2-$TiCl_3$ dehydrogenated at 5 bar exhibits a much stronger relative intensity. Nevertheless, besides some residual $LiBH_4$ also a noticeable fraction of $Li_2B_{12}H_{12}$ is detected. The formation of elemental boron was prevented, though.

In order to shed more light on the sequence of dehydrogenation reactions of the hydride composite $4LiBH_4$-Mg_2NiH_4-$TiCl_3$ and allow for the observation of intermediate crystalline phases, two *in situ* SR-PXD experiments were conducted at hydrogen pressures of 1 bar and 5 bar, respectively (figure 3.28). The as-milled material was heated from room temperature to 450 °C at a rate of 5 K min^{-1}. Since no chemical reactions but only the polymorphic transitions of $LiBH_4$ and Mg_2NiH_4 are observed at temperatures below 275 °C (see section 3.1.1 figure 3.3), the presented results focus on the temperature range from 275 °C to 450 °C. At both hydrogen pressures the diffraction patterns collected at 275 °C comprise exclusively the reflections of $LiBH_4$ (ht) and Mg_2NiH_4 (ht). At 1 bar H_2 (figure 3.28a) the first modification is caused by the abrupt disappearance of the $LiBH_4$ reflections at approximately 288 °C. At roughly 305 °C also the Mg_2NiH_4 diffraction peaks start to fade whereas those of Mg_2Ni arise. Upon further heating the reflections of $MgNi_{2.5}B_2$, Mg and UP emerge gradually. Whilst the latter reach a maximum around 415 °C, the intensities of $MgNi_{2.5}B_2$ and Mg reflections increase until the termination of this experiment. It must be emphasised that MgB_2 was

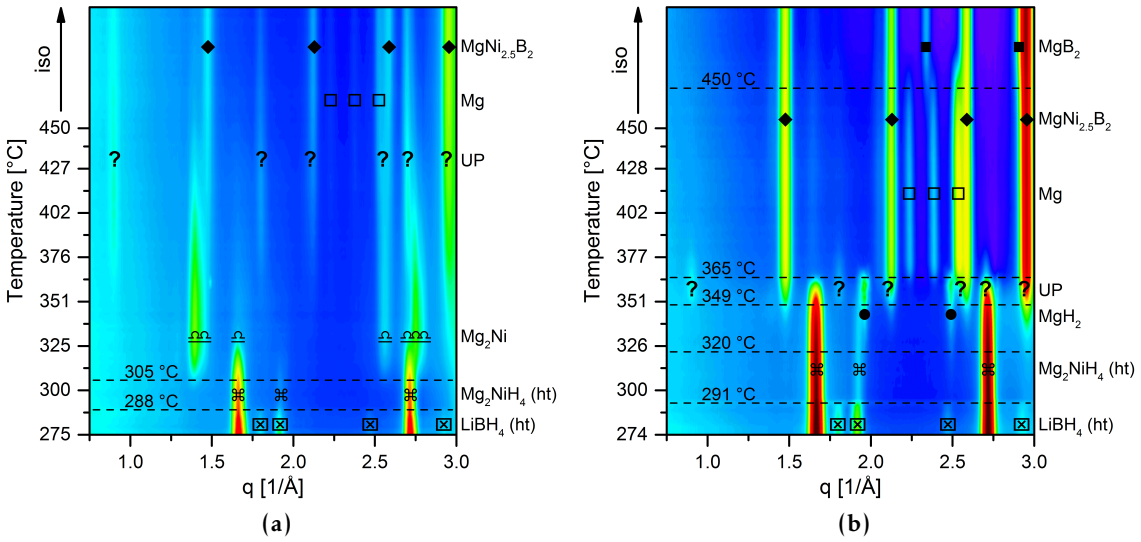

Figure 3.28: *In situ* SR-PXD experiments showing the dehydrogenation reactions of the $4LiBH_4$-Mg_2NiH_4-$TiCl_3$ RHC at hydrogen pressures of (a) 1 bar and (b) 5 bar. The specimens were heated from room temperature to 450 °C at a rate of 5 K min^{-1}.

not detected. Also at 5 bar H_2 (figure 3.28b) the first change in the diffraction patterns is induced by the vanishing of the $LiBH_4$ reflections (291 °C). In contrast to the experiment conducted at lower pressure, the first newly arising reflections can be attributed to $MgNi_{2.5}B_2$ and MgH_2. They appear at about 320 °C and are accompanied by an intensity reduction of Mg_2NiH_4. At approximately 349 °C the reflections of $MgNi_{2.5}B_2$ and MgH_2 intensify quickly and those of UP emerge. At the same time the diffraction pattern of Mg_2NiH_4 fades rapidly. The reflections of UP remain rather weak and vanish already below 400 °C. At 365 °C, MgH_2 decomposes and the reflections of Mg become visible. This compound is stable during the remaining heating period. However, within the isothermal region at 450 °C Mg disappears completely as MgB_2 is formed.

Rehydrogenation reactions and reversibility upon hydrogen cycling To evaluate the rehydrogenation reactions of the $4LiBH_4$-Mg_2NiH_4-$TiCl_3$ system, this material was desorbed in a 5 bar hydrogen atmosphere at 400 °C for 24 h. Afterwards a specimen of the desorbed powder was rehydrogenated in an *in situ* SR-PXD experiment (figure 3.29). In this experiment a hydrogen pressure of 150 bar was applied. The temperature was continuously increased to 365 °C at a rate of 5 K min^{-1} and subsequently kept constant for 60 min. The diffractogram collected at room temperature before starting the hydrogenation comprises the reflections of $MgNi_{2.5}B_2$, MgB_2, LiH and LiCl. The first modification of the diffraction patterns is observed at about 317 °C as the reflections of LiCl vanish suddenly. Shortly after, at approximately 345 °C, the reflections of Mg_2NiH_4 emerge. Simultaneously the diffraction intensities of $MgNi_{2.5}B_2$ and MgB_2 start to decrease noticeably. Whilst the reflections of $MgNi_{2.5}B_2$ – although fading continuously – remain visible throughout the whole experiment, those of

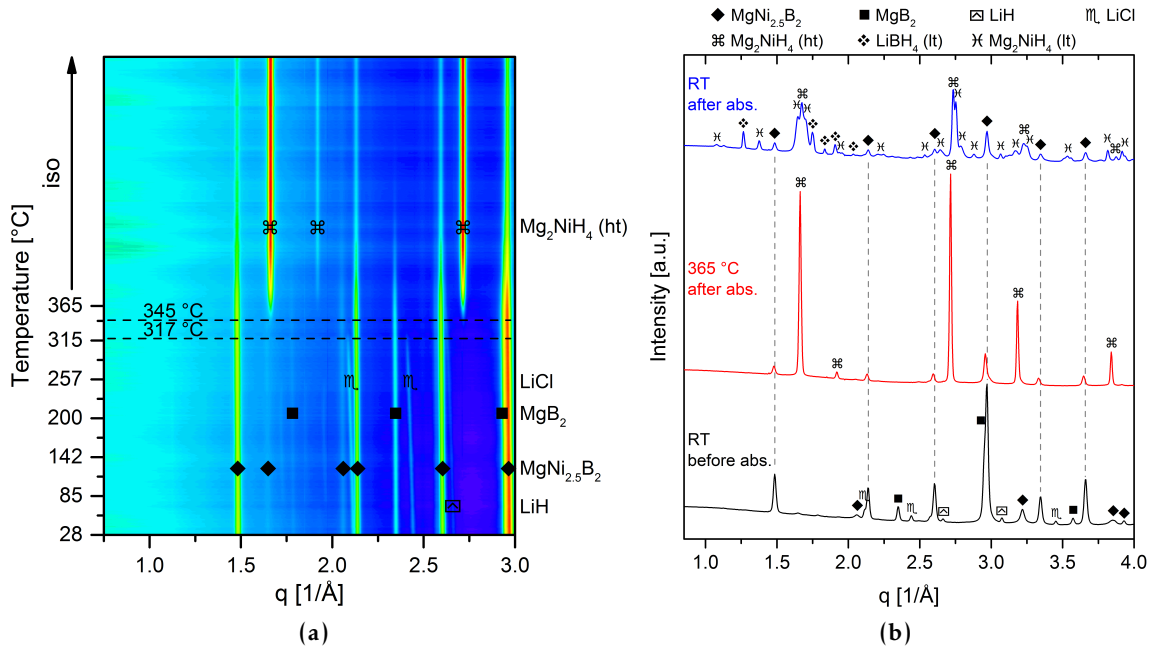

Figure 3.29: SR-PXD experiment probing the rehydrogenation reactions of the $4LiBH_4$-Mg_2NiH_4-$TiCl_3$ composite: (a) contour plot showing the full *in situ* analysis and (b) diffraction patterns taken before heating, at 365 °C after hydrogenation and at room temperature after cooling down. The hydrogen absorption was conducted at a pressure of 150 bar. The sample was heated from room temperature to 365 °C at 5 K min^{-1}.

MgB_2 disappear completely within the isothermal period. In contrast, the reflections of Mg_2NiH_4 intensify until the termination of the experiment. The diffractogram collected at room temperature after cooling down (figure 3.29b) clearly contains the reflections of $LiBH_4$ (lt) and Mg_2NiH_4 (lt and ht) but also those of unreacted $MgNi_{2.5}B_2$. It should be pointed out that MgH_2/Mg could not be detected at any time upon hydrogenation.

In order to evaluate the reversibility of the sorption processes and thus the stability of the storage capacity of the $4LiBH_4$-Mg_2NiH_4 system upon hydrogen cycling, nine full desorption-reabsorption cycles were performed. As already described in section 3.2.1.1, the high plateau pressure of the first dehydrogenation reaction between $LiBH_4$ and Mg_2NiH_4 does not allow for the use of the volumetric apparatuses for these experiments. The cycling of the different specimens had thus to be conducted in the temperature controlled autoclave. In fact, the materials described in this section were actually cycled simultaneously together with the samples described in section 3.2.1.1. Hence, a temperature of 420 °C and a hydrogen pressure of approximately 5 bar were applied for the dehydrogenation periods. The nine rehydrogenations were performed at 360 °C and pressures of approximately 250 bar. To determine the influence of $TiCl_3$ addition on the reversibility of the $4LiBH_4$-Mg_2NiH_4 system, samples of both the doped and undoped material were investigated. In addition, a specimen of $LiBH_4$-MgH_2-$TiCl_3$ was included in the cycling experiments for comparison. The volumetric analyses (5 bar H_2, 5 K min^{-1} up to 400 °C) of the tenth dehydrogenations

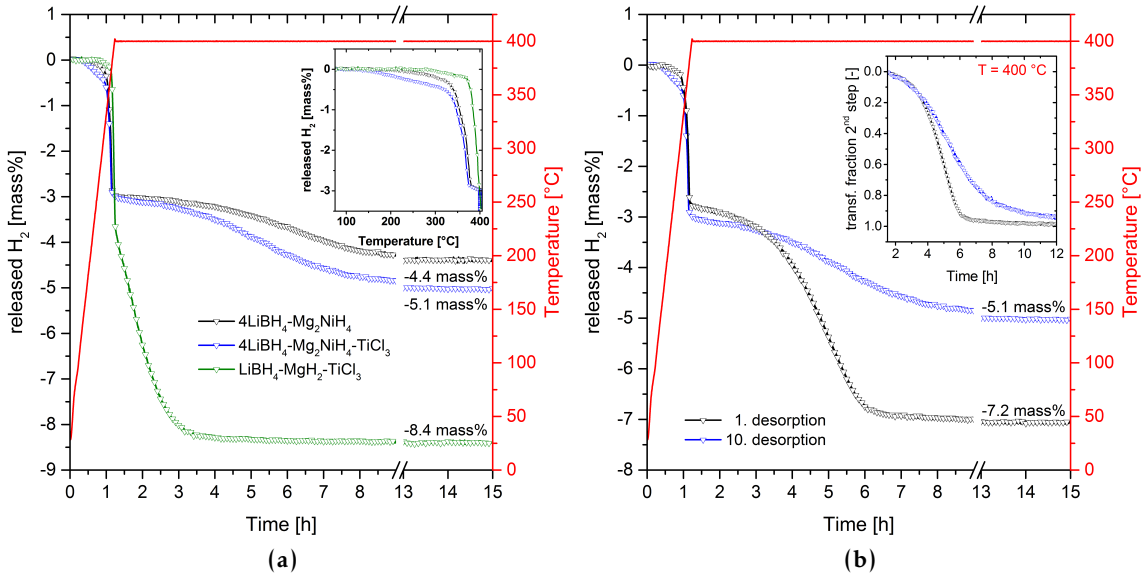

Figure 3.30: (a) Volumetric analyses of the 10. dehydrogenation of $4LiBH_4$-Mg_2NiH_4, $4LiBH_4$-Mg_2NiH_4-$TiCl_3$ and $LiBH_4$-MgH_2-$TiCl_3$, the samples were heated at $5\,K\,min^{-1}$ up to 400 °C in 5 bar H_2. (b) Direct comparison between the 1. and the 10. dehydrogenation of $4LiBH_4$-Mg_2NiH_4-$TiCl_3$.

of all three materials are presented in figure 3.30a. The direct comparison between pure $4LiBH_4$-Mg_2NiH_4 and the sample with $TiCl_3$ addition shows that this additive has a positive effect not only on the reaction kinetics but also on the capacity after cycling. In case of the doped system, the dehydrogenation appears to (slowly) start already below 200 °C, whereas the pure material releases hydrogen only above 250 °C. However, what both samples have in common is that a significant improvement of the sorption kinetics is observed at approximately 330 °C. At roughly 3 mass% the total amount of hydrogen released in the first dehydrogenation step is similar for the doped and undoped $4LiBH_4$-Mg_2NiH_4 system and almost unchanged compared to the first dehydrogenations of these two materials. However, the quantities of hydrogen that evolve in the second step clearly differ between these two samples: at 5.1 mass% the $TiCl_3$ doped material releases 0.7 mass% more hydrogen than the pure material. At approximately 360 °C, the dehydrogenation of $LiBH_4$-MgH_2-$TiCl_3$ starts at perceptibly higher temperatures as compared to the two $4LiBH_4$-Mg_2NiH_4 samples. However, in contrast to the latter, $LiBH_4$-MgH_2-$TiCl_3$ has no incubation period before the second reaction step starts and also the kinetics of this step are much faster. In addition, at 8.4 mass% the total amount of evolved hydrogen is significantly larger for this hydride composite. This large discrepancy is mainly caused by the considerable capacity drops in the second reaction step of the two cycled $4LiBH_4$-Mg_2NiH_4 samples. This can be seen clearly by comparing the volumetric analyses of the first and the tenth dehydrogenation of $4LiBH_4$-Mg_2NiH_4-$TiCl_3$ directly (figure 3.30b). Although the cycled material even exhibits a slight capacity increment for the first reaction step, the quantity of hydrogen released in

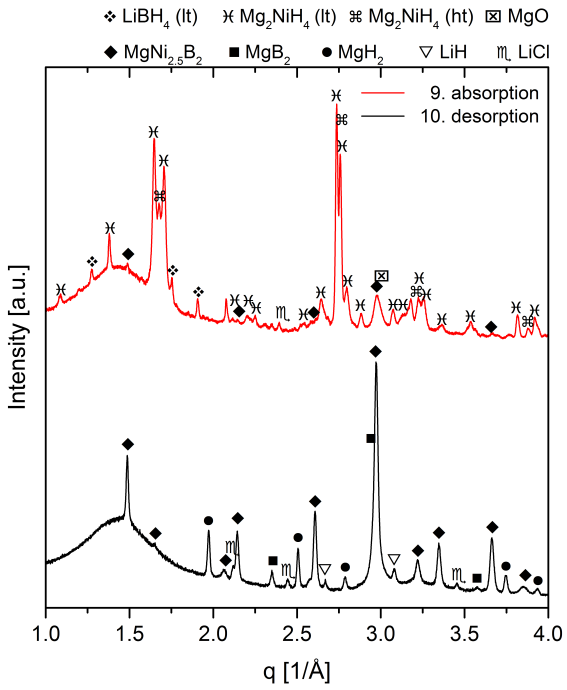

Figure 3.31: Determination of the chemical composition of $4LiBH_4$-Mg_2NiH_4-$TiCl_3$ by means of PXD analyses before and after the 10. dehydrogenation.

the second step decreased distinctly. In fact, if solely the gas evolved in this second step is considered, a capacity reduction of roughly 50 % is recorded. Moreover, also a noticeable degradation of the reaction kinetics is observed as depicted by the time dependencies of the transformed fraction of the second reaction step.

By means of PXD analyses the chemical composition of the cycled material was determined before and after the tenth dehydrogenation (figure 3.31). In the absorbed state six diffractive phases can be identified, namely Mg_2NiH_4 (lt and ht), $LiBH_4$, $MgNi_{2.5}B_2$, LiCl and MgO. No MgH_2 and MgB_2 are detected, though. The reflections of $MgNi_{2.5}B_2$ are fairly weak proving the rather low concentration of this compound in the hydrogenated state. However, by comparing the reflections intensities of Mg_2NiH_4 with those of $LiBH_4$, it is evident that $LiBH_4$ was not fully recovered upon rehydrogenation. After the tenth desorption of $4LiBH_4$-Mg_2NiH_4-$TiCl_3$ strong reflections of $MgNi_{2.5}B_2$ and MgB_2 are identified in the respective diffractogram besides the weak diffraction patterns of LiH and LiCl. However, also the intense reflections of MgH_2 are clearly discernible.

3.2.2.2 Discussion

The Reactive Hydride Composite $4LiBH_4$-Mg_2NiH_4 dehydrogenates in multiple steps. However, as confirmed by the PXD and ^{11}B NMR analyses presented in figure 3.27, the overall dehydrogenation reaction of $4LiBH_4$-Mg_2NiH_4 is in accordance with chemical equation 3.19 if an appropriate hydrogen pressure – for the presented experiments a value of 5 bar was

chosen – is applied. The intermediate reaction steps and phase changes could be monitored by means of the *in situ* SR-PXD experiments. At 5 bar H_2 (figure 3.28b), the first desorption step is the concerted reaction between $LiBH_4$ and Mg_2NiH_4 (see chemical equation 3.9). It can be seen clearly that the reflections of $MgNi_{2.5}B_2$ and MgH_2 arise first (approx. 320 °C). Especially the absence of Mg_2Ni reflections at this temperature proves unambiguously that Mg_2NiH_4 does not decompose before reacting with $LiBH_4$. Consequently, this first reaction step in the $4LiBH_4$-Mg_2NiH_4 system is concerted and can be written as follows:

$$4\,LiBH_4 + Mg_2NiH_4 \xrightarrow{\text{concerted}} 3.2\,LiBH_4 + 0.8\,LiH + 0.4\,MgNi_{2.5}B_2 + 1.6\,MgH_2 + \underbrace{1.6\,H_2}_{1.6\,\text{mass\%}}. \tag{3.20}$$

Moreover, at this pressure the unknown phase UP is just formed in small quantities and only above 350 °C. At this temperature the remaining reflections of Mg_2NiH_4 weaken quickly and slight increments of the background intensity are observed at those scattering vector values where the reflections of Mg_2Ni would occur. Hence, the following explanation appears to be most likely: the decomposition temperature of Mg_2NiH_4 is reached and some Mg_2Ni is produced which thereupon reacts with $LiBH_4$ to form UP. Due to the immediate and fast consumption of Mg_2Ni the growth of larger crystallites is hindered and this compound remains (almost) unrecognised in the diffraction experiment. This model also suggests that Mg_2Ni is an essential reactant for the formation of UP. Another interesting finding is that MgB_2 is formed only above the decomposition temperature of MgH_2 and after a certain dwelling time. This disproves the initial idea that the homogeneous and steady release of magnesium on an atomic level due to the reaction between $LiBH_4$ and Mg_2NiH_4 could foster the reactivity between these magnesium atoms and $LiBH_4$ and thus allow for the formation of MgB_2 already below the decomposition temperature of MgH_2. Instead, the kinetics of MgH_2 nucleation and growth appear to be much faster. The direct comparison between $4LiBH_4$-Mg_2NiH_4 and $LiBH_4$-MgH_2 in the volumetric and DSC analyses presented in figures 3.25 and 3.26, respectively, confirms that the first hydride composite starts to dehydrogenate at considerably lower temperatures. In particular, the DSC analyses demonstrate this improvement. The four thermal events recorded for $4LiBH_4$-Mg_2NiH_4-$TiCl_3$ at 5 bar H_2 (black labels A to D) are associated to the melting of $LiBH_4$, the concerted reaction 3.20, the decomposition of MgH_2 and the formation of MgB_2, respectively. In case of the $LiBH_4$-MgH_2-$TiCl_3$ system only three thermal events are observed (red labels A to C) which can be attributed to the melting of $LiBH_4$, the decomposition of MgH_2 and the formation of MgB_2, respectively. Therefore, the dehydrogenation of $4LiBH_4$-Mg_2NiH_4 starts at approximately 295 °C (black event B, reaction 3.20) whereas the release of hydrogen in $LiBH_4$-MgH_2 starts with the decomposition of MgH_2 (red event B) only above 370 °C. It is worth mentioning that also the decomposition of MgH_2 occurs at lower temperatures (about 350 °C) in the $4LiBH_4$-Mg_2NiH_4 system. Probably a finer microstructure of the MgH_2

particles formed in reaction 3.20 enables lower dehydrogenation activation energies.

As shown by the respective *ex situ* PXD and NMR analyses (figure 3.27) as well as the *in situ* SR-PXD experiment (figure 3.28a), the reaction path of $4LiBH_4$-Mg_2NiH_4 changes fundamentally if the system is dehydrogenated at just 1 bar H_2. In addition, the final desorption products differ significantly from the composition predicted in equation 3.19. First of all, the concerted reaction between $LiBH_4$ and Mg_2NiH_4 is not observed because the latter hydride decomposes independently at lower temperatures. Thus, Mg_2Ni is formed in high concentration and, as a result of this, a much greater fraction of UP is formed further on. However, the most decisive change is certainly the largely suppressed boron transfer from $LiBH_4$ to magnesium: no MgB_2 was formed in the course of the *in situ* SR-PXD experiment. In fact, the ^{11}B NMR analyses (figure 3.27b) confirms that some MgB_2 is actually produced upon dwelling at 400 °C for more than 17 h but most boron is bonded in $Li_2B_{12}H_{12}$ and elemental boron, though. These two compounds are known for their inertness to reversibly donate boron and thus allow for the recovery of $LiBH_4$ upon rehydrogenation. The absence of Mg_2Ni reflections in the diffractogram collected after full dehydrogenation (figure 3.27a) proves that the formation of $MgNi_{2.5}B_2$ is complete and not impeded by the reduced hydrogen pressure. This observation is in agreement with the results obtained for the $LiBH_4$-Mg_2NiH_4 system (see section 3.2.1) which clearly show that, independently from the applied hydrogen pressure, no elemental boron or $Li_2B_{12}H_{12}$ are formed. Consequently, the presence of these unwanted side products must be ascribed solely to the second reaction step in the $4LiBH_4$-Mg_2NiH_4 system, i. e. the incomplete formation of MgB_2. The same reaction behaviour is observed in the $LiBH_4$-MgH_2-$TiCl_3$ system upon dehydrogenation at 1 bar H_2. Although some MgB_2 is present among the desorption products, the largest fraction of boron is bonded in the elemental state and $Li_2B_{12}H_{12}$. This observation must be attributed to the tendency of $LiBH_4$ to dehydrogenate independently into these two compounds if the hydrogen pressure is too low. In contrast to Mg_2Ni – its reactivity with $Li_2B_{12}H_{12}$ and elemental boron is demonstrated in sections 3.2.1 and 3.3 – magnesium does not react with either of the two under moderate conditions. The implications of these findings are obvious: similar to $LiBH_4$-MgH_2 also the composite $4LiBH_4$-Mg_2NiH_4 must be dehydrogenated at sufficient hydrogen back pressures in order to suppress the independent desorption of $LiBH_4$ and thus ensure a complete reaction according to equation 3.19.

As revealed by the *in situ* SR-PXD rehydrogenation experiment (figure 3.29a), hydrogen absorption from desorbed $4LiBH_4$-Mg_2NiH_4-$TiCl_3$ appears to start only above 300 °C. At roughly 317 °C the reflections of LiCl suddenly vanished. Since this salt is highly stable, it must be assumed that it dissolved in newly formed $LiBH_4$ which is liquid and thus non-diffractive at this temperature. Mg_2NiH_4, however, crystallises with some delay at approximately 345 °C. Another quite interesting finding is the absence of any other diffractive compound besides Mg_2NiH_4 formed upon hydrogenation. If initial $LiBH_4$ formation was dominated by boron transfer from MgB_2, one would expect to find MgH_2 as an intermediate phase. As opposed to this, a dominant boron donation from $MgNi_{2.5}B_2$ would lead to

the formation of additional nickel containing compounds (such as $MgNi_2$ or elemental Ni). Consequently, it must be assumed that $MgNi_{2.5}B_2$ and MgB_2 are consumed relatively evenly for the production of $LiBH_4$. Although the *in situ* experiment was terminated before rehydrogenation could complete, a high degree of conversion was reached within the short 60 min isothermal period (figure 3.29b).

In contrast to the quite promising results of the first dehydrogenation and the consequent rehydrogenation of $4LiBH_4$-Mg_2NiH_4, reversibility of the sorption reactions upon several full hydrogen cycles – although performed at a dehydrogenation pressure of 5 bar – proved to be rather poor. The volumetric analyses of the tenth dehydrogenations show that the total hydrogen capacity of $4LiBH_4$-Mg_2NiH_4 dropped by approximately 29 % and 39 % for the samples with and without $TiCl_3$ addition, respectively (figure 3.30a). This significant reduction is mainly caused by a degradation of the second reaction step, i. e. the incomplete formation of MgB_2. Instead, the amount of hydrogen released in the first step is – independent of $TiCl_3$ addition – practically unchanged after ten sorption cycles. This is supported by the PXD analyses of $4LiBH_4$-Mg_2NiH_4-$TiCl_3$ shown in figure 3.31. After the nineth absorption, the reflections of $MgNi_{2.5}B_2$ are barely visible proving that almost all nickel is bonded in Mg_2NiH_4. In contrast, after the subsequent desorption, no traces of Mg_2NiH_4/Mg_2Ni are detected confirming that all nickel was transferred back to $MgNi_{2.5}B_2$. Thus, the first reaction step shows a very high degree of reversibility – similar to the $LiBH_4$-Mg_2NiH_4 composite described in section 3.2.1. However, the amount of hydrogen released in the second reaction step dropped by approximately 51 % for the sample containing $TiCl_3$ and even 67 % for the pure $4LiBH_4$-Mg_2NiH_4 composite. Again the diffractograms presented in figure 3.31 provide useful insights into this matter: the hydrogenated material does not contain any diffractive side products. As compared to the intensities of Mg_2NiH_4 reflections, those of $LiBH_4$ are clearly too weak to match the initial 4 : 1 molar ratio, though. The desorbed material features intense MgH_2 reflections proving that MgB_2 did not develop completely. Consequently, a significant fraction of boron did not participate in the reversible cycle between $LiBH_4$ and MgB_2 anymore. This finding points towards an agglomeration of $Li_2B_{12}H_{12}$ and/or elemental boron upon cycling continuously diminishing the capacity of the second reaction step. This could be explained by the fact that also at a hydrogen pressure of approximately 5 bar $LiBH_4$ slowly decomposes into $Li_2B_{12}H_{12}$, LiH and hydrogen [47, 122]. Therefore, if the incubation period of the second step, i. e. the duration for MgB_2 nucleation, is too long, larger amounts of $Li_2B_{12}H_{12}$ might be formed. A similar behaviour is also known from the $LiBH_4$-MgH_2 composite [47]. Typically, the addition of Ti based additives, such as $TiCl_3$, causes a shortening of this incubation period because fine TiB_2 particles (nanometre scale) formed upon ball milling and distributed evenly in the host material act as heterogeneous nucleation agents for MgB_2 [130]. This effectively reduces the activation energy for nucleation and thus accelerates the reaction between $LiBH_4$ and magnesium. Comparing the first and the tenth dehydrogenation of $4LiBH_4$-Mg_2NiH_4-$TiCl_3$ (figure 3.30b), it can be seen that the kinetics of hydrogen release in the second reaction step are slower in case of the cycled

material. This observation suggests that the enhancing effect of the Ti additive weakens upon hydrogen cycling. It might be that TiB_2 nano particles are not stable within this composite. This could possibly be explained by an energetically more favourable bonding of boron in $MgNi_{2.5}B_2$, by a potential formation of Ti-Ni phases or perhaps even an inclusion of Ti as substitutional atoms into the $MgNi_{2.5}B_2$ crystal. In order to shed more light on this issue, specific experiments, e. g. XAS measurements at the Ti K-edge, would have to be conducted to clarify the chemical state of titanium in these samples before and after cycling.

In addition, $TiCl_3$ appears to have a positive influence on the first reaction step in the $4LiBH_4$-Mg_2NiH_4 system, i. e. the concerted reaction between $LiBH_4$ and Mg_2NiH_4 (equation 3.20), as the dehydrogenation onset temperature is reduced and the sorption rate enhanced (figure 3.25b). After several hydrogen cycles this effect even seems to be more pronounced (figure 3.30a). At the moment the origin of this influence is unclear. In contrast to $LiBH_4$-MgH_2 (hydrogen release starts with decomposition of MgH_2), the initial evolution of hydrogen in $4LiBH_4$-Mg_2NiH_4 is due to a direct reaction between the two mutually destabilised hydrides. Consequently, modified thermodynamic properties of the individual hydrides could change the dehydrogenation temperature. The substitution of Cl^- anions into $LiBH_4$, for instance, is known to change the thermodynamics of this borohydride. However, the effect of this process was described to be negligible [132] and, moreover, dissolution of LiCl in liquid $LiBH_4$ was even shown to have a minor stabilising effect causing a slight increment of the hydrogen release temperatures [133]. Also below the melting point of $LiBH_4$, the formed hexagonal solid solution $Li(BH_4)_{1-x}Cl_x$ is reported to be slightly stabilised [133]. A significant improvement of the ionic conductivity in $LiBH_4$ by Cl^- substitution was discovered for the orthorhombic phase [134]. This could also affect reaction kinetics in diffusion limited processes. However, in the temperature range of interest, i. e. above 200 °C, $LiBH_4$ is present in the hexagonal structure and the ionic conductivity of this polymorph (superionic conduction) is much higher than for the orthorhombic phase and not improved further by the Cl^- substitution [134]. Altogether, no satisfactory explanation for the $TiCl_3$ induced enhancement of the direct reaction between $LiBH_4$ and Mg_2NiH_4 can be provided based on the available experimental data. More specific experiments would have to be performed in order to identify the underlying mechanism.

3.3 The $Ca(BH_4)_2$-Mg_2NiH_4 Reactive Hydride Composite

Thorough investigations of the dehydrogenation and rehydrogenation reactions of the $Ca(BH_4)_2$-Mg_2NiH_4 composite are presented in this section. Special emphasis is placed on the determination of the influence of the hydrogen pressure on the dehydrogenation reaction path as well as on the study of the reactivity between typical decomposition products of $Ca(BH_4)_2$ with Mg_2NiH_4. Furthermore, a set of samples was dehydrogenated at different temperatures and times to assess the impact of these two parameters on the desorbed state and on the reversibility of this system. Finally, the rehydrogenation reactions are analysed in detail and special actions to improve the hydrogen absorption yield are described.

3.3.1 Experimental Results

Influence of H_2 pressure on dehydrogenation reactions If reaction kinetics are sluggish it can be difficult to distinguish between thermodynamically controlled and kinetically hindered events, i. e. experimental techniques might not be able to resolve overlapping steps. In the *in situ* SR-PXD dehydrogenation experiment of the $Ca(BH_4)_2$-Mg_2NiH_4 composite conducted at 1 bar H_2 (section 3.1.5, figure 3.15), it can be seen that basically all desorption reaction steps occur at the same time. In order to shed more light on these reactions, the measurement was repeated at pressures of 7.5 bar, 20 bar and 50 bar of hydrogen. The underlying idea is that all equilibrium temperatures of solid-gas reactions are shifted to higher values with increasing pressure. Kinetic constraints solely depend on the temperature, though. Therefore, at a certain pressure the equilibrium temperature of a particular reaction step is high enough to directly allow overcoming this step's activation energy. As a consequence, differences between thermodynamic equilibrium temperatures and measured dehydrogenation onsets (governed by kinetics) shrink with increasing hydrogen pressure and distinct reaction steps can be isolated on the temperature axis.

The evolution of crystalline phases upon dehydrogenation of $Ca(BH_4)_2$-Mg_2NiH_4 was monitored by *in situ* SR-PXD experiments (figure 3.32). The sequences of diffraction patterns obtained under 1 bar, 7.5 bar, 20 bar and 50 bar H_2 are shown in a, b, c and d, respectively. As described in section 3.1.5, at temperatures below 300 °C only the polymorphic transitions of $Ca(BH_4)_2$ and Mg_2NiH_4 are observed. For this reason, the temperature axis of the presented results is reduced to the range from 300 °C to 450 °C. Irrespective of the applied pressure, the diffraction patterns taken at 300 °C exhibit exclusively the reflections of the high temperature polymorphs β-$Ca(BH_4)_2$ and cubic Mg_2NiH_4. At 1 bar (figure 3.32a), the dehydrogenation starts with the decomposition of Mg_2NiH_4 to Mg_2Ni and hydrogen at about 318 °C. The intensity of $Ca(BH_4)_2$ diffraction peaks begins to weaken soon after, while the reflections of four other phases occur and intensify, namely $MgNi_{2.5}B_2$, Mg, CaH_2 and UP. At 365 °C the peaks of $Ca(BH_4)_2$ finally vanish. Simultaneously, the intensity of Mg_2Ni reflections maximises and quickly declines afterwards. The reflections of UP intensify up to roughly 410 °C and fade out subsequently. On the contrary, diffraction intensities of CaH_2, $MgNi_{2.5}B_2$ and Mg increase

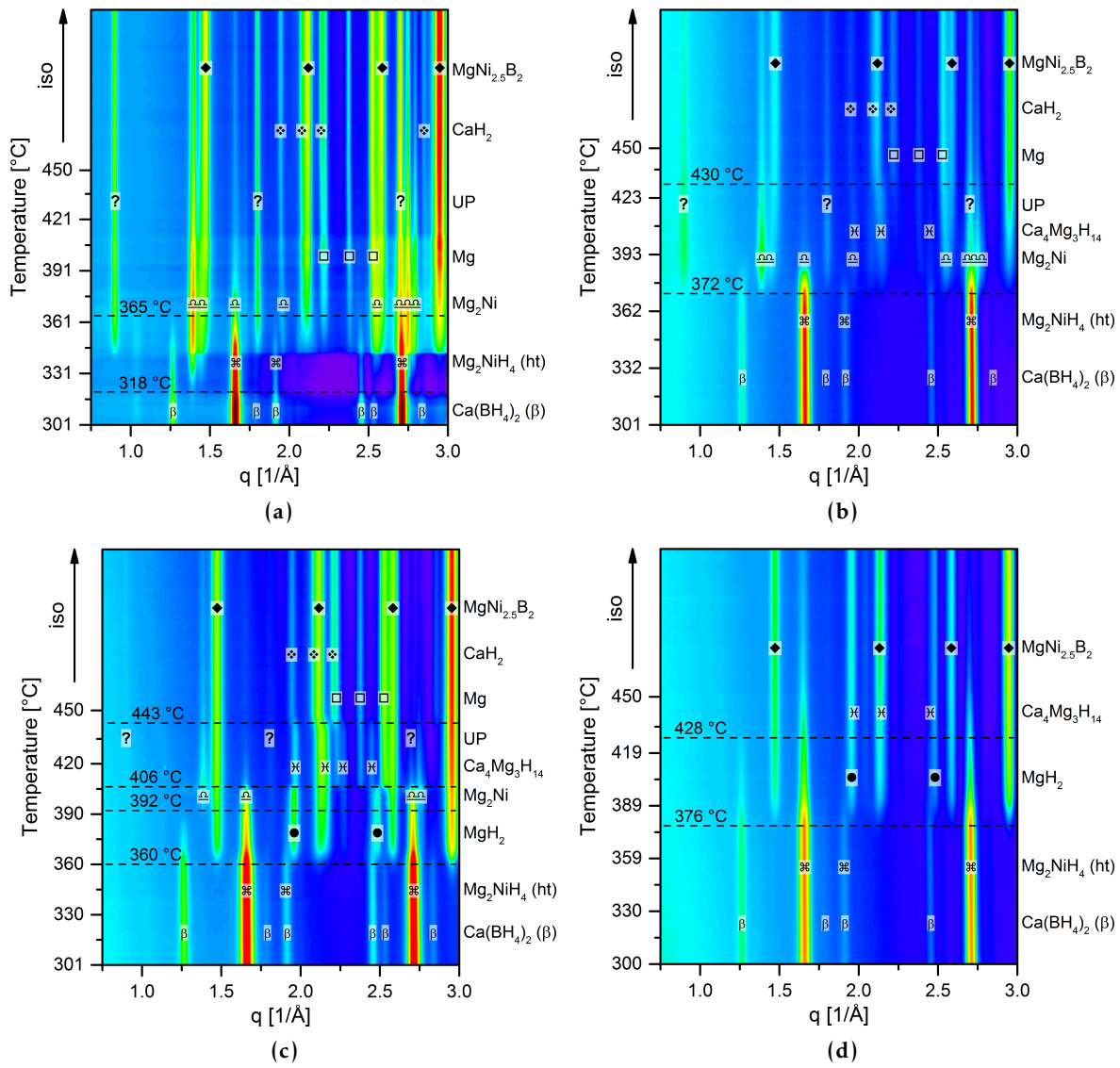

Figure 3.32: *In situ* SR-PXD dehydrogenation experiments of $Ca(BH_4)_2$-Mg_2NiH_4 conducted at different hydrogen pressures: (a) 1 bar, (b) 7.5 bar, (c) 20 bar and (d) 50 bar. The material was heated from room temperature to 450 °C at 5 K min^{-1}.

till the last diffractogram is taken. In the case of the dehydrogenation performed at 7.5 bar (figure 3.32b), the sequence of events looks almost similar to the experiment conducted at 1 bar H_2. The respective events are shifted to higher temperatures, though. Here, Mg_2NiH_4 starts to decompose at approximately 372 °C. However, differently from the experiment performed at 1 bar H_2, $Ca_4Mg_3H_{14}$ is formed instead of CaH_2. At 430 °C $Ca_4Mg_3H_{14}$ decomposes and the reflections of CaH_2 and Mg arise. The dehydrogenation of $Ca(BH_4)_2$-Mg_2NiH_4 at 20 bar H_2 (figure 3.32c) proceeds differently from the previous experiments. As it can be seen, the very first modification in the diffraction patterns is the appearance of $Ca_4Mg_3H_{14}$, $MgNi_{2.5}B_2$ and MgH_2 at about 360 °C, accompanied by intensity reductions of $Ca(BH_4)_2$ and Mg_2NiH_4. At 392 °C the diffraction peaks of Mg_2Ni appear whereas those of Mg_2NiH_4 vanish completely. Additionally, rather weak peaks of UP can be recognised shortly after. MgH_2 decomposes at 406 °C and the reflections of Mg become visible. At 443 °C $Ca_4Mg_3H_{14}$ dehydrogenates to CaH_2 and Mg. Also in this experiment the intensities of Mg_2Ni and UP reduce gradually up to the last diffractogram. As with the experiment conducted at 20 bar, the very first event at a back pressure of 50 bar H_2 (figure 3.32d) is the appearance of reflections that can be attributed to $Ca_4Mg_3H_{14}$, $MgNi_{2.5}B_2$ and MgH_2 at roughly 376 °C. From this temperature on, the intensities of $Ca(BH_4)_2$ and Mg_2NiH_4 decrease. In contrast to the continuously fading reflections of Mg_2NiH_4, the peaks of $Ca(BH_4)_2$ disappear abruptly at about 428 °C. Diffraction intensities of $Ca_4Mg_3H_{14}$, $MgNi_{2.5}B_2$ and MgH_2 increase till the last diffractogram. At this pressure, neither reflections of Mg_2Ni nor those belonging to UP can be perceived within the chosen temperature range.

In order to correlate the crystallographic changes of $Ca(BH_4)_2$-Mg_2NiH_4 upon dehydrogenation to thermal transitions and the release of hydrogen, combined calorimetric and volumetric analyses were performed replicating the experimental conditions of the SR-PXD experiments (figure 3.33). For comparison, also the DSC curves of pure $Ca(BH_4)_2$ and Mg_2NiH_4 are included in this graph. These pure compounds were ball milled in exactly the same manner as all other samples to ensure comparable kinetic properties. Figure 3.33a shows the results of the desorptions conducted at 1 bar H_2. The composite $Ca(BH_4)_2$-Mg_2NiH_4 features one broad endothermic peak (A_1) with an onset temperature of 293 °C. This is 60 K lower than the onset temperature of pure $Ca(BH_4)_2$ at 353 °C but 21 K higher than the one of pure Mg_2NiH_4 at 272 °C. The material releases about 4.5 mass% H_2. At 7.5 bar (figure 3.33b), the DSC trace of the hydride composite exhibits two separate endothermic peaks with onset temperatures of 339 °C ($A_{7.5}$) and 414 °C ($B_{7.5}$), respectively. Both peaks are related to the release of hydrogen. In the first event 4.1 mass% is evolved and additional 0.4 mass% in the second one. Hence, 4.5 mass% H_2 are desorbed in total. Compared to the pure compounds, the composite starts desorbing at about the same temperature as Mg_2NiH_4 (onset 343 °C) and 27 K below the temperature of $Ca(BH_4)_2$. The dehydrogenation experiments performed at a pressure of 20 bar H_2 are presented in figure 3.33c. As it can be seen, the DSC curve of the composite comprises four endothermic events. The onset temperatures of the peaks A_{20}, C_{20} and D_{20} are 343 °C, 410 °C and 451 °C, respectively. The second peak (B_{20}) is rather small,

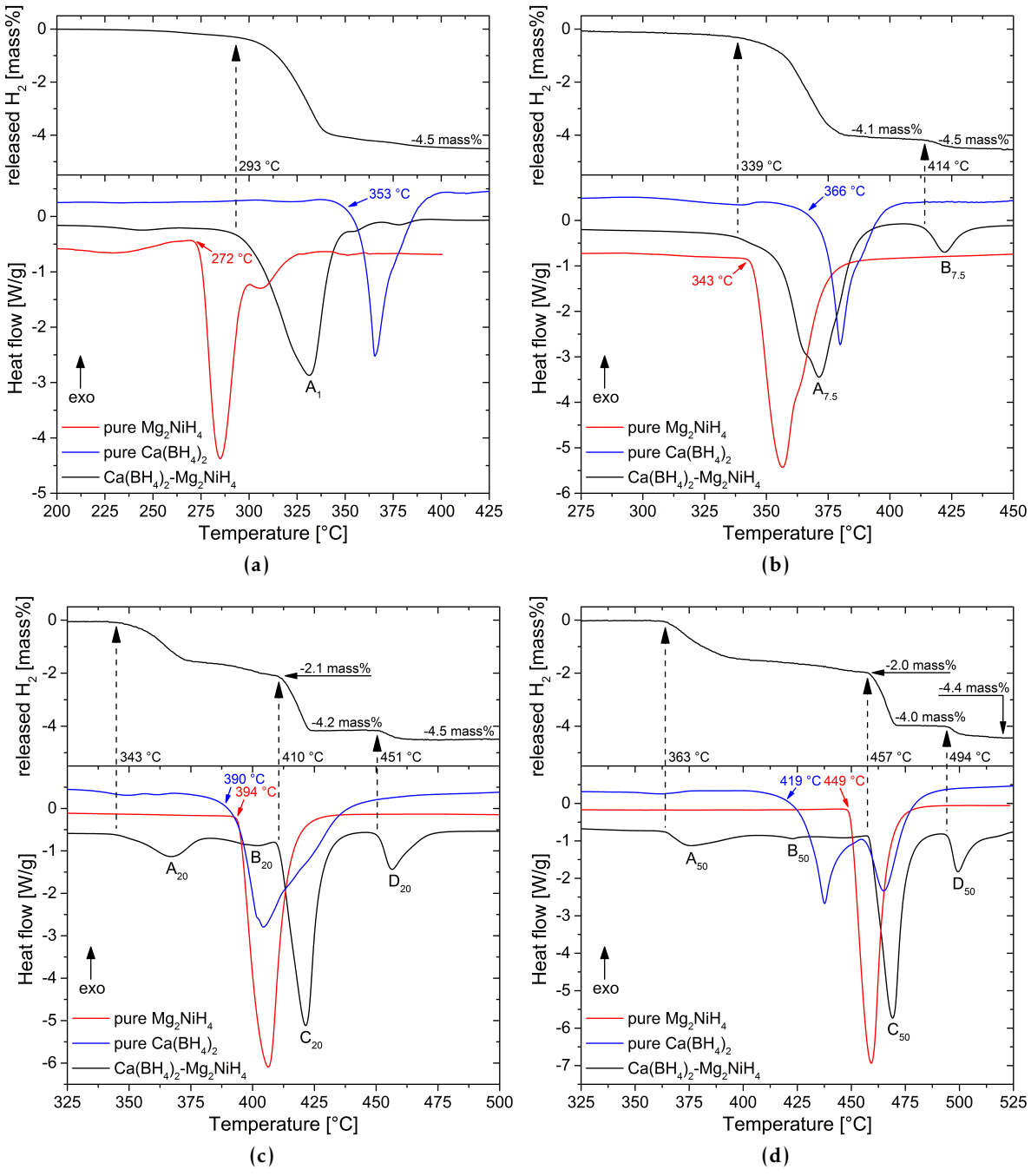

Figure 3.33: Combined DSC and volumetric analyses of $Ca(BH_4)_2$-Mg_2NiH_4, pure $Ca(BH_4)_2$ and pure Mg_2NiH_4. Hydrogen pressures of (a) 1 bar, (b) 7.5 bar, (c) 20 bar and (d) 50 bar were applied, respectively. The materials were heated from room temperature to 550 °C at a rate of 5 K min^{-1}.

though. Its onset temperature cannot be determined clearly, also because this peak might be overlapping partially with A_{20}. Nevertheless, the onset of B_{20} is certainly below 390 °C. All four peaks are associated with the evolution of hydrogen. Approximately 2.1 mass% are released in the first two reaction steps (A_{20} and B_{20}) and another 2.1 mass% in the reaction linked to C_{20}. In the last dehydrogenation step (D_{20}) 0.3 mass% H_2 evolves achieving an overall hydrogen loss of 4.5 mass%. Compared to pure $Ca(BH_4)_2$ and Mg_2NiH_4 (onsets at 390 °C and 394 °C), the temperature of the first dehydrogenation step of $Ca(BH_4)_2$-Mg_2NiH_4 (A_{20}) is reduced by about 50 K. Figure 3.33d shows the analyses performed at 50 bar H_2. Similar to the results obtained at 20 bar, the DSC curve of the composite features four endothermic peaks (A_{50}, B_{50}, C_{50} and D_{50}). Due to its low intensity, the onset temperature of the second peak (B_{50}) is difficult to estimate, however, it seems to lay at around 420 °C. The other three onset temperatures are approximately at 363 °C (A_{50}), 457 °C (C_{50}) and 494 °C (D_{50}). Each thermal event is associated with the evolution of hydrogen. During the first two reaction steps (A_{50} and B_{50}) about 2.0 mass% are released. 2.0 mass% and 0.4 mass% H_2 are released in the third (C_{50}) and fourth (D_{50}) desorption step, respectively. Therefore, the total amount of desorbed hydrogen reaches 4.4 mass%. The onset temperature of the first dehydrogenation step (A_{50}) is about 56 K lower than the onset temperature of pure $Ca(BH_4)_2$ (419 °C) and 86 K lower than the one of Mg_2NiH_4 (onset at 449 °C). By correlating the area of peak A_{50} with the amount of released hydrogen, the reaction enthalpy of this desorption step is estimated to be approximately 15 kJ $(mol\,H_2)^{-1}$.

If amorphous and/or nano-crystalline phases are involved in a chemical reaction, X-ray diffraction as well as calorimetric analyses do not provide sufficient information to fully elucidate the process. Thus, MAS NMR was employed to characterise the composition of desorbed samples with respect to ^{11}B containing phases. For this purpose, three specimens of $Ca(BH_4)_2$-Mg_2NiH_4 were dehydrogenated at 50 bar H_2 and final temperatures of 370 °C, 400 °C and 450 °C for 20 h. The normalised NMR spectra are shown in figure 3.34. The chemical shifts of $Ca(BH_4)_2$ at −31 ppm [55, 59], $CaB_{12}H_{12}$ at −15 ppm [63], boron at −1 ppm [55] and $MgNi_{2.5}B_2$ at 142 ppm are denoted. All the other signals visible in figure 3.34 are spinning sidebands of either $Ca(BH_4)_2$ or $MgNi_{2.5}B_2$. The spectrum of the sample desorbed at 370 °C features major resonance signals of $MgNi_{2.5}B_2$ and $Ca(BH_4)_2$. In addition, there is a minor signal of $CaB_{12}H_{12}$. The sample heated to 400 °C contains a smaller amount of $Ca(BH_4)_2$ and more of $MgNi_{2.5}B_2$ but also the fraction of $CaB_{12}H_{12}$ increased significantly. Furthermore, this sample seems to contain a small amount of boron. The sample heated to 450 °C exhibits the highest degree of conversion to $MgNi_{2.5}B_2$ – the resonance of $Ca(BH_4)_2$ almost disappeared – but, as compared to the 400 °C sample, an even greater fraction of boron is bonded in $CaB_{12}H_{12}$ and in the elemental state.

Reactivity with decomposition products of $Ca(BH_4)_2$ By analysing the course of reflection intensities in the *in situ* SR-PXD experiments conducted at 1 bar, 7.5 bar and 20 bar H_2 (figures 3.32a–c) it is possible to notice that the peaks of Mg_2Ni fade out whilst those of

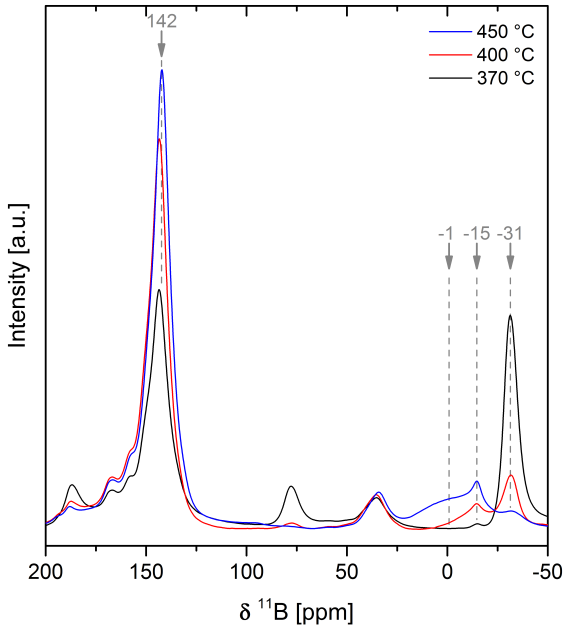

Figure 3.34: Solid-state ^{11}B MAS NMR spectra of samples of $Ca(BH_4)_2$-Mg_2NiH_4 dehydrogenated at 50 bar H_2 and temperatures of 370 °C, 400 °C and 450 °C, respectively. Chemical shifts of $Ca(BH_4)_2$, $CaB_{12}H_{12}$, elemental boron and $MgNi_{2.5}B_2$ are highlighted by arrows.

$MgNi_{2.5}B_2$ intensify after the diffraction peaks of $Ca(BH_4)_2$ already vanished. Since an additional boron source is required to form $MgNi_{2.5}B_2$ from Mg_2Ni, it is reasonable to consider non-diffractive decomposition products of $Ca(BH_4)_2$ as potential boron donors. In order to investigate this possibility, the three most common boron containing decomposition products of $Ca(BH_4)_2$, namely $CaB_{12}H_{12}$, CaB_6 and elemental boron, were chosen for an investigation of their reactivity with Mg_2NiH_4.

Mixtures of Mg_2NiH_4 with $CaB_{12}H_{12}$, CaB_6 and elemental boron were prepared in molar ratios of 15 : 1, 7.5 : 1 and 1.25 : 1, respectively, in order to meet the atomic ratio of Ni and boron in $MgNi_{2.5}B_2$. Samples of these three mixtures were heated to 450 °C in 1 bar H_2 and kept isothermally for 20 h. Afterwards PXD measurements were conducted on the obtained materials (figure 3.35a). All diffraction patterns clearly show the reflections of $MgNi_{2.5}B_2$ and Mg. In case of the samples initially prepared with $CaB_{12}H_{12}$ and CaB_6, no diffraction peaks of other compounds can be recognised. Rietveld analyses of these two diffraction patterns suggest the presence of CaH_2, though. The low intensity reflections are covered by peaks of $MgNi_{2.5}B_2$. In contrast, the diffractogram of dehydrogenated Mg_2NiH_4-B additionally displays the reflections of UP. Solid-state ^{11}B MAS NMR analyses of the same samples are presented in figure 3.35b and show the extent of boron transfer to $MgNi_{2.5}B_2$ upon heat treatment. The resonances of $MgNi_{2.5}B_2$ (complex signal with maxima at approx. 168 ppm, 152 ppm and 146 ppm), $CaB_{12}H_{12}$ (about −15 ppm), CaB_6 (two features at about 8 ppm and 0 ppm) and boron (approx. −1 ppm) are marked. In all three samples most of the boron is bonded in $MgNi_{2.5}B_2$. In the case of dehydrogenated Mg_2NiH_4-$CaB_{12}H_{12}$, $MgNi_{2.5}B_2$

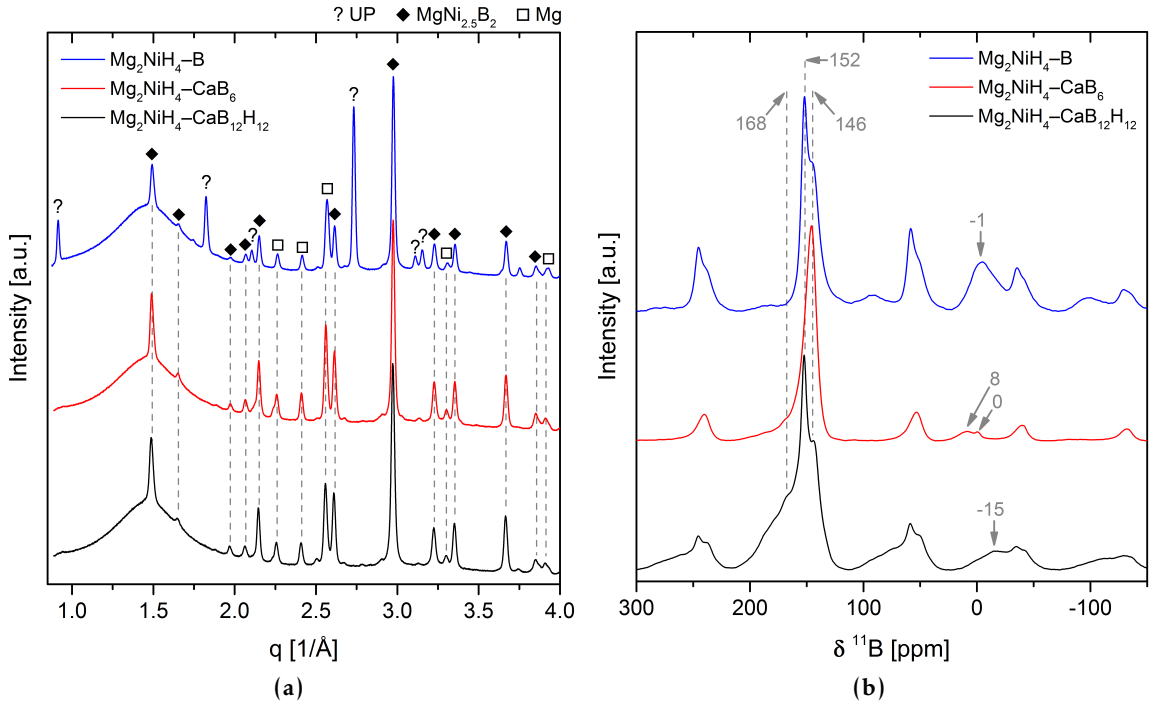

Figure 3.35: Chemical composition analyses of the reaction products between Mg_2NiH_4 and $CaB_{12}H_{12}$, CaB_6 and elemental boron, respectively: (a) X-ray powder diffractograms and (b) ^{11}B MAS NMR spectra. All samples were heated to 450 °C at a hydrogen pressure of 1 bar for 20 h.

contains about 96 % of all boron atoms – the rest is bonded in residual $CaB_{12}H_{12}$. Hence, the molar ratio of $MgNi_{2.5}B_2$ and $CaB_{12}H_{12}$ is roughly 144 : 1. For reacted Mg_2NiH_4-CaB_6 approximately 97 % of the boron atoms were transferred to $MgNi_{2.5}B_2$ which is equivalent to a molar ratio of about 97 : 1 for $MgNi_{2.5}B_2$ and CaB_6. The heated specimen of Mg_2NiH_4-B possesses the highest fraction of initial reactants: about 28 % of boron is still present in the elemental state. This corresponds to a molar ratio of $MgNi_{2.5}B_2$ and B of approximately 1.3 : 1. SR-PXD measurements showing the reactions upon heating of Mg_2NiH_4-$CaB_{12}H_{12}$ and Mg_2NiH_4-CaB_6 are presented in figure 3.36. Reaction kinetics of Mg_2NiH_4-B was too sluggish to allow for the observation by *in situ* diffraction analysis in a reasonable time frame and for this reason the experiment was not performed. The specimens of the two other composites were heated to 450 °C in 1 bar H_2. Since $CaB_{12}H_{12}$ is typically non-diffractive, only peaks of Mg_2NiH_4 can be identified in figure 3.36a up to 319 °C. At this temperature Mg_2NiH_4 decomposes and the reflections of Mg_2Ni arise. At about 383 °C $MgNi_{2.5}B_2$ and UP are formed simultaneously. Their peaks intensify till the termination of this experiment. Also in case of Mg_2NiH_4-CaB_6 the decomposition of Mg_2NiH_4 occurs at 319 °C but unlike the previously discussed experiment the emerging reflections of Mg_2Ni remain the only new peaks during the heating period. Nevertheless, after a short incubation time at 450 °C the peaks of $MgNi_{2.5}B_2$ and UP arise at roughly the same time. Possibly the growth of UP crystallites is slightly faster in this initial stage.

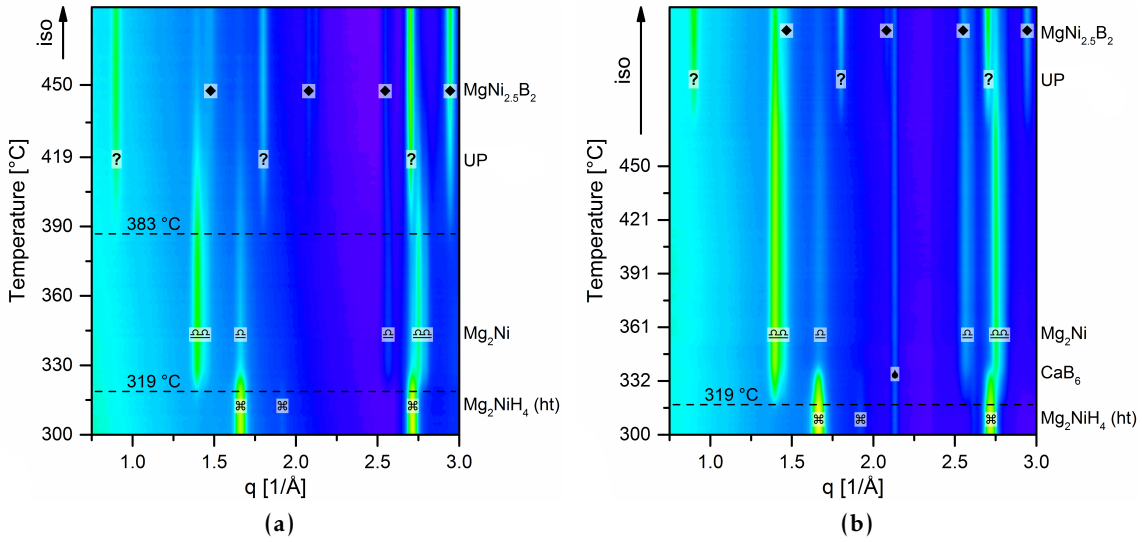

Figure 3.36: *In situ* SR-PXD dehydrogenation experiments of (a) Mg_2NiH_4-$CaB_{12}H_{12}$ and (b) Mg_2NiH_4-CaB_6, the specimens were heated in a hydrogen atmosphere of 1 bar from room temperature to 450 °C at 5 K min^{-1}.

Influence of desorption time and temperature on the dehydrogenated state and the reversibility of the system In general, the chosen temperature and duration for dehydrogenation potentially influence the reaction path as well as the degree of conversion and thus the composition and microstructure of the desorbed state. Furthermore, intermediate phases can be metastable at lower temperatures. On the contrary, longer annealing times and higher temperatures result in larger crystallite and grain sizes of the desorption products in addition to a reduction of the number of crystallographic defects. Hence, changes in the related activation energies might also affect the reabsorption reactions and therefore the degree of reversibility. In order to characterise these influences on $Ca(BH_4)_2$-Mg_2NiH_4, a set of samples was desorbed at 350 °C and 450 °C, respectively, with increasing desorption times and reabsorbed afterwards.

In total six samples were dehydrogenated at a pressure of 1 bar H_2 and then characterised by *ex situ* PXD and NMR analyses. Figures 3.37a and b show the diffraction patterns of these samples and the related ^{11}B NMR spectra, respectively. All samples were heated to their respective maximum temperatures at the same rate but the subsequent isothermal dwell time was varied. Charts with the same colour represent samples with equal total desorption time, i. e. the isothermal time was altered in such a manner that the overall time of both, heating period and dwell time, was equal for desorptions of the same set. Charts of samples with a total desorption time of 150 min are shown in black. Red and blue charts indicate total desorption times of 6 h and 42 h, respectively. All diffractograms presented in figure 3.37a exhibit the reflections of $MgNi_{2.5}B_2$, Mg and CaH_2. The samples dehydrogenated at 350 °C additionally feature the diffraction peaks of UP. The highest intensity of these reflections can be perceived in the diffractogram of the sample with a total dehydrogenation time of

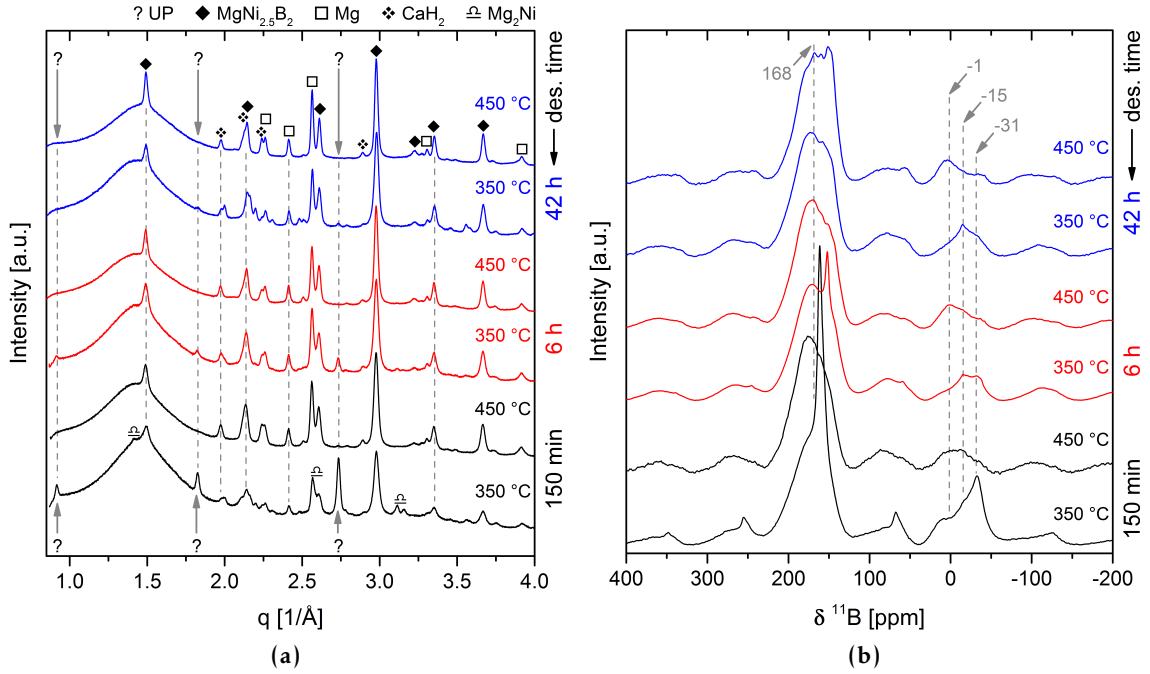

Figure 3.37: Differences in the dehydrogenation products of $Ca(BH_4)_2$-Mg_2NiH_4 evaluated by means of (a) PXD measurements and (b) ^{11}B MAS NMR analyses, all samples were heated to their respective maximum temperatures (350 °C or 450 °C) in 1 bar H_2, the dwell time was varied in order to establish equal total desorption times (150 min, 6 h and 42 h) for samples of the same set (same colour).

150 min. By increasing the isothermal heating period the respective peak intensities first decline (6 h) and eventually almost vanish (42 h). Traces of Mg_2Ni can only be recognised in case of the sample desorbed at 350 °C for 150 min. As can be seen in figure 3.37b, in all samples by far the largest fraction of boron is bonded in $MgNi_{2.5}B_2$. In all NMR spectra, the resonance of this compound is very broad and exhibits a rather asymmetric shape – the particular centerband positions are all at about 168 ppm. The resonances of $Ca(BH_4)_2$ (−31 ppm), $CaB_{12}H_{12}$ (−15 ppm), CaB_6 (0 ppm and 8 ppm) and elemental boron (−1 ppm) are all overlapping with the second spinning sideband of $MgNi_{2.5}B_2$ at lower frequencies. In conjunction with the irregular shapes of the $MgNi_{2.5}B_2$ peak in these spectra, it is hard to separate contributions of individual compounds if they are present just in small quantities. However, some general assumptions can be made. Among the samples heated to 350 °C, the one dehydrogenated for only 150 min clearly contains residual $Ca(BH_4)_2$, minor amounts of $CaB_{12}H_{12}$ and presumably traces of elemental boron or CaB_6. The sample desorbed for 6 h also shows weak signals that can be attributed to $CaB_{12}H_{12}$ and $Ca(BH_4)_2$ – the amount of $Ca(BH_4)_2$ is yet much less than in the sample with the short dehydrogenation time. After 42 h at 350 °C no more $Ca(BH_4)_2$ is discernible but only a small fraction of $CaB_{12}H_{12}$. In contrast, by heating $Ca(BH_4)_2$-Mg_2NiH_4 to 450 °C all $Ca(BH_4)_2$ already decomposes in the first 150 min. However, weak signals of what could be CaB_6 and/or elemental boron can be noticed also after 42 h. In addition, mean crystallite sizes of $MgNi_{2.5}B_2$ and Mg in the desorbed samples were evaluated as part of the Rietveld analyses and are presented in

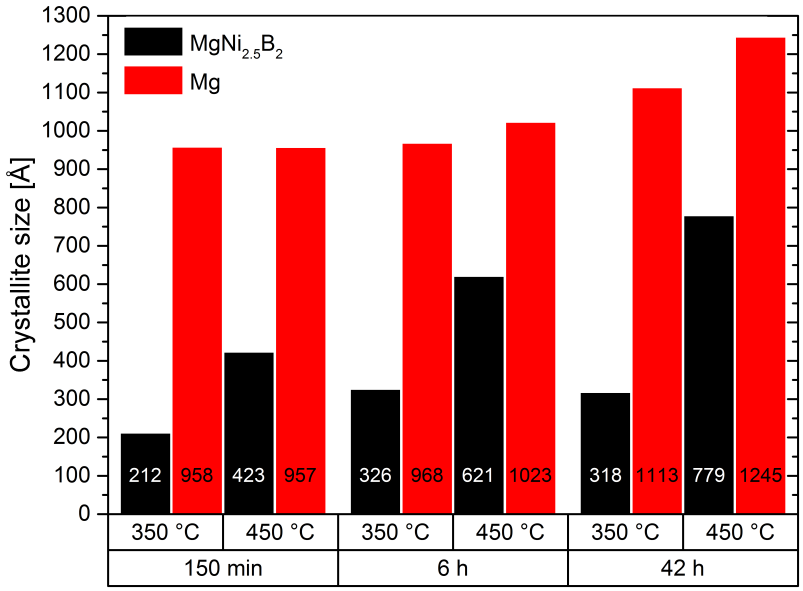

Figure 3.38: Mean crystallites sizes of $MgNi_{2.5}B_2$ and Mg in the samples presented in figure 3.37 determined by means of Rietveld analyses.

figure 3.38. As expected from the respective melting temperatures, in all investigated samples the crystallites of $MgNi_{2.5}B_2$ are significantly smaller than those of Mg. The influence of the dehydrogenation time and temperature on the crystallite growth of these two compounds is apparent as, for instance, $MgNi_{2.5}B_2$ crystallites are approximately doubled in size if the desorption temperature is increased from 350 °C to 450 °C.

In order to investigate the influence of the desorption temperature and time on the reversibility of this hydride composite, the samples were rehydrogenated. For the sake of comparability the hydrogenation of all six samples was performed simultaneously in the same experiment. After charging the autoclave with 250 bar H_2 at room temperature, the system was heated to 400 °C within 80 min and subsequently kept at this temperature for 16 h. Diffractograms and ^{11}B NMR spectra of the rehydrogenated powders are presented in figure 3.39. All samples contain $MgNi_{2.5}B_2$, $Ca_4Mg_3H_{14}$ and MgH_2. These are the only diffractive phases present in larger quantities (figure 3.39a). The specimen previously dehydrogenated at 350 °C for 6 h features two small peaks at 1.21 $Å^{-1}$ and 1.28 $Å^{-1}$ that could be assigned to the (111) reflection of α- and the (110) reflection of β-$Ca(BH_4)_2$. However, the intensities of these peaks are very low and all other potential reflections of the two $Ca(BH_4)_2$ polymorphs are possibly overlapping with other diffractions peaks. Therefore, the presence of $Ca(BH_4)_2$ in this sample cannot be confirmed with a sufficient degree of accuracy and reliability by a Rietveld refinement of the X-ray diffractogram. At this point the ^{11}B NMR analyses provide clear evidence that $Ca(BH_4)_2$ is actually present not only in this particular sample but in all samples. However, the rehydrogenated sample that was initially desorbed at 350 °C for 6 h apparently contains the highest fraction of $Ca(BH_4)_2$ among all presented samples. Although the $Ca(BH_4)_2$ resonance exhibits the highest intensity of all peaks in this

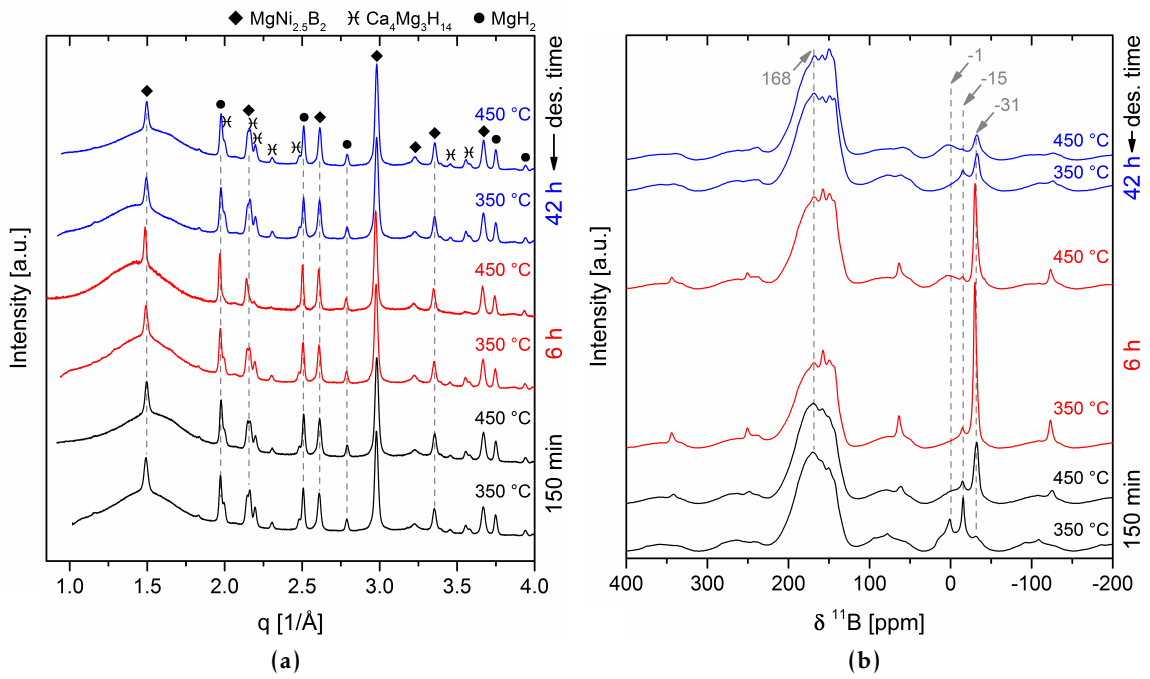

Figure 3.39: Chemical compositions of $Ca(BH_4)_2$-Mg_2NiH_4 samples desorbed at different temperatures and for different durations (see figure 3.37) after rehydrogenation: (a) PXD analyses and (b) ^{11}B MAS NMR.

spectrum, the molar ratio of $Ca(BH_4)_2$ and $MgNi_{2.5}B_2$ is only about 0.25. Considering the amount of formed $Ca(BH_4)_2$ as a measure for the degree of reversibility, a value of roughly 20 % was reached. With approximately 14 % of all boron bonded in $Ca(BH_4)_2$, the sample previously desorbed at 450 °C for 6 h shows the second highest degree of reversibility. All other samples feature reversibility levels well below 10 %. In addition, small quantities of $CaB_{12}H_{12}$ can be detected in all samples. The highest amount is found in the sample initially desorbed at 350 °C for 150 min. This sample as well as all samples dehydrogenated at 450 °C additionally seem to contain traces of elemental boron and/or CaB_6.

Analysing the absorption process by hydrogenation of different as-prepared desorbed state samples In order to obtain deeper insights into the absorption processes and potential constraints, the role and importance of the different components in the fully desorbed state was examined. As described earlier, these components are CaH_2, $MgNi_{2.5}B_2$ and Mg. In particular, the possibility to hydrogenate specimens without either CaH_2 or Mg should be investigated. Moreover, upon rehydrogenation of desorbed $Ca(BH_4)_2$-Mg_2NiH_4 a first partially hydrogenated state is created as MgH_2 is formed. Subsequently, CaH_2 is gradually consumed for the formation of $Ca_4Mg_3H_{14}$. Since this reaction proceeds without absorption of gaseous hydrogen, the degree of hydrogenation remains unchanged. However, for the chosen absorption conditions the formation of $Ca_4Mg_3H_{14}$ reduces the Gibbs free energy G of the partially hydrogenated state [56]. Therefore, the Gibbs free energy change ΔG for

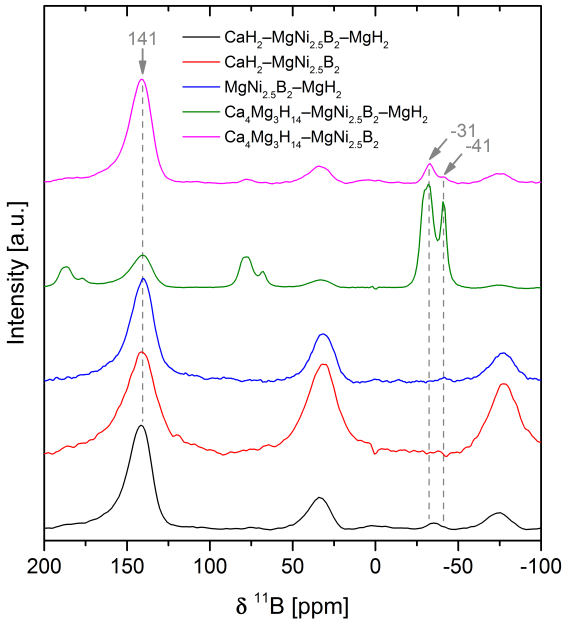

Figure 3.40: ^{11}B NMR analyses of the five different as-prepared desorbed state samples after hydrogenation.

the formation of $Ca(BH_4)_2$ from $Ca_4Mg_3H_{14}$ is reduced with respect to "$4\,CaH_2 + 3\,MgH_2$". Consequently, the formation of $Ca_4Mg_3H_{14}$ in the absorption process is expected to increase the sorption equilibrium pressure. In addition, kinetic barriers (i. e. activation energies) for the development of $Ca(BH_4)_2$ are probably changed by this intermediate reaction step as well. A similar reaction behaviour could be observed in the system CaH_2-MgB_2: $Ca_4Mg_3H_{14}$ formed in a side reaction would not react with MgB_2 and thus stop further formation of $Ca(BH_4)_2$ unless certain minimum temperature and hydrogen pressure conditions were applied [48, 135, 136].

Five samples with different compositions were prepared by ball milling: CaH_2-$MgNi_{2.5}B_2$-MgH_2, CaH_2-$MgNi_{2.5}B_2$, $MgNi_{2.5}B_2$-MgH_2, $Ca_4Mg_3H_{14}$-$MgNi_{2.5}B_2$-MgH_2 and $Ca_4Mg_3H_{14}$-$MgNi_{2.5}B_2$. The molar ratios are summarised in table 2.2. Due to the ductility of elemental magnesium and the resulting cold welding phenomena under ball milling, MgH_2 was used instead as the Mg source. Hereby, the absorption properties remain unimpaired because due to the fast hydrogenation kinetics of magnesium the formation of MgH_2 would be the first reaction step in any case. The five samples were hydrogenated simultaneously in the autoclave. The vessel was charged with 230 bar of hydrogen at room temperature and heated to 400 °C within 80 min. A final pressure of 410 bar was reached and kept for 48 h. ^{11}B NMR analyses of the hydrogenated samples are presented in figure 3.40. All samples show the resonance of unreacted $MgNi_{2.5}B_2$ at 141 ppm. The sample CaH_2-$MgNi_{2.5}B_2$-MgH_2 that resembles the composition of the dehydrogenation products of $Ca(BH_4)_2$-Mg_2NiH_4 additionally features a weak signal of $Ca(BH_4)_2$ at −31 ppm. The two samples without either CaH_2 or MgH_2 do not show any signals besides $MgNi_{2.5}B_2$. In contrast, hydrogenation of

$Ca_4Mg_3H_{14}$-$MgNi_{2.5}B_2$-MgH_2 led to the highest degree of $Ca(BH_4)_2$ formation as can be seen from the strong intensity of its resonance peak. An additional resonance at –41 ppm can be recognised. This signal can be attributed to $Mg(BH_4)_2$ [137, 138]. Also absorbed $Ca_4Mg_3H_{14}$-$MgNi_{2.5}B_2$ exhibits the signals of the two different borohydrides, the intensities are yet much lower than in the case of the material containing MgH_2. The two samples with $Ca_4Mg_3H_{14}$ as an initial reactant show the highest absorption yields among the five samples that are presented here.

Optimising the hydrogenation yield The results of the last section suggest that the rather low absorption yields that were achieved in most hydrogenation attempts must be attributed to sluggish reaction kinetics due to poor solid-state diffusion rates. A common way to address such kinetic limitations is the reduction of material particle sizes [81, 82]. This leads to shorter diffusion lengths and larger contact areas between the different reactants. The preparation of special desorbed state material with a low mean particle size is described in detail in section 2.1. This material is referred to as BMH (for ball milled in heptane).

The as-milled material (approx. 7 g) was hydrogenated in the autoclave that was initially charged with 250 bar H_2 at room temperature, heated to 400 °C within 80 min and then kept isothermally for 15 h. At the end of the hydrogenation period and before cooling down a pressure of 310 bar was measured. A specimen of the absorbed material was kept as a reference (BMH, 1st abs. step). One part of the remaining material was additionally milled in the Spex mill for 100 min and placed into the autoclave afterwards. Without additional treatment, the rest of the powder was separately placed into the autoclave, too. The second absorption step was performed in the exact same manner as the first one (final pressure[6] 420 bar). Afterwards, the material that was milled after the first absorption experiment was milled further for 100 min and returned to the autoclave. A third hydrogenation step was conducted similarly to the previous ones (final pressure 420 bar). Subsequently, specimens were taken from both the material with the intermediate milling cycles (BMH, 3rd abs. step, intermediate milling) and the material that was simply absorbed in three steps without additional treatment (BMH, 3rd abs. step, w/o intermediate milling). For comparison, an additional specimen of as-milled BMH was absorbed (2. BMH, 1st abs. step). In contrast to the previous three absorption iterations, this time only 200 mg of material were used and the autoclave was charged with an initial hydrogen pressure of 270 bar. As a consequence, the final pressure before cooling down was 440 bar. ^{11}B NMR spectra of the two different samples after just one absorption step and of the two samples after three absorption steps are presented in figure 3.41. Due to the normalisation of spectral intensities (total areas set to 1) the different spectra are directly comparable. After the first absorption step (BMH, 1st abs. step) an absorption yield of approximately 63 % was reached. Without the application

[6] As revealed by the analyses presented hereinafter, the hydrogen uptake by the sample material during the second and third absorption step was much lower than during the first. Therefore, considerably higher final hydrogen pressures were reached in these steps.

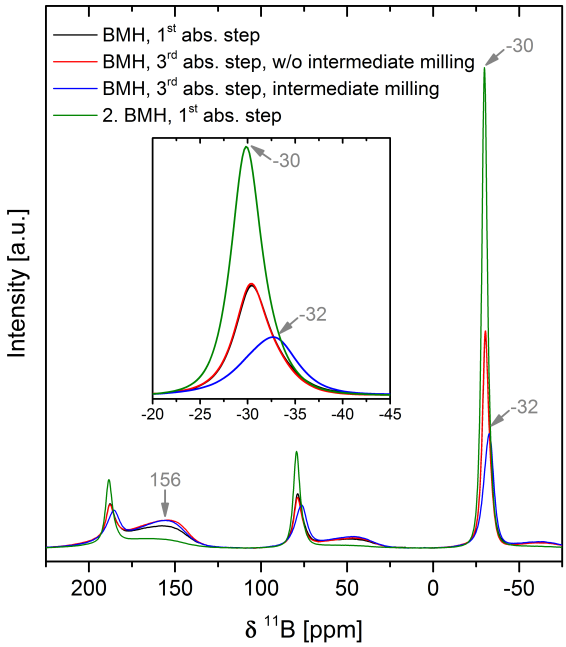

Figure 3.41: ^{11}B NMR spectra of BMH samples (i. e. CaH_2-$MgNi_{2.5}B_2$-MgH_2 with low mean particle size due to intense ball milling in heptane) after different hydrogenation approaches.

of intermediate milling cycles the two additional absorption iterations did not lead to an improved absorption yield. The corresponding spectrum (BMH, 3rd abs. step, w/o intermediate milling) looks almost identical to the one after the first absorption. In contrast, after three absorption steps with intermediate milling cycles (BMH, 3rd abs. step, intermediate milling) the intensity of the $Ca(BH_4)_2$ resonance dropped and the peak maximum shifted from −30 ppm to −32 ppm. However, the fraction of the total spectral intensity that is related to $Ca(BH_4)_2$ (areas of $Ca(BH_4)_2$ centerband incl. all spinning sidebands with respect to total area) remained unchanged because the centerband width as well as the relative intensities of the spinning sidebands increased. Thus, also after three absorption steps with intermediate milling procedures the absorption yield did not improve and remained at 63 %. The sample of as-milled BMH hydrogenated at higher hydrogen pressure led to improved conversion of the starting reactants. An absorption yield of 87 % was reached.

3.3.2 Discussion

The experiments conducted varying the hydrogen pressure clearly confirm the strong influence of this parameter on the dehydrogenation path of $Ca(BH_4)_2$-Mg_2NiH_4. At 1 bar H_2 several reaction steps take place simultaneously (figures 3.32a and 3.33a). The initial event is the desorption of Mg_2NiH_4. Immediately afterwards, the newly formed alloy Mg_2Ni reacts with $Ca(BH_4)_2$ to form $MgNi_{2.5}B_2$, CaH_2, Mg and UP. The broad DSC peak A_1 embraces all these overlapping steps. As discussed above, UP is an intermediate compound that degrades slowly. Also at 7.5 bar H_2, the first reaction step is still the independent dehydrogenation of

Mg_2NiH_4 but the follow-up reactions differ slightly from the processes 1 bar. The increased pressure enables the formation of $Ca_4Mg_3H_{14}$ – a ternary hydride that is more stable than MgH_2 [89] – besides $MgNi_{2.5}B_2$, Mg and UP. The DSC peak $A_{7.5}$ in figure 3.33b comprises these reactions. The second peak in this figure ($B_{7.5}$) is associated with the decomposition of $Ca_4Mg_3H_{14}$. The dehydrogenation of $Ca(BH_4)_2$-Mg_2NiH_4 conducted at 20 bar H_2 shows one significant difference in comparison to those performed at lower pressures: the first reaction step – the formation of $MgNi_{2.5}B_2$, $Ca_4Mg_3H_{14}$ and MgH_2 (figure 3.32c at 360 °C, figure 3.33c peak A_{20}) – occurs prior to the desorptions of residual Mg_2NiH_4 and $Ca(BH_4)_2$ (figure 3.32c at 392 °C, figure 3.33c peak B_{20}). This result suggests that the two complex hydrides, $Ca(BH_4)_2$ and Mg_2NiH_4, actually destabilise each other and react directly without initial dehydrogenation of the less stable hydride. By comparing the DSC analysis with the related *in situ* SR-PXD experiment, the DSC peaks C_{20} and D_{20} can be assigned to the desorptions of MgH_2 and $Ca_4Mg_3H_{14}$, respectively. Furthermore, weak reflections of UP appear in conjunction with those of Mg_2Ni once the decomposition temperature of Mg_2NiH_4 is exceeded (figure 3.32c at 392 °C). This observation implies once more that the reaction path leading to UP requires Mg_2Ni as reactant. Similarly to the experiment performed at 20 bar H_2, the first reaction step observed at 50 bar is the formation of $MgNi_{2.5}B_2$, $Ca_4Mg_3H_{14}$ and MgH_2 (figure 3.32d at 376 °C, figure 3.33d peak A_{50}) without the direct decomposition of Mg_2NiH_4. Due to the hydrogen back pressure of 50 bar, the equilibrium temperature of Mg_2NiH_4 was not exceeded in the course of the entire SR-PXD experiment (max. temperature limited to 450 °C) and consequently no Mg_2Ni was formed. There are also no reflections of UP discernible throughout the whole experiment which supports the proposed model of Mg_2Ni being an essential reactant for the formation of UP. In contrast to Mg_2NiH_4, residual $Ca(BH_4)_2$ decomposes independently as can be seen from the disappearance of its reflections at about 428 °C in figure 3.32d and the small DSC peak B_{50} in figure 3.33d. The last two DSC events in this figure, C_{50} and D_{50}, are related to the desorptions of MgH_2 and $Ca_4Mg_3H_{14}$, respectively. As just pointed out, at higher hydrogen pressures (here at 20 bar and 50 bar) the first dehydrogenation step seems to be a concerted reaction between $Ca(BH_4)_2$ and Mg_2NiH_4. This conclusion appears reasonable because the onset temperature of this reaction is lower than the decomposition temperatures of the pure compounds. Additionally, no reflections of Mg_2Ni are discernible in the corresponding SR-PXD experiments. However, decomposition products of $Ca(BH_4)_2$ tend to be non-diffractive [54, 55, 59, 61, 62]. Thus, it is possible that a partial or gradual desorption of $Ca(BH_4)_2$ into any of these non-diffractive phases initialises the first, presumably concerted reaction step. A rather conclusive argument that also $Ca(BH_4)_2$ does not desorb independently prior to the reaction forming $MgNi_{2.5}B_2$ is provided by the ^{11}B NMR analyses of the specimens desorbed at 50 bar H_2 and temperatures of 370 °C, 400 °C and 450 °C. The presence of residual $Ca(BH_4)_2$ in all samples shows that none of them dehydrogenated completely. Consequently, the spectra provide insights into an intermediate dehydrogenation state. At all temperatures the transfer of boron to $MgNi_{2.5}B_2$ proceeds with the fastest reaction rate since this com-

pound constitutes the highest molar fraction among all boron containing phases. Although a very small fraction of $CaB_{12}H_{12}$ is discernible already at 370 °C indicating that $Ca(BH_4)_2$ decomposed partially by itself, the peaks of $CaB_{12}H_{12}$ and elemental boron are much more pronounced at 400 °C and 450 °C. Therefore, by lowering the temperature below 370 °C the decomposition of $Ca(BH_4)_2$ can be suppressed without restraining the reaction path forming $MgNi_{2.5}B_2$. This finding is in accordance with the DSC and SR-PXD results and supports the assumption of a concerted reaction between $Ca(BH_4)_2$ and Mg_2NiH_4 at hydrogen pressures higher than (at least) 7.5 bar.

Considering only those crystalline compounds that could be detected in the SR-PXD experiments, hence neglecting the possible presence of small quantities of amorphous and/or nano-crystalline phases (i. e. CaB_xH_y, elemental boron), the release of hydrogen can be attributed to the following three thermodynamic reaction steps:

$$\begin{aligned} &Ca(BH_4)_2 + 2.5\,Mg_2NiH_4 \\ &\xrightarrow{\text{concerted}} 0.25\,Ca_4Mg_3H_{14} + MgNi_{2.5}B_2 + 3.25\,MgH_2 + \underbrace{4\,H_2}_{2.3\,\text{mass\%}} && (3.21) \\ &\longrightarrow 0.25\,Ca_4Mg_3H_{14} + MgNi_{2.5}B_2 + 3.25\,Mg + \underbrace{7.25\,H_2}_{4.2\,\text{mass\%}} && (3.22) \\ &\longrightarrow CaH_2 + MgNi_{2.5}B_2 + 4\,Mg + \underbrace{8\,H_2}_{4.6\,\text{mass\%}}. && (3.23) \end{aligned}$$

These reactions do not include Mg_2Ni and UP because these two phases do not exist in thermodynamic equilibrium but must be considered as intermediates. The theoretical amounts of hydrogen that evolve in each step are expressed in mass% with respect to the initial mass of the composite. At a pressure of 1 bar H_2, the material desorbs directly according to reaction 3.23 involving Mg_2Ni and UP as intermediate phases. By increasing the pressure to 7.5 bar, two dehydrogenation steps could be observed, namely the reactions 3.22 – again containing Mg_2Ni and UP temporarily – and 3.23. At 20 bar and 50 bar, the dehydrogenation proceeds *via* all three steps where reaction 3.21 constitutes the concerted reaction. For all investigated pressures the determined quantities of hydrogen that are released in the particular steps (figure 3.33a-d) are in good agreement with the theoretical values. This fact already indicates that no or just minor fractions of non-diffractive, hydrogen containing side products were formed upon desorption. Furthermore, it is noteworthy that at approximately 15 kJ $(mol\,H_2)^{-1}$ the estimated enthalpy change of reaction 3.21 is rather low for reversible hydrogen sorption processes. Compared to thermodynamic data obtained from pressure-composition isotherms, enthalpy values collected from DSC analyses are typically less accurate, especially if the investigated reaction proceeds with sluggish kinetics. However, the measured value still provides the correct magnitude. Moreover, for the system $LiBH_4$-Mg_2NiH_4 a similarly low reaction enthalpy was determined for the equivalent dehydrogenation step

(see section 3.2.1). The enthalpy of reaction 3.21 corresponds to an equilibrium temperature much lower than the observed dehydrogenation onsets substantiating that sluggish kinetics are governing the dehydrogenation of $Ca(BH_4)_2$-Mg_2NiH_4.

The experiments conducted to shed light on the reactivity between typical decomposition products of $Ca(BH_4)_2$ and Mg_2NiH_4 clearly show that the latter hydride or, more precisely, Mg_2Ni reacts with $CaB_{12}H_{12}$, CaB_6 and elemental boron (figures 3.35 and 3.36). This is quite remarkable since especially $CaB_{12}H_{12}$ and elemental boron are, in the range of experimental conditions investigated in this work, stable and often considered as boron sinks that reduce reversibility in pure $Ca(BH_4)_2$ as well as in $Ca(BH_4)_2$ based hydride composites [54–56, 59, 62, 63, 136, 139]. In all three mixtures $MgNi_{2.5}B_2$ was created. This phase is – except for minor amounts of the initial reactants – the only boron containing compound in fully reacted Mg_2NiH_4-$CaB_{12}H_{12}$ and Mg_2NiH_4-CaB_6 (figure 3.35). As confirmed by the *in situ* SR-PXD experiments, also the dehydrogenation reaction paths of these two mixtures involve UP as intermediate phase. For that reason it seems reasonable to assume that UP is also an intermediate compound in the reaction of Mg_2NiH_4-B and can still be detected in the *ex situ* powder diffractogram due to the highly sluggish reaction kinetics. The hydrogenation experiments (figures 3.39, 3.40 and 3.41) clearly prove the possibility to form $Ca(BH_4)_2$ by absorbing material that only contains $MgNi_{2.5}B_2$ as sole boron donor. As a consequence, it is possible to produce $Ca(BH_4)_2$ from $CaB_{12}H_{12}$, CaB_6 and elemental boron *via* formation of $MgNi_{2.5}B_2$ as a transitional compound.

The systematic variation of the dehydrogenation temperature and time for the composite $Ca(BH_4)_2$-Mg_2NiH_4 revealed that there is indeed an influence of these two parameters on the composition and microstructure of the dehydrogenated materials and on the degree of reversibility (figures 3.37, 3.38 and 3.39). Independently of the dehydrogenation conditions and in accordance with reaction3.23, the main chemical compounds of all desorbed samples are $MgNi_{2.5}B_2$, Mg and CaH_2. The temperature restriction to 350 °C leads to generally slower reaction kinetics (presence of unreacted $Ca(BH_4)_2$ after 150 min and 6 h) but also seems to promote the development of UP as an intermediate compound. This can be seen by comparing the relative intensities of UP reflections with those of $MgNi_{2.5}B_2$ in figure 3.37a and in the *in situ* experiment (figure 3.32a). If the temperature is limited to 350 °C, the following model appears to be the case: the ratio of UP formation and decomposition kinetics changes such that the net formation rate of this compound is enhanced. Moreover, also kinetics of the reaction path directly leading to the formation of $MgNi_{2.5}B_2$ could be constrained even more by the temperature restriction. Reversely, $MgNi_{2.5}B_2$ forming reactions accelerate if the temperature is continuously increased to 450 °C which results in a lower maximum concentration of UP. As will be discussed separately, the extent of solid-state diffusion required for the formation of UP is probably smaller than for the formation of $MgNi_{2.5}B_2$. Since diffusion coefficients increase with temperature, the same applies to the formation rate of $MgNi_{2.5}B_2$ – at the cost of diminished UP concentrations.

Besides $MgNi_{2.5}B_2$ all rehydrogenated samples comprise the crystalline phases MgH_2

and $Ca_4Mg_3H_{14}$ (figure 3.39a). The first is formed directly from metallic magnesium upon absorption, the latter is the product of the reaction between MgH_2 and CaH_2. Although $Ca(BH_4)_2$ was formed with an absorption yield of up to 20 % (figure 3.39b), its reflections could not be detected (unambiguously) in the related PXD analyses (figure 3.39a). Compared to the high reflection intensities of nickel containing compounds, the scattering capability of $Ca(BH_4)_2$ is rather poor. However, the complete absence of detectable reflections certainly points towards particular microstructural properties of $Ca(BH_4)_2$ such as a nanometric mean crystallite size or a high degree of disorder. Probably, the formation of this hydride is confined in some way. The highest degrees of reversibility were obtained for the two samples initially dehydrogenated for 6 h at 350 °C and 450 °C, respectively. These results suggest that different properties of the desorbed samples need to be considered in order to explain the lower absorption yields of samples with shorter (150 min) and longer (42 h) desorption time. Typically, mean crystallite and particle sizes can have a significant influence on reaction kinetics. However, in this particular case no direct correlation between crystallite sizes and the degree of reversibility can be drawn as, for instance, the sample desorbed for 42 h at 350 °C features a significantly lower mean size of $MgNi_{2.5}B_2$ crystallites than the sample desorbed for 6 h at 450 °C. The latter showed the higher degree of reversibility, though. Thus, at this point no satisfying explanation can be provided based on the presented experimental results. As the processes upon rehydrogenation seem to be rather complex, more specific experiments need to be conducted.

Hydrogenation of $MgNi_{2.5}B_2$ with solely CaH_2 or MgH_2 addition was not successful (figure 3.40). The presence of both hydrides (or their respective cations) seems to be crucial for the formation of borohydrides in this system. Interestingly, in contrast to the initial assumption that the formation of $Ca_4Mg_3H_{14}$ upon reabsorption of the decomposition products of $Ca(BH_4)_2$-Mg_2NiH_4 could hinder further formation of $Ca(BH_4)_2$ and thus impede full absorption, the opposite seems to be the case as the two samples with $Ca_4Mg_3H_{14}$ as a starting reactant feature the best absorption yields. Hence, the increased equilibrium pressure for borohydride formation due to the presence of $Ca_4Mg_3H_{14}$ did not turn out to be an obstacle. Instead, activation energies of these samples appear to be low enough to lead to higher degrees of absorption. These kinetic barriers are most likely related to solid-state diffusion processes. Since all three phases, i. e. $MgNi_{2.5}B_2$, CaH_2 and MgH_2, are required for the formation of $Ca(BH_4)_2$, the absorption reaction must take place at interfaces common to all three compounds. The further the reaction proceeds, the more diffusion of at least one of the components is necessary. If the desorbed state is prepared with $Ca_4Mg_3H_{14}$, the formation of $Ca(BH_4)_2$ will occur also at the interface of just the two phases $MgNi_{2.5}B_2$ and $Ca_4Mg_3H_{14}$. This can be seen directly for the sample $Ca_4Mg_3H_{14}$-$MgNi_{2.5}B_2$ that only features these two-phase interfaces and still contains borohydrides after absorption. Within $Ca_4Mg_3H_{14}$ the two compounds CaH_2 and MgH_2 are virtually mixed on an atomic level whereby the extent of required solid-state diffusion for borohydride formation at the interfaces with $MgNi_{2.5}B_2$ is minimized. In contrast to $Ca_4Mg_3H_{14}$-$MgNi_{2.5}B_2$-MgH_2, the sample

without the addition of MgH_2 offers a worse absorption yield. This is due to the mismatch in stoichiometry as the magnesium content in $Ca_4Mg_3H_{14}$ is just not high enough to allow for full absorption. It is noteworthy that upon hydrogenation of the two samples that were initially prepared with $Ca_4Mg_3H_{14}$, not only $Ca(BH_4)_2$ but also $Mg(BH_4)_2$ was formed. Since no $Mg(BH_4)_2$ could be detected after absorption of $MgNi_{2.5}B_2$-MgH_2, the presence of this borohydride must be directly related to $Ca_4Mg_3H_{14}$. Most likely $Mg(BH_4)_2$ is thermodynamically not stable in these systems but was formed as a metastable phase due to cation exchange reactions at the interface with $Ca_4Mg_3H_{14}$.

The preparation of the desorbed state material (BMH CaH_2-$MgNi_{2.5}B_2$-MgH_2) with strongly reduced particle size in order to enhance hydrogenation kinetics and improve the absorption yield was a great success (figure 3.41). Compared to all previous (re)hydrogenation attempts in which absorption yields of maximum 30 % to 40 % were reached, the formation of $Ca(BH_4)_2$ was 2 to 3 times more effective in this experiment. Hence, the low mean particle sizes of the reactants clearly improved the absorption kinetics of this hydride composite. Since the amount of formed borohydride did not increase upon the second and third absorption step, all $Ca(BH_4)_2$ must have been created already in the very first absorption iteration. This is easily comprehensible in case of the sample that was solely hydrogenated without additional treatment (BMH, 3rd abs. step, w/o intermediate milling). Here, already in the first absorption period, crystallite and particle sizes increased and diffusion impeding structures were created by the newly formed phases. Due to these kinetic barriers further absorption was hindered. Surprisingly, also the sample that was milled in between the individual absorption steps (BMH, 3rd abs. step, intermediate milling) did not feature an improved absorption yield compared to the reference specimen with just one absorption step (BMH, 1st abs. step). It appears that the impact of the comparatively short intermediate ball milling cycles was not enough in order to break inert structures and create new reactive interfaces of the residual reactants. Considering the low absorption yields of previous samples that were initially prepared by 300 min of ball milling in the SPEX mill, the insignificant influence of the intermediate milling cycles on the formation of $Ca(BH_4)_2$ is consistent. The milling had an impact on the microstructure of $Ca(BH_4)_2$, though. The shift of the ^{11}B resonance as well as the increased peak width are caused by a polymorphic conversion. The resonance peak is, in fact, a superposition of the two resonances of α- and β-$Ca(BH_4)_2$ at −30 ppm and −32 ppm, respectively [54, 59]. Typically, β-$Ca(BH_4)_2$ is the stable modification above approximately 175 °C [50, 116]. In this experiment, β-$Ca(BH_4)_2$ was partially stabilised at low temperatures as a consequence of the intermediate milling treatment. Furthermore, the increased relative intensity of the spinning sidebands of $Ca(BH_4)_2$ must be attributed to a reduction in the symmetry of the electronic distribution, i. e. the chemical environment, around the nucleus. The presented results not only imply that absorption of as-milled BMH basically occurred in the first hydrogenation step but also that the formation of $Ca(BH_4)_2$ must have stopped rather early. This becomes evident when considering also the second hydrogenation of as-milled BHM (2. BMH, 1st abs. step). At 87 % this sample features a significantly higher

absorption yield than the reference sample (BMH, 1st abs. step). However, this improvement cannot simply be attributed to higher hydrogen pressure in general. In fact, during the second and third absorption step of the first hydrogenation routine the pressure rose to 420 bar. It appears rather unlikely that the pressure increment from 420 bar to 440 bar could boost the absorption yield to such an extent, especially since this composite's equilibrium pressure at 400 °C must be lower than 310 bar. The particular difference between the first and the second hydrogenation of as-milled BMH was that in case of the latter already upon heating and also during the first dwelling period at maximum temperature the hydrogen pressure was considerably higher. Consequently, the stronger driving force could promote reaction kinetics and lead to an improved conversion within the same timeframe. The dwell time at 400 °C seems to be an important factor for the absorption process. The longer the powder is kept at this temperature, the more its crucial properties (very small crystallite and particle sizes, high number of defects and dislocations) induced by the intense milling process vanish and growing kinetic constraints hinder further hydrogenation. Therefore, additional absorption time – in this experiment further absorption steps – do not improve the absorption yield.

The variety of results also provides important information on $MgNi_{2.5}B_2$ which allow to draw conclusions about this compound's properties and its reactivity in the $Ca(BH_4)_2$-Mg_2NiH_4 system. In accordance with the results of the $LiBH_4$-Mg_2NiH_4 discussed in section 3.2.1, the characteristics of $MgNi_{2.5}B_2$ in the different PXD and ^{11}B NMR analyses presented in this section clearly differ due to the aforementioned homogeneity range. For instance, the comparison of the $MgNi_{2.5}B_2$ diffraction patterns in figures 3.35a and 3.37a reveals obvious differences in the reflection intensities indicating altered scattering capabilities of the Wyckoff sites, i. e. modified occupancies and/or substitutional effects. Consequently, also in the $Ca(BH_4)_2$-Mg_2NiH_4 system the experimental conditions (desorption temperature, time and hydrogen pressure as well as the type of boron donor) determine not only the reaction path and kinetics but also the state of the formed $MgNi_{2.5}B_2$. In addition, the diffractograms of the six rehydrogenated specimens (figure 3.39a) contain valuable information. By means of the Rietveld method the mass fractions of the diffractive compounds were evaluated. All samples show rather similar values that are in good agreement with the theoretical mass fractions that would be expected if only MgH_2 and $Ca_4Mg_3H_{14}$ were formed in the absorption process (56.7 mass%, 25.1 mass% and 18.2 mass% for $MgNi_{2.5}B_2$, MgH_2 and $Ca_4Mg_3H_{14}$, respectively). This applies also to the reabsorbed sample initially dehydrogenated at 350 °C for 6 h. However, the ^{11}B NMR spectrum (figure 3.39b) of this sample reveals that about 20 % of the boron is bonded in $Ca(BH_4)_2$. Thus, one would expect to find the corresponding 20 % of magnesium and nickel from $MgNi_{2.5}B_2$ in another chemical state. Besides $MgNi_{2.5}B_2$ no other nickel containing phases can be identified, though. That includes especially Mg_2Ni and Mg_2NiH_4 as well as $MgNi_2$ and elemental nickel. This observation might be ascribed to the homogeneity range of $MgNi_{2.5}B_2$, too. Since 20 % of the boron initially bonded in $MgNi_{2.5}B_2$ was transferred to $Ca(BH_4)_2$ without formation of

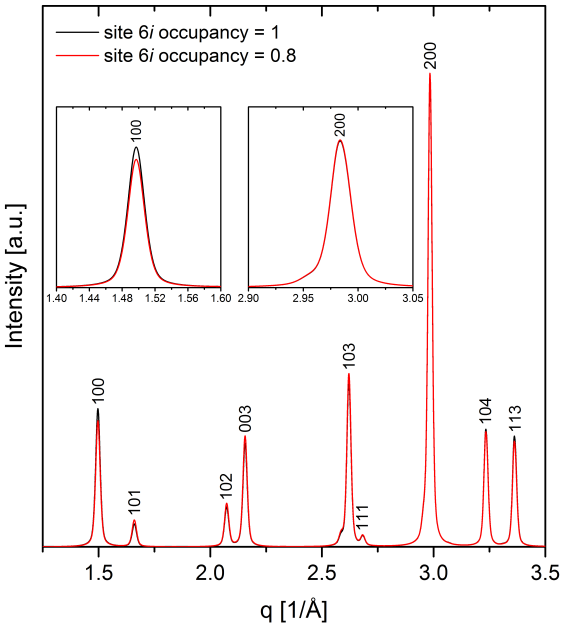

Figure 3.42: Calculated diffraction patterns of $MgNi_{2.5}B_2$ for two different occupancies (1 and 0.8) of the Wyckoff site 6*i* which is occupied by the boron atoms.

additional nickel containing compounds, the occupancy of the boron site 6*i* in the $MgNi_{2.5}B_2$ crystal must be reduced to roughly 0.8. The homogeneous reduction of the boron concentration in $MgNi_{2.5}B_2$ requires a certain mobility of boron atoms within the crystal. For a long range diffusion of boron vacancies two different interatomic distances of 1.94 Å and 3.02 Å need to be overcome alternatingly. Hence, solely from this structural point of view a reasonable mobility of boron atoms in $MgNi_{2.5}B_2$ seems possible. A reduction of the boron concentration by 20 % in $MgNi_{2.5}B_2$ would certainly affect the diffraction pattern of this phase. However, since the atomic scattering factor of boron is rather small compared to the one of magnesium and especially to the one of nickel, the impact of a reduced occupancy of site 6*i* on the reflection intensities would be relatively low. In fact, as shown in figure 3.42 the intensities of the four brightest peaks, i. e. the (200), (103), (100) and (104) reflections, would be changed by only 0.7 %, 4.3 %, 8.8 % and 2.1 %, respectively. Moreover, the (100) reflection which would be affected the most by this structural modification is superimposed by the broad background peak caused by the PMMA dome used for the *ex situ* diffraction experiments. Therefore, an experimental confirmation of the reduced boron occupancy in $MgNi_{2.5}B_2$ cannot be provided due to the resolution limit of the laboratory diffractometer. Furthermore, it should be noticed that the measured chemical shifts of $MgNi_{2.5}B_2$ differ significantly for the different experiments (figures 3.34, 3.35b and 3.37b). The respective centerband positions range from 142 ppm to 168 ppm. In addition, the shape and width of the $MgNi_{2.5}B_2$ ^{11}B NMR resonance vary noticeably for the different dehydrogenation conditions (figures 3.34 and 3.37b). These observations provide additional evidence for the variations in the crystal structure of this ternary boride. The strongly broadened ^{11}B resonance linewidth

that is observed after dehydrogenation of $Ca(BH_4)_2$-Mg_2NiH_4 at 1 bar H_2 (figure 3.37b) must be attributed to several local magnetic, i. e. chemical, environments experienced by the boron atoms. This can be motivated as well by the partial occupancy of the atomic sites providing a crystalline disordered structure. Similar to the $MgNi_{2.5}B_2$ diffraction pattern which is obtained upon dehydrogenation of $LiBH_4$-Mg_2NiH_4 at 50 bar H_2 (see section 3.2.1), also the $MgNi_{2.5}B_2$ ^{11}B resonance in the $Ca(BH_4)_2$-Mg_2NiH_4 samples desorbed at 50 bar (figure 3.34) shows the closest resemblance to the as-synthesised material (figure 2.2b). Independently from the temperature, a chemical shift of 142 ppm was determined in all these samples. This value is almost identical to the chemical shift measured for the as-synthesised $MgNi_{2.5}B_2$ (141 ppm). In contrast to the spectra of all samples desorbed at 1 bar H_2, considerably lower widths and higher symmetries of the $MgNi_{2.5}B_2$ resonance signal can be recognised in case of the specimens dehydrogenated at 50 bar. Also these characteristics are very similar to the reference material. As discussed above, at 50 bar H_2 the two hydrides $Ca(BH_4)_2$ and Mg_2NiH_4 react mutually. Especially the formation of Mg_2Ni – which seems to be an essential reactant for the formation of UP – is avoided. As for the $LiBH_4$-Mg_2NiH_4 system, also in case of $Ca(BH_4)_2$-Mg_2NiH_4 the altered reaction path at high hydrogen pressures, i. e. the concerted reaction between the borohydride and Mg_2NiH_4, facilitates the development of a more homogeneous micro- and crystal structure of $MgNi_{2.5}B_2$ which leads to the rather sharp resonance peak at the well-defined chemical shift. Most likely, the particular crystal structure of $MgNi_{2.5}B_2$ also affects the rehydrogenation kinetics and thus the degree of reversibility of $Ca(BH_4)_2$-Mg_2NiH_4. However, as set out above the state of the formed $MgNi_{2.5}B_2$ depends on many experimental parameters. Consequently, a systematic control of the crystal structure appears extremely difficult. Therefore, the influence of the $MgNi_{2.5}B_2$ crystal structure on the reversibility of this hydride composite could not be investigated in an isolated way.

The PXD and NMR analyses presented in figure 3.35 contain sufficient information to obtain a first quantitative estimate for the chemical composition of UP. Besides the reflections of $MgNi_{2.5}B_2$ and UP, the diffractogram of reacted Mg_2NiH_4-B in figure 3.35a shows neither peaks of Mg_2Ni nor any other nickel containing phase although roughly 28 % of boron remained unreacted (proven by the respective ^{11}B NMR spectrum in figure 3.35b) and the ratio of Mg_2NiH_4 and boron was chosen exactly to meet the atomic ratio of nickel and boron in $MgNi_{2.5}B_2$. The Rietveld refinement of this diffractogram – computed on those sections that do not contain reflections of UP – revealed a $MgNi_{2.5}B_2$ to magnesium weight ratio of about 72 : 28. The corresponding values for reacted Mg_2NiH_4-$CaB_{12}H_{12}$ and Mg_2NiH_4-CaB_6 are 75 : 25 and 72 : 28, respectively. These three ratios are very similar although (almost) full boron transfer to $MgNi_{2.5}B_2$ only occurred in case of the latter two samples. This implies that all or at least the majority of magnesium in reacted Mg_2NiH_4-B was released as a by-product of the $MgNi_{2.5}B_2$ formation. Consequently, for the formation of UP from the reactants Mg_2NiH_4 and boron no or just very minor amounts of magnesium are consumed or set free. Therefore, the atomic ratio of magnesium and nickel in UP must be equal or close to 2 : 1. The three ratios slightly differ from the theoretical weight ratio of $MgNi_{2.5}B_2$ and magnesium

of 67 : 33 that is expected to be present in all samples if boron is transferred exclusively to $MgNi_{2.5}B_2$. This small deviation might be caused by differences between the actual atomic composition of $MgNi_{2.5}B_2$ obtained under these experimental conditions and the structure (and thus composition) used for the Rietveld refinements which is based on Jung's publication [85]. In other words, the structural freedom of $MgNi_{2.5}B_2$ due to the homogeneity range was not taken into account at this point. Furthermore, the total atomic ratio of nickel and boron in the sample Mg_2NiH_4-B equals 2.5 : 2. Since all nickel is either bonded in $MgNi_{2.5}B_2$ or UP but about 28 % of boron remained in the elemental state, the atomic ratio of nickel and boron in UP must be greater than 2.5 : 2. These considerations can be expressed in the following chemical equation (here assuming the atomic ratio of magnesium and nickel in UP to be exactly 2 : 1):

$$
\begin{aligned}
2.5\,Mg_2NiH_4 + 2\,B &\longrightarrow 2.5\,Mg_2Ni + 2\,B + 5\,H_2\uparrow \\
&= x\,(2.5\,Mg_2Ni + 2\,B) + (1-x)(2.5\,Mg_2Ni + 2\,y\,B + 2\,(1-y)\,B) \\
&\longrightarrow x\,(MgNi_{2.5}B_2 + 4\,Mg) + (1-x)(Mg_5Ni_{2.5}B_{2y} + 2\,(1-y)\,B) \\
&= x\,MgNi_{2.5}B_2 + 4\,x\,Mg + (1-x)\underbrace{Mg_5Ni_{2.5}B_{2y}}_{\approx \text{UP}} + \underbrace{2\,(1-x)(1-y)}_{\approx 0.28}\,B
\end{aligned}
\tag{3.24}
$$

, with $x, y \in]0, 1[$.

Unfortunately, it is not possible to determine x and y because a second boundary condition cannot be extracted from the experimental results. Since UP is an intermediate phase in the reaction between a boron donor and Mg_2Ni to $MgNi_{2.5}B_2$, the estimated atomic composition of UP appears plausible. The ratio of magnesium and nickel is similar or equal to the one in Mg_2Ni and the relative boron content is lower than the one in $MgNi_{2.5}B_2$. Considering that solid-state diffusion is often the rate limiting step in solid-solid reactions, the formation of thermodynamically less favourable, intermediate phases might occur that require less atomic diffusion. Comparing the atomic compositions of $MgNi_{2.5}B_2$ and UP, the necessary extent of solid-state diffusion to form the latter compound from the described starting reactants is certainly smaller. Interestingly, the ^{11}B NMR spectrum of reacted Mg_2NiH_4-B only appears to exhibit the resonances of $MgNi_{2.5}B_2$ and boron. No other distinct signals could be resolved. Therefore the resonance of UP seems to overlap with the one of $MgNi_{2.5}B_2$. Hence, the chemistry of boron must be rather similar in these two compounds.

4 Summary and Conclusion

In the present work a new class of Reactive Hydride Composites was systematically investigated. These materials are combinations of the most interesting alkali and alkaline earth metal borohydrides $M(BH_4)_n$ ($M \in \{Li, Na, K, Mg, Ca\}$ and $n \in \{1, 2\}$) with Mg_2NiH_4. The new results and conclusions on these representative model systems are important from both the scientific point of view as well as with regards to possible applications. The new findings are summarised here.

Initially screening experiments were conducted for the five systems. The overall dehydrogenation reactions for the $LiBH_4$, $NaBH_4$, $Mg(BH_4)_2$ and $Ca(BH_4)_2$ based composites follow the same pattern: boron is successively transferred to $MgNi_{2.5}B_2$ as the reactions proceed. The KBH_4 based system represents an exception, as the borohydride remains stable within the investigated temperature range. This can be attributed to the higher thermodynamic stability of KBH_4 as compared to the other borohydrides investigated here. In terms of reversibility of the sorption process, (partial) rehydrogenation and thus recovery of the initial borohydrides could be achieved for the three composites based on $LiBH_4$, $NaBH_4$ and $Ca(BH_4)_2$. In addition, KBH_4 could easily be synthesised from an as-prepared mixture of KH, $MgNi_{2.5}B_2$ and MgH_2, proving that the reverse reaction is in principle feasible under appropriate conditions. In conclusion, only the recovery of $Mg(BH_4)_2$ was not successful. Whether this is due to rather high and thus experimentally not accomplished thermodynamic conditions required for (re)hydrogenation, i. e. highly demanding temperature and hydrogen pressure conditions, or due to kinetic constraints could not be clarified based on the experiments performed here. Given its comparatively high hydrogen content, fast reaction kinetics and promising reversibility, the $LiBH_4$-Mg_2NiH_4 system was chosen for further studies. In addition, also $Ca(BH_4)_2$-Mg_2NiH_4 was the subject of additional investigations because the complete boron transfer to the reaction partner is a unique feature among all reversible $Ca(BH_4)_2$ based hydride composites.

Different compositions of the RHC based on $LiBH_4$ and Mg_2NiH_4 were characterised systematically. The system with the molar ratio 2 : 2.5, i. e. the $LiBH_4$-Mg_2NiH_4 composite, shows some very interesting and unique properties. First of all, the two hydrides react mutually if the dehydrogenation of Mg_2NiH_4 is prevented by the application of a certain temperature dependant minimum hydrogen pressures. The restriction of the temperature during dehydrogenation was also proven to facilitate this concerted reaction: at 270 °C, i. e. below the melting point of $LiBH_4$, the reaction between solid $LiBH_4$ and Mg_2NiH_4 was observed. The mutual destabilisation between these two compounds reduces the system's

reaction enthalpy significantly. A value of about 13 kJ $(\mathrm{mol\,H_2})^{-1}$ was experimentally determined by evaluation of DSC analyses. In addition, a rather low entropy change – less than 70 J $(\mathrm{K\,mol\,H_2})^{-1}$ appears plausible – could be estimated. Furthermore, independent of the applied hydrogen pressure chosen for dehydrogenation, (almost) no $Li_2B_{12}H_{12}$ could be detected among the reaction products. As the dedicated experiment revealed, Mg_2Ni also reacts with $Li_2B_{12}H_{12}$ and forms $MgNi_{2.5}B_2$. Hence, $Li_2B_{12}H_{12}$ can be regarded as an intermediate phase in the $LiBH_4$-Mg_2NiH_4 RHC and therefore, unlike the $LiBH_4$-MgH_2 system, no special dehydrogenation conditions (i. e. a certain minimum hydrogen pressure) need to be applied in order to preserve the system's hydrogen storage capacity. Interestingly, larger quantities of MgB_2 were identified in completely dehydrogenated $LiBH_4$-Mg_2NiH_4. Thermodynamic estimations suggest that the formation of MgB_2 is energetically less favourable than the intended reaction. However, this compound is formed *via* an accessible (side) reaction path between free magnesium and yet unreacted $LiBH_4$. It must be emphasised that the formation of MgB_2 does not impede reversibility. A high hydrogenation yield of approximately 90 % was achieved after ten hydrogen cycles.

For the $4LiBH_4$-Mg_2NiH_4 composite, i. e. for a molar ratio of 4 : 1, the formation of MgB_2 is intended. At 5 bar H_2 the reaction proceeds as expected and the two borides $MgNi_{2.5}B_2$ and MgB_2 are formed. However, similar to the $LiBH_4$-MgH_2 system a certain minimum hydrogen pressure is required to promote the formation of MgB_2. At a dehydrogenation pressure of 1 bar H_2 significant amounts of $Li_2B_{12}H_{12}$ and amorphous boron are formed and drastically diminish the reversible hydrogen capacity of the system. The direct comparison between $4LiBH_4$-Mg_2NiH_4 and $LiBH_4$-MgH_2 revealed that the onset temperatures of all dehydrogenation steps – including the formation of MgB_2 – are noticeably reduced in case of the former system. Moreover, the addition of Ti-based compounds ($TiCl_3$ used in experiments) clearly enhanced the general dehydrogenation kinetics of the $4LiBH_4$-Mg_2NiH_4 system. A beneficial effect is not only observed for the nucleation and growth of MgB_2 but also for the concerted reaction between $LiBH_4$ and Mg_2NiH_4. However, the positive influence of the additive appears to cease upon hydrogen cycling. The reason for this behaviour is still unknown. In order to shed more light on this issue specific experiments, e. g. XAS measurements at the Ti K-edge, are required to determine the chemical state of titanium within the samples before and after cycling. If the performance of the additive can be stabilised, the $4LiBH_4$-Mg_2NiH_4 composite could pose an attractive alternative to the $LiBH_4$-MgH_2 system.

The Reactive Hydride Composite $Ca(BH_4)_2$-Mg_2NiH_4 was also characterised in detail. The results demonstrate that the dehydrogenation reaction path of this composite strongly depends on the applied hydrogen pressure. Independent of this pressure, only CaH_2, $MgNi_{2.5}B_2$ and Mg are present after full dehydrogenation. Three consecutive reaction steps could be distinguished. The first step can be observed at hydrogen pressures higher than (at least) 7.5 bar and appears to be a concerted reaction between $Ca(BH_4)_2$ and Mg_2NiH_4 forming the three dehydrogenation products $Ca_4Mg_3H_{14}$, $MgNi_{2.5}B_2$ and MgH_2. This reaction occurs at temperatures lower than the dehydrogenation temperatures of pure $Ca(BH_4)_2$ and Mg_2NiH_4

confirming the mutual destabilisation between the two hydrides. By means of DSC analyses, the enthalpy of this concerted reaction was estimated to be approximately 15 kJ $(\mathrm{mol\,H_2})^{-1}$. At lower hydrogen pressures the dehydrogenation of the composite starts with the desorption of Mg_2NiH_4 under formation of Mg_2Ni. In addition, the successful synthesis of $MgNi_{2.5}B_2$ from Mg_2NiH_4 and each of the three typical boron containing decomposition products of $Ca(BH_4)_2$, i. e. CaB_6, $CaB_{12}H_{12}$ and elemental boron was demonstrated. Consequently, these compounds cannot be found (in larger quantities) among the reaction products of $Ca(BH_4)_2$-Mg_2NiH_4 after full dehydrogenation. $CaB_{12}H_{12}$ and elemental boron are usually considered as stable boron sinks that hinder (full) reversibility of $Ca(BH_4)_2$ and its respective composites. The transfer of boron from these compounds to the phase $MgNi_{2.5}B_2$ is a very important discovery for the utilisation of $Ca(BH_4)_2$ as a reversible hydrogen storage medium because $MgNi_{2.5}B_2$ is capable to donate the boron for the recovery of $Ca(BH_4)_2$. Although the reversibility of $Ca(BH_4)_2$-Mg_2NiH_4 is rather limited without special treatment due to slow solid-state diffusion processes, an absorption yield of about 87 % was reached by intense ball milling prior to the hydrogenation procedure.

It should be emphasised once again that $LiBH_4$-Mg_2NiH_4 and $Ca(BH_4)_2$-Mg_2NiH_4 are the only known reversible borohydride based composites so far that feature a mutual destabilisation mechanism. It appears very likely that the concerted reaction between the hydrides is somehow enabled by Mg_2NiH_4. In contrast to simple binary ionic hydrides such as MgH_2, Mg_2NiH_4 contains molecular anions. Whether the $[NiH_4]^{4-}$ complex may interact with the $[BH_4]^-$ anion in a particular way or a certain catalytic activity is introduced due to the presence of nickel is yet to be understood, though. In order to obtain a more comprehensive understanding of the underlying mechanism, specific experiments probing the molecular dynamics are necessary.

The chemistry of boron appears to be diverse in all systems introduced here. Especially the processes involved in the formation of the Mg-Ni-B compounds show some very interesting properties. The presented results clearly show that the reactions between Mg_2Ni and any of the considered boron donors results in the intermediate formation of a yet unknown phase (UP). The atomic composition of this ternary boride could be estimated to $\mathrm{Mg:Ni:B} = 2:1:x$ with $x < 0.8$. The determined ratio of Mg and Ni is similar to the one in Mg_2Ni and the relative boron content is lower than in $MgNi_{2.5}B_2$. Considering the atomic compositions of the samples investigated here, the formation of UP is thermodynamically less favourable as compared to $MgNi_{2.5}B_2$. However, the reduced extent of solid-state diffusion required for its nucleation and growth seems to be a plausible explanation for the intermediate character of UP in the dehydrogenation process. As the reaction progresses, more and more boron is available and the boron rich phase $MgNi_{2.5}B_2$ can form. As pointed out above, $MgNi_{2.5}B_2$ features a certain homogeneity range. The atomic composition of this compound is not fixed. Instead, the substitution of nickel and magnesium atoms and the relatively strong variations in the occupancy factors of the different atomic sites give $MgNi_{2.5}B_2$ a great structural diversity. The state of this compound highly depends on the way it is formed, i. e. on the

experimental conditions.

5 Outlook

The results presented so far provide valuable information from both a scientific and application-oriented perspective. With regard to hydrogen storage applications, the systems based on $LiBH_4$ and Mg_2NiH_4 certainly show the greatest potential. The $4LiBH_4$-Mg_2NiH_4 Reactive Hydride Composite in particular should be considered for future investigations. The high hydrogen capacity of 8.1 mass% already makes this system very attractive and the concerted reaction mechanism of the first dehydrogenation step leads to lower operation temperatures than those required in the $LiBH_4$-MgH_2 system. The decisive factor is whether the problem of capacity loss of the second dehydrogenation step upon cycling, i. e. the impaired formation of MgB_2, can be solved. In principle, the reversible exchange of boron between $LiBH_4$ and MgB_2 should work very well. After all, this exchange mechanism is the basis for the reversible sorption reactions in the $LiBH_4$-MgH_2 system. Thus, further studies should certainly investigate the exact cause of this deterioration. The presented results indicate that the effect of the additive decreases through cycling. It should be determined whether this is related to reactions involving titanium. In this case, suitable non-titanium based additives whose performance is known from the $LiBH_4$-MgH_2 system should be tested. In addition, by means of a systematised parameter study, optimal temperature and pressure conditions for both dehydrogenation as well as rehydrogenation should be assessed under which the storage capacity of the $4LiBH_4$-Mg_2NiH_4 can be maintained.

Taking into account the moderate hydrogen capacity of only 4.6 mass% and the still high dehydrogenation temperatures, $Ca(BH_4)_2$-Mg_2NiH_4 is certainly not the most appealing solution for practical hydrogen storage applications. The problematic reversibility of this system (challenging absorption conditions, necessary activation of desorbed state for high hydrogenation yields) is another critical issue. In this context, the kinetic limitations due to low solid-state diffusion rates are surely the biggest obstacle. From a scientific point of view, however, the $Ca(BH_4)_2$-Mg_2NiH_4 system represents an extremely interesting research subject. If the mechanism behind the mutual destabilisation between $Ca(BH_4)_2$ and Mg_2NiH_4 can be understood better, the obtained knowledge can be transferred and used to develop other Reactive Hydride Composites with higher hydrogen capacities. Furthermore, particular emphasis should be placed on the peculiarities of the Mg-Ni-B system. It is extremely exciting that Mg_2Ni appears to be capable of reacting with a broad variety boron containing compounds of which many are typically considered as kinetically stable and thus non-reactive under moderate temperature conditions, e. g. amorphous boron or $[B_{12}H_{12}]^{2-}$ compounds. The development of a theoretical model describing the molecular dynamics and

thus providing useful explanations for the significantly lowered activation energies associated with these reactions would be extremely important. It is clear that the transport of boron in the Mg-Ni-B system is the most crucial mechanism to understand. That includes the transfer of boron atoms from one phase to another as well as the diffusion of these atoms within each of the different phases. The presented results unambiguously indicate the good mobility of boron within $MgNi_{2.5}B_2$ as well as a rather broad homogeneity range of this compound, i. e. a high degree of freedom with respect to atomic occupancies. Therefore, future research should aim for an even better understanding of the specific features and characteristics of the Mg-Ni-B system. Dedicated *in situ* experiments (e. g. TEM, NMR or EXAFS) allowing to monitor the formation and decomposition of the different phases would be the first choice in this regard. Special attention should be paid to the as yet unknown phase referred to as UP. In the experiments this phase showed faster kinetics in taking up boron than $MgNi_{2.5}B_2$. An approach worth considering would be the development of RHCs in which the formation of UP is intended as the final and sole boron containing reaction product. Perhaps UP proves to be an even better boron donor for the recovery of borohydrides than $MgNi_{2.5}B_2$. In order to characterise the pivotal properties of this compound, its exact composition and crystal structure need to be determined. In a first attempt to do so, Mg_2NiH_4 and boron were mixed in a ratio according to the calculations presented in chapter 3.3, i. e. a sample with the molar ratio Mg_2NiH_4 : B of 5 : 2 was prepared. The atomic ratio Mg : Ni : B within this material was 2 : 1 : 0.4. Considering that the boron content in UP was estimated between 0 and 0.8, a value of 0.4 appeared to be a reasonable choice. The material was heated to 700 °C for 60 min and afterwards its diffraction pattern was collected. As can be seen in figure 5.1a (bottom), the diffractogram displays very strong reflections of UP. This compound is by far the most intense phase and other compounds are only present in minor quantities. This result confirms that the estimated composition of UP is actually very good and its molecular formula must be (similar to) $Mg_5Ni_{2.5}B$. A Rietveld refinement of the known crystalline phases – $MgNi_{2.5}B_2$, Mg_2Ni, Mg, MgO, Fe and $Mg_{3.58}Ni_{6.42}B_2$ were identified – was prepared. For that purpose all regions containing UP reflections were excluded from the optimisation (figure 5.1a (top)). Afterwards the final refinement was subtracted from the experimental data. The obtained result is presented in figure 5.1b. This diffraction pattern (theoretically) should only contain reflections of UP and, in deed, all major Bragg peaks[1] can be attributed to this compound. By means of the modified diffractogram it was intended to determine the crystal structure of UP. However, there are several minor reflections visible in figure 5.1b that cannot be attributed to UP unambiguously. Although these reflections are just very small, for the proper determination of the crystal structure it is crucial to know whether these peaks are related to UP or not. Especially the assignment of the small Bragg peak at about $1.5\,Å^{-1}$ has a significant influence on the determination of the correct lattice system and cell parameters. So far, a cubic or rhombohedral lattice can be excluded. Most likely UP crystallises in a tetragonal or

[1] For the reliable identification of UP reflections also several *in situ* SR-PXD experiments were analysed carefully in order to attribute the Bragg peaks to the different crystalline compounds.

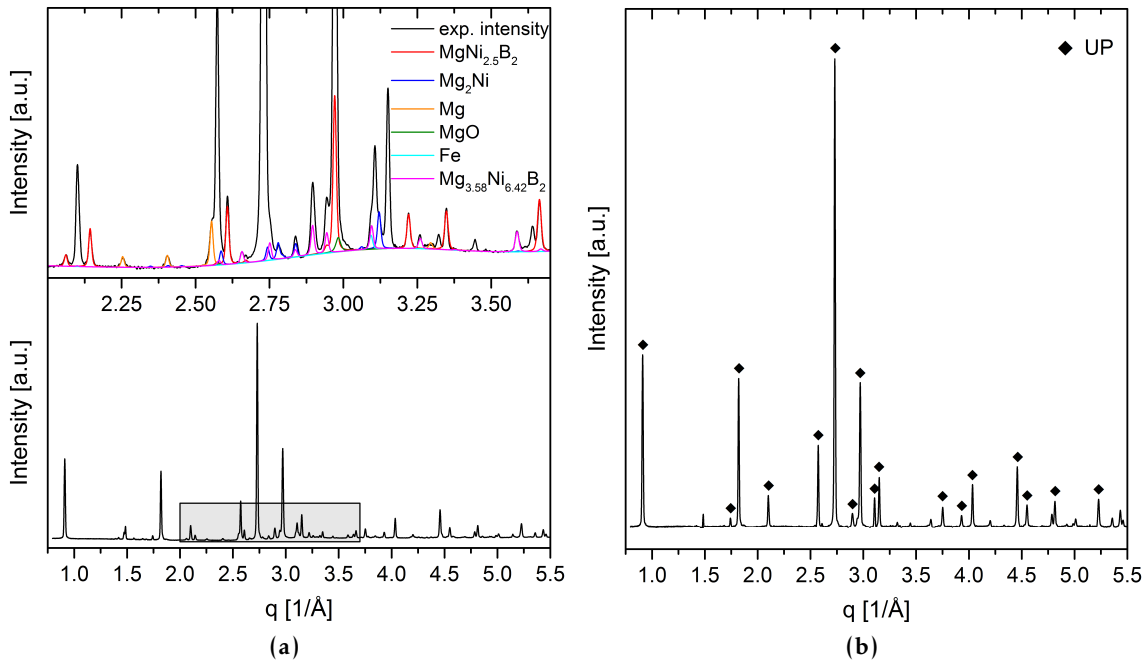

Figure 5.1: X-ray diffraction analysis of annealed "$5\,Mg_2NiH_4 + 2\,B$": (a) the full diffraction pattern is shown at the bottom, the greyed out area is presented enlarged at the top, contributions of identified known compounds are displayed based on a Rietveld analysis, (b) experimental intensity minus the calculated contributions of the known compounds providing an almost single-phase diffractogram of UP.

orthorhombic structure. However, there are several equally good solutions. Consequently, for the clear determination of the correct crystal structure more diffraction data of UP is required. Samples with small variations of the boron content should be prepared to promote or suppress the formation of other compounds. This approach should allow for a clear identification of UP reflections and thus enable the structure solution.

Bibliography

[1] T. M. I. Mahlia, T. J. Saktisahdan, A. Jannifar, M. H. Hasan and H. S. C. Matseelar. 'A review of available methods and development on energy storage; Technology update'. In: *Renewable and Sustainable Energy Reviews* 33 (2014), pp. 532–545.

[2] B. Zakeri and S. Syri. 'Electrical energy storage systems: A comparative life cycle cost analysis'. In: *Renewable and Sustainable Energy Reviews* 42 (2015), pp. 569–596.

[3] B. Zakeri and S. Syri. 'Corrigendum to "Electrical energy storage systems: A comparative life cycle cost analysis" [Renew. Sustain. Energy Rev. 42 (2015) 569–596]'. In: *Renewable and Sustainable Energy Reviews* 53 (2016), pp. 1634–1635.

[4] M. A. Pellow, C. J. M. Emmott, C. J. Barnhart and S. M. Benson. 'Hydrogen or batteries for grid storage? A net energy analysis'. In: *Energy & Environmental Science* 8 (2015), pp. 1938–1952.

[5] A. Züttel, A. Remhof, A. Borgschulte and O. Friedrichs. 'Hydrogen: the future energy carrier'. In: *Philosophical Transactions of the Royal Society A: Mathematical, Physical and Engineering Sciences* 368 (2010), pp. 3329–3342.

[6] A. Züttel, A. Borgschulte and L. Schlapbach, eds. *Hydrogen as a Future Energy Carrier*. WILEY-VCH Verlag GmbH & Co. KGaA, 2008.

[7] M. Hirscher, ed. *Handbook of Hydrogen Storage: New Materials for Future Energy Storage*. WILEY-VCH Verlag GmbH & Co. KGaA, 2010.

[8] T. Q. Hua, R. K. Ahluwalia, J.-K. Peng, M. Kromer, S. Lasher, K. McKenney, K. Law and J. Sinha. 'Technical assessment of compressed hydrogen storage tank systems for automotive applications'. In: *International Journal of Hydrogen Energy* 36 (2011), pp. 3037–3049.

[9] T. Brunner and O. Kircher. 'Cryo-compressed Hydrogen Storage'. In: *Hydrogen Science and Engineering: Materials, Processes, Systems and Technology*. Wiley-Blackwell, 2016. Chap. 29, pp. 711–732.

[10] Toyota Motor Europe. *Hydrogen? Is that safe?* URL: https://blog.toyota.eu/safety/hydrogen-is-that-safe/ (visited on 26/01/2018).

[11] A. Goodwin. *Hyundai Nexo: We drove Hyundai's hydrogen prototype to CES 2018*. URL: https://www.cnet.com/roadshow/news/we-drove-hyundais-new-hydrogen-prototype-to-ces-2018/ (visited on 26/01/2018).

[12] L. Schlapbach and A. Züttel. 'Hydrogen storage-materials for mobile applications'. In: *Nature* 414 (2001), pp. 353–358.

[13] S. Orimo, Y. Nakamori, J. R. Eliseo, A. Züttel and C. M. Jensen. 'Complex Hydrides for Hydrogen Storage'. In: *Chemical Reviews* 107 (2007), pp. 4111–4132.

[14] Q. Lai, M. Paskevicius, D. A. Sheppard, C. E. Buckley, A. W. Thornton, M. R. Hill, Q. Gu, J. Mao, Z. Huang, H. K. Liu, Z. Guo, A. Banerjee, S. Chakraborty, R. Ahuja and K. F. Aguey-Zinsou. 'Hydrogen Storage Materials for Mobile and Stationary Applications: Current State of the Art'. In: *ChemSusChem* 8 (2015), pp. 2789–2825.

[15] K. T. Møller, T. R. Jensen, E. Akiba and H.-w. Li. 'Hydrogen - A sustainable energy carrier'. In: *Progress in Natural Science: Materials International* 27 (2017), pp. 34–40.

[16] H. Hemmes, A. Driessen and R. Griessen. 'Thermodynamic properties of hydrogen at pressures up to 1 Mbar and temperatures between 100 and 1000 K'. In: *Journal of Physics C: Solid State Physics* 19 (1986), pp. 3571–3585.

[17] M. H. Mendelsohn, D. M. Gruen and A. E. Dwight. '$LaNi_{5-x}Al_x$ is a versatile alloy system for metal hydride applications'. In: *Nature* 269 (1977), pp. 45–47.

[18] J. J. Reilly. 'Metal Hydride Technology'. In: *Zeitschrift für Physikalische Chemie* 117 (1979), pp. 155–184.

[19] J. F. Stampfer Jr., C. E. Holley Jr. and J. F. Suttle. 'The Magnesium-Hydrogen System'. In: *Journal of the American Chemical Society* 82 (1960), pp. 3504–3508.

[20] A. Zaluska, L. Zaluski and J. O. Ström–Olsen. 'Nanocrystalline magnesium for hydrogen storage'. In: *Journal of Alloys and Compounds* 288 (1999), pp. 217–225.

[21] J. Huot, G. Liang, S. Boily, A. Van Neste and R. Schulz. 'Structural study and hydrogen sorption kinetics of ball-milled magnesium hydride'. In: *Journal of Alloys and Compounds* 293–295 (1999), pp. 495–500.

[22] W. Oelerich, T. Klassen and R. Bormann. 'Metal oxides as catalysts for improved hydrogen sorption in nanocrystalline Mg-based materials'. In: *Journal of Alloys and Compounds* 315 (2001), pp. 237–242.

[23] B. Bogdanović and M. Schwickardi. 'Ti-doped alkali metal aluminium hydrides as potential novel reversible hydrogen storage materials'. In: *Journal of Alloys and Compounds* 253-254 (1997), pp. 1–9.

[24] H.-W. Li, Y. Yan, S. Orimo, A. Züttel and C. M. Jensen. 'Recent Progress in Metal Borohydrides for Hydrogen Storage'. In: *Energies* 4 (2011), pp. 185–214.

[25] L. H. Rude, T. K. Nielsen, D. B. Ravnsbæk, U. Bösenberg, M. B. Ley, B. Richter, L. M. Arnbjerg, M. Dornheim, Y. Filinchuk, F. Besenbacher and T. R. Jensen. 'Tailoring properties of borohydrides for hydrogen storage: A review'. In: *Physica Status Solidi A: Applications and Materials Science* 208 (2011), pp. 1754–1773.

[26] M. B. Ley, L. H. Jepsen, Y.-S. Lee, Y. W. Cho, J. M. Bellosta von Colbe, M. Dornheim, M. Rokni, J. O. Jensen, M. Sloth, Y. Filinchuk, J. E. Jørgensen, F. Besenbacher and T. R. Jensen. 'Complex hydrides for hydrogen storage – new perspectives'. In: *Materials Today* 17 (2014), pp. 122–128.

[27] M. Paskevicius, L. H. Jepsen, P. Schouwink, R. Černý, D. B. Ravnsbæk, Y. Filinchuk, M. Dornheim, F. Besenbacher and T. R. Jensen. 'Metal borohydrides and derivatives – synthesis, structure and properties'. In: *Chemical Society Reviews* 46 (2017), pp. 1565–1634.

[28] J. Puszkiel, S. Garroni, C. Milanese, F. Gennari, T. Klassen, M. Dornheim and C. Pistidda. 'Tetrahydroborates: Development and Potential as Hydrogen Storage Medium'. In: *Inorganics* 5 (2017), p. 74.

[29] R. Mohtadi, M. Matsui, T. S. Arthur and S.-J. Hwang. 'Magnesium Borohydride: From Hydrogen Storage to Magnesium Battery'. In: *Angewandte Chemie International Edition* 51 (2012), pp. 9780–9783.

[30] R. Mohtadi and S. Orimo. 'The renaissance of hydrides as energy materials'. In: *Nature Reviews Materials* 2 (2017), p. 16091.

[31] R. Mohtadi, A. Remhof and P. Jena. 'Complex metal borohydrides: multifunctional materials for energy storage and conversion'. In: *Journal of Physics: Condensed Matter* 28 (2016), p. 353001.

[32] G. Barkhordarian, T. Klassen and R. Bormann. *Patent CA2590210A1: Composite material storing hydrogen, and device for the reversible storage of hydrogen*. 2004. URL: https://patents.google.com/patent/CA2590210A1/en.

[33] G. Barkhordarian, T. Klassen, M. Dornheim and R. Bormann. 'Unexpected kinetic effect of MgB_2 in reactive hydride composites containing complex borohydrides'. In: *Journal of Alloys and Compounds* 440 (2007), pp. L18–L21.

[34] J. J. Vajo, S. L. Skeith and F. Mertens. 'Reversible Storage of Hydrogen in Destabilized $LiBH_4$'. In: *The Journal of Physical Chemistry B* 109 (2005), pp. 3719–3722.

[35] Y. Nakamori, K. Miwa, A. Ninomiya, H.-W. Li, N. Ohba, S. Towata, A. Züttel and S. Orimo. 'Correlation between thermodynamical stabilities of metal borohydrides and

cation electronegativites: First-principles calculations and experiments'. In: *Physical Review B* 74 (2006), p. 045126.

[36] Y. Nakamori, K. Miwa, H. W. Li, N. Ohba, S. Towata and S. Orimo. 'Tailoring of Metal Borohydrides for Hydrogen Storage Applications'. In: *MRS Proceedings* 971 (2006), Z02–01.

[37] J. J. Reilly and R. H. Wiswall. 'The Reaction of Hydrogen with Alloys of Magnesium and Copper'. In: *Inorganic Chemistry* 6 (1967), pp. 2220–2223.

[38] Y. W. Cho, J.-H. Shim and B.-J. Lee. 'Thermal destabilization of binary and complex metal hydrides by chemical reaction: A thermodynamic analysis'. In: *Calphad* 30 (2006), pp. 65–69.

[39] J. Yang, A. Sudik and C. Wolverton. 'Destabilizing $LiBH_4$ with a Metal (M = Mg, Al, Ti, V, Cr, or Sc) or Metal Hydride (MH_2 = MgH_2 , TiH_2 , or CaH_2)'. In: *The Journal of Physical Chemistry C* 111 (2007), pp. 19134–19140.

[40] X.-D. Kang, P. Wang, L.-P. Ma and H.-M. Cheng. 'Reversible hydrogen storage in $LiBH_4$ destabilized by milling with Al'. In: *Applied Physics A* 89 (2007), pp. 963–966.

[41] M. Dornheim. 'Thermodynamics of Metal Hydrides: Tailoring Reaction Enthalpies of Hydrogen Storage Materials'. In: *Thermodynamics: Interaction Studies – Solids, Liquids and Gases*. Ed. by J. C. Moreno Piraján. InTech, 2011. Chap. 33.

[42] P. Chen, Z. Xiong, J. Luo, J. Lin and K. L. Tan. 'Interaction of hydrogen with metal nitrides and imides'. In: *Nature* 420 (2002), pp. 302–304.

[43] S. Orimo, Y. Nakamori, G. Kitahara, K. Miwa, N. Ohba, S. Towata and A. Züttel. 'Dehydriding and rehydriding reactions of $LiBH_4$'. In: *Journal of Alloys and Compounds* 404–406 (2005), pp. 427–430.

[44] U. Bösenberg, S. Doppiu, L. Mosegaard, G. Barkhordarian, N. Eigen, A. Borgschulte, T. R. Jensen, Y. Cerenius, O. Gutfleisch, T. Klassen, M. Dornheim and R. Bormann. 'Hydrogen sorption properties of MgH_2-$LiBH_4$ composites'. In: *Acta Materialia* 55 (2007), pp. 3951–3958.

[45] U. Bösenberg, J. W. Kim, D. Gosslar, N. Eigen, T. R. Jensen, J. M. Bellosta von Colbe, Y. Zhou, M. Dahms, D. H. Kim, R. Günther, Y. W. Cho, K. H. Oh, T. Klassen, R. Bormann and M. Dornheim. 'Role of additives in $LiBH_4$-MgH_2 reactive hydride composites for sorption kinetics'. In: *Acta Materialia* 58 (2010), pp. 3381–3389.

[46] J. Jepsen, C. Milanese, A. Girella, G. A. Lozano, C. Pistidda, J. M. Bellosta von Colbe, A. Marini, T. Klassen and M. Dornheim. 'Compaction pressure influence on material properties and sorption behaviour of $LiBH_4$-MgH_2 composite'. In: *International Journal of Hydrogen Energy* 38 (2013), pp. 8357–8366.

[47] T.-T. Le, C. Pistidda, J. Puszkiel, M. V. Castro Riglos, F. Karimi, J. Skibsted, S. P. GharibDoust, B. Richter, T. Emmler, C. Milanese, A. Santoru, A. Hoell, M. Krumrey, E. Gericke, E. Akiba, T. R. Jensen, T. Klassen and M. Dornheim. 'Design of a Nanometric AlTi Additive for MgB_2-Based Reactive Hydride Composites with Superior Kinetic Properties'. In: *The Journal of Physical Chemistry C* 122 (2018), pp. 7642–7655.

[48] G. Barkhordarian, T. R. Jensen, S. Doppiu, U. Bösenberg, A. Borgschulte, R. Gremaud, Y. Cerenius, M. Dornheim, T. Klassen and R. Bormann. 'Formation of $Ca(BH_4)_2$ from Hydrogenation of CaH_2+MgB_2 Composite'. In: *The Journal of Physical Chemistry C* 112 (2008), pp. 2743–2749.

[49] F. E. Pinkerton, M. S. Meyer, G. P. Meisner, M. P. Balogh and J. J. Vajo. 'Phase Boundaries and Reversibility of $LiBH_4$/MgH_2 Hydrogen Storage Material'. In: *The Journal of Physical Chemistry C* 111 (2007), pp. 12881–12885.

[50] E. Rönnebro and E. H. Majzoub. 'Calcium Borohydride for Hydrogen Storage: Catalysis and Reversibility'. In: *The Journal of Physical Chemistry B* 111 (2007), pp. 12045–12047.

[51] J.-H. Kim, S.-A. Jin, J.-H. Shim and Y. W. Cho. 'Thermal decomposition behavior of calcium borohydride $Ca(BH_4)_2$'. In: *Journal of Alloys and Compounds* 461 (2008), pp. L20–L22.

[52] J. Y. Lee, D. B. Ravnsbæk, Y.-S. Lee, Y. Kim, Y. Cerenius, J.-H. Shim, T. R. Jensen, N. H. Hur and Y. W. Cho. 'Decomposition Reactions and Reversibility of the $LiBH_4$-$Ca(BH_4)_2$ Composite'. In: *The Journal of Physical Chemistry C* 113 (2009), pp. 15080–15086.

[53] F. Pendolino. '"Boron Effect" on the Thermal Decomposition of Light Metal Borohydrides MBH_4 (M = Li, Na, Ca)'. In: *The Journal of Physical Chemistry C* 116 (2012), pp. 1390–1394.

[54] Y. Yan, A. Remhof, D. Rentsch, A. Züttel, S. Giri and P. Jena. 'A novel strategy for reversible hydrogen storage in $Ca(BH_4)_2$'. In: *Chemical Communications* 51 (2015), pp. 11008–11011.

[55] C. Bonatto Minella, S. Garroni, C. Pistidda, R. Gosalawit-Utke, G. Barkhordarian, C. Rongeat, I. Lindemann, O. Gutfleisch, T. R. Jensen, Y. Cerenius, J. Christensen, M. D. Baró, R. Bormann, T. Klassen and M. Dornheim. 'Effect of Transition Metal Fluorides on the Sorption Properties and Reversible Formation of $Ca(BH_4)_2$'. In: *The Journal of Physical Chemistry C* 115 (2011), pp. 2497–2504.

[56] Y. Kim, D. Reed, Y.-S. Lee, J. Y. Lee, J.-H. Shim, D. Book and Y. W. Cho. 'Identification of the Dehydrogenated Product of $Ca(BH_4)_2$'. In: *The Journal of Physical Chemistry C* 113 (2009), pp. 5865–5871.

[57] V. Ozoliņš, E. H. Majzoub and C. Wolverton. 'First-Principles Prediction of Thermodynamically Reversible Hydrogen Storage Reactions in the Li-Mg-Ca-B-H System'. In: *Journal of the American Chemical Society* 131 (2009), pp. 230–237.

[58] Y. Zhang, E. Majzoub, V. Ozoliņš and C. Wolverton. 'Theoretical prediction of different decomposition paths for $Ca(BH_4)_2$ and $Mg(BH_4)_2$'. In: *Physical Review B* 82 (2010), p. 174107.

[59] Y. Kim, S.-J. Hwang, J.-H. Shim, Y.-S. Lee, H. N. Han and Y. W. Cho. 'Investigation of the Dehydrogenation Reaction Pathway of $Ca(BH_4)_2$ and Reversibility of Intermediate Phases'. In: *Journal of Physical Chemistry C* 116 (2012), pp. 4330–4334.

[60] Y. Kim, S.-J. Hwang, Y.-S. Lee, J.-Y. Suh, H. N. Han and Y. W. Cho. 'Hydrogen Back-Pressure Effects on the Dehydrogenation Reactions of $Ca(BH_4)_2$'. In: *The Journal of Physical Chemistry C* 116 (2012), pp. 25715–25720.

[61] C. J. Sahle, C. Sternemann, C. Giacobbe, Y. Yan, C. Weis, M. Harder, Y. Forov, G. Spiekermann, M. Tolan, M. Krisch and A. Remhof. 'Formation of CaB_6 in the thermal decomposition of the hydrogen storage material $Ca(BH_4)_2$'. In: *Physical Chemistry Chemical Physics* 18 (2016), pp. 19866–19872.

[62] Y. Yan, D. Rentsch and A. Remhof. 'Controllable decomposition of $Ca(BH_4)_2$ for reversible hydrogen storage'. In: *Physical Chemistry Chemical Physics* 19 (2017), pp. 7788–7792.

[63] C. Bonatto Minella, S. Garroni, D. Olid, F. Teixidor, C. Pistidda, I. Lindemann, O. Gutfleisch, M. D. Baró, R. Bormann, T. Klassen and M. Dornheim. 'Experimental Evidence of $CaB_{12}H_{12}$ Formation During Decomposition of a $Ca(BH_4)_2$ + MgH_2 Based Reactive Hydride Composite'. In: *The Journal of Physical Chemistry C* 115 (2011), pp. 18010–18014.

[64] C. Bonatto Minella, C. Pistidda, S. Garroni, P. Nolis, M. D. Baró, O. Gutfleisch, T. Klassen, R. Bormann and M. Dornheim. '$Ca(BH_4)_2$ + MgH_2: Desorption Reaction and Role of Mg on Its Reversibility'. In: *Journal of Physical Chemistry C* 117 (2013), pp. 3846–3852.

[65] F. Karimi, P. K. Pranzas, C. Pistidda, J. A. Puszkiel, C. Milanese, U. Vainio, M. Paskevicius, T. Emmler, A. Santoru, R. Utke, M. Tolkiehn, C. Bonatto Minella, A.-L. Chaudhary, S. Börries, C. E. Buckley, S. Enzo, A. Schreyer, T. Klassen and M. Dornheim. 'Structural and kinetic investigation of the hydride composite $Ca(BH_4)_2$ + MgH_2 system doped with NbF_5 for solid-state hydrogen storage'. In: *Physical Chemistry Chemical Physics* 17 (2015), pp. 27328–27342.

[66] J. Huang, M. Gao, Z. Li, X. Cheng, J. Gu, Y. Liu and H. Pan. 'Destabilization of combined $Ca(BH_4)_2$ and $Mg(AlH_4)_2$ for improved hydrogen storage properties'. In: *Journal of Alloys and Compounds* 670 (2016), pp. 135–143.

[67] H. Chu, Z. Xiong, G. Wu, J. Guo, X. Zheng, T. He, C. Wu and P. Chen. 'Hydrogen Storage Properties of $Ca(BH_4)_2$-$LiNH_2$ System'. In: *Chemistry - An Asian Journal* 5 (2010), pp. 1594–1599.

[68] N. Poonyayant, V. Stavila, E. H. Majzoub, L. E. Klebanoff, R. Behrens, N. Angboonpong, M. Ulutagay-Kartin, P. Pakawatpanurut, E. S. Hecht and J. S. Breit. 'An Investigation into the Hydrogen Storage Characteristics of $Ca(BH_4)_2$/$LiNH_2$ and $Ca(BH_4)_2$/$NaNH_2$: Evidence of Intramolecular Destabilization'. In: *The Journal of Physical Chemistry C* 118 (2014), pp. 14759–14769.

[69] Y. Kim, D. Reed, Y.-S. Lee, J.-H. Shim, H. N. Han, D. Book and Y. W. Cho. 'Hydrogenation reaction of CaH_2-CaB_6-Mg mixture'. In: *Journal of Alloys and Compounds* 492 (2010), pp. 597–600.

[70] F. Karimi, P. K. Pranzas, A. Hoell, U. Vainio, E. Welter, V. S. Raghuwanshi, C. Pistidda, M. Dornheim, T. Klassen and A. Schreyer. 'Structural analysis of calcium reactive hydride composite for solid state hydrogen storage'. In: *Journal of Applied Crystallography* 47 (2014), pp. 67–75.

[71] J. J. Reilly and R. H. Wiswall Jr. 'The Reaction of Hydrogen with Alloys of Magnesium and Nickel and the Formation of Mg_2NiH_4'. In: *Inorganic Chemistry* 7 (1968), pp. 2254–2256.

[72] Z. Gavra, M. H. Mintz, G. Kimmel and Z. Hadari. 'Allotropic Transitions of Mg_2NiH_4'. In: *Inorganic Chemistry* 18 (1979), pp. 3595–3597.

[73] J. Genossar and P. S. Rudman. 'Structural Transformation in Mg_2NiH_4'. In: *Journal of Physics and Chemistry of Solids* 42 (1981), pp. 611–616.

[74] D. Noréus and P.-E. Werner. 'The structure of the low temperature phase Mg_2NiH_4 (LT)'. In: *Materials Research Bulletin* 16 (1981), pp. 199–206.

[75] P. Zolliker, K. Yvon and C. H. Baerlocher. 'Low-Temperature Structure of Mg_2NiH_4: Evidence for Microtwinning'. In: *Journal of The Less-Common Metals* 115 (1986), pp. 65–78.

[76] K. Zeng, T. Klassen, W. Oelerich and R. Bormann. 'Thermodynamic analysis of the hydriding process of Mg–Ni alloys'. In: *Journal of Alloys and Compounds* 283 (1999), pp. 213–224.

[77] B. Ao, Z. Zhang, Y. He and Y. Zhao. 'Semiconducting ground-state of three polymorphs of Mg_2NiH_4 from first-principles calculations'. In: *International Journal of Hydrogen Energy* 38 (2013), pp. 16471–16476.

[78] J. J. Vajo, W. Li and P. Liu. 'Thermodynamic and kinetic destabilization in $LiBH_4$/Mg_2NiH_4: promise for borohydride-based hydrogen storage'. In: *Chemical Communications* 46 (2010), p. 6687.

[79] W. Li, J. J. Vajo, R. W. Cumberland, P. Liu, S.-J. Hwang, C. Kim and R. C. Bowman Jr. 'Hydrogenation of Magnesium Nickel Boride for Reversible Hydrogen Storage'. In: *The Journal of Physical Chemistry Letters* 1 (2010), pp. 69–72.

[80] G. Afonso, A. Bonakdarpour and D. P. Wilkinson. 'Hydrogen Storage Properties of the Destabilized $4NaBH_4/5Mg_2NiH_4$ Composite System'. In: *The Journal of Physical Chemistry C* 117 (2013), pp. 21105–21111.

[81] V. Bérubé, G. Radtke, M. Dresselhaus and G. Chen. 'Size effects on the hydrogen storage properties of nanostructured metal hydrides: A review'. In: *International Journal of Energy Research* 31 (2007), pp. 637–663.

[82] R. A. Varin, L. Zbroniec, M. Polanski and J. Bystrzycki. 'A Review of Recent Advances on the Effects of Microstructural Refinement and Nano-Catalytic Additives on the Hydrogen Storage Properties of Metal and Complex Hydrides'. In: *Energies* 4 (2010), pp. 1–25.

[83] R. Janot and D. Guerard. 'Ball-milling in liquid media: Applications to the preparation of anodic materials for lithium-ion batteries'. In: *Progress in Materials Science* 50 (2005), pp. 1–92.

[84] C. Wall, A. Pohl, M. Knapp, H. Hahn and M. Fichtner. 'Production of nanocrystalline lithium fluoride by planetary ball-milling'. In: *Powder Technology* 264 (2014), pp. 409–417.

[85] W. Jung. 'Darstellung und Kristallstruktur von $MgNi_{2,5}B_2$ und $Li_{1,2}Ni_{2,5}B_2$'. In: *Zeitschrift für Naturforschung B* 32 (1977), pp. 1371–1374.

[86] K. J. Gross, A. Züttel and L. Schlapbach. 'On the possibility of metal hydride formation: Part I. The synthesis of $MgNi_3B_2$ by mechanical milling and sintering'. In: *Journal of Alloys and Compounds* 274 (1998), pp. 239–247.

[87] P. Manfrinetti, M. Pani, S. K. Dhar and R. Kulkarni. 'Structure, transport and magnetic properties of $MgNi_3B_2$'. In: *Journal of Alloys and Compounds* 428 (2007), pp. 94–98.

[88] F. Gingl, F. Bonhomme, K. Yvon and P. Fischer. 'Tetracalcium trimagnesium tetradecahydride, $Ca_4Mg_3H_{14}$: the first ternary alkaline earth hydride'. In: *Journal of Alloys and Compounds* 185 (1992), pp. 273–278.

[89] K. Yvon and B. Bertheville. 'Magnesium based ternary metal hydrides containing alkali and alkaline-earth elements'. In: *Journal of Alloys and Compounds* 425 (2006), pp. 101–108.

[90] S. Djellab, Y. Bouhadda, M. Bououdina, N. Fenineche and Y. Boudouma. 'Structural, Electronic and Elastic Properties of MgH_2, CaH_2 and $Ca_4Mg_3H_{14}$ for Hydrogen Storage Materials'. In: *Journal of Electronic Materials* 45 (2016), pp. 3935–3942.

[91] U. Bösenberg, C. Pistidda, M. Tolkiehn, N. Busch, I. Saldan, K. Suarez-Alcantara, A. Arendarska, T. Klassen and M. Dornheim. 'Characterization of metal hydrides by in-situ XRD'. In: *International Journal of Hydrogen Energy* 39 (2014), pp. 9899–9903.

[92] B. R. S. Hansen, K. T. Møller, M. Paskevicius, A.-C. Dippel, P. Walter, C. J. Webb, C. Pistidda, N. Bergemann, M. Dornheim, T. Klassen, J.-E. Jørgensen and T. R. Jensen. 'In situ X-ray diffraction environments for high-pressure reactions'. In: *Journal of Applied Crystallography* 48 (2015), pp. 1234–1241.

[93] C. Pistidda, A. Santoru, S. Garroni, N. Bergemann, A. Rzeszutek, C. Horstmann, D. Thomas, T. Klassen and M. Dornheim. 'First Direct Study of the Ammonolysis Reaction in the Most Common Alkaline and Alkaline Earth Metal Hydrides by in Situ SR-PXD'. In: *The Journal of Physical Chemistry C* 119 (2015), pp. 934–943.

[94] A. P. Hammersley, S. O. Svensson, M. Hanfland, A. N. Fitch and D. Hausermann. 'Two-dimensional detector software: From real detector to idealised image or two-theta scan'. In: *High Pressure Research* 14 (1996), pp. 235–248.

[95] A. P. Hammersley. 'FIT2D: An Introduction and Overview'. In: *ESRF Internal Report* ESRF97HA02 (1997).

[96] OriginLab Corporation. *Origin and OriginPro*. URL: https://www.originlab.com/Origin (visited on 16/02/2018).

[97] H. M. Rietveld. 'Line profiles of neutron powder-diffraction peaks for structure refinement'. In: *Acta Crystallographica* 22 (1967), pp. 151–152.

[98] H. M. Rietveld. 'A profile refinement method for nuclear and magnetic structures'. In: *Journal of Applied Crystallography* 2 (1969), pp. 65–71.

[99] B. H. Toby. 'R factors in Rietveld analysis: How good is good enough?' In: *Powder Diffraction* 21 (2006), pp. 67–70.

[100] L. Lutterotti. *MAUD – Materials Analysis Using Diffraction*. URL: http://maud.radiographema.eu/ (visited on 19/10/2017).

[101] L. Lutterotti. 'Total pattern fitting for the combined size-strain-stress-texture determination in thin film diffraction'. In: *Nuclear Instruments and Methods in Physics Research Section B: Beam Interactions with Materials and Atoms* 268 (2010), pp. 334–340.

[102] FIZ Karlsruhe GmbH. *ICSD – Inorganic Crystal Structure Database*. URL: http://www2.fiz-karlsruhe.de/icsd_home.html (visited on 19/10/2017).

[103] A. Züttel, S. Rentsch, P. Fischer, P. Wenger, P. Sudan, P. Mauron and C. Emmenegger. 'Hydrogen storage properties of $LiBH_4$'. In: *Journal of Alloys and Compounds* 356-357 (2003), pp. 515–520.

[104] Y. Filinchuk, D. Chernyshov and R. Cerny. 'Lightest Borohydride Probed by Synchrotron X-ray Diffraction: Experiment Calls for a New Theoretical Revision'. In: *The Journal of Physical Chemistry C* 112 (2008), pp. 10579–10584.

[105] Y. Filinchuk and H. Hagemann. 'Structure and Properties of $NaBH_4 \cdot 2\,H_2O$ and $NaBH_4$'. In: *European Journal of Inorganic Chemistry* 2008 (2008), pp. 3127–3133.

[106] Y. Kusadome, K. Ikeda, Y. Nakamori, S. Orimo and Z. Horita. 'Hydrogen storage capability of $MgNi_2$ processed by high pressure torsion'. In: *Scripta Materialia* 57 (2007), pp. 751–753.

[107] G. Renaudin, S. Gomes, H. Hagemann, L. Keller and K. Yvon. 'Structural and spectroscopic studies on the alkali borohydrides MBH_4 (M = Na, K, Rb, Cs)'. In: *Journal of Alloys and Compounds* 375 (2004), pp. 98–106.

[108] M. Paskevicius, M. B. Ley, D. A. Sheppard, T. R. Jensen and C. E. Buckley. 'Eutectic melting in metal borohydrides'. In: *Physical Chemistry Chemical Physics* 15 (2013), p. 19774.

[109] S. Kumar, Y. Kojima and G. K. Dey. 'Synergic effect of $ZrCl_4$ on thermal dehydrogenation kinetics of KBH_4'. In: *Journal of Alloys and Compounds* 718 (2017), pp. 134–138.

[110] W. I. F. David, S. K. Callear, M. O. Jones, P. C. Aeberhard, S. D. Culligan, A. H. Pohl, S. R. Johnson, K. R. Ryan, J. E. Parker, P. P. Edwards, C. J. Nuttall and A. Amieiro-Fonseca. 'The structure, thermal properties and phase transformations of the cubic polymorph of magnesium tetrahydroborate'. In: *Physical Chemistry Chemical Physics* 14 (2012), p. 11800.

[111] Y. Filinchuk, R. Černý and H. Hagemann. 'Insight into $Mg(BH_4)_2$ with Synchrotron X-ray Diffraction: Structure Revision, Crystal Chemistry, and Anomalous Thermal Expansion'. In: *Chemistry of Materials* 21 (2009), pp. 925–933.

[112] J.-H. Her, P. W. Stephens, Y. Gao, G. L. Soloveichik, J. Rijssenbeek, M. Andrus and J.-C. Zhao. 'Structure of unsolvated magnesium borohydride $Mg(BH_4)_2$'. In: *Acta Crystallographica Section B* 63 (2007), pp. 561–568.

[113] P. J. Brown, A. G. Fox, E. N. Maslen, M. A. O'Keefe and B. T. M. Willis. 'Intensity of diffracted intensities'. In: *International Tables for Crystallography*. Ed. by E. Prince. 3rd ed. Vol. C. Kluwer Academic Publishers, 2006. Chap. 6.1, pp. 554–595.

[114] J. J. Vajo, W. Li and P. Liu. 'Supplementary Material (ESI) for "Thermodynamic and kinetic destabilization in $LiBH_4$/ Mg_2NiH_4: promise for borohydride-based hydrogen storage"'. In: *Chemical Communications* 46 (2010), p. 6687.

[115] Y. Yan, A. Remhof, P. Mauron, D. Rentsch, Z. Łodziana, Y.-S. Lee, H.-S. Lee, Y. W. Cho and A. Züttel. 'Controlling the Dehydrogenation Reaction toward Reversibility of the $LiBH_4$–$Ca(BH_4)_2$ Eutectic System'. In: *The Journal of Physical Chemistry C* 117 (2013), pp. 8878–8886.

[116] Y. Filinchuk, E. Rönnebro and D. Chandra. 'Crystal structures and phase transformations in $Ca(BH_4)_2$'. In: *Acta Materialia* 57 (2009), pp. 732–738.

[117] F. Buchter, Z. Łodziana, A. Remhof, O. Friedrichs, A. Borgschulte, P. Mauron, A. Züttel, D. Sheptyakov, L. Palatinus, K. Chłopek, M. Fichtner, G. Barkhordarian, R. Bormann and B. C. Hauback. 'Structure of the Orthorhombic γ-Phase and Phase Transitions of $Ca(BD_4)_2$'. In: *The Journal of Physical Chemistry C* 113 (2009), pp. 17223–17230.

[118] M. R. Hansen, T. Vosegaard, H. J. Jakobsen and J. Skibsted. '^{11}B Chemical Shift Anisotropies in Borates from ^{11}B MAS, MQMAS, and Single-Crystal NMR Spectroscopy'. In: *The Journal of Physical Chemistry A* 108 (2004), pp. 586–594.

[119] B. V. Padlyak, N. A. Sergeev, M. Olszewski, V. T. Adamiv and Y. V. Burak. '^{11}B and ^{7}Li MAS NMR spectroscopy of glassy and crystalline borate compounds'. In: *Physics and Chemistry of Glasses: European Journal of Glass Science and Technology Part B* 55 (2014), pp. 25–33.

[120] H. I. Schlesinger and H. C. Brown. 'Metallo Borohydrides. III. Lithium Borohydride'. In: *Journal of the American Chemical Society* 62 (1940), pp. 3429–3435.

[121] O. Friedrichs, A. Remhof, S.-J. Hwang and A. Züttel. 'Role of $Li_2B_{12}H_{12}$ for the Formation and Decomposition of $LiBH_4$'. In: *Chemistry of Materials* 22 (2010), pp. 3265–3268.

[122] M. P. Pitt, M. Paskevicius, D. H. Brown, D. A. Sheppard and C. E. Buckley. 'Thermal stability of $Li_2B_{12}H_{12}$ and its role in the decomposition of $LiBH_4$'. In: *Journal of the American Chemical Society* 135 (2013), pp. 6930–6941.

[123] B. R. S. Hansen, D. B. Ravnsbæk, J. Skibsted and T. R. Jensen. 'Hydrogen reversibility of $LiBH_4$–MgH_2–Al composites'. In: *Phys. Chem. Chem. Phys.* 16 (2014), pp. 8970–8980.

[124] M. Matsuo, Y. Nakamori, S. Orimo, H. Maekawa and H. Takamura. 'Lithium superionic conduction in lithium borohydride accompanied by structural transition'. In: *Applied Physics Letters* 91 (2007), p. 224103.

[125] M. Dornheim, S. Doppiu, G. Barkhordarian, U. Boesenberg, T. Klassen, O. Gutfleisch and R. Bormann. 'Hydrogen storage in magnesium-based hydrides and hydride composites'. In: *Scripta Materialia* 56 (2007), pp. 841–846.

[126] P. Martelli, R. Caputo, A. Remhof, P. Mauron, A. Borgschulte and A. Züttel. 'Stability and Decomposition of $NaBH_4$'. In: *The Journal of Physical Chemistry C* 114 (2010), pp. 7173–7177.

[127] The National Institute of Standards and Technology (NIST). *NIST Chemistry WebBook*. URL: https://webbook.nist.gov/ (visited on 16/02/2018).

[128] T. E. C. Price, D. M. Grant, I. Telepeni, X. B. Yu and G. S. Walker. 'The decomposition pathways for $LiBD_4$-MgD_2 multicomponent systems investigated by in situ neutron diffraction'. In: *Journal of Alloys and Compounds* 472 (2009), pp. 559–564.

[129] R. D. Shannon. 'Revised Effective Ionic Radii and Systematic Studies of Interatomic Distances in Halides and Chalcogenides'. In: *Acta Crystallographica Section A* 32 (1976), pp. 751–767.

[130] F. Karimi, M. V. C. Riglos, A. Santoru, A. Hoell, V. S. Raghuwanshi, C. Milanese, N. Bergemann, C. Pistidda, P. Nolis, M. D. Baro, G. Gizer, T.-T. Le, P. K. Pranzas, M. Dornheim, T. Klassen, A. Schreyer and J. Puszkiel. 'In Situ Formation of TiB_2 Nanoparticles for Enhanced Dehydrogenation/Hydrogenation Reaction Kinetics of $LiBH_4$–MgH_2 as a Reversible Solid-State Hydrogen Storage Composite System'. In: *The Journal of Physical Chemistry C* 122 (2018), pp. 11671–11681.

[131] J. Jepsen, C. Milanese, J. Puszkiel, A. Girella, B. Schiavo, G. Lozano, G. Capurso, J. Bellosta von Colbe, A. Marini, S. Kabelac, M. Dornheim and T. Klassen. 'Fundamental Material Properties of the $2\,LiBH_4$-MgH_2 Reactive Hydride Composite for Hydrogen Storage: (II) Kinetic Properties'. In: *Energies* 11 (2018), p. 1170.

[132] O. Zavorotynska, M. Corno, E. Pinatel, L. H. Rude, P. Ugliengo, T. R. Jensen and M. Baricco. 'Theoretical and Experimental Study of $LiBH_4$-LiCl Solid Solution'. In: *Crystals* 2 (2012), pp. 144–158.

[133] L. M. Arnbjerg, D. B. Ravnsbæk, Y. Filinchuk, R. T. Vang, Y. Cerenius, F. Besenbacher, J.-E. Jørgensen, H. J. Jakobsen and T. R. Jensen. 'Structure and Dynamics for $LiBH_4$–LiCl Solid Solutions'. In: *Chemistry of Materials* 21 (2009), pp. 5772–5782.

[134] M. Matsuo, H. Takamura, H. Maekawa, H.-W. Li and S. Orimo. 'Stabilization of lithium superionic conduction phase and enhancement of conductivity of $LiBH_4$ by LiCl addition'. In: *Applied Physics Letters* 94 (2009), p. 084103.

[135] B. Schiavo, A. Girella, F. Agresti, G. Capurso and C. Milanese. 'Ball-milling and AlB_2 addition effects on the hydrogen sorption properties of the CaH_2 + MgB_2 system'. In: *Journal of Alloys and Compounds* 509S (2011), S714–S718.

[136] C. Pistidda, F. Karimi, S. Garroni, A. Rzeszutek, C. Bonatto Minella, C. Milanese, T. T. Le, L. H. Rude, J. Skibsted, T. R. Jensen, C. Horstmann, C. Gundlach, M. Tolkiehn, P. K. Pranzas, A. Schreyer, T. Klassen and M. Dornheim. 'Effect of the Partial Replacement of CaH_2 with CaF_2 in the Mixed System CaH_2 + MgB_2'. In: *The Journal of Physical Chemistry C* 118 (2014), pp. 28409–28417.

[137] H.-W. Li, E. Akiba and S. Orimo. 'Comparative study on the reversibility of pure metal borohydrides'. In: *Journal of Alloys and Compounds* 580 (2013), S292–S295.

[138] Z. Łodziana, P. Błoński, Y. Yan, D. Rentsch and A. Remhof. 'NMR Chemical Shifts of ^{11}B in Metal Borohydrides from First-Principle Calculations'. In: *The Journal of Physical Chemistry C* 118 (2014), pp. 6594–6603.

[139] C. Bonatto Minella, S. Garroni, C. Pistidda, M. D. Baró, O. Gutfleisch, T. Klassen and M. Dornheim. 'Sorption properties and reversibility of Ti(IV) and Nb(V)-fluoride doped-$Ca(BH_4)_2$-MgH_2 system'. In: *Journal of Alloys and Compounds* 622 (2015), pp. 989–994.

Publications

Parts of this thesis were published in the following peer reviewed articles:

- N. Bergemann, C. Pistidda, C. Milanese, T. Emmler, F. Karimi, A.-L. Chaudhary, M. R. Chierotti, T. Klassen and M. Dornheim. 'Ca$(BH_4)_2$-Mg_2NiH_4: on the pathway to a Ca$(BH_4)_2$ system with a reversible hydrogen cycle'. In: *Chemical Communications* 52 (2016), pp. 4836–4839.
- N. Bergemann, C. Pistidda, C. Milanese, M. Aramini, S. Huotari, P. Nolis, A. Santoru, M. R. Chierotti, A.-L. Chaudhary, M. D. Baró, T. Klassen and M. Dornheim. 'A hydride composite featuring mutual destabilisation and reversible boron exchange: Ca$(BH_4)_2$-Mg_2NiH_4'. In: *Journal of Materials Chemistry A* 6 (2018), pp. 17929–17946.
- N. Bergemann, C. Pistidda, M. Uptmoor, C. Milanese, A. Santoru, T. Emmler, J. Puszkiel, M. Dornheim and T. Klassen. 'A new mutually destabilized reactive hydride system: $LiBH_4$-Mg_2NiH_4'. In: *Journal of Energy Chemistry* 34 (2019), pp. 240–254.

Acknowledgements

I would like to thank everyone who supported me during my PhD studies and helped me to collect the results, interpret them and finally assemble the many pieces of the puzzle. I thank Prof. Dr. Thomas Klassen and Dr. Martin Dornheim who made it possible for me to do these studies at Helmholtz-Zentrum Geesthacht. I want to express my gratitude to Dr. Claudio Pistidda who trained me when I started my work at the research centre. In the following years, he was always very supportive in many ways, a reliable advisor and a pleasant person to work with and talk to. I would like to thank all my collaborators, especially Prof. Dr. Chiara Milanese and her colleagues from the University of Pavia who carried out several relevant measurements for me. Prof. Dr. Maria D. Baró and Dr. Pau Nolis from the Autonomous University of Barcelona allowed me to use their facilities and measure my samples with their NMR spectrometer. I thank them for that. Prof. Dr. Michele R. Chierotti from the University of Turin measured a series of NMR spectra for me and I would like to express my gratitude to him. I also want to thank Dr. Matteo Aramini from the Rutherford Appleton Laboratory for accompanying me during our X-ray Raman Spectroscopy experiments at ESRF and for spending a lot of time on the data evaluation afterwards. Of course, I want to thank all my colleagues from Helmholtz-Zentrum Geesthacht. Especially, I am grateful to Dr. Thomas Emmler who performed several NMR measurements that helped me to understand the investigated systems better. Dr. Anna-Lisa Chaudhary supported me during our long shifts at different synchrotron facilities and made these hours a lot of fun. I also want to thank Oliver Metz for always having a helping hand in all technical matters and for all our nice conversations. Dr. Fahim Karimi often had interesting and good ideas for solving problems and finding answers and I want to thank him for sharing these ideas with me. In particular, I am grateful to Dr. Antonio Santoru who was not only very helpful in the lab and regarding diffraction data evaluation but also a competent sparring partner and a very pleasant fellow. My special thanks go to Dr. Stefan Börries with whom I always had very stimulating discussions on a wide range of different topics. In addition, he brought a lot of joy into my PhD time by being an always-cheerful office neighbour and great sailing partner with whom I often stopped on the way to work at the Geesthacht outdoor pool to swim some lanes. Eventually, I want to thank my son Bo and my wife Rina from the bottom of my heart. Although Bo deprived me of so much sleep, he has always given me new energy and momentum. All the time, Rina has been there for me and had my back. She has always encouraged me and made me stronger.